



PB99-126690

NCHRP Report 412

Fatigue-Resistant Design of Cantilevered Signal, Sign and Light Supports

Transportation Research Board
National Research Council

REPRODUCED BY: **NTIS**
U.S. Department of Commerce
National Technical Information Service
Springfield, Virginia 22161

TRANSPORTATION RESEARCH BOARD EXECUTIVE COMMITTEE 1998

OFFICERS

Chairwoman: Sharon D. Banks, General Manager, AC Transit

Vice Chairman: Wayne Shackelford, Commissioner, Georgia Department of Transportation

Executive Director: Robert E. Skinner, Jr., Transportation Research Board

MEMBERS

THOMAS F. BARRY, JR., Secretary of Transportation, Florida Department of Transportation

BRIAN J. L. BERRY, Lloyd Viel Berkner Regental Professor, Bruton Center for Development Studies, University of Texas at Dallas

SARAH C. CAMPBELL, President, TransManagement, Inc., Washington, DC

E. DEAN CARLSON, Secretary, Kansas Department of Transportation

JOANNE F. CASEY, President, Intermodal Association of North America, Greenbelt, MD

JOHN W. FISHER, Director, ATLSS Engineering Research Center, Lehigh University

GORMAN GILBERT, Director, Institute for Transportation Research and Education, North Carolina State University

DELON HAMPTON, Chair and CEO, Delon Hampton & Associates, Washington, DC

LESTER A. HOEL, Hamilton Professor, Civil Engineering, University of Virginia

JAMES L. LAMMIE, Director, Parsons Brinckerhoff, Inc., New York, NY

THOMAS F. LARWIN, General Manager, San Diego Metropolitan Transit Development Board

BRADLEY L. MALLORY, Secretary of Transportation, Pennsylvania Department of Transportation

JEFFREY J. MCCAIG, President and CEO, Trimac Corporation, Calgary, Alberta, Canada

JOSEPH A. MICKES, Chief Engineer, Missouri Department of Transportation

MARSHALL W. MOORE, Director, North Dakota Department of Transportation

ANDREA RINIKER, Executive Director, Port of Tacoma

JOHN M. SAMUELS, VP-Operations Planning & Budget, Norfolk Southern Corporation, Norfolk, VA

LES STERMAN, Executive Director, East-West Gateway Coordinating Council, St. Louis, MO

JAMES W. VAN LOBEN SELS, Director, CALTRANS (Past Chair, 1996)

MARTIN WACHS, Director, University of California Transportation Center, University of California at Berkeley

DAVID L. WINSTEAD, Secretary, Maryland Department of Transportation

DAVID N. WORMLEY, Dean of Engineering, Pennsylvania State University (Past Chair, 1997)

MIKE ACOTT, President, National Asphalt Pavement Association (ex officio)

JOE N. BALLARD, Chief of Engineers and Commander, U.S. Army Corps of Engineers (ex officio)

ANDREW H. CARD, JR., President and CEO, American Automobile Manufacturers Association (ex officio)

KELLEY S. COYNER, Acting Administrator, Research and Special Programs, U.S. Department of Transportation (ex officio)

MORTIMER L. DOWNEY, Deputy Secretary, Office of the Secretary, U.S. Department of Transportation (ex officio)

FRANCIS B. FRANCOIS, Executive Director, American Association of State Highway and Transportation Officials (ex officio)

DAVID GARDINER, Assistant Administrator, U.S. Environmental Protection Agency (ex officio)

JANE F. GARVEY, Federal Aviation Administrator, U.S. Department of Transportation (ex officio)

JOHN E. GRAYKOWSKI, Acting Maritime Administrator, U.S. Department of Transportation (ex officio)

ROBERT A. KNISELY, Deputy Director, Bureau of Transportation Statistics, U.S. Department of Transportation (ex officio)

GORDON J. LINTON, Federal Transit Administrator, U.S. Department of Transportation (ex officio)

RICARDO MARTINEZ, National Highway Traffic Safety Administrator, U.S. Department of Transportation (ex officio)

WALTER B. McCORMICK, President and CEO, American Trucking Associations, Inc. (ex officio)

WILLIAM W. MILLAR, President, American Public Transit Association (ex officio)

JOLENE M. MOLITORIS, Federal Railroad Administrator, U.S. Department of Transportation (ex officio)

KAREN BORLAUG PHILLIPS, Senior Vice President, Association of American Railroads (ex officio)

VALENTIN J. RIVA, President, American Concrete Pavement Association

GEORGE D. WARRINGTON, Acting President and CEO, National Railroad Passenger Corporation (ex officio)

KENNETH R. WYKLE, Federal Highway Administrator, U.S. Department of Transportation (ex officio)

NATIONAL COOPERATIVE HIGHWAY RESEARCH PROGRAM

Transportation Research Board Executive Committee Subcommittee for NCHRP

SHARON BANKS, AC Transit (Chairwoman)

FRANCIS B. FRANCOIS, American Association of State Highway and Transportation Officials

LESTER A. HOEL, University of Virginia

WAYNE SHACKELFORD, Georgia Department of Transportation

ROBERT E. SKINNER, JR., Transportation Research Board

DAVID N. WORMLEY, Pennsylvania State University

KENNETH R. WYKLE, Federal Highway Administration

Project Panel 10-38 Field of Materials and Construction Area of Specifications, Procedures, and Practices

JOHN J. PANAK, D-5 Engineering, Austin, TX (Chair)

CHAO HU, Delaware DOT

F. WAYNE KLAIBER, Iowa State University

ALLEN F. LAFFOON, Missouri Highway and Transportation Department

CLARENCE MABIN, Custom Engineering, Inc., Independence, MO

JOHN NYDAHL, University of Wyoming

ROGER D. TILL, Michigan DOT

KRISHNA K. VERMA, FHWA

WILLIAM WRIGHT, FHWA Liaison Representative

D. WILLIAM DEARASAUGH, TRB Liaison Representative

Program Staff

ROBERT J. REILLY, Director, Cooperative Research Programs

CRAWFORD F. JENCKS, Manager, NCHRP

DAVID B. BEAL, Senior Program Officer

LLOYD R. CROWTHER, Senior Program Officer

B. RAY DERR, Senior Program Officer

AMIR N. HANNA, Senior Program Officer

EDWARD T. HARRIGAN, Senior Program Officer

RONALD D. MCCREADY, Senior Program Officer


KENNETH S. OPIELA, Senior Program Officer

EILEEN P. DELANEY, Managing Editor

HELEN CHIN, Assistant Editor

JAMIE FEAR, Assistant Editor

HILARY FREER, Assistant Editor

REPORT DOCUMENTATION PAGE		Form Approved OMB No. 0704-0188	
Public reporting burden for this collection of information is estimated to average 1 hour response, including the time for reviewing instructions, searching existing data sources, gathering and maintaining the data needed, and completing and reviewing the collection of information. Send comments regarding this burden estimate or any other aspect of this collection of information, including suggestions for reducing this burden, to Washington Headquarters Services, Directorate for Information Operations and Reports, 1215 Jefferson Davis Highway, Suite 1204, Arlington, VA 22202-4302, and to the Office of Management and Budget, Paperwork reduction Project (0704-0188), Washington, DC 20503			
1. AGENCY USE ONLY (Leave blank)	2. REPORT DATE 1998	3. REPORT TYPE AND DATES COVERED Final Report	
4. TITLE AND SUBTITLE NCHRP Report 412: Fatigue-Resistant Design of Cantilevered Signal, Sign and Light Supports		5. FUNDING NUMBERS D10-38	
6. AUTHOR(S): M.R. Kaczinski et al.		 PB99-126690	
7. PERFORMING ORGANIZATION NAME(S) AND ADDRESS(ES) ATLSS Engineering Research Center Lehigh University Bethlehem, PA		8. PERFORMING ORGANIZATION REPORT NUMBER HR 10-38	
9. SPONSORING/MONITORING AGENCY NAME(S) AND ADDRESS(ES) American Association of State Highway and Transportation Officials 444 North Capitol Street, N.W. Suite 249 Washington, D.C. 20001		10. SPONSORING/MONITORING AGENCY REPORT NUMBER	
11. SUPPLEMENTARY NOTES Sponsored in cooperation with the Federal Highway Administration			
12a. DISTRIBUTION/AVAILABILITY STATEMENT Available 2101 Constitution Avenue, N.W., Washington, D.C. 20418		12b. DISTRIBUTION CODE: unlimited	
13. ABSTRACT (Maximum 200 words) This report contains the findings of a study on fatigue resistance of cantilevered signal, sign, and light supports. Recommended specifications for the fatigue-resistant design of these structures are included. The contents of this report will be of immediate interest to bridge and structural engineers, traffic engineers, and manufacturers.			
14. SUBJECT TERMS Bridges, Other Structures, and Hydraulics and Hydrology		15. NUMBER OF PAGES	
		16. PRICE CODE	
17. SECURITY CLASSIFICATION Unclassified	18. SECURITY CLASSIFICATION OF THIS PAGE Unclassified	19. SECURITY CLASSIFICATION OF ABSTRACT Unclassified	20. LIMITATION OF ABSTRACT

Report 412

Fatigue-Resistant Design of Cantilevered Signal, Sign and Light Supports

M. R. KACZINSKI

R. J. DEXTER

J.P. VAN DIEN

ATLSS Engineering Research Center

Lehigh University

Bethlehem, PA

PROTECTED UNDER INTERNATIONAL COPYRIGHT
ALL RIGHTS RESERVED.
NATIONAL TECHNICAL INFORMATION SERVICE
U.S. DEPARTMENT OF COMMERCE

Subject Areas

Bridges, Other Structures, and Hydraulics and Hydrology

Research Sponsored by the American Association of State
Highway and Transportation Officials in Cooperation with the
Federal Highway Administration

TRANSPORTATION RESEARCH BOARD
NATIONAL RESEARCH COUNCIL

NATIONAL ACADEMY PRESS
Washington, D.C. 1998

NATIONAL COOPERATIVE HIGHWAY RESEARCH PROGRAM

Systematic, well-designed research provides the most effective approach to the solution of many problems facing highway administrators and engineers. Often, highway problems are of local interest and can best be studied by highway departments individually or in cooperation with their state universities and others. However, the accelerating growth of highway transportation develops increasingly complex problems of wide interest to highway authorities. These problems are best studied through a coordinated program of cooperative research.

In recognition of these needs, the highway administrators of the American Association of State Highway and Transportation Officials initiated in 1962 an objective national highway research program employing modern scientific techniques. This program is supported on a continuing basis by funds from participating member states of the Association and it receives the full cooperation and support of the Federal Highway Administration, United States Department of Transportation.

The Transportation Research Board of the National Research Council was requested by the Association to administer the research program because of the Board's recognized objectivity and understanding of modern research practices. The Board is uniquely suited for this purpose as it maintains an extensive committee structure from which authorities on any highway transportation subject may be drawn; it possesses avenues of communications and cooperation with federal, state and local governmental agencies, universities, and industry; its relationship to the National Research Council is an insurance of objectivity; it maintains a full-time research correlation staff of specialists in highway transportation matters to bring the findings of research directly to those who are in a position to use them.

The program is developed on the basis of research needs identified by chief administrators of the highway and transportation departments and by committees of AASHTO. Each year, specific areas of research needs to be included in the program are proposed to the National Research Council and the Board by the American Association of State Highway and Transportation Officials. Research projects to fulfill these needs are defined by the Board, and qualified research agencies are selected from those that have submitted proposals. Administration and surveillance of research contracts are the responsibilities of the National Research Council and the Transportation Research Board.

The needs for highway research are many, and the National Cooperative Highway Research Program can make significant contributions to the solution of highway transportation problems of mutual concern to many responsible groups. The program, however, is intended to complement rather than to substitute for or duplicate other highway research programs.

Note: The Transportation Research Board, the National Research Council, the Federal Highway Administration, the American Association of State Highway and Transportation Officials, and the individual states participating in the National Cooperative Highway Research Program do not endorse products or manufacturers. Trade or manufacturers' names appear herein solely because they are considered essential to the object of this report.

NCHRP REPORT 412

Project 10-38 FY'93

ISSN 0077-5614

ISBN 0-309-06274-8

L. C. Catalog Card No. 98-60839

© 1998 Transportation Research Board

NTIS is authorized to reproduce and sell this report. Permission for further reproduction must be obtained from the copyright owner.

NOTICE

The project that is the subject of this report was a part of the National Cooperative Highway Research Program conducted by the Transportation Research Board with the approval of the Governing Board of the National Research Council. Such approval reflects the Governing Board's judgment that the program concerned is of national importance and appropriate with respect to both the purposes and resources of the National Research Council.

The members of the technical committee selected to monitor this project and to review this report were chosen for recognized scholarly competence and with due consideration for the balance of disciplines appropriate to the project. The opinions and conclusions expressed or implied are those of the research agency that performed the research, and, while they have been accepted as appropriate by the technical committee, they are not necessarily those of the Transportation Research Board, the National Research Council, the American Association of State Highway and Transportation Officials, or the Federal Highway Administration, U.S. Department of Transportation.

Each report is reviewed and accepted for publication by the technical committee according to procedures established and monitored by the Transportation Research Board Executive Committee and the Governing Board of the National Research Council.

To save time and money in disseminating the research findings, the report is essentially the original text as submitted by the research agency. This report has not been edited by TRB.

Published reports of the

NATIONAL COOPERATIVE HIGHWAY RESEARCH PROGRAM

are available from:

Transportation Research Board
National Research Council
2101 Constitution Avenue, N.W.
Washington, D.C. 20418

and can be ordered through the Internet at:

<http://www.nas.edu/trb/index.html>

Printed in the United States of America

FOREWORD

*By Staff
Transportation Research
Board*

This report contains the findings of a study on fatigue resistance of cantilevered signal, sign, and light supports. Recommended specifications for the fatigue-resistant design of these structures are included. The contents of this report will be of immediate interest to bridge and structural engineers, traffic engineers, and manufacturers.

Cantilevered signal, sign, and light supports are susceptible to fatigue cracking from numerous cycles of wind and other loads. Because these structures are often positioned over major roadways, there is widespread concern regarding their reliability. In rare cases, cantilevered sign supports have failed, crashing into the roadway and presenting a hazard to the traveling public.

Many bridge engineers believe that the design guidance in the AASHTO "Standard Specifications for Structural Supports for Highway Signs, Luminaires, and Traffic Signals" should be improved with respect to guarding against fatigue. In particular, the response of these structures to wind is not well understood. Similar structures, under similar environmental conditions, may perform in radically different ways. Engineers also have questions regarding the fatigue resistance of various connection details, both welded and bolted, that are used in various parts of these structures. Although most such existing structures have not exhibited substantial problems, the state of the practice should be improved to ensure the safe performance of such structures in the future.

NCHRP Project 10-38, "Fatigue-Resistant Design of Cantilevered Signal, Sign and Light Supports," was initiated with the objective of developing rational design procedures and recommended specifications that consider wind-induced cyclic stresses in cantilevered signal, sign, and light support structures. The research was performed at Lehigh University, in Bethlehem, Pennsylvania, and included a comprehensive literature study, a survey of practice (of both designers and manufacturers), aeroelastic and aerodynamic wind-tunnel tests, and an experimental fatigue-testing program. This report summarizes the findings from the study and includes fatigue categories for connection details, fatigue design examples, and recommended specifications and commentary for consideration by AASHTO.

The research determined that, for a typical sign or signal support structure, galloping is the primary cause of vibrations that may result in fatigue damage. It was also determined that the number of structures observed to be galloping in field applications is low. Much variation in the detailing of connections was found, and several details of low fatigue resistance are in use. The research suggests that, through changes in the recommended design wind loads used for design of these structures and avoidance of fatigue-susceptible details, the probability of failure of these structures may be reduced. In addition, the research suggests that mitigation of wind-induced vibrations of structures, once they are observed in the field, may also be a desirable action. The report recommends additional research in this area. Finally, the report provides guidance that designers may consider pending any formal changes to design specifications by AASHTO.

CONTENTS

S-1 SUMMARY

1 CHAPTER 1 Introduction and Research Approach

- 1.1 Research Problem Statement, 1
- 1.2 Wind Loads on Cantilevered Support Structures, 2
 - 1.2.1 Galloping, 3
 - 1.2.2 Vortex Shedding, 6
 - 1.2.3 Natural Wind Gusts, 11
 - 1.2.4 Truck-Induced Wind Gusts, 12
- 1.3 Variable Amplitude Fatigue, 19
- 1.4 Research Objectives and Approach, 20
- 1.5 Organization of the Report, 22

23 CHAPTER 2 Findings

- 2.1 Wind Tunnel Tests, 23
 - 2.1.1 Aerodynamic Test Program, 24
 - 2.1.2 Aeroelastic Test Program, 25
- 2.2 Analyses to Determine Fatigue Design Loads, 56
 - 2.2.1 Finite-Element Models, 57
 - 2.2.2 Modal Analyses to Simulate Galloping and Vortex Shedding, 58
 - 2.2.3 Spectral Analyses to Simulate Natural Wind Gusts, 80
 - 2.2.4 Static Pressure Range for Truck-Induced Gusts, 93
 - 2.2.5 Recommendations for Fatigue Loads, 94
- 2.3 Anchor Bolt Fatigue Tests, 95
 - 2.3.1 Background, 96
 - 2.3.2 Description of Experiments, 101
 - 2.3.3 Results of Experiments, 104
 - 2.3.4 Recommendations for Fatigue Design of Anchor Bolts, 112
- 2.4 Relationship Between Support-Structure Forces and Anchor-Bolt Stresses, 132
 - 2.4.1 Description of Experiments, 132
 - 2.4.2 Results of Experiments, 135
 - 2.4.3 Recommendations for Calculating Design Stresses in Anchor Bolts, 140
- 2.5 Fatigue Categorization of Connection Details, 148
 - 2.5.1 Fatigue of Welded Details, 148
 - 2.5.2 Categorization of Connection Details, 149

154 CHAPTER 3 Interpretation, Appraisal and Applications

- 3.1 Review of Existing Specification, 154
 - 3.1.1 Wind-Induced Limit State Fatigue Loads, 154
 - 3.1.2 Allowable Deflection Limits, 156
 - 3.1.3 Fatigue Resistance of Connection Details, 157
- 3.2 Development of the Proposed Specification, 157
 - 3.2.1 Fatigue Limit State Loads and Importance Factors, 157
 - 3.2.2 Resistance to Fatigue Damage and Excessive Mast Arm Deflections, 164
- 3.3 Impact of the Proposed Specification, 167

170 CHAPTER 4 Conclusions and Suggested Research

- 4.1 Conclusions, 170
- 4.2 Suggested Research, 171

173 REFERENCES

A-1 APPENDIX A Fatigue Categorization of Support Structure Connection Details

B-1 APPENDIX B Fatigue Design Examples

C-1 APPENDIX C Proposed Specification and Commentary

AUTHOR ACKNOWLEDGMENTS

The research reported herein was performed under NCHRP Project 10-38 by the ATLSS Engineering Research Center at Lehigh University and the Department of Aeronautics and Astronautics at Massachusetts Institute of Technology (MIT). The work undertaken at MIT was under a subcontract with Lehigh University.

Mark R. Kaczinski, Research Engineer at the ATLSS Center, was the principal investigator. The other authors of this report are Robert J. Dexter, Senior Research Engineer, and James P. Van Dien, Research Assistant at the ATLSS Center. The authors would like to acknowledge Professor John W. Fisher for providing invaluable

guidance over the course of the research program. Special thanks are also extended to Elizabeth Dechant, Robert Connor, Eric J. Kaufmann, and the entire ATLSS Laboratory technician staff.

The wind-tunnel experimental program was conducted at the Wright Brothers Memorial Wind Tunnel Facility at MIT under the direction of Eugene E. Covert, Professor of Aeronautics and Astronautics. Other members of the research team at MIT included Frank H. Durgin, Research Engineer, and Philip Cali, Research Assistant.

Finally, the authors would like to acknowledge the patience and guidance of the NCHRP project panel members.

SUMMARY

Experimental and analytical research was performed to develop guidelines for the fatigue design of cantilevered sign, signal, and luminaire support structures. Four wind-loading phenomena were identified as possible sources of large amplitude vibrations which could lead to fatigue failures, i.e. galloping, vortex shedding, natural wind gusts, and truck-induced wind gusts. Aerodynamic and aeroelastic wind tunnel tests characterized the potential susceptibility and dynamic response of cantilevered sign and signal support structures to the galloping and vortex shedding phenomena. Signs and signal attachments with backplates which are rigidly mounted to a cantilevered mast-arm produced large amplitude galloping-induced vibrations. These findings were consistent with the observed dynamic responses of cantilevered signal support structures in the field. The wind tunnel tests also confirmed that sign and signal support structures are not susceptible to vortex-induced vibrations from the attachments to these structures or, in most cases, from the members themselves. Vortex shedding induced loads are most significant in non-tapered structural members. Static and dynamic finite element analyses were performed to estimate the magnitude of galloping, vortex shedding, and natural wind gust equivalent static fatigue limit-state loads. In addition, calculations were performed to validate a very simple static load model for truck-induced gust loads.

Fatigue-sensitive connection details (e.g. mast arm-to-column, column-to-base plate) were identified from state department of transportation standard drawings and manufacturer literature. The fatigue strengths of these details were categorized according to the AASHTO and AWS fatigue design curves. This review revealed that many cantilevered support structure connection details exhibit very low fatigue strengths (i.e. AASHTO Category E' or lower). Additional emphasis was placed on determining the fatigue resistance of anchor bolts and also the relationship of anchor bolt stresses to support structure forces.

Static tests on full-scale, eight-bolt pattern, anchor bolt groups indicated that the relationship between support structure forces and anchor bolt stresses can be accurately predicted by applying the flexure equation using the moment of inertia of the bolt group. Full-scale fatigue tests were conducted on 47 anchor bolt specimens. These results indicated that the constant-amplitude fatigue limit corresponding to the AASHTO Category D design curve (48 MPa or 7 ksi) is a reasonable lower bound estimate for snug- and fully tightened axially loaded anchor bolts. Several fatigue tests on the full-scale foundations confirmed the validity of the proposed approaches.

The fatigue limit-state wind loads and the fatigue detail categorization were incorporated into a proposed specification for the fatigue-resistant design of cantilevered signal, sign, and luminaire support structures. In the proposed specification, Importance Factors are used to adjust the level of structural reliability for three categories of cantilevered support structures. The most important cantilevered support structures will be designed to resist rarely occurring wind-loading phenomena. Most existing support structure designs would require changes to comply with the provisions of the proposed specification for structures in the most important category. To meet the design specifications, increases in member section properties and/or the selection of more fatigue-resistant connection details will be required. No significant increase of section properties, on average, should be required to meet the proposed provisions for non-critical structures, which are calibrated to achieve the same average level of reliability as existing designs. (The evaluation and retrofit of existing structures in service were not part of the scope.) Sample fatigue design calculations for a sign, signal, and luminaire support structure are included in the report. Recommendations for future research are presented.

Chapter One

INTRODUCTION AND RESEARCH APPROACH

1.1 RESEARCH PROBLEM STATEMENT

Cantilevered sign, signal, and luminaire support structures are used extensively on major interstate highways and at local intersections for traffic control and roadway illumination. The cantilevered support structures are supported by a single vertical support rather than two supports for a traditional overhead support structure. The single support increases motorist safety by lessening the likelihood of vehicle collision; but, the single support also significantly increases the flexibility of the cantilevered structures relative to overhead structures.

The flexibility of the cantilevered support structures has increased over the years as the span of horizontal mast arm has increased. The span of the cantilevers has increased because the setback distance of the column from the roadway has increased for safety reasons and because these structures are increasingly being used on roads with more lanes. Today, it is not unusual for the cantilever to span more than 12 meters (40 ft).

The flexibility, combined with low mass, gives these structures low resonant frequencies of about 1 Hz. The damping is extremely low, typically less than one percent of the critical damping. These conditions make cantilevered support structures particularly susceptible to large-amplitude vibration and/or fatigue cracking because of wind-loading.

Cantilevered sign, signal, and luminaire support structures are designed in accordance with the AASHTO Standard Specifications for Structural Supports for Highway Signs, Luminaires, and Traffic Signals [1]. Historically, the performance of most of the structures designed with these specifications has been satisfactory. However, a survey of state DOTs, conducted as part of this research [2], revealed that the occurrence of problems is increasing. Among the 36 states which responded, approximately one-half had had problems with wind-induced vibration of cantilevered support structures. Several states reported occurrences of horizontal mast-arm displacement ranges in excess of 1200 mm (48 in) under steady-state winds with velocities in the range of 5 m/s to 15 m/s (10 to 35 mph) [2]. Generally, the reported vibrations were observed to occur in the plane of the structure (i.e. vertical-plane vibrations of the horizontal mast arm) in a direction normal to the direction of wind flow.

The large-amplitude, across-wind vibrations observed in cantilevered sign and signal support structures can in most cases be attributed to an aeroelastic phenomenon known as galloping, also known as Den Hartog instability. Galloping requires a non-symmetric cross section, which is provided by the sign and signal attachments. In some cases, vibration has occurred prior to the installation of the attachments. Also, luminaires with symmetric cross-section have been observed to vibrate. In these cases, the vibration may be due to vortex shedding. Both galloping and vortex shedding are characterized by large-amplitude resonant vibrations which occur normal to the direction of wind flow.

Truck-induced gusts have also been identified as a possible source of large-amplitude vertical oscillations in cantilevered support structures, while natural wind gusts create displacements in the horizontal direction. Although the amplitude of stress ranges caused by truck or natural wind-induced vibrations may be smaller than the previously discussed aeroelastic phenomenon, the number of cycles which can be accumulated over the life of a structure is quite large. In fact, it is possible that truck and natural wind-induced vibrations are responsible for the accumulation of fatigue damage in structures which have been in service for over 15 to 20 years.

In most cases, the stress ranges resulting from vibrations due to the four wind-loading phenomena are relatively small. In these cases, the vibration is only a serviceability problem; i.e. motorists cannot clearly see the signals or signs or are concerned about driving under the vibrating structure. Because of the excessive number of complaints that are generated, vibration with a displacement range exceeding 200 mm (8 in) is deemed unacceptable.

However, there have been many cases where the magnitude of the stress ranges in critical connection details was large enough to cause fatigue cracks. The 36 state departments of transportation, which responded to the survey, reported a total of 80 occurrences of fatigue damage in cantilevered support structures resulting from wind-loading. Most of the occurrences of fatigue damage were reported at either the mast-arm-to-column connection, column-to-base-plate connection, or anchor bolts. The propagation of these cracks has resulted in the collapse of several cantilevered support structures [3].

The provisions of the AASHTO Standard Specifications for Structural Supports for Highway Signs, Luminaires, and Traffic Signals are vague and insufficient with respect to the design of structures for vibration and fatigue. Furthermore, the commentary to the specifications does not contain adequate guidance for the application of the current provisions. The reported problems with the performance of cantilevered support structures underscore the need for improvements in the current specifications with respect to the provisions pertaining to vibration and fatigue.

1.2 WIND LOADS ON CANTILEVERED SUPPORT STRUCTURES

Cantilevered sign, signal, and luminaire support structures are susceptible to four types of wind-loading which are critical with respect to the design for vibration and fatigue: (1) galloping; (2) vortex shedding; (3) natural wind gusts; and, (4) truck-induced wind gusts. The following section provides a summary of the four wind loading phenomena as they relate to the performance of cantilevered sign, signal, and luminaire support structures.

1.2.1 GALLOPING

1.2.1.1 General - Galloping and vortex shedding lock-in are aeroelastic phenomena caused by a coupling between the aerodynamic forces which act on a structure (caused by the action of wind) and the structural vibrations [4]. Galloping-induced oscillations primarily occur in flexible, lightly damped structures with non-symmetrical cross-sections (e.g. circular cylinders are not susceptible to galloping-induced vibrations). The phenomenon has been extensively studied in various structures such as square and rectangular prismatic members and ice-coated transmission conductors.

Galloping-induced oscillations are caused by forces which act on a structural element as it is subjected to periodic variations in the angle of attack of the wind flow. The periodically varying angle of attack is generated by across-wind oscillation of the structure. When the forces are aligned with the direction of across-wind motion, the result is successively larger amplitudes of oscillation, i.e. galloping. A derivation of the conditions under which galloping-induced oscillations occur is included in Reference 5 and additional discussion pertaining to the mechanics of the galloping phenomenon can be found in References 6, 7, 8, and 9.

The potential susceptibility of a structure to galloping from the equilibrium position is evaluated using the following equation:

$$\left(\frac{dC_{Fy}}{d\alpha}\right)\bigg|_{\alpha=0} = -\left(\frac{dC_L}{d\alpha} + C_D\right)\bigg|_{\alpha=0} > 0 \quad (1.1)$$

where C_{Fy} is the aerodynamic lift force coefficient acting normal to the free stream velocity, α is the angle of attack, C_L is the lift force coefficient, and C_D is the drag force coefficient which act in respect to the relative wind velocity. The free-stream velocity is defined as the relative wind velocity times the cosine of the angle of attack. Equation 1.1 is commonly referred to as the Den Hartog stability criterion [10]. The Den Hartog stability criterion states that "a section is dynamically unstable if the negative slope of the lift curve is greater than the ordinate of the drag curve." As shown in Equation 1.1, this condition is satisfied when the slope of the lift force coefficient normal to the free-stream velocity, $dC_{Fy}/d\alpha$, is positive (i.e. when the term $dC_L/d\alpha + C_D$ is negative). This condition is called "negative aerodynamic damping."

Galloping from the equilibrium position can only occur if the magnitude of the negative aerodynamic damping is greater than the magnitude of the positive mechanical damping possessed by the structure (i.e. galloping can only occur if the effective damping is less than zero). Therefore, the minimum wind velocity required to initiate galloping is directly proportional to the mechanical damping possessed by the structure [11]. This onset wind velocity is also proportional to the mass and stiffness of the structure and the inverse of the slope of the lift force coefficient curve, C_{Fy} . Thus, a highly flexible structure with low damping (such as a typical cantilevered support structure) will be susceptible to galloping-induced oscillations at relatively low wind velocities provided, of course, that the Den Hartog stability criterion is satisfied.

Several researchers have proposed analytical models to predict the dynamic characteristics of prismatic structures subjected to galloping [4, 11, 12]. For complicated geometrical configurations however, the analysis is highly uncertain. Thus, analytical models which attempt to predict the dynamic response of structures to the galloping phenomenon are not well suited for inclusion in a design specification.

In summary, a structure will be subject to galloping-induced oscillations from the equilibrium condition when two conditions are satisfied: (1) the structure possesses aerodynamic characteristics which satisfy the Den Hartog stability criterion; and, (2) the structure is subjected to a certain minimum onset wind velocity.

1.2.1.2 Evaluation of the Susceptibility to Galloping - The oscillations observed in cantilevered support structures in the field are consistent with the characteristics of the galloping phenomenon. These characteristics include the sudden onset of large-amplitude, across-wind vibrations which increase with wind velocity and occur at the natural frequency of the structure.

Most cantilevered support structures are composed of structural members with circular cross-sections. The symmetry of a circular cylinder lends to the development of a pure drag force when subjected to a periodically varying angle of attack of the wind flow. As a result, the aerodynamic force, which develops normal to the free-stream velocity, is always oriented opposite to the direction of across-wind motion (i.e. circular cylinders always experience positive aerodynamic damping). Thus, circular cylinders are not susceptible to the galloping instability. This fact is important because it indicates that the across-wind vibrations observed in the cantilevered support structures in the field are the result of the aerodynamic characteristics possessed by the attachments to these structures (i.e. signs/signals).

This fact was confirmed by McDonald et al. [13] in a research program which was recently conducted to evaluate the susceptibility of cantilevered signal support structures to the galloping phenomenon. McDonald performed tow tank tests to measure the aerodynamic forces acting on horizontally mounted signal attachments (i.e. signals mounted parallel to the horizontal mast-arm) composed of various geometrical configurations under flow directions from the front and the rear. The results of these tests indicated that the configuration of the signal attachments and the direction of flow significantly influence the susceptibility for galloping. Signal attachments configured with backplates and subjected to flow from the rear were found to be most susceptible to galloping (i.e. the slope of the lift force coefficient curve, C_{Fy} , was greatest for this configuration and flow direction).

These observations regarding signals with backplates were confirmed in wind tunnel tests conducted at the Wright Brothers facility at the Massachusetts Institute of Technology as part of this project. These wind-tunnel tests are described in detail in Section 2.1.

McDonald also showed that signal attachments configured without backplates were found not to be susceptible to galloping for flow from both the front and the rear (i.e. the slope of the lift force coefficient curve, C_{Fy} , indicated positive aerodynamic damping).

Tests were also performed on two cantilevered signal support structures to evaluate the dynamic response exhibited by these structures during occurrences of galloping-induced oscillations. One of the structures tested had a horizontal mast-arm length of 12.2 m (40 ft) and the other had a horizontal mast-arm length of 14.6 m (48 ft). Each of the structures was mounted to a rotatable foundation which permitted the structures to be oriented normal to the prevailing wind direction.

Tests on the 12.2 m (40 ft) structure were conducted with the structure configured with signal attachments which were found to be both susceptible and not susceptible to galloping during the tow tank experiments. Tests in which the structure was mounted with signal attachments found not to be susceptible to galloping from the equilibrium position during the tow tank experiments did not exhibit galloping-induced oscillations when tested in the field. However, when configured with signal attachments found to be susceptible to galloping during the tow tank tests, the structure was observed to experience galloping oscillations with displacement amplitudes at the tip of the horizontal support estimated at between 300 to 400 mm (12 to 16 in). The results of tests on the 14.6 m (48 ft) structure were similar. Galloping was observed in this structure at a wind velocity equal to 4.5 m/s (10 mph) with a maximum measured stress range in the vertical support (at a location 330 mm (13 in) from the base) equal to approximately 34 MPa (4.9 ksi). As will be discussed in Section 2.5, fatigue cracks would be expected to form under a 34 MPa (4.9 ksi) stress range for most cantilevered support structure connection details.

In summary, the results of previous research programs confirm that cantilevered signal support structures are susceptible to galloping as a result of the aerodynamic characteristics possessed by the attachments to these structures. Full-scale field tests showed that galloping cantilevered signal support structures exhibit excessive displacement ranges and stress ranges. These findings are consistent with (1) observations of wind-induced vibration of signal support structures in the field (see Section 2.2) and (2) the results of wind-tunnel tests (see Section 2.1). Because the vibration persists over long time periods at a frequency of about 1 Hz, large numbers of cycles are quickly accumulated. The large numbers of cycles require that structures be designed to resist galloping loads for "infinite-life," as described in Section 1.3 below.

1.2.1.3 Mitigation of Galloping-Induced Vibrations - Two possible means exist by which to mitigate galloping-induced oscillations in cantilevered support structures. First, the dynamic characteristics of the structure could be changed such that the magnitude of the onset wind velocity is greater than the wind velocity for which steady-state flows are typically maintained. Alternatively, the aerodynamic characteristics of the attachments could be changed such that the structure will experience positive aerodynamic damping when subjected to a periodically varying angle of attack of the wind flow.

The dynamic properties of a cantilevered support structure can be altered by changing the structure's mass, stiffness, and/or damping. Increasing any of the three dynamic properties increases the magnitude of the onset wind velocity required to initiate galloping vibrations. Increases in stiffness and mass can be obtained by increasing the sizes of the structural members. Increases in damping can be obtained by mounting various external damping devices to the structure.

McDonald et al. [13] evaluated the effectiveness of several types of external damping devices for mitigating galloping-induced vibrations in cantilevered signal support structures. A tuned-mass damper was dismissed as a potential mitigation measure following an evaluation which indicated that the installation of such a device to the horizontal mast-arm of a cantilevered support structure would be impractical. The liquid-tuned damper, which consisted of a 914 mm (36 in) long PVC pipe filled with water and inserted into the end of the horizontal mast-arm of a full-scale signal support structure, was found to be ineffective in mitigating galloping-induced vibrations.

The aerodynamic properties of the attachments to cantilevered support structures can be altered by (1) changing the geometric configuration of the attachment to either minimize or eliminate the characteristics which result in negative aerodynamic damping; or, (2) installing a device which is known to provide positive aerodynamic damping. In terms of changing the geometry, there are many signal configurations which are believed to be not susceptible to galloping, e.g. signals configured without a backplate and signals which have an articulated connection to the support. However, these configurations may not be acceptable from a traffic control perspective. The tradeoff between suitability for traffic control and susceptibility to galloping should be investigated further. Until greater certainty is achieved in distinguishing susceptible configurations from non-susceptible configurations, it will be assumed that all types of signals may be susceptible.

With respect to devices, McDonald et al. evaluated the effectiveness of a damping plate mounted to the horizontal support of a cantilevered signal support structure. The damping plate consisted of a sign blank measuring 410 x 1680 mm (16 x 66 in) mounted horizontally (i.e. parallel to the horizon) directly above the signal attachment located closest to the tip of the horizontal mast-arm. The results of full-scale tests indicated that the damping plate provided enough positive aerodynamic damping to mitigate effectively galloping-induced vibrations. Smaller damping plates did not effectively mitigate the vibrations. In addition, damping plates mounted at locations other than directly above the outermost signal were also not effective at mitigating the galloping-induced vibrations. This promising mitigation technique and others should be further tested so that they may be approved as an alternative to design to resist galloping.

1.2.2 Vortex Shedding

1.2.2.1 General - Vortex shedding, like galloping, typically develops during steady, uniform flows and produces resonant oscillations in a plane normal to the direction of flow. Unlike galloping, which results from a periodic variation in the angle of attack of the wind flow, vortex shedding is caused by the shedding of vortices in a regular, alternating pattern in the wake of a structural element. The phenomenon has been observed in a wide range of structures, including chimneys, hyperbolic cooling towers, antenna masts, and pipelines.

When a structural element is exposed to a steady, uniform flow, vortices are shed in the wake behind the element in an alternating pattern called a von Karman vortex street (Figure 1.1). The frequency at which vortices are shed from the element, f_s , is given by the Strouhal relation:

$$f_s = \frac{SV}{D} \quad (1.2)$$

where S is the Strouhal number, D is the across-wind dimension of the element, and V is the free-stream wind velocity. As is indicated by Equation 1.2, the frequency at which vortices are shed depends on the velocity of the flow, the across-wind dimension of the element, and the shape of the element (as defined by the magnitude of the Strouhal number). Table 1.1 summarizes the magnitude of the Strouhal number for typical cantilevered support structure attachments and structural members obtained from References 9, 13, and 16.

When the frequency of vortex shedding, as predicted by the Strouhal relation, does not match one of the natural frequencies of the structure, the shedding of vortices in the wake of a structure will elicit only a nominal periodic response. However, when the frequency of vortex shedding approaches one of the natural frequencies of a flexible, lightly damped structure, significant displacement ranges and stress ranges can result. The across-wind resonant vibration has a strong organizing effect on the pattern with which vortices are shed. The result is an increase in vortex strength, an increase in the spanwise correlation of the vortex shedding forces, and a tendency for the vortex shedding frequency to become coupled to the natural frequency of the structure. This phenomenon is called "lock-in" (see Figure 1.2). The critical wind velocity, V_{cr} , at which lock-in occurs is given by the Strouhal relation:

$$V_{cr} = \frac{f_n D}{S} \quad (1.3)$$

where f_n is the natural frequency of the structure. The result is a condition of resonant vibration that persists over a range of wind velocities.

The amplitudes of vibration associated with the lock-in phenomenon are generally limited by the ability of vortices to be shed from the structure symmetrically. Large amplitudes of vibration tend to interfere with the symmetric pattern of vortex formation. Previous research indicates that the maximum amplitudes of displacements associated with the lock-in phenomenon rarely exceed approximately 1 to 1.5 times the across-wind dimension of the structural element from which vortices are shed [6, 8].

1.2.2.2 Evaluation of the Susceptibility to Vortex Shedding -That uniform steady-state flow is required for vortex shedding can be used to bound the velocities under which various elements of cantilevered support structures could possibly be susceptible to vortex-induced vibrations. Previous research indicates that the level of turbulence associated with wind velocities above approximately 15 to

20 m/s (35 to 45 mph) limits the symmetric formation of periodic vortices [8]. Also, vortex formation at wind velocities below approximately 5 m/s (10 mph) generates forces with magnitudes insufficient to excite most structures. Based upon this knowledge, structures may be susceptible to vortex-induced vibrations in the range of wind velocities between approximately 5 and 15 m/s (10 to 35 mph).

The range of wind velocities for which vortex-induced vibrations can be expected to occur provides a convenient criterion by which to evaluate the potential susceptibility of cantilevered sign, signal, and luminaire support structures to this wind-loading phenomenon. The following paragraphs provide a brief discussion of the critical wind velocities for which lock-in could possibly occur for the range of member and attachment dimensions typically used in cantilevered support structures. A comparison of these critical wind velocities with the range of wind velocities for which vortex-induced vibrations can be expected to occur suggests that the susceptibility of cantilevered support structures to vortex shedding lock-in is generally quite limited.

Figure 1.3 depicts the wind velocities required to initiate vortex-induced vibrations due to the shedding of vortices from circular supports of cantilevered support structures in the supercritical flow regime. For a given member diameter, wind velocities greater than the curved line will initiate vortex shedding. The subcritical and supercritical flow regimes are defined by the Reynolds number. For a detailed explanation of this relationship see Reference 2. Figure 1.3 indicates that the wind velocities required to initiate vortex shedding in the supercritical flow regime are well above the maximum velocity for which uniform, steady-state flows are typically maintained (i.e. 20 m/s or 45 mph). As a result, only the subcritical flow regime need be considered when evaluating the susceptibility of cantilevered support structures to vortex-induced vibration caused by the shedding of vortices from the supports.

Figure 1.4 depicts the critical wind velocities required to initiate lock-in due to the shedding of vortices from circular supports of cantilevered support structures in the subcritical flow regime. The results are based upon the Strouhal relation in Equation 1.3, where f_n is assumed to be 1 Hz and the Strouhal number is 0.18. Again, the diameters selected are representative of the range of diameters typically used in cantilevered signal, sign, and luminaire support structures. Figure 1.4 indicates that the wind velocities for which vortices will be shed from the circular supports of cantilevered support structures fall below the minimum wind velocity of 5 m/s (10 mph) required to initiate vibration in most structures. Thus, cantilevered support structures are not expected to be susceptible to vortex-induced vibrations due to the shedding of vortices from the supports.

The contention that cantilevered signal, sign, and luminaire support structures are generally not susceptible to significant vibrations due to the shedding of vortices from the supports was supported by a series of water table and tow tank experiments conducted by McDonald et al. [13] at Texas Tech University. The experiments simulated wind velocities of 4.5 m/s (10 mph) (about the minimum velocity for initiation of vortex shedding) and 9 m/s (20 mph). Table 1.2 shows the frequencies of the vortex shedding from experiments on two sections. The frequencies at which vortices were shed from the circular and octagonal support sections at the two flow velocities considered were well above the natural frequency of approximately 1 Hz possessed by a majority of cantilevered support structures.

Tapered circular support members will be even less susceptible to vortex-induced vibrations. Coherent vortex shedding can only occur over some fraction of the member's length as a result of the variation in diameter along the length. Therefore, insufficient energy will be available to generate large-amplitude oscillations of the structure.

The Strouhal relation in Equation 1.3 was also used to predict the critical wind velocities at the onset of lock-in of vortex shedding from signal attachments. The results depicted in Figure 1.5 were calculated using a natural frequency equal to 1 Hz and a Strouhal number equal to 0.20. Examination of these critical wind velocities indicates that vortex-induced vibrations would be expected for signal depths greater than approximately 1000 mm (39 in). Thus, horizontally mounted signal attachments (i.e. mounted with the directional lights oriented parallel to the horizontal mast-arm), with typical depths ranging from approximately 300 mm to 500 mm (12 to 20 in), would not be expected to experience vortex-induced vibrations. Vertically mounted signal attachments (i.e. mounted with the directional lights oriented perpendicular to the horizontal mast-arm), however, with depths ranging from approximately 900 mm to 1300 mm (35 to 51 in), could be susceptible to vortex-induced vibrations.

Note that having a critical velocity in the range 5 to 15 m/s (10 to 35 mph) is a necessary but not sufficient condition for vortex shedding lock-in. Many other factors can interfere with coherent vortex shedding. In fact, full-scale flow-visualization tests conducted in a tow tank by McDonald et al. indicated that the three-dimensional characteristics of signal attachments interfered with the formation of a regular pattern of vortices at a well-defined frequency. The frequency at which vortices were shed was observed to be highly random. In addition, the vortices shed in the wake of the attachments were disorganized. As a result, it was concluded that cantilevered signal support structures were unlikely to experience significant amplitudes of across-wind oscillation due to the shedding of vortices from the signal attachments. Thus, even though the calculated critical flow velocities for a majority of signal attachments fall in the range for which vortex shedding would be expected, the occurrence of significant amplitudes of vibration are unlikely due to the incoherent, random characteristics of the vortex street in the wake of a signal attachment.

Critical wind velocities for which lock-in is possible for sign attachments are shown in Figure 1.6. The results in Figure 1.6 correspond to a natural frequency equal to 1 Hz and a Strouhal number equal to 0.14. Examination of these critical wind velocities indicates that vortex-induced vibrations could be possible for sign depths ranging from approximately 800 mm to 2800 mm (31 to 109 in). Tests conducted at the Wright Brothers wind-tunnel facility at MIT (which are described in detail in Section 2.1) show that galloping is the dominant driving force for wind-induced vibration. However, it is possible that vortex shedding may play a role in the initiation of the galloping.

In summary, it is concluded that

- Only those support structures with very large member dimensions, e.g. diameter greater than 900 mm (35 in), will potentially be susceptible to vortex-induced vibrations because of the

shedding of vortices from the support members. Tapered sections are far less susceptible than prismatic sections.

- Galloping, rather than vortex shedding, is the most probable cause of excessive wind-induced vibration of signal and sign support structures.

1.2.2.3 Mitigation of Vortex-Induced Vibrations - Effects of vortex shedding can be mitigated by either altering the dynamic properties of the structure (i.e. mass, stiffness, and/or damping), or altering the aerodynamic characteristics of the structure.

Significant amplitudes of vibration associated with vortex shedding can be avoided by ensuring that the critical wind velocity associated with lock-in falls outside the range of wind velocities for which vortex shedding would be expected (i.e. 5 to 15 m/s or 10 to 35 mph). This can be achieved by either increasing or decreasing the natural frequency of the structure (through variations in the mass and stiffness). Of course, decreasing the natural frequency such that the critical wind velocity is less than the lower limit for vortex shedding (i.e. 5 m/s or 10 mph) is generally not feasible for a majority of cantilevered support structures. Existing cantilevered support structures are already quite flexible and additional reductions in stiffness may increase the susceptibility for galloping-induced oscillations. Increasing the natural frequency, however, could readily be achieved through increased member dimensions such that the critical wind velocity falls above the upper-bound velocity for which uniform, steady-state flows are typically maintained (i.e. 15 m/s or 35 mph). The increased levels of stiffness associated with increases in natural frequency would also be beneficial in limiting the susceptibility of cantilevered support structures to the galloping phenomenon.

The dynamic properties of cantilevered support structures can also be altered through the use of external damping devices such as tuned-mass and impact dampers. As was discussed in Section 1.2.1.3, however, the results of research conducted by McDonald et al. indicated that (1) the use of tuned-mass dampers in cantilevered support structures was impractical and (2) a liquid-tuned damper was ineffective in mitigating galloping-induced vibrations. Also, previous experience [14] obtained with the use of impact dampers to reduce cantilevered support structure vibrations indicates that such damping devices are not effective for structures with natural frequencies of vibration below approximately 1 Hz.

Vortex-induced vibrations can also be affected by altering the aerodynamic characteristics of the element from which vortices are shed. Vibrations may be minimized by altering the cross-section of the element such that the formation of a coherent pattern of vortices at one well-defined frequency is prevented. With respect to the shedding of vortices from members with circular cross-sections, helical strakes, shrouds, and rectangular plates installed at intervals along the members have proven to be an effective method by which to mitigate vibrations in structures such as stacks and chimneys [6, 15]. Although the use of such devices has proven effective in a variety of structures, their effectiveness for preventing vortex-induced vibrations in cantilevered support structures has been questioned by Edwards et al. [16]. Results of wind-tunnel tests conducted by Edwards suggest that the installation of strakes to

the support members of cantilevered support structures does not significantly reduce the response of these structures to vortex shedding.

In summary, there is significant uncertainty about the effectiveness of various vibration mitigation devices. Further testing is recommended before these devices are approved as an alternative to designing the structures to resist vortex-induced vibration.

1.2.3 Natural Wind Gusts

1.2.3.1 General - Natural wind gusts arise from the inherent variability in the velocity and direction of air flow. Natural wind gusts are characterized by a spectrum of fluctuating velocity components which oscillate over a broad range of frequencies as a result of turbulence inherently present in any natural air flow. These fluctuations in flow velocity induce fluctuating pressures on the various structural components of a wind-loaded structure which may then induce vibration in that structure. As expected for structures with very low damping, the structural response to natural wind gusts is dominated by the response at the resonant frequency. However, unlike the almost constant-amplitude harmonic response due to galloping or vortex shedding, the amplitude of the response to natural wind gusts is variable and randomly distributed. The magnitudes of the variable stress ranges induced in the connection details of a structure may, in some cases, be such that fatigue cracking is possible due to the long-term cumulative effect of these natural wind gusts.

For ultimate strength design, the most common approach for estimating the maximum pressure (load) imposed on a structure by a gust is through the use of a gust factor. A gust factor is defined as the ratio of the expected peak displacement (load) during a specified period to the mean displacement (load). The value of a gust factor is a function of several parameters, some of which include the roughness of the surrounding terrain, the height of the structure, and the geometry of the structure. This factor can then be employed to determine the design wind pressure. This design pressure represents the maximum expected equivalent static wind pressure which produces the same response a structure would be subjected to under a maximum expected dynamic wind loading.

Research conducted on the characteristics of the variations in velocity fluctuations associated with gusts indicates that the intensity of turbulence of wind is typically between 5 and 25 percent [7]. The intensity of turbulence is defined as the ratio of the root mean square (rms) of the wind velocity fluctuation to the mean wind velocity. The AASHTO Specifications conservatively imply the use of a 30 percent (through the use of a factor of 1.3) intensity of turbulence in the design of sign, signal, and luminaire support structures. Since the pressure imposed upon a structure by wind is proportional to the square of the velocity (as is exhibited in the dynamic pressure equation), the actual gust factor indicated in the Specifications for use in ultimate strength design is equal to the square of 1.3, or 1.69. This factor has been used by the Specifications without modification since approximately 1959.

All available evidence indicates that cantilevered support structures perform satisfactorily under extreme wind conditions. No reported failures have been directly attributed to the exceedence of the

ultimate strength of cantilevered support structures due to extreme gust loading conditions. As a result, the gust factor of 1.3 seems adequate for the ultimate strength design of cantilevered support structures.

Although convenient for use in an ultimate strength design to estimate the maximum expected pressures associated with natural wind gusts, gust factors cannot be implemented in a fatigue design due to the fact that such a design is based on the loads imposed upon a structure at the service level.

1.2.3.2 Evaluation of the Susceptibility to Natural Wind Gusts - All outdoor structures with significant cross-sectional area are susceptible to natural wind gusts. Typically, the damping is high enough such that vibration from the natural wind gusts and associated dynamic amplification is not a problem. Therefore, the significance of natural wind gusts is primarily that the gusts increase the design ultimate wind load. However, the damping in cantilevered support structures is so low that the dynamic response to the gust loading is significant and could possibly result in excessive displacement and/or fatigue cracking.

1.2.3.3 Mitigation of Natural Wind Gust Vibrations - The effects of natural wind gusts can be mitigated by altering the damping of the structure to lower the dynamic amplification factor. As discussed above, external damping devices such as tuned-mass and impact dampers have been proposed to reduce the effects of galloping and vortex shedding; and mixed results have been obtained.

Unlike the aeroelastic phenomena (galloping or vortex shedding), the natural-wind-gust loading is essentially aerodynamic, meaning there is negligible structural interaction with the loading. Therefore, although stiffening the structure reduces the stresses for a given loading, stiffening the structure or adding mass does not reduce the loading effect as it does for aeroelastic phenomena. Also, changing the natural frequency through changes in mass and/or stiffness does not reduce the load effect significantly because the wind velocity and pressure spectra have significant excitation over a broad range of frequencies. Since uniform flow is not required for the gust loading, as opposed to vortex shedding, there is no lower limiting velocity for the natural wind loading. Similarly, there is no upper bound wind velocity.

1.2.4 Truck-Induced Wind Gusts

1.2.4.1 General - The passage of trucks beneath cantilevered support structures tends to induce gust loads on the frontal area and the underside of the members and the attachments mounted on the mast arms of these structures. The effects of these loads are most significant in cantilevered sign-support structures due to the relatively large frontal areas of signs which are exposed to these gusts. The horizontal gust load exerts torsional and bending moments in the column supports of these structures. The torsional moment is, of course, a function of the frontal area of the sign and the length of the horizontal support arm. The bending moment (about an axis parallel to the horizontal support) is a function of the frontal area of the sign and the height of the structure. As explained in Section 2.2, the magnitude of natural wind gust pressure is much larger than the pressures from truck-induced loading (in the horizontal

direction). Therefore, for the purposes of fatigue design, truck-induced wind loads normal to the sign are not critical.

However, in addition to the horizontal loads exerted on these support structures, truck-induced gusts also generate vertical loads on the underside of the members and attachments which induce bending moments about an axis parallel to the direction of traffic. These bending moments are a function of the exposed areas (projected on a horizontal plane). The area increases with the depth of the sign, walkways, or lighting fixtures, in a direction parallel to the direction of traffic flow, and with the length of the horizontal support arm. The relatively new electronic variable message signs (VMS), which are being installed on cantilevered sign support structures, are particularly susceptible. These signs have a relatively large depth (up to approximately 0.6 m or 2 ft) in the direction parallel to traffic flow. In some cases, vertical truck-induced wind gusts may create larger bending moments than those due to galloping; therefore, these vertical loads are important to consider for fatigue.

1.2.4.2 Evaluation of the Susceptibility to Truck-Induced Gusts - A study by Creamer, Frank, and Klingner [17] has been the most extensive program performed to date on the subject of truck-induced gust loads. The major objectives of this research program included the determination of the overall sign response characteristics and member forces associated with vehicle-induced gust loads through field testing of three cantilevered sign support structures, identification of the parameters affecting these characteristics, development of a forcing function to simulate the observed field responses, and application of that forcing function in an analytical study to evaluate the dynamic response of a variety of sign configurations. Results of the experimental study resulted in the development of a static loading function which simulates the member forces observed in the field. This loading function is represented by a horizontal triangular pressure distribution applied to the face of the sign panel with a peak pressure of 60 Pa (1.25 psf) and a vertical uniform pressure distribution of 60 Pa (1.25 psf) applied to any walkways or lighting fixtures. The development of this forcing function was based upon the maximum loading event observed in the field and corresponds to a gust velocity of approximately 8.5 m/s (19 mph).

This forcing function was then implemented in an analytical study to determine the full range of response characteristics exhibited by a variety of sign support structures. Results of this analytical study indicate that the forces induced in sign support structures due to truck-induced gust loads are below levels necessary to cause fatigue damage. Stress ranges at critical member connections in all of the structures included in this study were found to fall below approximately 14 MPa (2 ksi). Additionally, anchor bolt stress ranges were below the constant-amplitude fatigue limit.

In addition to the above research program, several other studies have been conducted to determine the loads induced in conventional sign support structures resulting from truck-induced wind gusts. Although these other studies are more limited in scope, they support the conclusions drawn by Creamer. For example, field testing of one support structure conducted by the University of North Carolina determined that the maximum pressure induced on the face of the sign was equal to 67.5 Pa (1.41 psf) [16]. Another field study conducted by the Michigan Department of Transportation determined that the

maximum axial stress range, induced in the anchor bolts of a cantilevered sign support structure, is equal to just over 21 MPa (3 ksi) [19]. This axial stress range was observed during the simultaneous passage of two trucks beneath the structure.

However, recently reported failures of cantilevered variable message sign (VMS) structures in Virginia [20] and California [21] have suggested that truck-induced gust loads are a potential source of vibration in structures with relatively large horizontally projected areas (i.e. 300 to 600 mm or 1 to 2 ft). It has been reported that state DoT engineers observed vertical vibrations in the mast arms of these structures with the passage of vehicles under the sign. It has been suggested that the wind deflectors, which are now commonly placed on the cab of tractor-trailers to improve fuel economy, act as a wedge and produce vertical wind gust pressures larger than those estimated in previous research [20]. Desantis reasoned that the velocity of these wind gusts can be assumed to be at least equal to the speed of the vehicle. However, a vehicle travelling into strong head winds can produce even higher magnitude vertical gusts.

1.2.4.3 Mitigation of Truck-Induced Gust Vibrations - Unlike the aeroelastic wind loading phenomena discussed earlier (i.e. galloping and vortex shedding lock-in), there are not many options to effectively mitigate oscillations of horizontal mast arms due to truck-induced gust loads. It would seem possible, however, to reduce the magnitude of vertical truck gust pressures on the bottom of the sign by increasing the vertical clearance of the sign panel above the tops of trucks. This option may be limited by roadway geometric constraints and sight distance requirements. Additionally, the use of perforated panels and open grating can be used to reduce the effective horizontally projected area.

Geometry	Flow Regime	Strouhal Number
Circular Cylinder	Subcritical	0.18
	Critical	NA
	Supercritical	0.25
Sign	NA	0.14
Signal	NA	0.13 - 0.28

NA = not applicable

Table 1.1 - Strouhal Number for Circular Supports, Sign Attachments, and Signal Attachments.

Configuration	Vortex Shedding Frequency (Hz) for Wind of	
	4.5 m/s	9.0 m/s
Octagonal Cylinder	3.8	7.7
Circular Cylinder	4.5	8.9

Table 1.2 - Selected Water Table Test Results Obtained by McDonald et al. [13].



Figure 1.1 - Schematic of a von Karman Vortex Street in the Wake of a Circular Cylinder.

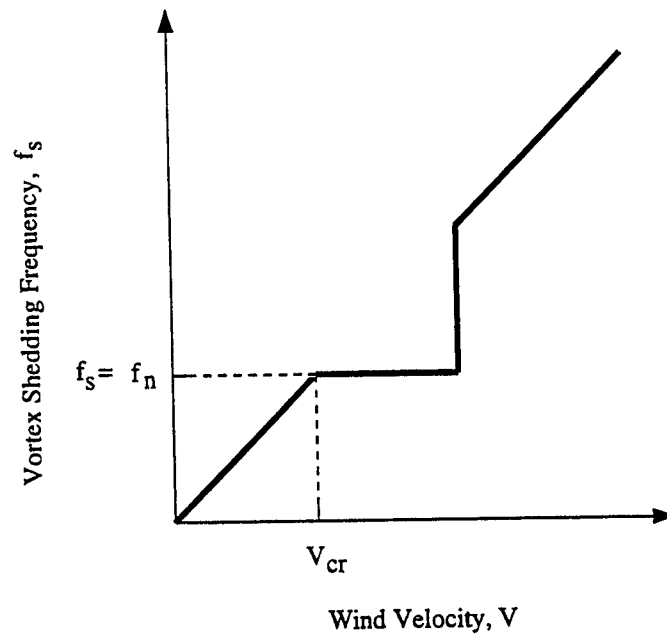


Figure 1.2 - Schematic of Vortex Shedding Lock-In.

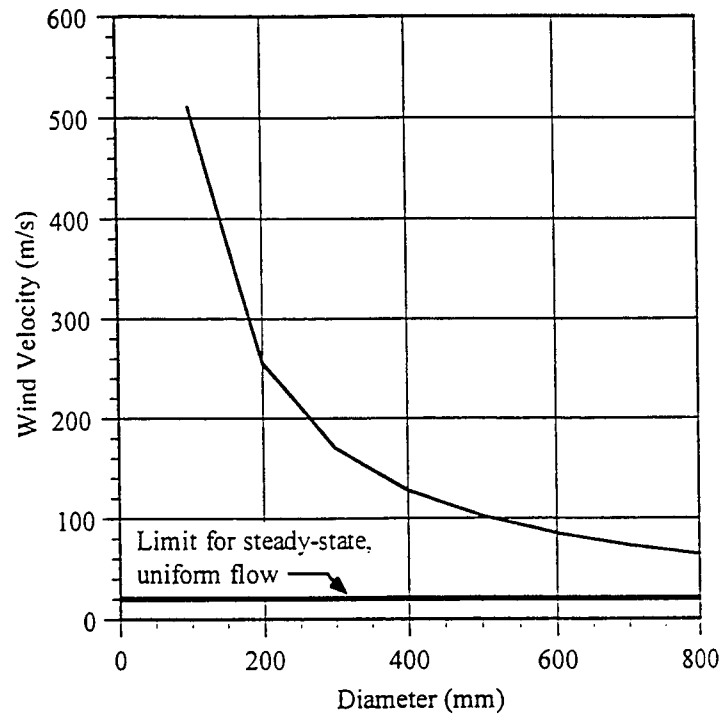


Figure 1.3 - Wind Velocities Required to Enter Supercritical Flow Regime for Flow Around a Circular Support.
(Velocities above curved line /will initiate vortex shedding.)

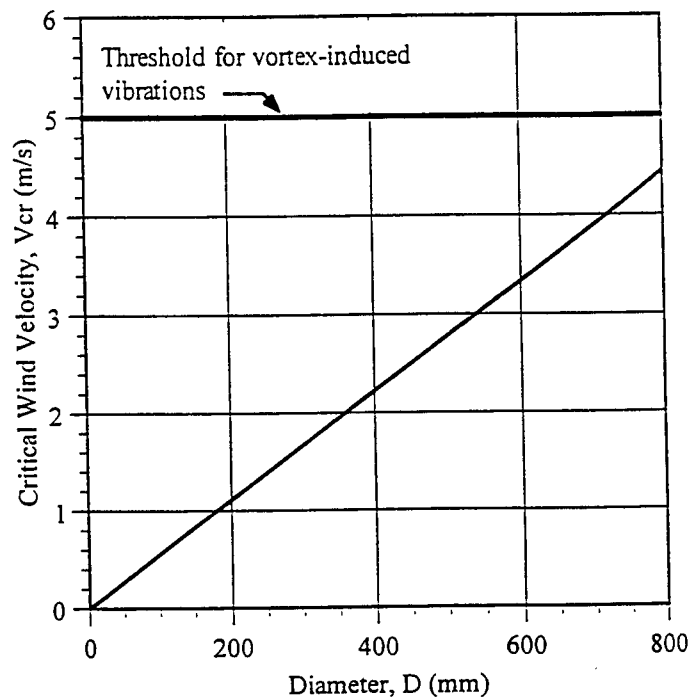


Figure 1.4 - Critical Wind Velocities Required For Vortex Shedding Lock-In For Circular Supports.

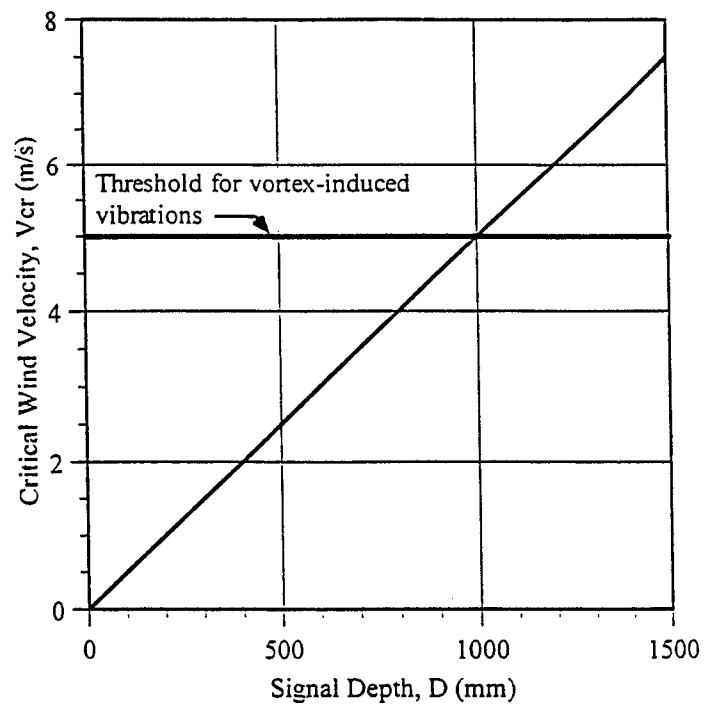


Figure 1.5 - Critical Wind Velocities Required For Vortex Shedding Lock-In For Signal Attachments.

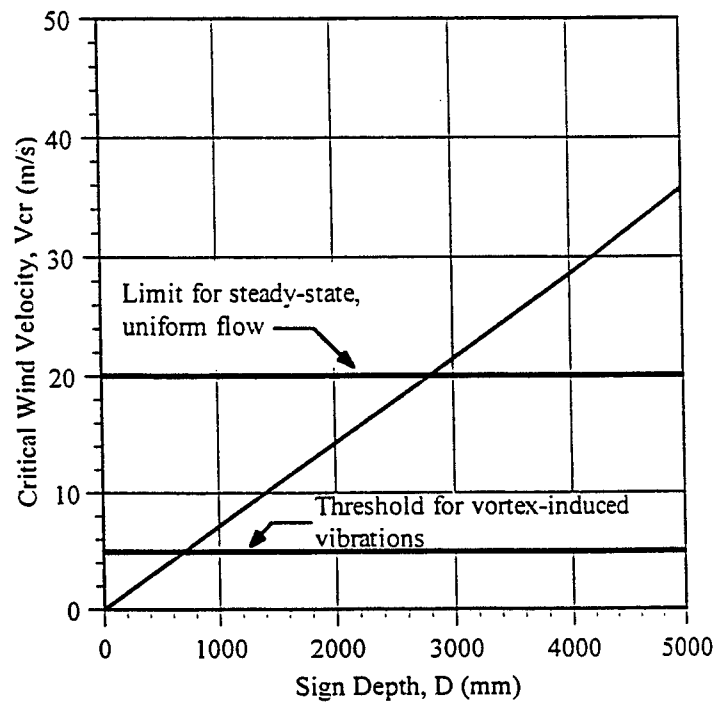


Figure 1.6 - Critical Wind Velocities Required For Vortex Shedding Lock-In For Sign Attachments.

1.3 VARIABLE AMPLITUDE FATIGUE

The AASHTO and AWS S-N curves for fatigue design are based on constant-amplitude-loading tests with relatively short lives, typically less than two million cycles. The S-N curves are used to predict the fatigue lives of structures subjected to numbers of cycles which are orders of magnitude greater than two million, but smaller and variable in amplitude. Miners's rule for linear damage accumulation is an accepted means of predicting fatigue lives for variable-amplitude loading. If the slope of the S-N curve is equal to 3, then the relative damage of stress ranges is proportional to the cube of the stress range. An "effective" constant-amplitude stress range, which would cause an equivalent amount of fatigue damage for the given number of cycles of variable-amplitude loading, is defined. Miner's rule implies that the effective stress range is equal to the cube root of the mean cube of the stress ranges, i.e.:

$$S_{effective} = \left[\left(\frac{n_i}{N_{total}} \right) \times S_i^3 \right]^{\frac{1}{3}} \quad (1.4)$$

The Guide Specifications for Fatigue Design of Steel Bridges [22] uses this effective stress range (root-mean-cube or RMC) that results from Miner's rule.

Constant-amplitude fatigue test results exhibit a constant-amplitude fatigue limit (CAFL). The CAFL is a stress range below which the fatigue life appears to be infinite. Infinite life is only a theoretical possibility, practically the term implies a fatigue life greater than the typical service life of the structure, usually 25 years in the case of cantilever signal, sign, and luminaire support structures. Infinite life only occurs for constant-amplitude testing or for variable-amplitude testing where practically all of the applied stress ranges are below the CAFL. When occasional large load cycles, which exceed the fatigue limit, are mixed with cycles that are below the fatigue limit, the lower bound to the test data appears to continue to follow the extrapolation of the S-N curve below the CAFL [23]. In order to perform a cumulative damage calculation to predict a finite fatigue life, the numbers of cycles of stress ranges in certain intervals of magnitude are required, i.e. the complete histogram of the loading for all future events. In view of the uncertainty involved in wind loading of cantilevered support structures, the development of a sufficiently accurate histogram of the lifetime history of the stress ranges is practically impossible.

However, in most cases, the number of wind load cycles expected in the 25-year or greater lifetime of a support structure is expected to exceed 100 million, which is much greater than the number of cycles at the CAFL. For example, the CAFL for Category E and E' support structure welded details occurs at ten to twenty million cycles. In these cases, an "infinite-life" fatigue design approach may be used.

The infinite-life approach was developed in a recent NCHRP study [23], where full-scale, long-life, variable-amplitude tests on severe details with varying percentages of the stress ranges exceeding the CAFL were performed. It was observed that failure could still occur if 0.05 percent or more of the stress ranges exceeded the CAFL and that infinite life resulted when 0.01 percent or fewer of the cycles exceeded the CAFL.

The infinite-life variable-amplitude fatigue design approach recommended in NCHRP Report 354 is described below. The response of the structure (including any dynamic amplification) which has a probability of exceedence of only 0.01 percent must be estimated. Typically, equivalent static load ranges are given which will produce a static response similar to this dynamic response. These static load ranges are referred to as the "fatigue limit-state" load ranges. Stress ranges are determined at critical details using the fatigue limit-state load ranges. These stress ranges must be less than the CAFL of each detail.

For the infinite-life fatigue design approach, the only important characteristic of the distribution of wind loads is the fatigue limit-state wind load. Note that the fatigue limit-state wind load is not at all related to the maximum wind load which is used for strength design in Section 2 of the existing AASHTO Specifications for structural supports. The maximum wind load is typically governed by extreme storms rather than these galloping, vortex shedding, natural gust, and truck-induced gust loads. It is believed that the design loads for ultimate strength are adequate.

Aside from the maximum load and the fatigue limit-state wind load range, the rest of the loading spectrum does not matter when using this approach. Also, the actual number of cycles is not required. The infinite-life approach is considerably simpler than trying to account for the cumulative damage of a distribution of future wind loads.

The simplicity of the infinite-life approach narrowed the objectives of the wind-load investigation described in Chapter Two. When the infinite-life approach is used for fatigue design, only an estimate of the 0.01 percent exceedence (fatigue limit-state) load range is required. The upper bound of the limited number of observed load ranges during wind-loading events was used; load ranges larger than those observed are surely possible. The design loads must not be excessively conservative and lead to overdesigned and costly cantilevered support structures. It is recognized that this is an imprecise estimate of the limit-state load range, but it is thought to be sufficiently accurate to ensure fatigue lives longer than 25 years.

1.4 RESEARCH OBJECTIVES AND APPROACH

A comprehensive research program was undertaken to develop guidelines for preventing excessive vibration and fatigue of cantilevered sign, signal, and luminaire support structures. The specific objectives of the research were as follows:

- Identify and characterize the susceptibility of cantilevered support structures to excessive displacement and/or fatigue damage due to galloping, vortex shedding, natural wind gusts, and truck-induced wind gusts.
- Develop equivalent static load-range models which reasonably represent the magnitude of the dynamic response of cantilevered support structures subjected to galloping, vortex shedding, natural wind gusts, and truck-induced wind gusts.

- Identify fatigue-sensitive cantilevered support structure connection details and categorize those details according to the AASHTO [1] and/or AWS [24] fatigue design curves.
- Determine the relationship between support structure forces and anchor bolt stresses.
- Determine the fatigue strength of axially loaded, snug and fully tightened anchor bolts.

The approach to this research was as follows:

- A literature review and survey of state departments of transportation were performed to determine the nature and extent of fatigue damage in cantilevered support structures and to identify the conditions under which cantilevered support structures have been observed to oscillate in the field. These tasks resulted in the identification of galloping, vortex shedding, natural wind gusts, and truck-induced gusts as the most critical fatigue-loading mechanisms.
- Aerodynamic wind tunnel tests were performed to evaluate the susceptibility of cantilevered support structures to galloping phenomenon. Aeroelastic wind tunnel tests were performed to investigate the characteristics of the dynamic response of cantilevered support structures subjected to galloping- and vortex-induced vibrations. Data obtained from the aeroelastic tests (lift moment amplitudes at the base of the vertical support) were used to estimate the magnitude of the across-wind pressure fluctuations associated with galloping and vortex shedding.
- Dynamic finite-element analyses of the wind-tunnel test models and the full-scale prototype structures represented by the models were used to verify scaling laws and determine the applied dynamic load ranges associated with galloping and vortex shedding. Then, full-scale cantilevered support structures observed galloping in the field were modeled to determine the amplitude of the across-wind load ranges on the sign and signal attachments which correspond to the observed displacement amplitudes. The upper bound of the applied loads was used to develop an equivalent static limit-state load range to be used in the fatigue design of cantilevered support structures subject to galloping.
- Dynamic finite-element analyses were conducted for a range of cantilevered support structures subjected to upper-bound spectral loading representative of natural wind gusts and transient loading representative of truck-induced wind gusts. The load models for both types of gust loading were obtained from the literature. Calculated stress ranges and displacement ranges were compared with those observed for cantilevered support structures subjected to gust loading, including some with fatigue failures. These results were relatively consistent and, therefore, the load models from the literature were used to develop equivalent static limit-state load ranges to represent natural and truck-induced gust loads.

- Static tests were conducted on a full-scale, eight-bolt anchor bolt group to determine the relationship between support structure forces and anchor bolt stresses. The effects of bolt misalignment, exposed length, and nut looseness were evaluated.
- Full-scale fatigue tests were performed to determine lower-bound estimates of the fatigue strength of axially loaded, snug and fully tightened anchor bolts in the regimes of finite and infinite life.
- Fatigue-sensitive cantilevered support structure connection details were identified through a review of state department of transportation standard drawings for cantilevered support structures. Existing knowledge of the fatigue of weldments was used to categorize the fatigue strengths of these details according to the AASHTO and/or AWS fatigue design curves.

1.5 ORGANIZATION OF THE REPORT

Chapter Two is a detailed presentation of the research findings. Included in this chapter is (1) a summary of the wind-tunnel experiments; (2) results of dynamic finite-element analyses used to determine equivalent static limit-state load ranges for galloping, vortex shedding, natural wind gusts and truck-induced gusts; (3) findings from anchor bolt fatigue tests and full-scale tests to determine the relationship between support structure forces and anchor bolt stresses; and (4) a fatigue categorization of typical support structure connection details.

In addition to providing a review of existing specifications currently used for the design of cantilevered support structures, Chapter Three synthesizes the results of this research into a series of design guidelines for vibration and fatigue. Design examples and a discussion concerning the impact of these proposed guidelines is also presented.

Chapter Four presents generalized conclusions from the research and outlines several recommendations for future research.

Chapter Two

FINDINGS

Chapter Two presents the specific findings of research conducted to determine the dynamic wind loading and fatigue resistance of cantilevered sign, sign and luminaire support structures. The chapter is organized into five sections. Section 2.1 summarizes the results of aerodynamic and aeroelastic wind tunnel experiments. Section 2.2 presents results of analyses conducted to determine "equivalent" static load ranges which approximate the dynamic load ranges to which cantilevered support structures are subjected during galloping, vortex shedding, natural wind gusts, and truck-induced gusts. The results of tests to determine the constant-amplitude fatigue limit (CAFL) of axially loaded anchor bolts are presented in Section 2.3 and the results of static tests to determine the relationship between support structure forces and anchor bolt stresses are presented in Section 2.4. Finally, Section 2.5 presents a fatigue categorization of typical cantilevered sign, signal, and luminaire support structure connection details.

2.1 WIND-TUNNEL TESTS

This section summarizes the results of wind-tunnel tests which were performed to evaluate galloping and vortex shedding on scale-models of cantilevered support structures. The wind-tunnel tests were conducted in two phases. The first phase consisted of a series of aerodynamic tests (i.e. not including the effects of structural interaction) to determine the relative susceptibility of various cantilevered support structure attachments (i.e. signs and signals) to the galloping phenomenon. The susceptibility for galloping was evaluated by applying the Den Hartog stability criterion (see Section 1.2.1) to the measured aerodynamic lift and drag forces exerted on each of the test specimens under steady-state flow conditions. The second, and most important, phase consisted of a series of aeroelastic tests (i.e. including the effects of structural interaction) to study the dynamic behavior of cantilevered sign and signal support structures subjected to galloping- and vortex-induced vibrations.

Wind-tunnel tests were conducted at the Wright Brothers Memorial Wind Tunnel at the Massachusetts Institute of Technology (MIT) [25]. The wind tunnel at the MIT facility is a closed, single return test system capable of wind velocities up to 76 m/s (170 mph). The elliptical test area measures 2290 mm high x 3050 mm wide x 4570 mm long (90 in x 120 in x 180 in).

As is the case with most wind-tunnel tests, the limited size of the test area at the MIT facility required that testing be conducted on scale models. Selection of a model scale was based primarily upon the level of wind tunnel blockage below which two-dimensional flow conditions could be maintained (i.e. three percent blockage). For the prototype dimensions of the cantilevered support structures considered in the aeroelastic test program, a three percent blockage required that the aeroelastic model specimens be fabricated to one-eighth scale. In order to maintain consistency between the aeroelastic and aerodynamic test programs, the aerodynamic test models were also fabricated to one-eighth scale. However, tests on

one of the aerodynamic test specimens were duplicated using a specimen fabricated to one-half scale in order to investigate possible scale effects. Tests on the one-half scale aerodynamic specimen verified that scale effects were not excessive, and therefore the one-eighth scale aerodynamic and aeroelastic test results are expected to be representative of the behavior exhibited by full-scale cantilevered support structures.

2.1.1 Aerodynamic Test Program

As was discussed in Chapter One, a structure is potentially susceptible to galloping-induced oscillations when a periodically varying angle of attack of the wind flow produces aerodynamic forces which are aligned with the across-wind motion of the structure. The alignment of these forces with the across-wind motion of the structure generates negative aerodynamic damping. If the total damping possessed by the structure (mechanical damping plus aerodynamic damping) is less than zero, the structure becomes unstable and large-amplitude, across-wind galloping oscillations occur. Thus, one of the primary factors (besides the level of mechanical damping) which drives the galloping phenomenon consists of the aerodynamic characteristics of the structure (i.e. the relation between the aerodynamic lift and drag forces under varying angles of attack of the wind flow). These aerodynamic forces can be measured in the wind tunnel under static conditions to evaluate the potential susceptibility for galloping-induced oscillations.

For example, recent research conducted by McDonald et al. [13] has established that cantilevered signal support structures possess aerodynamic characteristics which make these structures susceptible to galloping. This research indicates that the galloping-induced vibrations observed in cantilevered signal support structures in the field are generated by the aerodynamic lift and drag forces exerted on the attachments (i.e. signals). The scope of this previous work, however, was limited to horizontally mounted signal attachments (i.e. signals which are mounted parallel to the horizontal mast arm) and also did not consider the possibility of galloping-induced oscillations in cantilevered sign support structures.

The aerodynamic test program reported herein was conducted to evaluate the aerodynamic characteristics of various cantilevered support structure attachments (which were not considered within the scope of previous research programs) to determine their susceptibility to the galloping phenomenon. Specifically, tests were conducted on two types of attachments: (1) a vertically mounted signal (i.e. mounted perpendicular to the horizontal mast arm) configured with and without a backplate, and (2) a sign. The primary objective of these tests was to qualitatively evaluate the relative susceptibility of each of the attachments to the galloping phenomenon with respect to attachment geometry and flow direction. Since the aeroelastic tests described below (Section 2.1.2) are the most important tests for measuring galloping induced loads, these aerodynamic tests will only be briefly discussed. For a detailed description of the aerodynamic test set-up, experimental procedure and test results, the reader is referred to Reference 5.

Results of the aerodynamic test program indicate that cantilevered sign and signal support structures are potentially susceptible to large-amplitude, across-wind vibrations resulting from the galloping phenomenon. Specifically, this susceptibility arises from the aerodynamic characteristics possessed by the

attachments (i.e. signs and signals) to these structures, which is in agreement with the results of previous research programs [13]. Furthermore, the results of the aerodynamic research program indicate that

- Signal attachments, configured with or without a backplate, are more susceptible to galloping when subjected to flow from the rear,
- Signal attachments are more susceptible to galloping when configured with a backplate, and
- The susceptibility of sign attachments to the galloping phenomenon is independent of aspect ratio (i.e., height to width ratio) and flow direction.

The results of the aerodynamic test program are in agreement with conditions under which galloping-induced oscillations have been observed in cantilevered support structures in the field. For example, a majority of cantilevered signal support structures have been observed to vibrate when the signals are configured with a backplate and the direction of flow is from the rear. Inspection of the lift coefficient data obtained from the aerodynamic tests indicates that signal attachments are most susceptible to galloping under these conditions, i.e. the slope of the lift coefficient with respect to angle of attack was largest (most positive) for tests in which the signals were configured with a backplate and flow was from the rear. This observation provides a level of confidence that the wind-tunnel tests reasonably simulated the aerodynamic characteristics of full-scale support structures in the field.

2.1.2 Aeroelastic Test Program

2.1.2.1 Objectives - Results of the aerodynamic test program described above indicate that cantilevered support structure attachments (i.e. signs and signals) possess aerodynamic characteristics which are potentially favorable for the occurrence of galloping. The aerodynamic tests, however, provided no information concerning the dynamic behavior of cantilevered support structures subjected to galloping- and vortex-induced vibrations. Therefore, aeroelastic tests were performed to evaluate the magnitude of the support structure forces (in terms of moments at the base of the vertical supports of the test specimens) to which cantilevered support structures are subjected during occurrences of galloping- and vortex-induced vibrations (the magnitudes of the across-wind loads could not be directly measured). Dynamic finite-element analyses (described in Section 2.2 below) were then used to estimate the amplitude of the loads on the attachments which corresponded to the measured base-moment amplitudes.

2.1.2.2 Specimen Details and Test Matrix - A total of five cantilevered-support-structure configurations (two signal supports and three sign supports) were included in the aeroelastic test program. Details of each of the specimens are summarized in Figures 2.1 through 2.5. The specimens are identified as Specimens A through E with the prototype (i.e full-scale) dimensions, from which each of the models were fabricated, shown in boldface. All selected prototype structures were constructed with steel

members. The material, from which each of the model specimens were fabricated (steel or aluminum), is shown in the upper-left corner of each figure. All of the model specimens were fabricated to one-eighth scale.

Details of the two cantilevered signal support structures are shown in Figures 2.1 and 2.2. Specimen A, shown in Figure 2.1, was a one-eighth scale model of a signal support structure known to have experienced galloping-induced vibrations. The prototype structure, from which the model was scaled, was observed to experience vertical-plane, galloping-induced vibrations in the field when flow was from the rear with velocities in the range of 16 m/s (36 mph). Under these flow velocities, the displacement amplitudes at the tip of the horizontal mast arm, were estimated at approximately 305 to 610 mm (12 to 24 in). As shown in Figure 2.1, the prototype structure was composed of uniformly tapered structural elements. Because of difficulties encountered in fabrication, the model specimen was made using non-uniformly tapered structural elements which approximately simulated the mass and stiffness of the prototype structure.

Specimen B, shown in Figure 2.2, was a one-eighth scale model of a signal support structure that was tested to evaluate the effects of slight variations in structural stiffness on the dynamic response to galloping and/or vortex shedding. As shown, Specimen B was identical to Specimen A with the exception of the horizontal support being prismatic.

Details of the three cantilevered sign-support structures are shown in Figures 2.3 through 2.5. Each of the model sign-support structures was fabricated from aluminum in order to adequately simulate the mass and stiffness properties of the prototype structures. Specimen C, shown in Figure 2.3, was a one-eighth scale model of a single-arm sign support structure composed of prismatic vertical and horizontal supports. Specimen D, shown in Figure 2.4, was a one-eighth scale model of a sign-support structure with a prismatic vertical support and a two-chord truss horizontal support. To study the effect of mast arm stiffness, the geometry and dimensions for Specimen C were selected for comparison with the truss used in Specimen D. Specimen D was detailed with member sizes and dimensions found in standard drawings of truss-type cantilever sign structures supplied by state DOTs. Specimen E, shown in Figure 2.5, was identical to Specimen D with the exception of the vertical support being replaced with a vertical support of reduced stiffness.

As shown in Figures 2.1 through 2.5, each of the specimens was configured with a variety of attachment details. Specimens A and B were tested with signal attachments configured with and without backplates (details of each of these attachments are shown in Figure 2.6). Specimen C was tested with two sign attachments as shown in Figures 2.7 and 2.8. Specimen D was tested with the sign attachment shown in Figure 2.7 and Specimen E was tested with the two sign attachments shown in Figures 2.7 and 2.9. As shown in these figures, the geometric dimensions of the attachment details included in the aeroelastic test program were identical to the dimensions of the attachment details included in the aerodynamic test program. Thus their susceptibility to galloping was expected to be identical. The weights of each of the attachments are shown in the upper left corner of each figure.

The test matrix for the aeroelastic test program is shown in Tables 2.1(a) and 2.1(b). Each specimen was tested under two basic conditions: (1) configured with attachments, and (2) configured without attachments. Tests in which the specimens were configured with attachments were performed with flows from both the front and the rear.

2.1.2.3 Aeroelastic Test Set-Up and Experimental Procedure - A schematic of the aeroelastic test set-up is provided in Figure 2.10. The specimens were mounted in the wind tunnel so that the flow was normal to the plane of the structure. The vertical support of each test specimen was mounted to a dynamic balance which was used to measure the moments to which each specimen was subjected during testing. The dynamic balance was instrumented with two pairs of strain gages located on orthogonal planes. These gages permitted the measurement of the drag and lift moments shown schematically in Figure 2.10.

The dynamic properties (i.e. natural frequency and damping) of each model were determined from vertical-plane, free vibration tests. Strain output (i.e. strain versus time) was used to estimate the natural frequency corresponding to the first vertical mode of vibration of each model. In addition, the level of damping possessed by the model was calculated using the log decrement method [26]. Each of the models was then subjected to discrete increments of increasing flow velocity. At each increment in velocity, uniform, steady-state flow conditions were maintained and data from each of the strain gages attached to the dynamic balance were recorded by the data acquisition system. The strain data were then processed to determine the lift and drag moment amplitudes.

2.1.2.4 Results Regarding Galloping - Figure 2.11 shows the observed dynamic response of Specimen A (a structure with documented galloping-induced vibrations) configured with signal attachments without backplates (Test Series I-A) under flow from the front. The data are presented in terms of the lift moment amplitude versus flow velocity. The arrows indicate the progression of the test with respect to flow velocity. As is indicated, the specimen did not exhibit significant vertical-plane oscillations when subjected to increasing flow velocities. Similar results were obtained when Specimen A was subjected to flow from the rear.

Figures 2.12(a) and 2.12(b) show the observed lift-moment amplitude for Specimen A configured with signal attachments with backplates (Test Series II-A) under flow from the front and the rear, respectively. As is shown in Figure 2.12(a), the specimen exhibited no significant dynamic response in the vertical plane for flow from the front. However, for flow from the rear (Figure 2.12(b)), the specimen exhibited severe oscillations resulting from the galloping phenomenon. The characteristics of the response observed in this test consisted of significant amplitudes of vibration perpendicular to the direction of flow (i.e. the oscillations were oriented in the vertical plane).

Figures 2.13(a) through 2.13(c) depict time histories of the dynamic response depicted in Figure 2.12(b) at three discrete flow velocities. The data are presented in terms of the root-mean-square (rms) variation in lift moment versus time. Again, note the increase in magnitude of the lift moment with

respect to the drag moment for increasing flow velocities, which is characteristic of the galloping phenomenon. At low flow velocities (Figure 2.13(a)), the specimen exhibited no significant dynamic response in the vertical plane. As the flow velocity was increased, as depicted in Figures 2.13(b) and 2.13(c), the galloping instability became apparent as the range in lift moment increased in much greater proportion than the range in drag moment. At the peak flow velocity (Figure 2.13(c)), the response of the structure was oriented primarily in the vertical plane. The measured column-base moment for the cases where significant response occurred is discussed further in Section 2.2 where it is used in analysis.

Several interesting characteristics can be observed with regard to the dynamic response depicted in Figure 2.12(b). First, note the persistent nature of the galloping phenomenon as the flow velocity was decreased from a peak of 18.2 m/s (40.7 mph). Significant vertical-plane oscillations continued even with decreases in the flow velocity. This type of behavior has been observed in various other types of structures which are susceptible to galloping-induced vibrations (e.g. transmission lines) [27] and suggests that once galloping-induced oscillations are initiated in a structure, damaging stress cycles may continue to occur even with reductions in the flow velocity.

Second, note the reduction in the relative magnitude of the lift-moment amplitude as the flow velocity was increased a second time. This is evidence of the inherent variability in the dynamic response of a structure to the galloping phenomenon and indicates the highly specific conditions which must be present in order for significant across-wind vibrations to occur. As further evidence of the dependence of galloping to specific flow conditions, the galloping response of Specimen A shown in Figure 2.12(b) occurred only once during the aeroelastic test program. Repeated testing of Specimen A under identical flow conditions failed to reproduce the results shown in Figure 2.12(b).

Tests conducted on Specimen B (Test Series I-B and II-B) did not exhibit a significant vertical-plane response when configured with either attachment TS-1D or TS-2D and subjected to flow from either the front or the rear. In general, the dynamic response of Specimen B under each of the conditions considered was similar to that shown in Figure 2.11. The lack of response in the across-wind direction may have resulted from the absence of very specific conditions which must be present for galloping to occur. Therefore, it cannot be concluded with certainty that the increased stiffness of the horizontal support prevented galloping-induced oscillations in this specimen.

Figures 2.14(a) and 2.14(b) illustrate the observed dynamic response of Specimen C for Test Series I-C under flow from the front and the rear, respectively. Each test was conducted with the specimen configured with attachment RS-1D. As indicated in Figure 2.14(a), the specimen exhibited a significant vertical-plane response due to galloping when subjected to flow from the front. However, the maximum response may not have been measured because the test was stopped to prevent damage to the model. A comparison of the characteristics of the response with those shown in Figure 2.12(b) indicate several similarities, the most notable of which are (1) the increase in response with increasing flow velocity and (2) the persistent nature of the galloping oscillations as the flow velocity was decreased. As shown in Figure 2.14(b), the specimen did not exhibit a significant vertical plane-response due to the galloping phenomenon when subjected to flow from the rear.

Figures 2.15(a) and 2.15(b) depict the observed dynamic response of Specimen C for Test Series II-C under flow from the front and rear, respectively. Each test was conducted with the specimen configured with attachment RS-3D. The vertically projected area of attachment RS-3D was one-half the projected area of specimen RS-1D. Again, for flow from the front, the specimen exhibited significant vertical-plane oscillations due to the galloping phenomenon. Similar to the results presented above, the test was stopped prior to reaching the maximum response to prevent damage to the model. In addition, a comparison of Figures 2.14(a) and 2.15(a) indicates that, at the flow velocity corresponding to the peak vertical-plane response, the magnitude of the lift moment for attachment RS-3D was approximately one-half the magnitude of the lift moment for attachment RS-1D. This observation suggests that the forces to which a cantilevered support structure is subjected during occurrences of galloping are directly proportional to the projected area of the attachment detail. As is shown in Figure 2.15(b), Specimen C did not exhibit significant vertical-plane response when configured with attachment RS-3D and subjected to flow from the rear.

Figure 2.16 depicts the observed dynamic response of Specimen D for Test Series I-D under flow from the front. As is indicated, Specimen D did not exhibit significant vertical-plane oscillations for flow from the front of the specimen. Similar results were obtained for flow from the rear. The observed dynamic response of Specimen E was similar to that of Specimen D for all of the flow conditions and attachment configurations considered (i.e. Test Series I-E and II-E). Reductions in the column stiffness (i.e. Test Series I-E) and sign mass (i.e. Test Series II-E) did not increase the susceptibility of Specimen E to galloping-induced vibrations. However, because of the sensitivity to specific conditions, it cannot be concluded that the truss structure is less susceptible to galloping than the single-arm cantilevered sign structure (i.e. Specimen C). In fact, failures of truss structures in the field have been attributed to vertical-plane vibrations which are consistent with the occurrence of galloping [3].

2.1.2.5 Results Regarding Vortex Shedding - Table 2.2 summarizes the predicted critical wind velocities at which each of the test specimens was expected to exhibit vortex-induced vibrations due to the shedding of vortices from the attachments. The table consists of seven columns of data. The first two columns summarize the test specimen and attachment detail, respectively. The third column indicates the average natural frequency of the test specimen as determined from vertical-plane, free-vibration tests. The fourth column indicates the depth of the attachment. The fifth column indicates the value of the Strouhal number used to predict the critical flow velocity at which lock-in was expected. Finally, the sixth and seventh columns summarize the values of the predicted and observed critical wind velocities for each specimen. Predicted values of the critical wind velocity, V_{cr} , were calculated using the Strouhal relation:

$$V_{cr} = \frac{f_n D}{S} \quad (2.1)$$

where f_n is the average measured natural frequency corresponding to the first vertical-plane mode of vibration, D is the depth of the attachment, and S is the Strouhal number.

As indicated in Table 2.2, none of the test specimens exhibited vortex-induced vibrations when configured with either sign or signal attachments. Inspection of the data presented in Table 2.2 indicates that the magnitudes of the predicted critical wind velocities for which lock-in of the signal support specimens (i.e. Specimens A and B) would be expected were near or below the threshold wind velocity (i.e. 5 m/s or 10 mph) below which the vortex shedding force is considered insufficient to excite significant amplitudes of vibration [8]. In addition, the results of research conducted by McDonald et al. [13] suggest that the three-dimensional characteristics of signal attachments disrupt the formation of coherent vortices at one well-defined frequency. As a result, vortex-induced vibration of the signal support specimens due to the shedding of vortices from the attachments would not be expected.

Inspection of the data for the cantilevered sign support specimens (i.e. Specimens C, D, and E) shows that the predicted critical wind velocities for each of the specimens is greater than the threshold velocity of 5 m/s (10 mph). Vortex-induced vibrations, however, were not observed. One possible explanation for the lack of vortex-induced vibration is that sign attachments also possess three-dimensional characteristics which interfere with the formation of coherent vortices at one well-defined frequency.

Table 2.3 summarizes the predicted critical wind velocities at which each test specimen without attachments was expected to exhibit vortex-induced vibrations due to the shedding of vortices from the horizontal mast-arms. As indicated in Table 2.3, the tapered and prismatic signal support structures (Specimens A and B) did not experience vortex-induced vibrations. Inspection of the predicted critical wind velocities for which vortex shedding lock-in would be expected in these specimens indicates that the predicted velocities fall below the threshold velocity of 5 m/s (10 mph) necessary for vortex-induced vibrations. As a result, vortex-induced vibrations would not be expected in these specimens.

The prismatic sign-support structure (Specimen C) did exhibit a significant vortex-induced response resulting from the shedding of vortices from the horizontal mast arm. As indicated in Table 2.3, the predicted velocity is approximately 18 percent less than the velocity at which the peak dynamic response was observed. This result is reasonable considering that lock-in probably began at a wind velocity slightly below the velocity at which peak across-wind response was observed. Figure 2.17 depicts the dynamic response of Specimen C. As is indicated, a sharp peak in the response occurs at the critical wind velocity at which the vortex-shedding frequency corresponds to the natural frequency of the specimen (i.e. lock-in). This is in contrast to the characteristic increase in across-wind response with increasing wind velocity associated with galloping (see Figure 2.14(a)). Figure 2.18 depicts a time history of the observed dynamic response at the critical wind velocity. The response is harmonic and dominated by the lift moment. The measured column-base moment for this case is discussed further in Section 2.2 where it is used in analysis.

The contrast in behavior between the signal support specimens (Specimens A and B) and the sign support specimen (Specimen C) can be attributed to the magnitudes of the critical wind velocities at which lock-in was expected for each of these structures when tested without attachments. The diameters of the support members for Specimens A and B resulted in critical wind velocities which were significantly less than the wind velocity of 5 m/s (10 mph) which previous researchers indicate as being the minimum wind

velocity required to initiate significant amplitudes of wind-induced vibration. The diameter of the support members for Specimen C resulted in a critical wind velocity which was very near the threshold velocity of 5 m/s (10 mph). Based on the results of these tests, it appears that the threshold wind velocity proposed by Kolousek [8] represents a reasonable estimate of the minimum wind velocity at which significant amplitudes of vibration can be expected.

2.1.2.6 Summary - Results of the aeroelastic test program permit several conclusions to be drawn concerning the dynamic response of cantilevered support structures to the galloping and vortex shedding phenomena. With respect to galloping

- Galloping is definitely possible for most types of signs and signal structures and has been observed to occur and cause problems in the field. However, the galloping phenomenon is very sensitive to the specific conditions and does not occur frequently. For example, galloping was difficult to reproduce in the wind tunnel experiments, even though the support structure models had extremely low levels of damping. Some models which theoretically should have been very susceptible to galloping did not exhibit galloping-induced vibrations. Just because a structure did not exhibit galloping in the wind tunnel does not mean that it is not susceptible to galloping. Susceptibility is better judged from the aerodynamic properties as explained in Section 1.2.1. Other models which exhibited galloping-induced vibration on one occasion did not exhibit an identical response in repeated tests. Difficulties encountered in reproducing the galloping phenomenon in many of the test series can be attributed to the specific conditions (dynamic properties of the structure, aerodynamic properties of the attachment details, and characteristics of the flow) which must be present in order for galloping-induced oscillations to occur. This sensitivity to very specific conditions is also evident in the observed dynamic responses of cantilevered support structures in the field. For example, structures which were observed to vibrate in the field very often had identical structures only blocks away, oriented the same way, which were not vibrating. In some cases, the risk of galloping and excessive deflection and fatigue failure may be acceptable. This is similar to the way tornados are dealt with for buildings. These events are considered sufficiently rare and the cost to design to resist tornados is not justified. However, structures located above high-volume high-speed roads should probably be designed to resist galloping-induced fatigue damage.
- Cantilevered signal support structures are most susceptible to galloping-induced oscillations when the signal attachments are rigidly mounted on the mast arm and are configured with backplates. This observation is in agreement with the results of the aerodynamic test program reported in this Chapter as well as tow-tank and full-scale field tests performed by McDonald et al. [13]. In addition, the results are consistent with the observed dynamic responses of cantilevered signal support structures in the field.

- The results suggest that, once the galloping instability is initiated, the resulting across-wind resonant vibrations persist even with reductions in the flow velocity. This is detrimental to the behavior of the structure with respect to fatigue, i.e. damaging stress cycles may persist in a structure subjected to galloping-induced oscillations even with reductions in the flow velocity.
- Once the galloping instability is initiated, the resulting across-wind resonant vibrations increase with increases in the flow velocity. Structures in the field have been observed to continue galloping despite gusts and to increase the range of vibration as the velocity increases.
- Trussed cantilevered sign-support structures considered in this test program did not exhibit a susceptibility to galloping-induced vibration. Enough tests were not conducted however, to exclude all truss cantilevers from being susceptible to galloping-induced vibrations. Aerodynamic tests confirm that any cantilevered sign structure may be susceptible to galloping, due primarily to the sign attachment.

With respect to vortex shedding

- Vortices shed from the attachments to cantilevered sign and signal support structures do not appear to be able to drive excessive vibration of these structures.
- The Strouhal relation provides a reasonable estimate of the critical wind velocity at which resonant vortex shedding can be expected.
- Cantilevered support structures are most susceptible to vortex-induced vibrations due to the shedding of vortices from the horizontal supports, i.e. vortex shedding from the column does not appear to be significant enough to excite structural vibrations. It appears that the column is less susceptible to aeroelastic vibration than the mast arm. For the column to vibrate, it must move the inertia of the mast arm along with it. The mast arm, which is essentially fixed at its end to the relatively stiff column, is free to vibrate as a cantilever.
- Vortex shedding need not be considered in the design of cantilevered support structures for fatigue when the critical wind velocity for lock-in (as computed by the Strouhal relation) falls significantly below 5 m/s (10 mph). As a result, only those structures with horizontal supports of relatively large diameter are susceptible to vortex-induced vibration (which is in agreement with the conclusions presented in Chapter One).
- The addition of attachments to the horizontal supports of cantilevered support structures appears to disrupt the spanwise correlation of the vortex shedding forces. As a result, vortex-

induced vibrations need only be considered prior to the installation of attachments to the structure.

- Cantilevered support structures composed of tapered structural members do not appear susceptible to vortex-induced vibrations. In general, the dimensions of the tapered elements are such that the critical wind velocities will fall below the threshold wind velocity of 5 m/s necessary for a significant across-wind pressure fluctuation. Furthermore, the vortex-shedding forces which develop in a tapered structural member will be correlated over a limited length of the member. As a result, the probability of generating a significant vortex shedding force in a tapered structural member is limited.

Test Series	Support Structure	Test Number	Attachments	Flow Direction
I-A	A	1	TS-1D	Front
		2	TS-1D	Rear
		3	None	NA
II-A	A	4	TS-2D	Front
		5	TS-2D	Rear
		6	None	NA
I-B	B	7	TS-1D	Front
		8	TS-1D	Rear
		9	None	NA
II-B	B	10	TS-2D	Front
		11	TS-2D	Rear
		12	None	NA

Note: NA = not applicable

Table 2.1(a) - Aeroelastic Test Matrix (Signal Support Specimens).

Test Series	Support Structure	Test Number	Attachments	Flow Direction
I-C	C	13	RS-1D	Front
		14	RS-1D	Rear
		15	None	NA
II-C	C	16	RS-3D	Front
		17	RS-3D	Rear
		18	None	NA
I-D	D	19	RS-1D	Front
		20	RS-1D	Rear
		21	None	NA
I-E	E	22	RS-1D	Front
		23	RS-1D	Rear
II-E	E	24	RS-2D	Front
		25	RS-2D	Rear

Note: NA = not applicable

Table 2.1(b) - Aeroelastic Test Matrix (Sign Support Specimens).

Specimen ¹	Attachments	Average Natural Frequency (Hz)	Depth, D (mm)	Strouhal Number	Predicted V_{cr} (m/s)	Observed V_{cr} (m/s)
A	TS-1D	7	133	0.20	4.7	- ²
A	TS-2D	7	165	0.20	5.8	-
B	TS-1D	5.5	133	0.20	3.7	-
B	TS-2D	5.5	165	0.20	4.5	-
C	RS-1D	10	230	0.14	16.4	-
C	RS-2D	11	230	0.14	18.1	-
D	RS-1D	13.5	230	0.14	22.2	-
E	RS-1D	11.3	230	0.14	18.6	-
E	RS-3D	12.8	230	0.14	21.0	-

¹See Figures 2.1 through 2.5 for details of each of the test specimens.

²Indicates vortex-induced vibrations were not observed.

Table 2.2 - Predicted and Observed Critical Wind Velocities for Vortex Shedding Lock-In Resulting From the Shedding of Vortices From the Attachments.

Specimen ¹	Attachments	Average Natural Frequency (Hz)	Diameter, D (mm)	Strouhal Number	Predicted V_{cr} (m/s)	Observed V_{cr} (m/s)
A	None	8.5	18 ² 8 ³	0.18	0.9 0.4	- ⁴
B	None	6.7	16	0.18	0.6	-
C	None	14.1	57	0.18	4.5	5.5

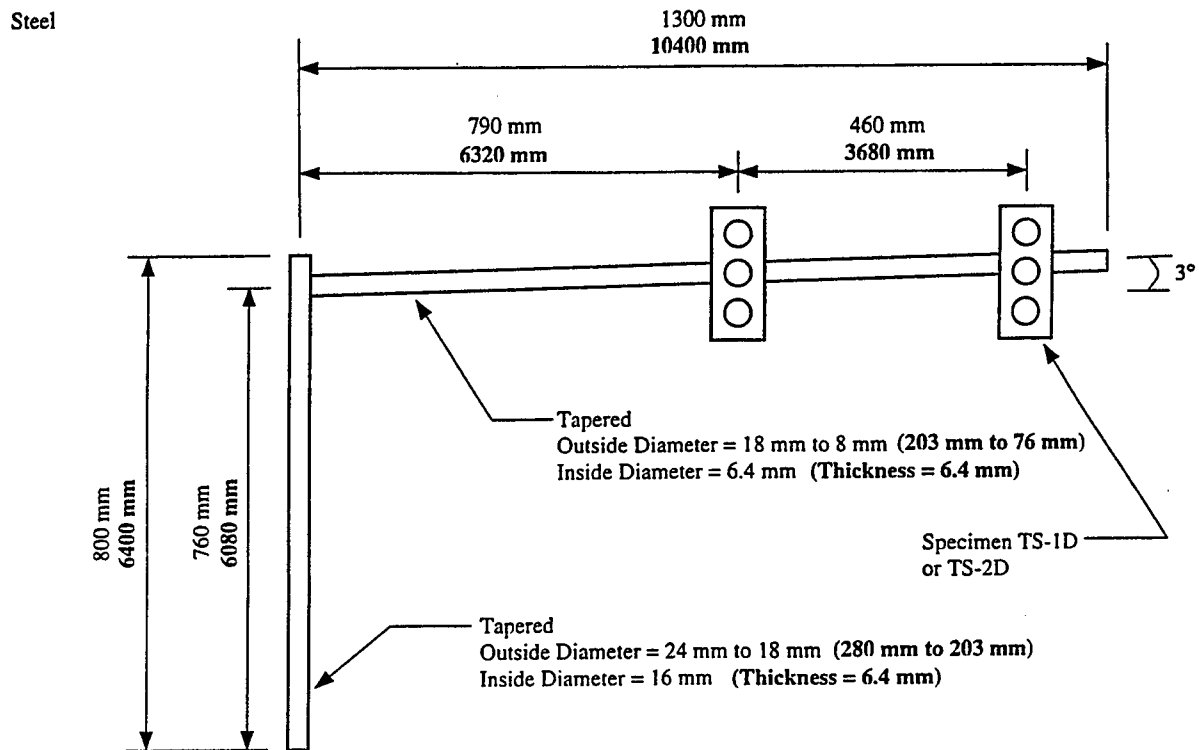
¹See Figures 2.1 through 2.5 for details of each of the test specimens.

²Diameter at base of mast arm.

³Diameter at tip of mast arm.

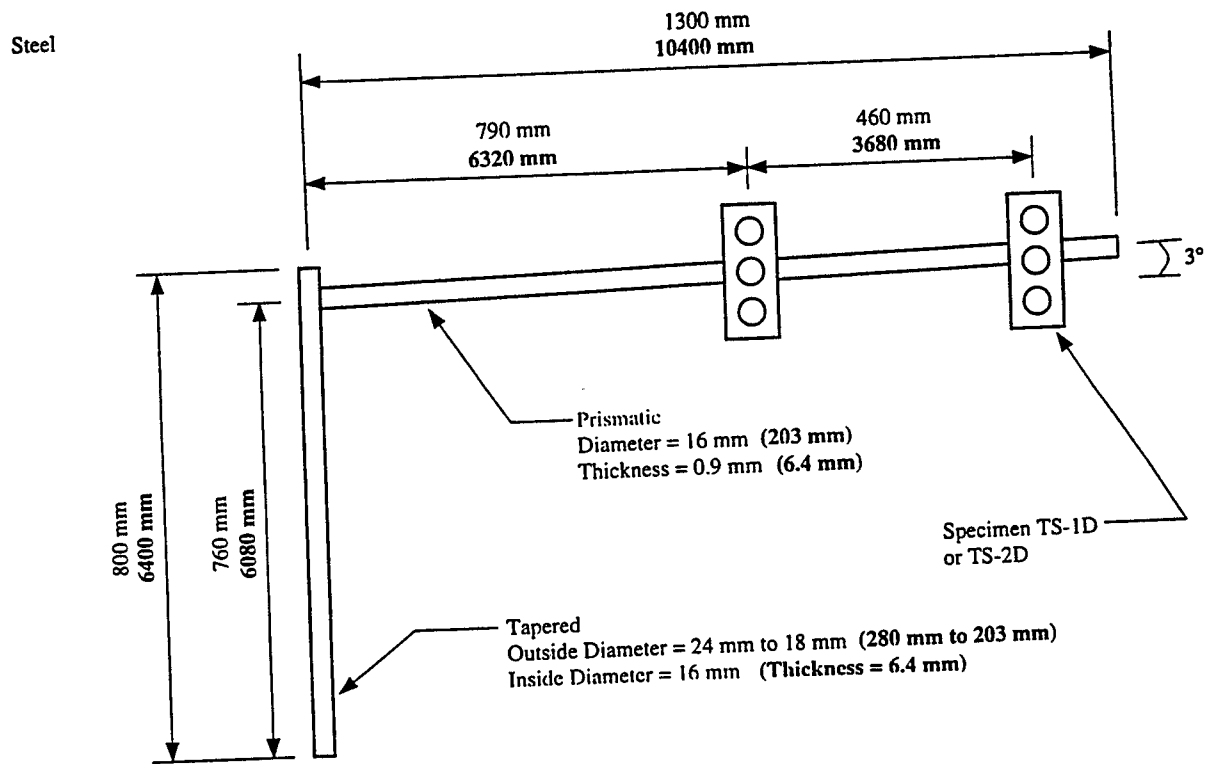
⁴Indicates vortex-induced vibrations were not observed.

Table 2.3 - Predicted and Observed Critical Wind Velocities for Vortex Shedding Lock-In Resulting From the Shedding of Vortices From the Supports.



Note:
Boldface indicates dimensions of prototype.

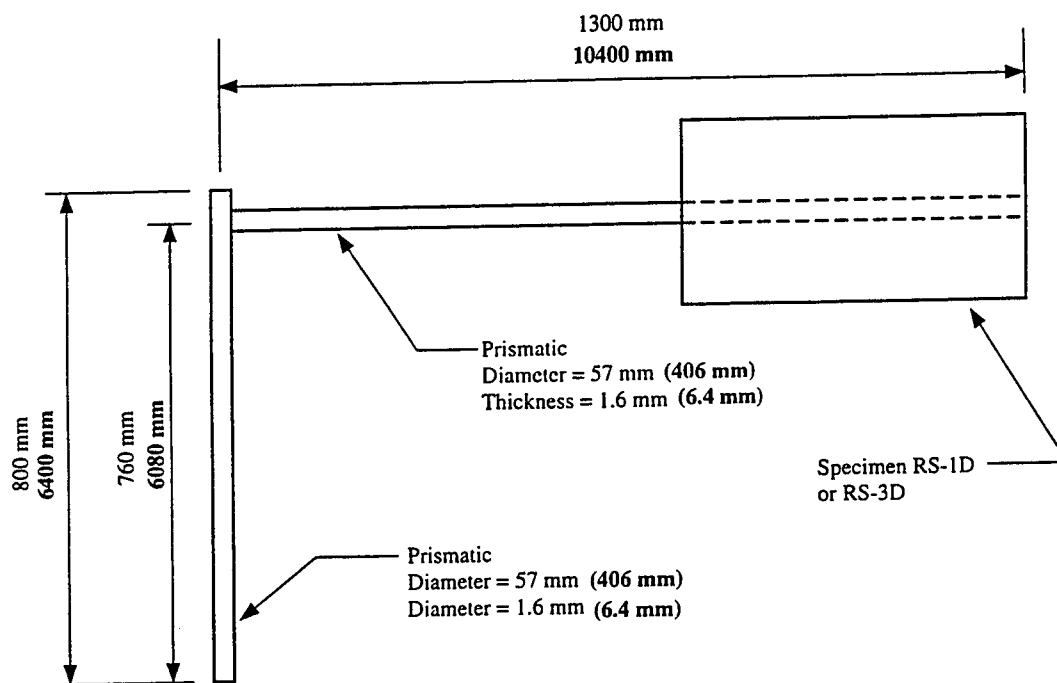
Figure 2.1 - Dimensions of the One-Eighth Scale Cantilevered Signal Support Structure (**Specimen A**) Included in the Aeroelastic Test Program.



Note:
Boldface indicates dimensions of prototype.

Figure 2.2 - Dimensions of the One-Eighth Scale Cantilevered Signal Support Structure (Specimen B) Included in the Aeroelastic Test Program.

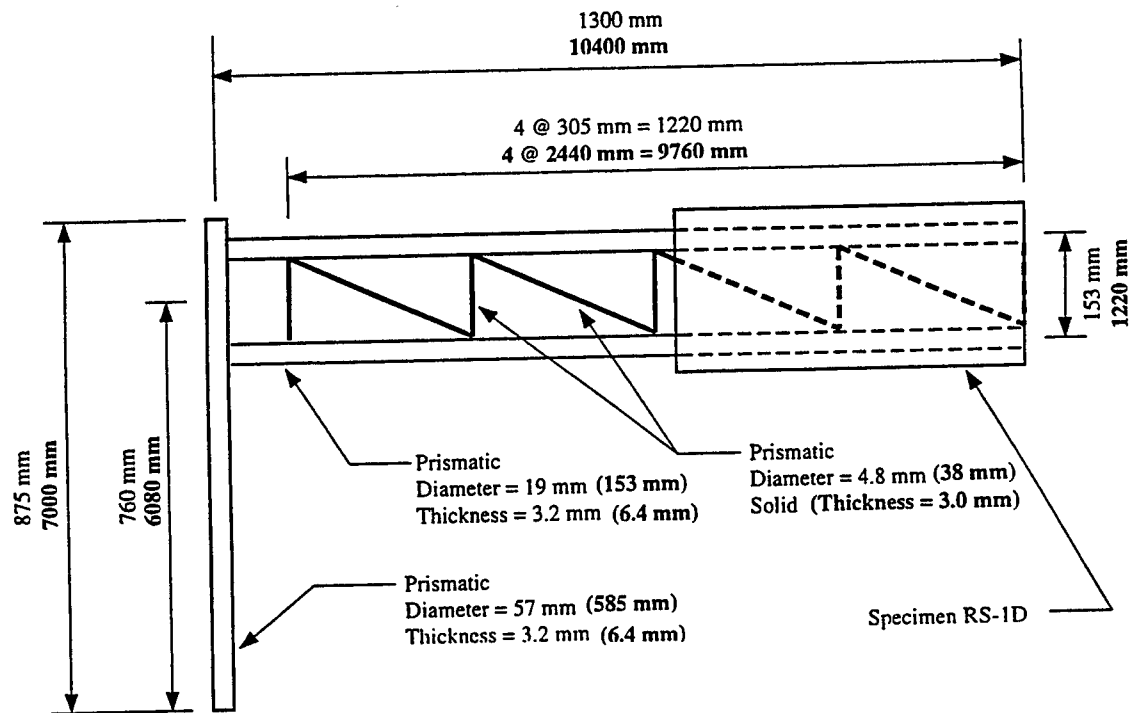
Aluminum



Note:
Boldface indicates dimensions of prototype.

Figure 2.3 - Dimensions of the One-Eighth Scale Cantilevered Sign-support structure (**Specimen C**) Included in the Aeroelastic Test Program.

Aluminum

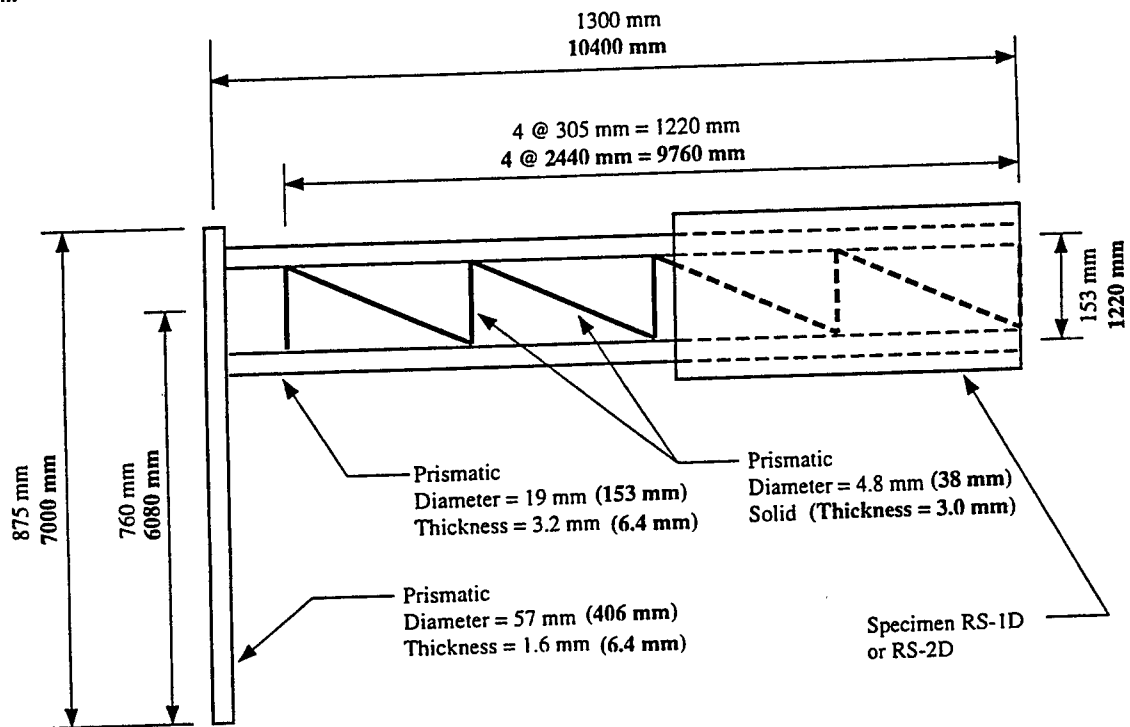


Note:

Boldface indicates dimensions of prototype.

Figure 2.4 - Dimensions of the One-Eighth Scale Cantilevered Sign-Support Structure (Specimen D) Included in the Aeroelastic Test Program.

Aluminum



Note:

Boldface indicates dimensions of prototype.

Figure 2.5 - Dimensions of the One-Eighth Scale Cantilevered Sign-Support Structure (Specimen E) Included in the Aeroelastic Test Program.

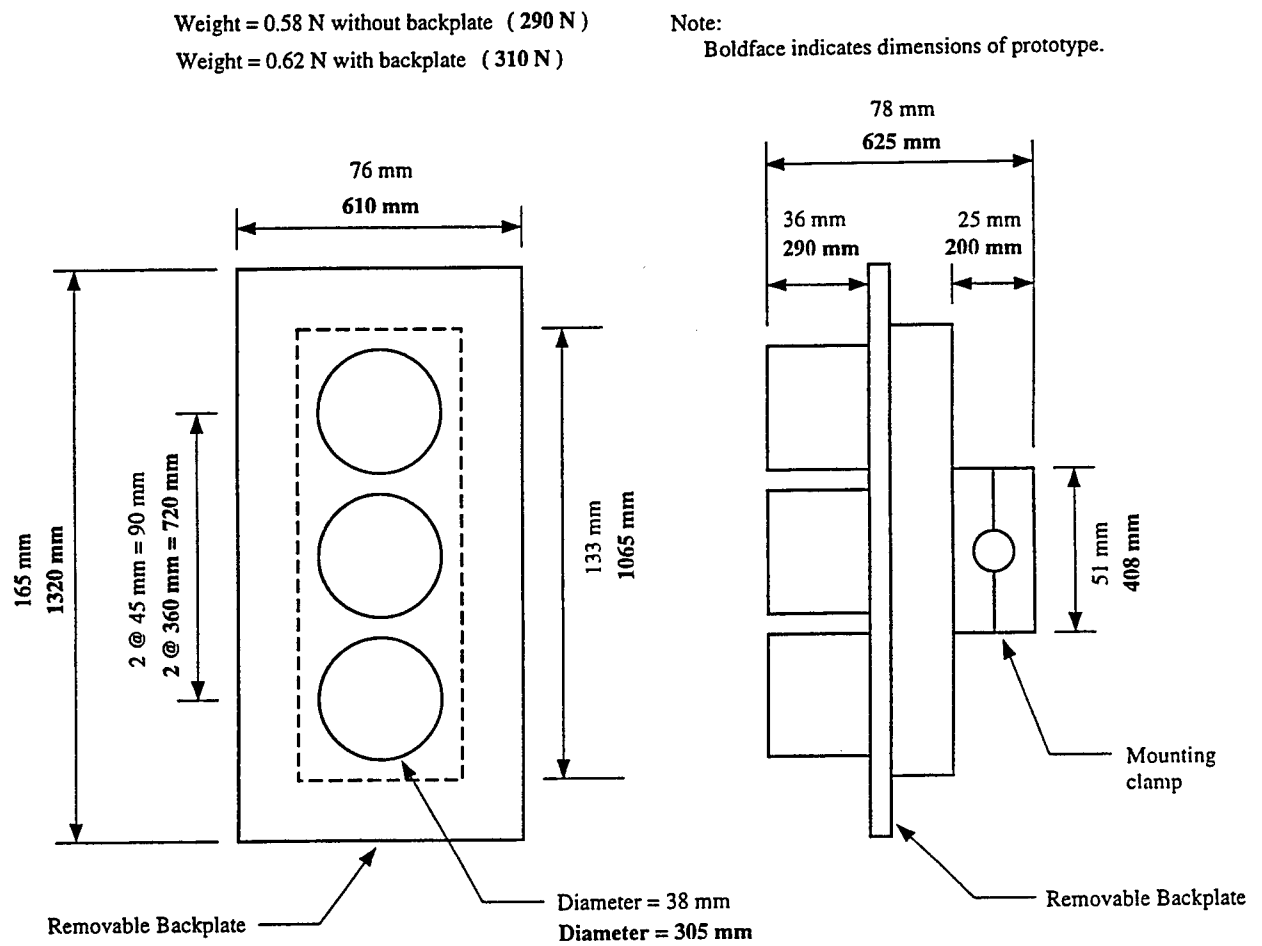
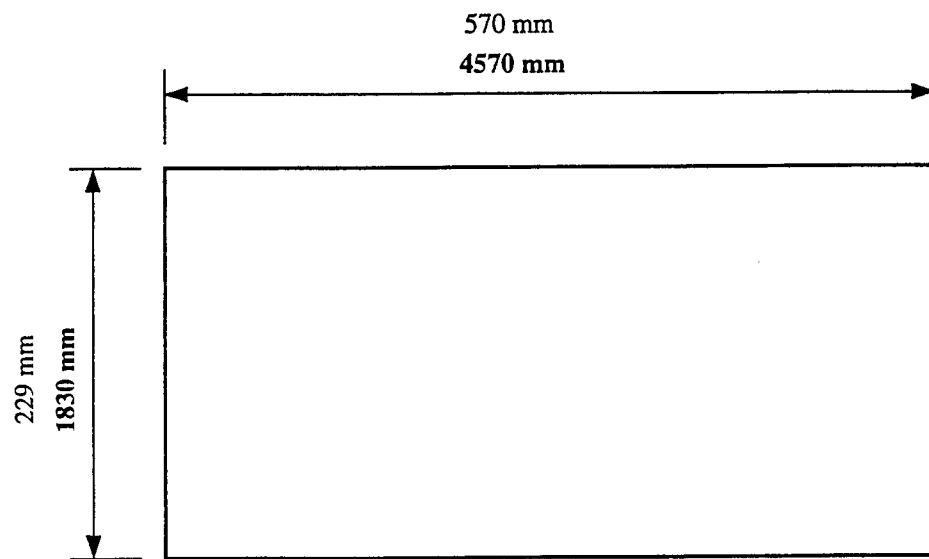


Figure 2.6 - Dimensions of the One-Eighth Scale Signal Attachments Mounted to Specimens A and B During the Aeroelastic Tests. **Specimen TS-1D** denotes signal without backplate. **Specimen TS-2D** denotes signal with backplate.

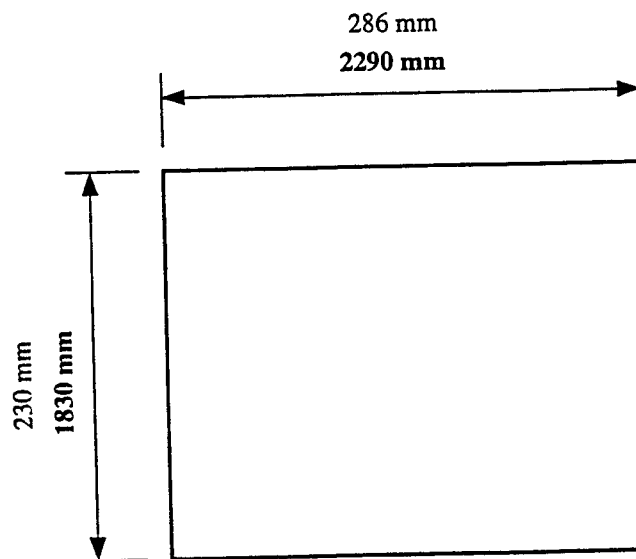
Weight = 4.2 N
Weight = 3110 N



Note:
Boldface indicates dimensions of prototype.

Figure 2.7 - Dimensions of the One-Eighth Scale "Full-Size" Sign Attachment (**Specimen RS-1D**) Mounted to Specimens C and D During the Aeroelastic Tests.

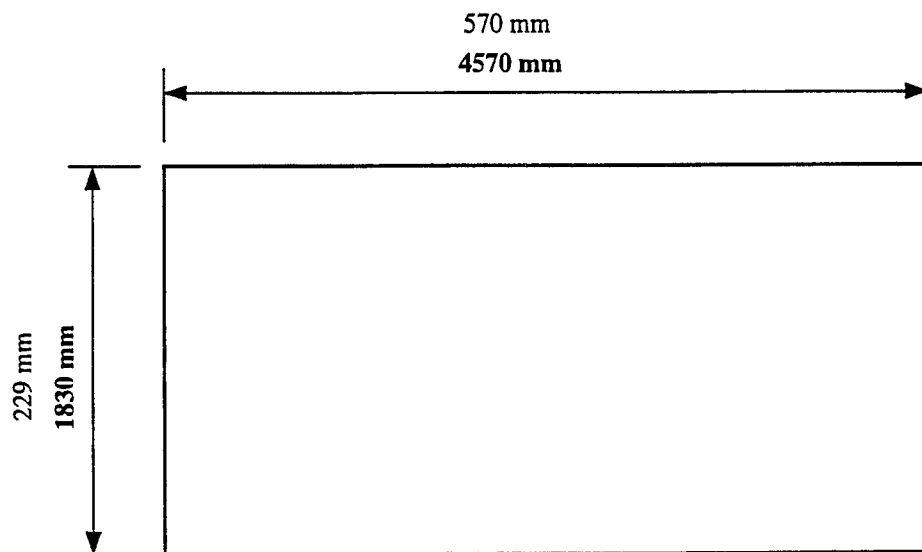
Weight = 2.1 N
Weight = 1560 N



Note:
Boldface indicates dimensions of prototype.

Figure 2.8 - Dimensions of the One-Eighth Scale "Half-Size" Sign Attachment (**Specimen RS-3D**) Mounted to Specimen C During the Aeroelastic Tests.

Weight = 1.0 N
Weight = 3110 N



Note:
Boldface indicates dimensions of prototype.

Figure 2.9 - Dimensions of the One-Eighth Scale "Full-Size" Sign Attachment (**Specimen RS-2D**) Mounted to Specimen E During the Aeroelastic Tests.

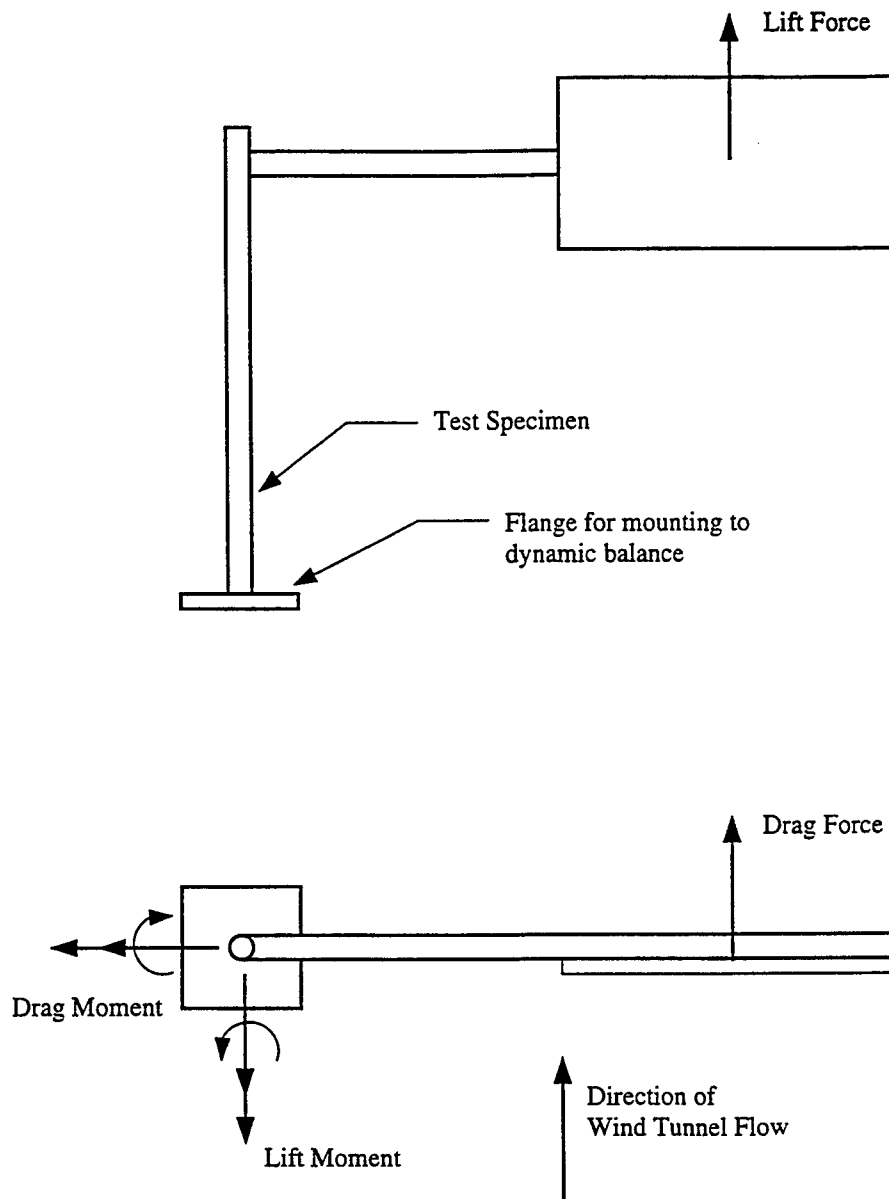


Figure 2.10 - Schematic Showing the Orientation of the Aeroelastic Test Specimens With Respect to the Wind Tunnel Flow and the Orientation of the Lift and Drag Moments Measured by the Dynamic Balance.

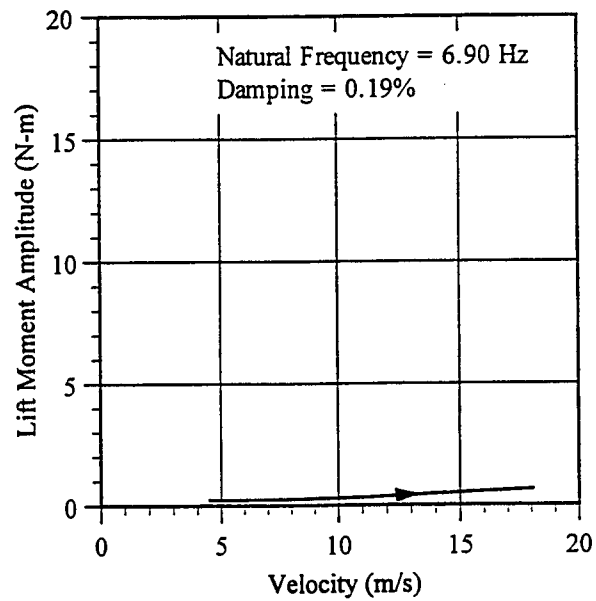
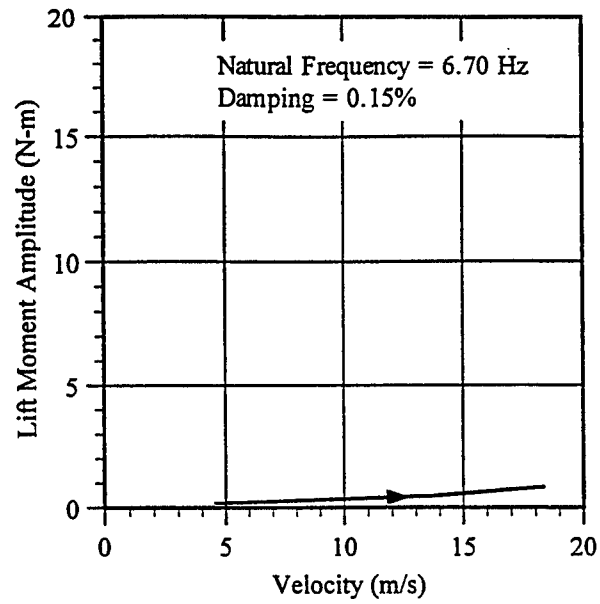
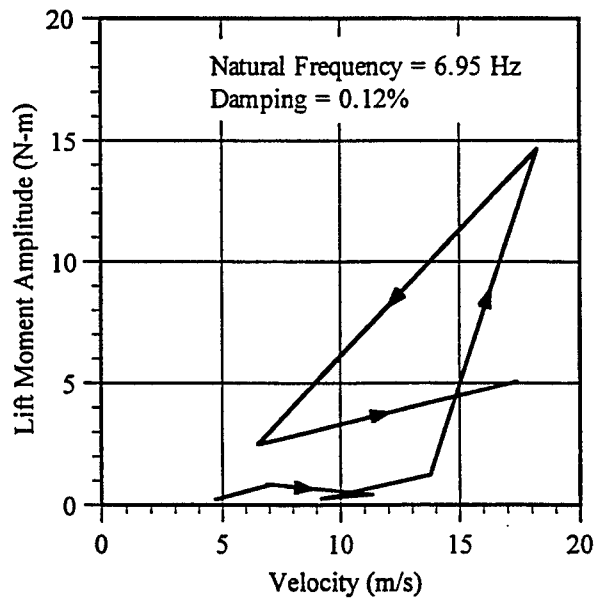


Figure 2.11 - Lift Moment Amplitude Versus Flow Velocity for Test Series I-A (Specimen A Configured with Signal without Backplates) for Flow From the Front. Note the lack of significant cross-wind response. Results for flow from the rear were similar.

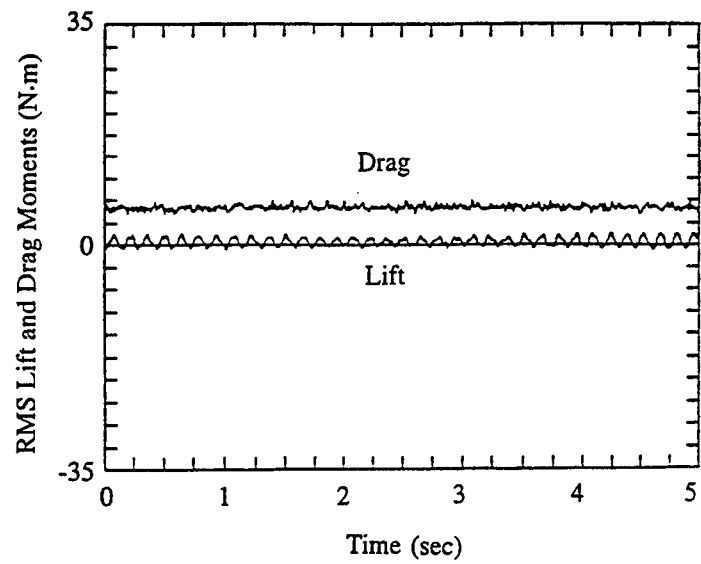


(a)

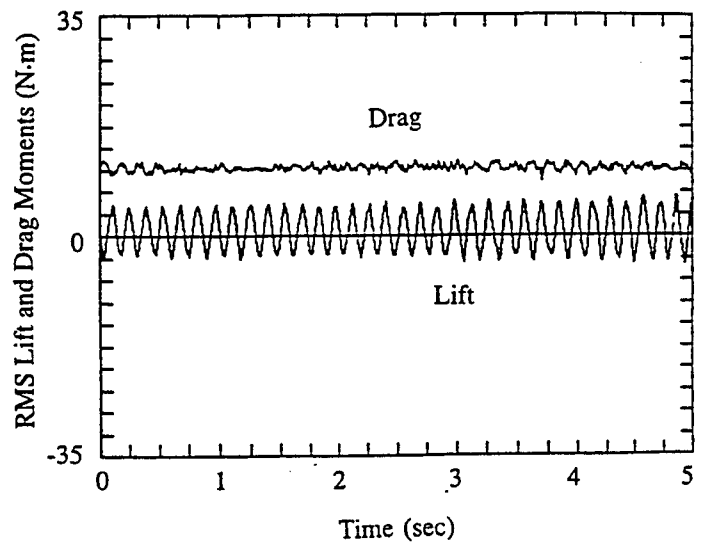


(b)

Figure 2.12 - Lift Moment Amplitude Versus Flow Velocity for Test Series II-A (Specimen A Configured with Signals with Backplates) for (a) Flow From the Front and (b) Flow From the Rear. Note the across-wind galloping response for flow from the rear.

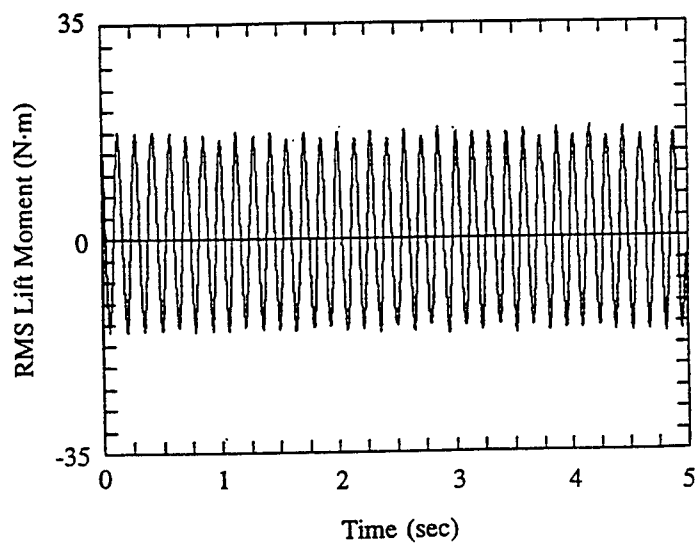


(a)



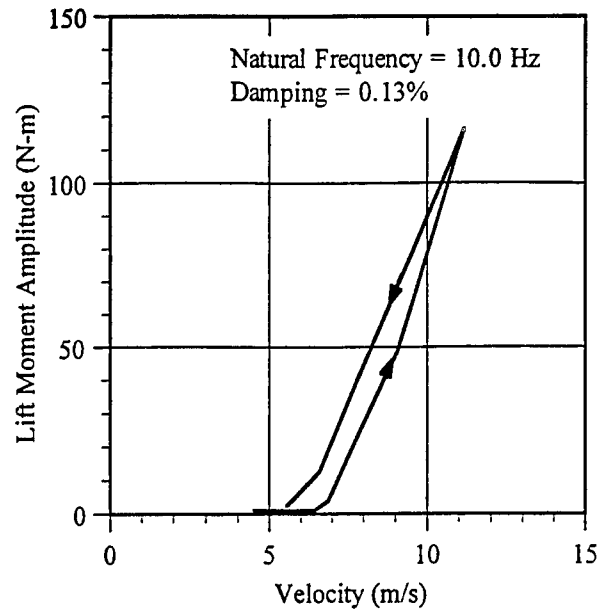
(b)

Figure 2.13 - Time History of the Dynamic Response for Test Series II-A (Flow from Rear) at (a) 13.4 m/s, (b) 17.4 m/s.

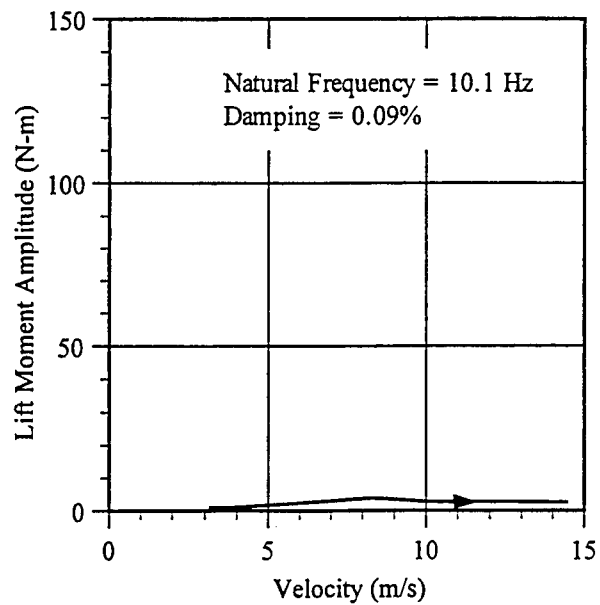


(c)

Figure 2.13 - Time History of the Dynamic Response for Test Series II-A (Flow from Rear) at (c) 18.2 m/s.

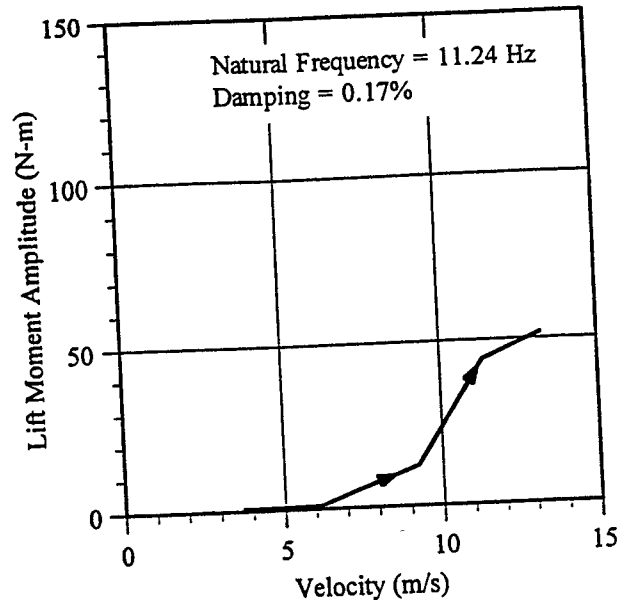


(a)

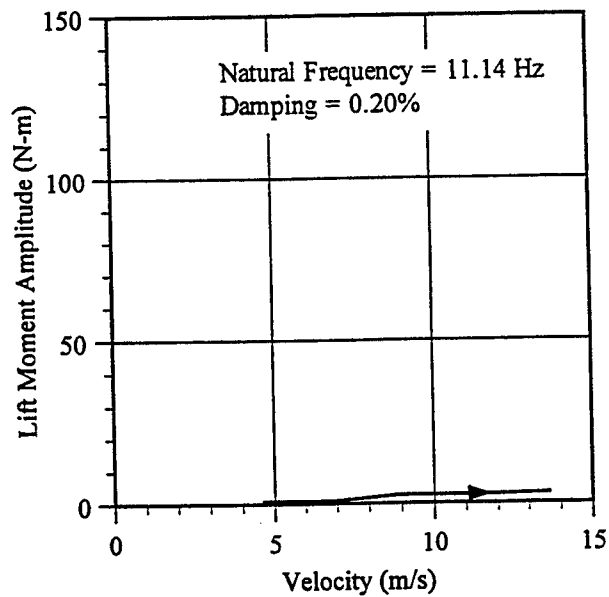


(b)

Figure 2.14 - Lift Moment Amplitude Versus Flow Velocity for Test Series I-C (Specimen C Configured with Sign RS-1D) for (a) Flow From the Front and (b) Flow From the Rear. Note the across-wind galloping response for flow from the front.



(a)



(b)

Figure 2.15 - Lift Moment Amplitude Versus Flow Velocity for Test Series II-C (Specimen C Configured with Sign RS-3D) for (a) Flow From the Front and (b) Flow From the Rear. Note the across-wind galloping response for flow from the front.

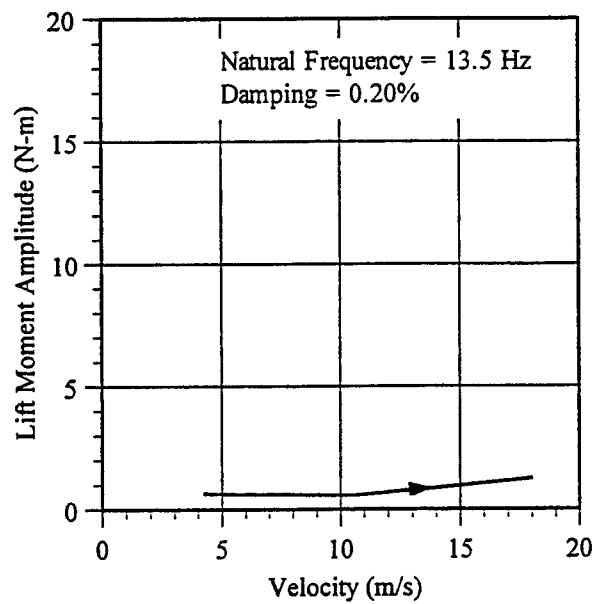


Figure 2.16 - Lift Moment Amplitude Versus Flow Velocity for Test Series I-D (Specimen D Configured with Sign RS-1D) for Flow From the Front. Note the lack of significant across-wind response. Similar results were obtained for flow from the rear and also for tests conducted on Specimen E.

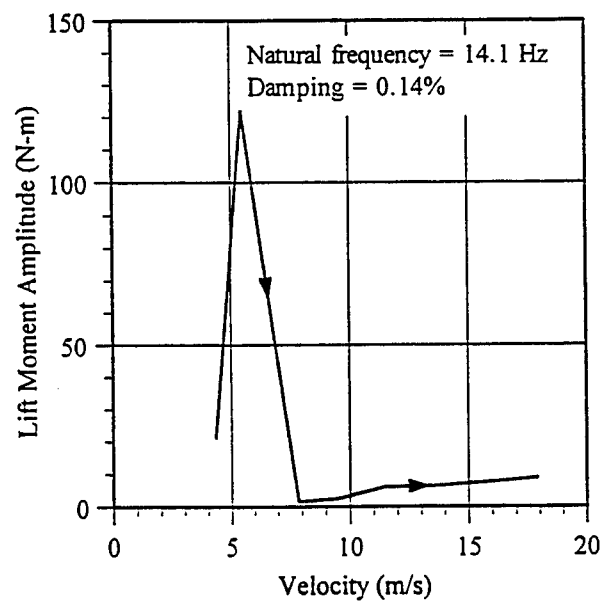


Figure 2.17 - Lift Moment Amplitude Versus Flow Velocity for Test Series I-C (Specimen C Configured with No Attachments). Note the sharp peak in the response indicative of vortex shedding.

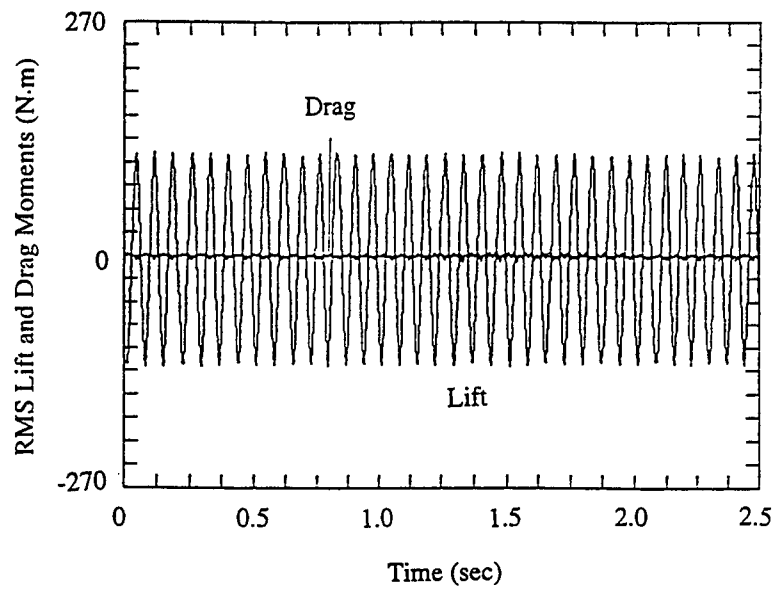


Figure 2.18 - Time History of the Dynamic Response for Test Series I-A (Specimen C Configured With No Attachments) at the Critical Wind Velocity of 5.5 m/s.

2.2 ANALYSES TO DETERMINE FATIGUE DESIGN LOADS

This Section summarizes the results of dynamic and static finite-element analyses and other calculations performed to estimate the magnitude of wind pressures to which cantilevered support structures are subjected during occurrences of galloping, vortex shedding, natural wind, and truck-induced gust vibrations. The following methods were used to accomplish this objective:

- Dynamic finite-element analyses of the wind-tunnel model specimens were performed to estimate the magnitude of the lift pressures required to simulate the across-wind response amplitudes (i.e. lift moment amplitudes at the base of the vertical supports) measured during the aeroelastic wind-tunnel tests exhibiting galloping or vortex shedding.
- Dynamic finite-element analyses of the wind tunnel prototype specimens were performed and verified that the mass and stiffness of the prototype specimens were reasonably represented by the model specimens.
- Dynamic finite-element analyses of several full-scale cantilevered support structures were performed to evaluate the validity of the experimentally-determined lift pressures. Structures selected for these analyses were known to have been subjected to across-wind vibrations consistent with galloping. In addition, estimates of at least one dynamic response amplitude from each of these structures was known (either displacements at the tip of the horizontal mast arm or stress measurements). Thus the dynamic response observed in the field could be simulated using finite-element analyses. The apparent loading from these events was in good agreement with the loading on the wind tunnel specimens.
- The response of typical cantilevered support structures to natural wind gusts was modelled using spectral finite-element analysis. The probability of exceedence of wind velocity is a Rayleigh distribution based on the annual mean wind velocity for a location. An upper-bound annual mean wind velocity was determined from data for U.S. cities. A standard wind velocity spectrum (which depends on the mean hourly wind velocity) was selected from the literature [28]. Analyses were performed over a range of mean hourly wind velocities. The velocity spectra were converted to force spectra which were applied in finite-element analyses to a range of structures. The analyses give an estimate of the effective stress range at critical details. A limit-states stress range associated with the 0.01 percent exceedence level was determined.
- Static finite-element analyses were performed on all of these structural models to calibrate "equivalent" static load ranges. When the equivalent static load range is applied in an analysis

(from zero mean load), the resulting stress values at critical details (interpreted as stress ranges) are approximately the same as the stress ranges caused by various dynamic wind-loading phenomena; including galloping, vortex shedding, and natural wind gusts. Note that only the stress range is needed for the fatigue strength check; the actual mean load is irrelevant. Therefore the static load range is applied from zero load, and the resulting peak stress is the stress range use for design.

- Calculations were performed using a very simple static load model for truck-induced gust loading. Several variable message sign (VMS) structures which have recently had fatigue failures were analyzed. The simple load model gave stress ranges in the critical details of these structures consistent with the fatigue lives of these structures prior to failure.

Section 2.2.1 describes the finite-element models which were used in all of the various analyses. Section 2.2.2 summarizes the modal analyses to simulate galloping and vortex shedding results for the model wind tunnel specimens, the prototype wind tunnel specimens, and the full-scale cantilevered support structures. Based on static analysis, equivalent static vertical lift pressure ranges are proposed for use in the design of cantilevered support structures for galloping- and vortex-induced fatigue. Section 2.2.3 summarizes spectral analysis simulating natural wind gusts. Finally, a simplified static pressure range model for truck-induced gusts is discussed in Section 2.2.4.

2.2.1 Finite-Element Models

The finite-element analyses were performed using the commercially available finite-element program ABAQUS [29]. Details of the analytical methods which were used in the various types of analyses are provided in Sections 2.2.2 through 2.2.5.

The cantilevered support structures considered in the analyses (i.e. wind-tunnel model specimens, wind-tunnel prototype specimens, and full-scale support structures) were modeled using continuous, three-noded, quadratic beam elements. Structures composed of prismatic structural members were modeled using beam elements of the same corresponding cross-sectional dimensions (i.e. the actual member dimensions were used in the finite-element model). Structures composed of uniformly tapered structural members were modeled using a series of "equivalent" prismatic elements arranged in a step fashion as is shown in Figure 2.19. The cross-sectional dimension of each "equivalent" prismatic element was equal to the average cross-sectional dimension of the corresponding tapered member.

A relatively fine mesh size was used in the analyses of all full-scale cantilevered support structures and prototype wind tunnel specimens (a nominal element length equal to 305 mm or 12 in). This mesh size was selected to ensure adequate representation of the variation in mass and stiffness along the length of the tapered structural members.

Signal attachments were modeled as lumped masses at the nodal points corresponding to the locations of the attachments on the actual support structure. Sign attachments were modeled as a series

of lumped masses at the nodal points corresponding to the length of the horizontal support over which the sign was mounted on the actual support structure. The mass at each nodal point was computed as the mass of the actual sign attachment divided by the number of nodal points over which the sign was mounted on the actual support structure. Both the sign and signal attachments do not substantially contribute to the stiffness of the mast arm and therefore any increase in stiffness was neglected.

The base of the vertical support of each of the models was assumed fixed. Effects of foundation flexibility and/or soil-structure interaction were neglected in each of the analyses. Kaczinski et al. [2] showed that the fixed base assumption results in worst-case estimates of the stress ranges at critical connection details. Therefore, the equivalent static load models developed from these finite-element analyses will conservatively predict the magnitudes of the stress ranges to which cantilevered support structures are subjected during galloping, vortex shedding, and natural wind gusts.

2.2.2 Modal Analyses to Simulate Galloping and Vortex Shedding

Finite-element analyses were performed to determine the magnitude of the lift pressures required to simulate a known dynamic response amplitude. For the wind-tunnel model and prototype specimens, the known dynamic response amplitude was the magnitude of the lift moment at the base of the vertical support. For the full-scale support structures, the known dynamic response amplitude was either an estimate of the displacement amplitude of the horizontal support or an estimate of the stress range at some location within the structure. Three finite-element analyses were performed on each of the structures considered within the scope of the analytical program. Each of the analyses are briefly discussed below.

Eigenvalue analyses were performed to determine the natural frequencies and mode shapes corresponding to the first six modes of vibration of the structure. The number of modes extracted in the eigenvalue analysis was arbitrarily selected. As will be discussed below, the dynamic response of cantilevered support structures to galloping and vortex shedding is dominated by the first vertical-plane mode of vibration.

Load models for the galloping and vortex shedding phenomena were developed based upon the wind-tunnel test results. As was discussed in Section 2.1, galloping of the cantilevered sign and signal model specimens was caused by the aerodynamic forces acting on the attachments to these specimens. As a result, the load model for galloping of the signal support structures was represented in the finite-element analyses as a concentrated load applied in the vertical-plane at the nodal points corresponding to the locations of the signal attachments in the actual structure (see Figure 2.20). The load model for galloping of the sign-support structures was represented as a uniformly distributed load applied in the vertical-plane over the length of the sign panel (see Figure 2.21). The wind tunnel test results indicated that vortex shedding of the cantilevered sign support model specimen (configured without attachments) was caused by the shedding of vortices from the horizontal mast arm. As a result, the load model for vortex shedding was represented as a uniformly distributed load applied to the structure in the vertical-plane over the length of the horizontal mast arm (see Figure 2.22).

Linear modal analyses were performed to determine the steady-state dynamic response of each of the structures to the galloping and/or vortex shedding phenomena. The load to which each of the structures was subjected was assumed to be a sinusoidal wave of the form:

$$F(t) = F_0 \sin \omega t \quad (2.2)$$

where F_0 is the amplitude of the dynamic load required to simulate the known dynamic response amplitude, ω is the circular natural frequency of the structure corresponding to the first mode of vibration in the vertical-plane, and t is time. The load given by Equation 2.2 was applied to the structure in accordance with one of the load models discussed above. Representation of the loading as a sinusoidal function is consistent with the time history of the dynamic response observed during the wind-tunnel tests for which galloping and vortex shedding were observed (see Figures 2.13 and 2.18, respectively). Each of the dynamic analyses was performed by only considering the contribution of the first vertical-plane mode of vibration (generally the second mode of vibration of each of the structures). The superposition of response amplitudes from higher vertical-plane modes were found to contribute less than 1 percent to the overall dynamic response of the structures.

Static analyses were also performed to determine the magnitude of the static load range required to obtain a response equal to the known dynamic response range for each of the structures. The static load range was applied to the structure with the same load distributions that were used in the dynamic analyses. The static analyses were performed to evaluate the accuracy of using equivalent static load models to simulate the forces to which cantilevered support structures are subjected during occurrences of galloping and vortex shedding. The use of equivalent static load models avoids the necessity for using dynamic analyses for design. The equivalent static pressure range is given as:

$$\text{Equivalent Static Pressure Range} = \frac{2 F_{\text{static}}}{A} \quad (2.3)$$

where F_{static} is the amplitude of the load required to simulate the lift moment amplitudes measured during the wind tunnel test and A is the projected area of the member subjected to loading (sign, signal, or horizontal support). Note that the static force amplitude has been multiplied by 2.0 to change the amplitude into a range.

An estimate of the static pressure range can also be obtained from the dynamic magnification factor. For a single-degree-of-freedom (SDOF) oscillator at resonance, the dynamic magnification factor equals $1/2\xi$, where ξ is the critical damping ratio [26].

$$\text{Estimated Static Pressure Range} = \frac{F_{\text{dynamic}}}{(A)(\xi)} \quad (2.4)$$

The magnification factor is multiplied with F_{dynamic} , the dynamic force amplitude required to obtain the lift moment amplitude recorded during the wind-tunnel test. Once again, this quantity has been multiplied by 2.0 to change from an amplitude into a range. A is the projected area of the member subjected to the loading (i.e. signal, sign, or horizontal support). This estimate of the static lift pressure range can be compared to the value obtained from the static analyses as a consistency check. The equivalent static pressure range determined from static finite-element analysis is considered the more accurate of the two.

2.2.2.1 - Analyses of Wind Tunnel Model Specimens - Table 2.4 provides a tabular summary of the data collected from the wind tunnel specimens which exhibited significant vertical-plane vibrations due to either galloping or vortex shedding. The data presented in Table 2.4 were presented graphically in Section 2.1 and represent the maximum values obtained from the wind tunnel tests. As discussed in Section 2.1, vortex-induced vibrations were only observed in the sign support specimen (i.e. Specimen C) configured without attachments. The remaining specimens shown in Table 2.4 exhibited galloping-induced vibrations. Member dimensions for each of the model specimens were also previously summarized in Section 2.1. The natural frequency (corresponding to the first vertical-plane mode of vibration) and percent critical damping (also corresponding to the first vertical-plane mode of vibration) were determined from free-vibration tests. The wind velocity indicated for each specimen is the velocity at which peak vertical-plane oscillations were observed. Similarly, the column moment amplitude is the lift moment measured at the base of the vertical support of the specimen at the time of peak vertical-plane oscillation.

Table 2.5 summarizes the dynamic finite-element analysis results for the wind-tunnel model specimens. The predicted natural frequencies in the table are for the vertical-plane mode of vibration of the specimen and agree to within 20 percent of the measured values. This level of agreement is considered very good for any type of analysis compared to experimentally determined resonant frequencies. As is indicated, the damping ratio for each specimen was set equal to the damping ratio obtained from vertical-plane, free-vibration tests of that specimen during the wind-tunnel tests.

The remaining columns of Table 2.5 depict the dynamic response amplitudes (i.e. moments and displacements) corresponding to the magnitude of the load required to obtain the lift moment amplitude recorded during the wind tunnel test. A comparison of the results for the sign-support structure (i.e. Specimen C) configured with the two sign attachments (i.e. Attachment RS-1D and Attachment RS-3D) indicates that the response is approximately proportional. That is, the response amplitudes associated with Specimen C configured with Attachment RS-1D (the "full-size" sign attachment) are approximately two times greater than the response amplitudes associated with Specimen C configured with Attachment RS-3D (i.e. the "half-size" sign attachment). This result verifies that the magnitude of the across-wind loads to which cantilevered support structures are subjected during occurrences of galloping are proportional to the

area of the attachment detail. In other words, the vertical lift pressure associated with galloping is approximately constant for different signs and signals.

The equivalent static pressure ranges indicated in Table 2.6 were calculated from Equation 2.3 using static elastic finite-element analysis with the same models that were used for the dynamic analysis. The static pressure range is calibrated to obtain the same base moment range as the dynamic analysis. Note that the static lift-pressure range is like a shear force which is applied vertically on the vertically projected area of the attachments. Examination of the equivalent static pressure ranges listed in Table 2.6 indicate that the lift pressure ranges associated with galloping vary from 1150 Pa (24 psf) for the signal-support structure to 1770 Pa (37 psf) for the sign structure configured with the "full-size" sign attachment (i.e. Attachment RS-1D). Considering the differences in these structures and the randomness of the galloping phenomenon, this range in equivalent static pressures is remarkably consistent.

The estimated static pressure ranges are also included in Table 2.6. These values were calculated from the computed dynamic driving force amplitudes using the simple SDOF magnification factor (Equation 2.4). The estimated static pressure ranges vary from 850 to 1480 Pa (17.8 to 30.9 psf), which compares to the equivalent static pressure range of 1150 to 1770 Pa (24.0 to 37.0 psf). The agreement is good considering the simplicity of the SDOF approximation and indicates that results from different analysis approaches are consistent.

However, a comparison of the arm moment amplitude in Tables 2.5 and 2.6 reveals a systematic variation between the dynamic and static response amplitudes. In particular, the dynamic analysis predicts that the arm moment will be approximately 65 to 75 percent of the column moment while the static analysis predicts that the arm and column moments should be equal. (Actually there is a small difference between the arm moment and the column moment in the static analysis. This difference occurs because the arm moments were computed at the face of the column while the column moments were computed at the longitudinal axis of the column. As a result, the arm moments computed from the static analyses are slightly less than the column moments.)

This variation between the static and dynamic results can be attributed to the inertial effects inherent in the dynamic analysis of a multi-degree-of-freedom system which are not accounted for in the static analysis. Use of the static analysis for design will result in overestimation of the mast arm moment by 30 to 50 percent, hence ignoring the dynamic effects is conservative. In view of the considerable variation in the lift pressures to which the model specimens were subjected under galloping, the fact that the static analyses overestimate the dynamic response amplitudes is not considered significant. It is therefore concluded that equivalent static load models provide a reasonable means by which to simulate the dynamic response amplitudes exhibited by cantilevered support structures subjected to galloping.

Also shown in Table 2.6, the equivalent static pressure range (from static finite-element analysis) for vortex shedding from the mast arm of the sign structure (i.e. Specimen C) without attachments is 5100 Pa (107 psf). This equivalent static pressure range can be compared to the equivalent static pressure range computed using the provisions of the present AASHTO Specifications [1] and Ontario Code [30].

The present AASHTO Specifications, which will be discussed in Section 3.1, contain provisions for the design of simple poles for vortex shedding. The critical wind velocity associated with vortex shedding lock-in, V_{cr} , can be calculated with the Strouhal relation, $V_{cr} = f_n D/s$. The measured natural frequency of Specimen C was 14.1 Hz, the diameter of the horizontal support was 57 mm, and the Strouhal number for vortex shedding from a circular cylinder is 0.18. Therefore, the predicted critical wind velocity is equal to 4.5 m/s (10 mph). Substituting this critical wind velocity and the measured damping ratio for Specimen C (0.14%) into the AASHTO provisions yields an equivalent static pressure range of 4760 Pa (99.5 psf). This value agrees very well with the calculated equivalent static pressure range (derived from wind-tunnel tests) of 5100 Pa (106.6 psf).

The Ontario Code also contains provisions for predicting the equivalent static transverse force amplitude per unit length associated with vortex shedding from a simple pole (described in detail in Section 3.1). These provisions predict an equivalent static transverse pressure range of 6160 Pa (128.7 psf).

Thus, for a measured value of damping, the equivalent static pressure predicted by the Ontario Code is more conservative than the equivalent static pressure predicted by the AASHTO Specifications. The Ontario code pressure range is also greater than the pressure range derived from the wind-tunnel tests.

Generally, the equivalent static pressures predicted by each of the design specifications correlate well with the equivalent static pressure derived from the dynamic finite-element analysis. As a result, it can be concluded that the design provisions for vortex shedding from a simple pole can be used to estimate the magnitude of the equivalent static pressure ranges to which cantilevered support structures are subjected during occurrences of vortex-induced vibration resulting from the shedding of vortices from the mast arm. Unfortunately, there are no equivalent load models specified in either the Ontario Code or the AASHTO Specifications for galloping. However, the relatively good agreement between the wind-tunnel results and the design specifications for vortex shedding increases the confidence in the wind-tunnel results for galloping as well.

2.2.2.2 Analyses of Wind Tunnel Prototypes - Dynamic and static finite-element analyses were also conducted on prototypes of the wind-tunnel specimens in a manner identical to that of the model specimens. Details of the dimensions of the prototype specimens were provided in Section 2.1. The prototypes are hypothetical full-size versions of the wind-tunnel models and may not be completely representative of actual cantilevered support structures. Scaling of the column moment amplitudes in the model specimens to the column moment amplitudes in the prototype specimens was based upon the one-eighth scaling factor used in the fabrication of the wind tunnel test specimens.

Results of these analyses indicated that the mass and stiffness properties of the model specimens were scaled with a reasonable level of accuracy. The laws of similitude indicate that the natural frequencies of the model specimens should be eight times the natural frequencies of the prototype specimens. A comparison of the natural frequencies (model versus prototype) indicates that this holds true with an error of less than 30 percent, which is considered excellent agreement. Similarly, for a given

applied lift pressure, the displacements of the prototype specimens would be expected to be eight times the displacements of the model specimens. The data indicate that this holds true with an error of less than 15 percent. As a result, it can be concluded that the dynamic behavior of the model specimens observed during the aeroelastic wind-tunnel tests were representative of the behavior which would be exhibited by full-scale cantilevered support structures in the field.

Finally, the magnitudes of the predicted stress ranges at the mast arm and column exceed 42 MPa (6 ksi) for each of the prototype structures. As will be discussed in Sections 2.3 and 2.5, these stress ranges would be in excess of the constant-amplitude fatigue limits for typical cantilevered support structure connection details. As a result, fatigue damage would be expected had these structures experienced galloping- and/or vortex-induced vibrations in the field.

2.2.2.3 Analyses of Actual Support Structures Observed to Gallop in the Field - Finite-element analyses of several full-scale cantilevered support structures were performed to validate the magnitudes of the equivalent static pressure ranges derived from finite-element analyses of the wind tunnel test specimens. The structures included in these analyses were known to have experienced vertical-plane vibrations consistent with galloping. Estimates of at least one dynamic response range was known (either displacements at the tip of the horizontal mast arm or stress measurements) so that the dynamic response observed in the field could be simulated using finite-element analyses. Details of the full-scale support structures are provided in Figures 2.23 through 2.25.

Signal Structure #1 - Figure 2.23 summarizes the details of a cantilevered signal support structure (identified as Signal Structure #1) which was observed to experience vertical-plane vibrations consistent with the galloping phenomenon. The dimensions of Signal Structure #1 are identical to the prototype dimensions of Specimen A (see Figure 2.1) which was tested in the wind tunnel.

Across-wind vibrations of Signal Structure #1 were documented on videotape. Observations of the videotape indicate that the natural frequency of the structure (corresponding to the vertical-plane mode of vibration) was approximately equal to 1.2 Hz. The typical range of vibration of the mast arm was estimated as 254 mm (10 in). During brief increases in wind velocity, the range increased to 610 mm (24 in).

Information obtained from the National Climatic Data Center indicated that the average hourly wind velocity on the day the vibrations were observed was between 11 and 13 m/s (24 to 29 mph) with gust velocities up to approximately 18 m/s (40 mph). As was shown in Section 2.1, these velocities are in good agreement with the velocities at which galloping occurred in Specimen A during the aeroelastic wind-tunnel tests.

Dynamic and static finite-element analyses were performed to determine the magnitudes of the equivalent static pressure ranges required to produce mast-arm dynamic displacement ranges of 254 mm or 10 in (indicated as Run A in Table 2.7) and 610 mm or 24 in (indicated as Run B in Table 2.7). A level of damping equal to 0.75 percent of critical was assumed in each of the dynamic analyses. This

level of damping is a conservative estimate of the level of damping possessed by signal support structures in the field and is specified in the Ontario Highway Bridge Design Code.

As is indicated in Table 2.7, the frequency corresponding to the vertical-plane mode of vibration predicted by finite-elements (1.13 Hz) correlates well with that observed on the videotape (1.2 Hz). The 775 Pa (16.2 psf) equivalent static pressure range required to produce a mast-arm displacement range of 254 mm (10 in) is less than but reasonably close to the equivalent static pressure ranges obtained from finite-element analyses of the wind tunnel specimens (1150 to 1770 Pa). The 1860 Pa equivalent static pressure required to produce a displacement range of 610 mm (24 in) is just greater than that obtained from the wind-tunnel tests. This large displacement was only observed during a short segment of the videotape and most likely corresponds to a brief increase in wind velocity. Therefore, it is not necessary to consider an occasional extreme equivalent static pressure such as this in the design of cantilevered support structures for fatigue. It is the cumulative effect of the response over a few hours that dominates the fatigue damage. However, the occurrence of this higher range of pressure confirms the trend observed in the wind tunnel that the range of the response increases with increasing wind velocity.

Signal Structure #2 - Figure 2.24 summarizes the details of a cantilevered signal support structure (identified as Signal Structure #2) which was subjected to a series of full-scale field tests in a research program conducted by McDonald et al. [13]. The scope of this research program was summarized in Chapter One. The results of these field tests indicated that Signal Support Structure #2 was subjected to a maximum measured stress range in the vertical support (at a location approximately 330 mm (13 in) from the base) equal to approximately 34 MPa (4.9 ksi) under wind velocities in the range of 4.5 m/s (10 mph). The results of vertical-plane free-vibration tests indicated that the natural frequency of the structure was 0.74 Hz and the damping was 0.62 percent of critical.

Static and dynamic finite-element analyses were performed to determine the equivalent static pressure amplitude required to produce a stress range equal to 34 MPa (4.9 ksi) at a location 330 mm (13 in) from the base of the vertical support. The results of this analysis are summarized in Table 2.8. As is indicated, good correlation was obtained between the predicted and measured natural frequencies. An equivalent static pressure range equal to 824 Pa (17.2 psf) was required to produce a stress range in the column equal to 34 MPa (4.9 ksi).

The equivalent static pressure range required to produce the observed dynamic response in this structure is less than the magnitudes of the equivalent static pressure ranges obtained from the wind tunnel test results. This result would be expected considering that the structure tested by McDonald et al. was only subjected to a 4.5 m/s (10 mph) wind velocity. Furthermore, this result highlights the fact that the load to which cantilevered support structures are subjected is a function of the wind velocity. It can reasonably be assumed that this structure would have been subjected to equivalent static lift pressure ranges significantly greater than 824 Pa (17.2 psf) had higher wind velocities been observed during the testing of this structure.

Sign Structure #1 - Figure 2.25 summarizes the details of a cantilevered sign-support structure (identified as Sign Structure #1) which collapsed as a result of the propagation of fatigue cracks in the anchor bolts. Fractographic analyses of the failed anchor bolts indicated that the structure was subjected to vertical-plane oscillations which resulted in anchor bolt stress ranges between 69 and 103 MPa (10 and 15 ksi) [3]. Based on measured critical damping values of 0.6 to 1.2 percent on other cantilevered sign structures [16,17], a level of damping equal to 1 percent of critical was assumed for this structure.

As is indicated in Table 2.9, an equivalent static pressure range of between 862 Pa (18 psf) and 1292 Pa (27 psf) is required to produce anchor bolt stress ranges of 69 MPa (10 ksi) and 103 MPa (15 ksi), respectively. Once again, the magnitude of this equivalent static pressure range correlates reasonably well with the pressure ranges obtained from finite-element analyses of the wind tunnel model specimens.

2.2.2.4 Summary - From the results of these finite-element analyses, the following conclusions can be made regarding galloping and vortex-shedding induced wind loads.

Galloping - The results of finite-element simulations of the wind tunnel experiments indicate that the model cantilevered sign and signal support structures were subjected to equivalent static lift-pressure ranges between 1150 and 1770 Pa (24 and 37 psf) during occurrences of galloping-induced vibrations. These pressures were derived from the maximum loads obtained from the wind tunnel tests (i.e. peak wind tunnel loads). It was observed that the magnitude of the loads increases with wind velocity, such that much larger loads are theoretically possible at higher wind velocities. However, testing was terminated to minimize potential damage to the wind tunnel specimen.

The actual structures for which field observations of galloping were available were subjected to equivalent static pressure ranges from 775 to 1290 Pa (16.2 to 27.0 psf) under continuous steady conditions, with one observation equivalent to a static pressure range of 1861 Pa (38.9 psf) during a brief increase in wind velocity. Thus, the wind tunnel data are conservative and reasonably consistent with respect to the field observations.

Considering the inherent variability in the response of a structure to galloping, the range in equivalent static pressure ranges observed in this study are remarkably consistent. Based upon these results, it is recommended that an equivalent static lift-pressure range equal to 1000 Pa (21 psf) be used in the design of cantilevered sign and signal support structures for galloping-induced fatigue. The value of 1000 Pa (21 psf) is the median (rounded to two significant figures) of the loads from the field observations (775 to 1290 Pa, notwithstanding the one brief excursion of Structure #1). This equivalent static lift-pressure range should be applied vertically as a shear stress on the surface area of all sign and signal attachments mounted to the horizontal mast arm as seen in the normal elevation.

The value of 1000 Pa (21 psf) is at the low end of the loads from the wind-tunnel tests, but the field data are considered more reliable. It is possible that this pressure range is not conservative for all situations. For example, it is theoretically possible, and was demonstrated briefly by Structure #1, that much larger loads could be experienced if the wind velocity increases significantly. However, it is already

a rare occurrence for structures to start galloping, and it was concluded that it would be too conservative to design for anything greater than the peak wind tunnel load or the observed field data. Fatigue calculations using this recommended load (see Appendix B) show that most existing structures would require better details or substantial increases in section properties to resist fatigue from galloping. Therefore, it seems unreasonable to postulate even greater fatigue loads.

Vortex Shedding - The results of finite-element simulations of the wind tunnel experiments indicated equivalent static pressure ranges that were consistent with the load models in the AASHTO Standard Specifications for Structural Supports for Highway Signs, Luminaires, and Traffic Signals, as well as the Ontario specifications. When the attachments are mounted on the structures, galloping occurs preferentially. Therefore, only cantilevered support structures erected without the attachments are susceptible to fatigue damage from vortex-shedding induced vibrations. In all cases however, the magnitude of critical wind velocity (as calculated by the Strouhal relation) must be greater than approximately 5 m/s (10 mph) for significant vortex shedding induced forces to be generated. The vortex-shedding loads should be applied to the mast arm only in the case of signal and sign structures. In most other respects, including the magnitude of the equivalent static lift pressure range, the provisions contained in the present AASHTO Specifications are adequate.

Support Structure¹	Attachment Detail¹	Flow Direction	Natural Frequency² (Hz)	Damping² (%)	Figure³	Flow Velocity⁴ (m/s)	Amplitude Column Moment⁵ (N-m)
A	TS-2D	Rear	6.95	0.12	2.12(b)	18.2	14.7
C	RS-1D	Front	10.00	0.13	2.14(a)	11.2	116.6
C	RS-3D	Front	11.24	0.17	2.15(a)	13.1	54.5
C	None	-	14.10	0.14	2.17	5.5	122.3

¹Specimen and attachment details summarized in Section 2.1.

²As measured from vertical-plane, free-vibration tests.

³Corresponding figure in Section 2.1.

⁴Velocity at which peak vertical-plane response was observed.

⁵Peak column moment amplitude measured at base of vertical support.

Table 2.4 - Observed Wind-Tunnel Test Results.

Support Structure	Attachment Detail	Predicted Natural Frequency (Hz)	Damping (%)	Dynamic Pressure Range (Pa)
A	TS-2D	6.1	0.12	1.02
C	RS-1D	12.4	0.13	1.92
C	RS-3D	13.6	0.17	2.02
D	None	16.6	0.14	5.85

Support Structure	Attachment Detail	Amplitude Column Moment (N-m)	Amplitude Arm Moment (N-m)	Amplitude Column Displacement (mm)	Amplitude Arm Displacement (mm)
A	TS-2D	14.7	10.3	2.5	21.9
C	RS-1D	116.6	83.5	4.1	18.9
C	RS-3D	54.5	38.9	1.9	8.8
D	None	122.3	79.4	4.2	18.6

Table 2.5 - Dynamic Finite-Element Analysis Results of Wind Tunnel Model Specimens.

Support Structure	Attachment Detail	Equivalent Static Pressure Range (1) (Pa)	Estimated Static Pressure Range (2) (Pa)
A	TS-2D	1150	850
C	RS-1D	1770	1480
C	RS-3D	1450	1190
C	None	5100	4180

Support Structure	Attachment Detail	Amplitude Column Moment (N-m)	Amplitude Arm Moment (N-m)	Amplitude Column Displacement (mm)	Amplitude Arm Displacement (mm)
A	TS-2D	14.7	14.6	2.9	31.1
C	RS-1D	116.6	112.9	4.5	23.0
C	RS-3D	54.5	53.2	2.1	11.0
C	None	122.3	115.8	4.8	23.0

Note:

1. Calculated from Equation 2.3
2. Calculated from Equation 2.4

Table 2.6 - Static Finite-Element Analysis Results of Wind Tunnel Model Specimens.

Support Structure	Run Number	Natural Frequency (Hz)	Assumed Damping (%)	Equivalent Static Pressure Range (Pa)	Amplitude Column Moment (N-m)	Amplitude Arm Moment (N-m)
Signal #1	A	1.13	0.75	775	4825	3560
Signal #1	B	1.13	0.75	1861	11600	8550

Support Structure	Run Number	Amplitude Column Displ. (mm)	Amplitude Arm Displ. (mm)	Column Stress Range (Pa)	Arm Stress Range (MPa)
Signal #1	A	15	127	37	57
Signal #1	B	36	305	90	135

Table 2.7 - Dynamic Finite-Element Analysis Results of Full-Scale Cantilevered Signal Support Structure (Signal Structure #1).

Support Structure	Natural Frequency (Hz)	Measured Damping (%)	Equivalent Static Pressure Range (Pa)	Amplitude Column Moment (N-m)	Amplitude Arm Moment (N-m)
Signal #2	0.83	0.62	824	8460	7510

Support Structure	Amplitude Column Displ. (mm)	Amplitude Arm Displ. (mm)	Column Stress Range (Pa)	Arm Stress Range (MPa)
Signal #2	10	151	34	47

Table 2.8 - Dynamic Finite-Element Analysis Results of Full-Scale Cantilevered Signal Support Structure (Signal Structure #2).

Support Structure	Run Number	Natural Frequency (Hz)	Assumed Damping (%)	Equivalent Static Pressure Range (Pa)	Amplitude Column Moment (N-m)	Amplitude Arm Moment Bot. Chord (N-m)
Sign #1	A	1.27	1.0	862	92800	4790
Sign #1	B	1.27	1.0	1292	139200	7190

Support Structure	Run Number	Amplitude Arm Moment Top Chord (N-m)	Amplitude Column Displ. (mm)	Amplitude Arm Displ. (mm)	Column Stress Range (MPa)	Anchor Bolt Stress Range (MPa)
Sign #1	A	912	24	53	20	69
Sign #1	B	1370	36	80	30	103

Table 2.9 - Dynamic Finite-Element Analysis Results of Full-Scale Cantilevered Sign Support Structure (Sign Structure #1)

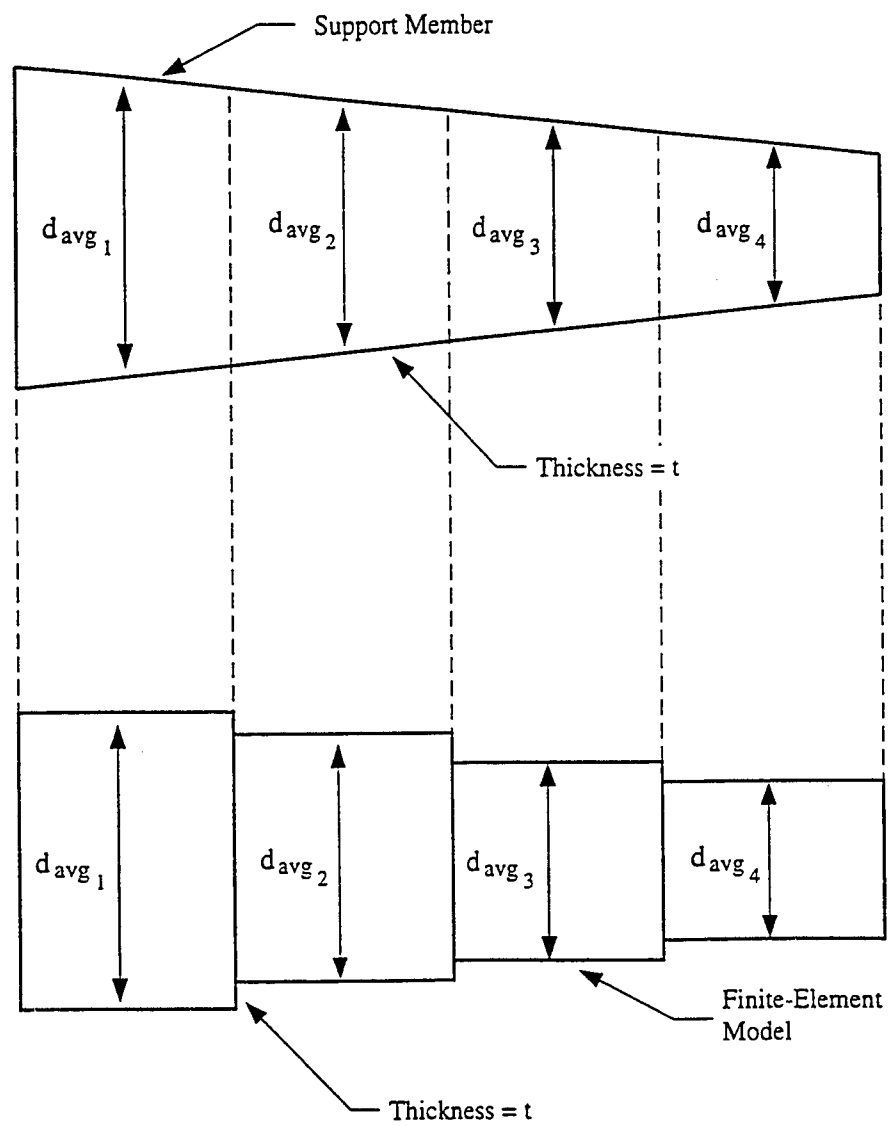


Figure 2.19 - Finite-Element Model of Tapered Members

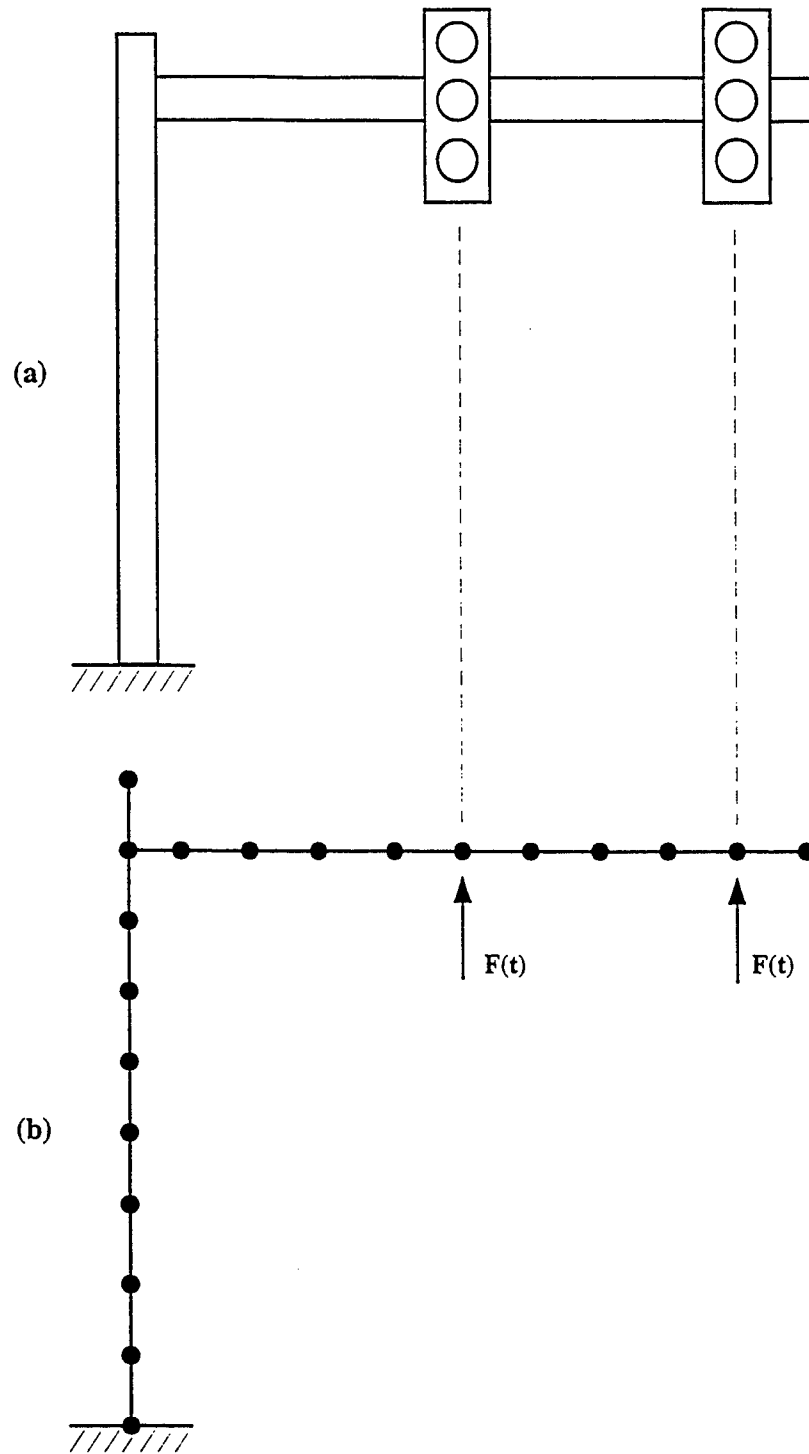


Figure 2.20 - Load Model for Galloping From Signals; (a) Support Structure (b) FEM Model

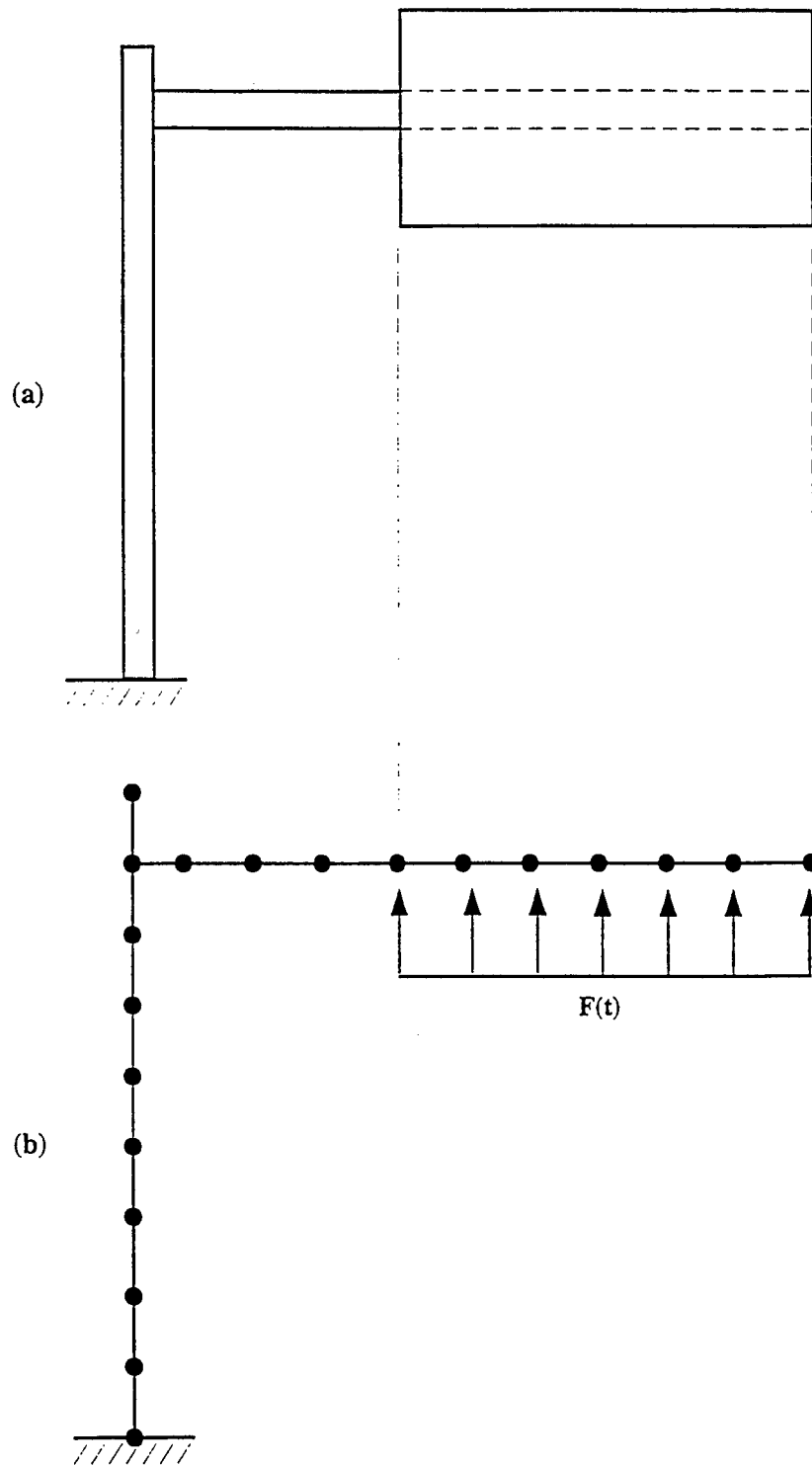


Figure 2.21 - Load Model for Galloping From Signs; (a) Support Structure (b) FEM Model

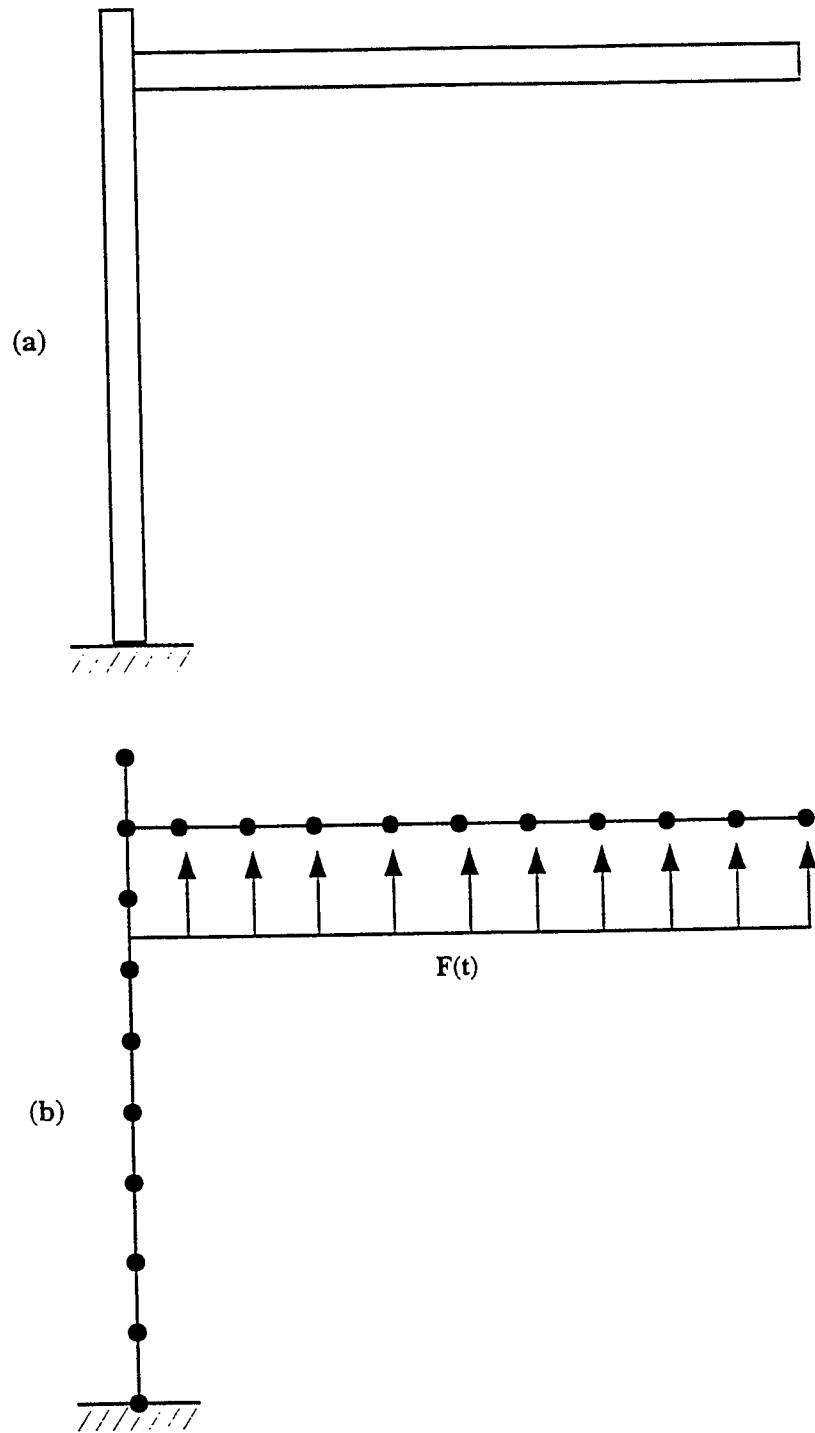


Figure 2.22 - Load Model for Vortex Shedding From Mast Arms; (a) Support Structure (b) FEM Model

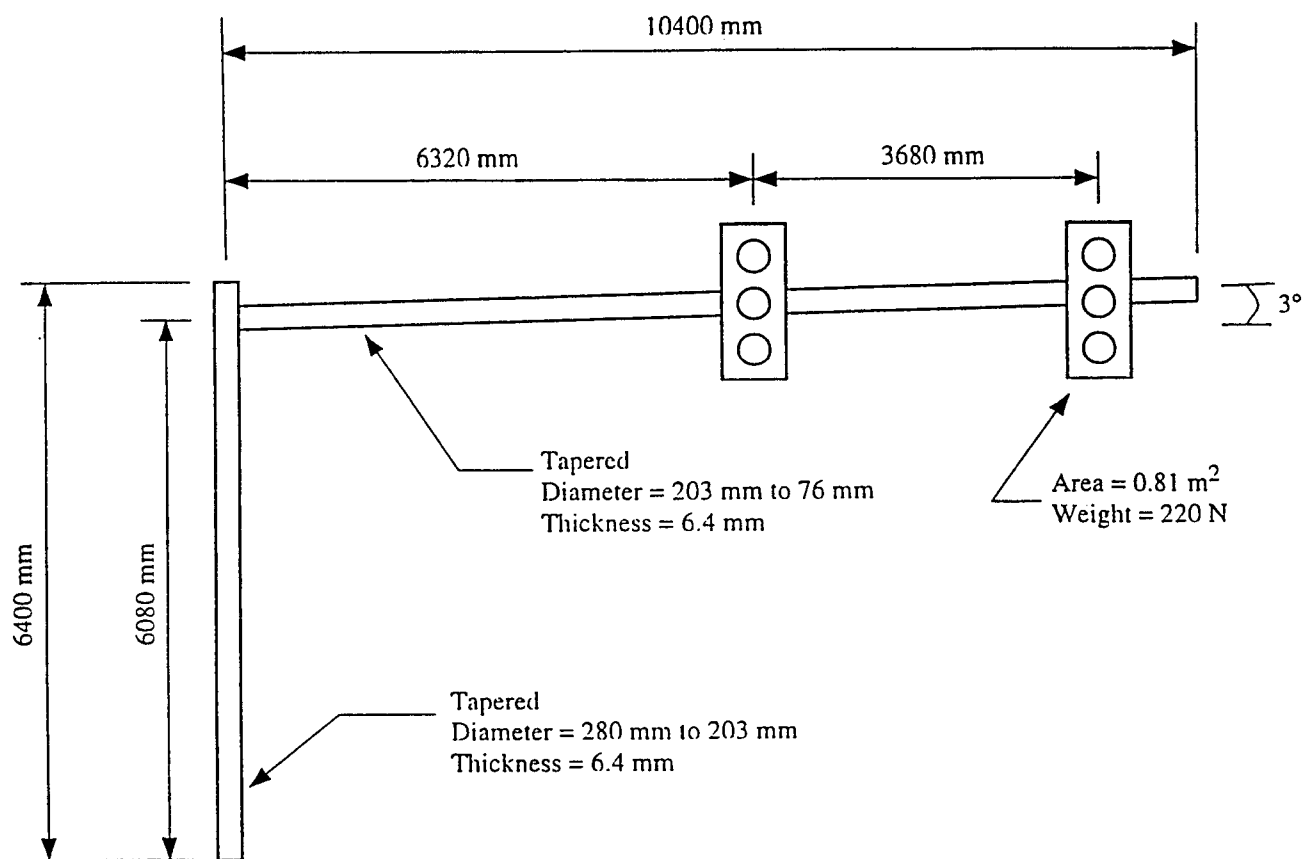


Figure 2.23 - Details of Full-Scale Cantilevered Signal Support Structure (Signal Support #1)

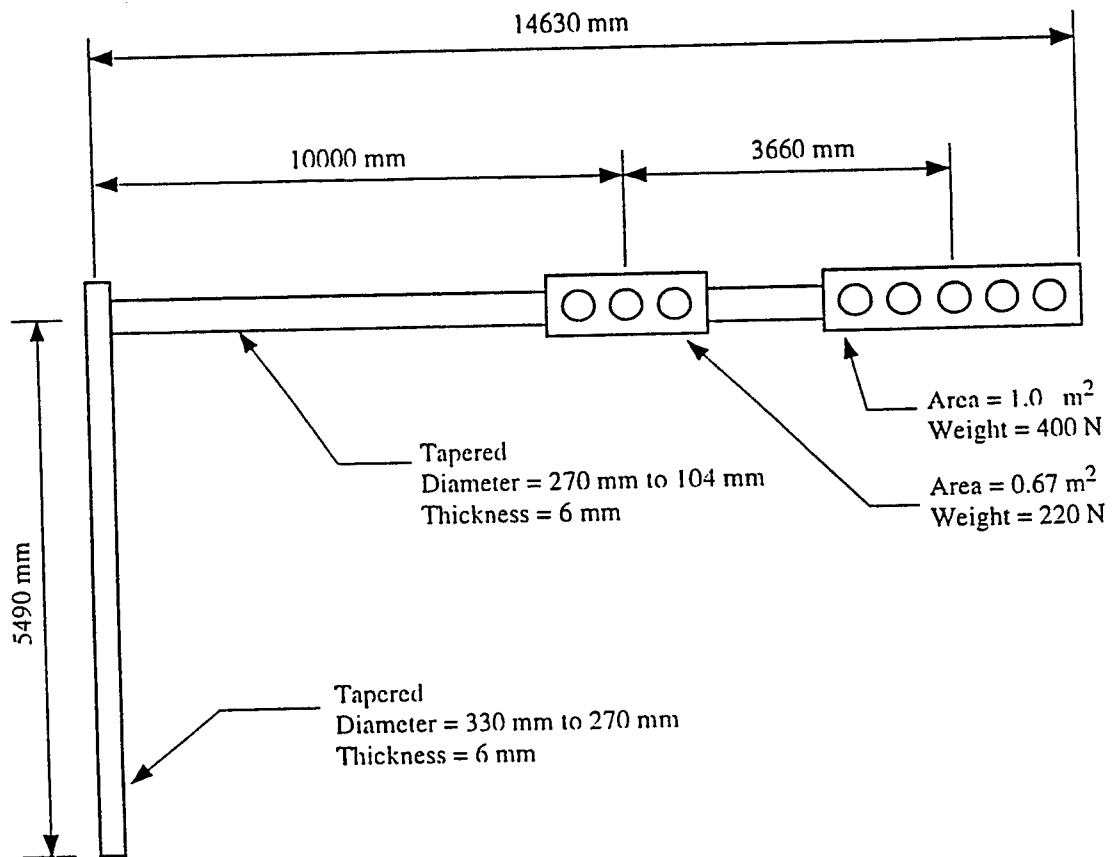


Figure 2.24 - Details of Full-Scale Cantilevered Signal Support Structure (Signal Support #2)

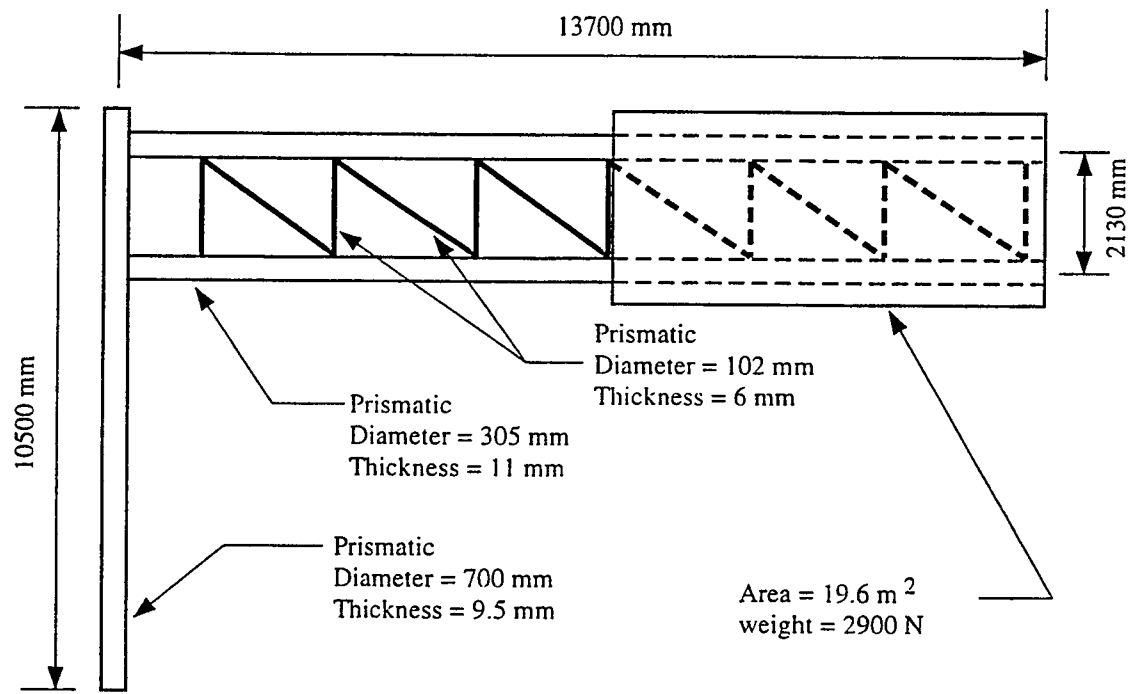


Figure 2.25 - Details of Full-Scale Cantilevered Sign Support Structure (Sign Support #1)

2.2.3 Spectral Analyses to Simulate Natural Wind Gusts

The response of typical cantilevered support structures to natural wind gusts was modelled using spectral finite-element analysis. Spectral analysis is explained in detail in many textbooks and handbooks, (e.g. References 9 and 15). The structure is broken up into several continuous areas such as signs or exposed portions of the structure. The fluctuating wind force on each area and the resulting response variables (such as column base moment) during a short interval are characterized as random processes with stationary means. In this case, the force is represented by a spectrum, i.e. the variation of the force as a function of frequency. The linear modal analyses (such as described in the previous section) are used as a transfer function to relate the value of the force spectrum at a particular frequency to the value of the response spectrum at that frequency. The response spectrum can be related back to the expected variable-amplitude history of the response as a function of time. Specifically, the root-mean-square (RMS) of the random response time history is found from the integration of the response spectrum over all significant frequencies. In the case of cantilevered support structures, there are only a few significant frequencies, so the integration is performed by simply summing the response at these frequencies.

The wind force spectrum is derived from the velocity spectrum. A standard wind velocity spectrum (which depends on the mean hourly wind velocity) was selected from the literature [28].

$$S_v(f) = \frac{4 K V_{10}^2 x^2}{f(1+x^2)^{4/3}} \quad (2.5)$$

where $S_v(f)$ is the spectral density of the velocity (which has units of velocity squared multiplied by time), f is the cyclic frequency (cps), K is a terrain coefficient (m/s^2), V_{10} is the mean wind velocity (m/s) at a reference height of 10 meters, and x is the quantity $(1200 \text{ meters} * f)/V_{10}$ (dimensionless for V_{10} in m/s). The terrain coefficient K was taken as 0.005 which is typical for open grassy terrain [28,31].

The drag force is proportional to the square of the velocity and both the force and the velocity can be represented as the sum of their mean and fluctuating components. Through algebraic manipulation of these relationships, the following relations can be obtained [31]:

$$\left(\frac{d}{v}\right)^2 = \frac{4 D^2}{V^2} = 4 C^2 A^2 V^2 \quad (2.6)$$

where d and D are the fluctuating and mean value of the drag force respectively, v and V are the fluctuating and mean value of the wind velocity respectively, A is the total frontal area of the surface which is causing the drag, and C is a constant equal to $0.5\rho C_d$ with ρ equal to the density of air and C_d equal to the drag force coefficient. The density was taken as 1.22 kg/m^3 which is the value for "standard air" (one atmosphere pressure at 14°C).

The force and velocity spectra are proportional to the square of the fluctuating components of force or velocity, therefore the ratio of these spectra is equal to the ratio in Equation 2.6, i.e.:

$$S_F(f) = 4 C^2 A^2 V^2 S_v(f) \quad (2.7)$$

The force spectrum must be calculated for the total frontal area of a surface and cannot be broken down into sub-areas. One spectrum is calculated for each sign and signal attachment. Additional spectra are calculated for each continuous exposed portion of the mast arm or column. These spectra must be completely correlated to each other in the analysis.

Important assumptions must be made regarding: 1) the mean wind velocity at which the support structures should be analyzed; and, 2) estimating the effective stress range from the RMS of the variable amplitude response. It is impractical to forecast the future wind history at each location for cantilevered support structures. Therefore, some very simple assumptions were made as explained below. The analyses discussed below and fatigue design calculations shown in Appendix B show that the assumptions appear reasonable. These calculations indicate that most structures will eventually be susceptible to cracking from natural wind gusts, but the recommended loads are not so large as to predict rapid failure. These results are consistent with observed service fatigue failures which can be attributed to natural wind gusts. Because of the uncertainty in these assumptions, the recommended equivalent static load range can be easily adjusted for other mean wind speeds.

The strategy for analyzing the natural wind gust loading is made easier by the "infinite-life" approach for variable amplitude fatigue. As explained in Chapter One, the "infinite-life" approach for variable amplitude fatigue involves comparing a fatigue "limit-state" stress range with only 0.01 percent exceedence to the constant-amplitude fatigue limit (CAFL). Therefore, the only result required from the analyses of natural wind gusts is an estimate of the limit-state stress range with 0.01 percent exceedence. However, there is no established way (and many possible ways) to estimate this limit-state stress range.

It was decided to idealize the wind loading as having a stationary mean velocity over one-hour periods. The limit-state stress range was defined as the average stress range resulting from a spectral analysis using the "limit-state" mean hourly wind velocity, i.e. the mean hourly wind velocity which was exceeded in only 0.01 percent of all hours.

It is accepted that the probability of exceedence of mean hourly wind velocity at a location is a Rayleigh distribution which depends only on the yearly mean wind velocity V_m [15], i.e.:

$$P_E(v) = e^{\frac{-\pi v^2}{4V_m^2}} \quad (2.8)$$

where $P_E(v)$ is the probability that a randomly occurring mean hourly velocity is greater than the velocity magnitude "v" and e is the base of the natural logarithms. The limit-state mean hourly velocity is found by setting P_E equal to 0.01 percent and solving for "v." Figure 2.26 shows that the result is a linear relation such that the limit-state hourly velocity is 3.4 times the annual mean wind velocity.

The yearly mean wind velocity also varies from place to place. A collection of yearly mean wind speed data from weather stations at 59 cities across the U.S. was examined. Most weather stations are

located at airports, therefore the data should be representative of most open terrain. The data showed that 81 percent of the cities had a mean wind velocity at 10 m (33 ft) above the ground less than 5 m/s (11 mph), and 98 percent of the cities had a mean wind speed less than 5.8 m/s (13 mph). The cities with greater annual wind speeds are generally in the Plains states from North Dakota to Oklahoma. It was decided to use 5 m/s (11 mph), which was exceeded in only 19 percent of U.S. cities, as the baseline case for a static design pressure in the specifications. As shown in Figure 2.26, the limit-state velocity for this yearly mean wind speed is 17 m/s (37 mph).

As a further indication that these assumptions are reasonable, 17 m/s is a relatively high wind velocity in comparison to wind speeds at the time of galloping events reported in the previous section. For example, the field test of a cantilevered signal support structure at Texas Tech University in Lubbock Texas took place when the mean wind velocity was approximately 5.5 m/s (12 mph) [13]. Signal Structure #1 (discussed previously in Section 2.2.2.3) vibrated when the mean hourly wind velocity was in the range of 11 to 13 m/s (24 to 29 mph).

Spectral analyses were performed over a range of mean hourly wind velocities for the same characteristic signal, sign and luminaire support structures that were analyzed for galloping and vortex shedding. The analyses on luminaires is particularly important because if the luminaire column is tapered, vortex shedding does not have to be checked, and natural wind gusts constitute the most likely dynamic wind loading to govern the design. (Some luminaires may gallop due to forces on the small cantilevered fixture. Also, some luminaires located on bridges may vibrate from the bridge response to traffic loads.) Signals and signs, on the other hand, are susceptible to galloping which gives much larger stress ranges and will therefore control the design in most cases. However, mitigation of galloping, if proven, may eliminate the need to check the design for galloping. In this case, natural wind gusts will govern the fatigue design of these structures as well.

The result of the analysis, the spectral density of the response, has units of the response (such as moment or stress) squared multiplied by time. When the spectral density of the response is integrated across a range of frequencies, the result (the area under the spectrum) is equivalent to the variance of the response about the mean. The square-root of this area is the root-mean-square (RMS) of the response. The time history of the response is narrow-banded (concentrated about one frequency), since the response is still dominated by the resonant frequency. For random, narrow-band time histories, the average or effective stress range S_r^{eff} can be estimated from the relationship which gives the stress range for a constant-amplitude response in terms of the RMS of the stress response, σ_{rms} [9], i.e.:

$$S_r^{eff} = 2.8\sigma_{rms} \quad (2.9)$$

Signal structure #2 was analyzed for a range of mean hourly wind velocities using the above procedures and assumptions. Signal structure #2, which was also analyzed for galloping as described in the previous section, has a mast arm length of 14.6 m (48 ft) and therefore is representative of these types of structures. Figures 2.27a and 2.27b show the effective stress ranges as a function of the mean hourly wind velocity at (a) the mast arm connection and (b) at the column base. Typically, these are Category

E' details with a CAFL of 18 MPa or 2.6 ksi (see Section 2.5) which govern the fatigue design of signal support structures. At the limit-state velocity of 17 m/s (37 mph) the mast arm and column limit-state stress ranges are 36 and 14 MPa (5.2 and 2.0 ksi), respectively. Thus, under these loads, the mast arm connection would have to be redesigned to lower the stress range or increase the fatigue strength through choice of a better detail. The column stress range appears to be acceptable.

The static pressure range recommended in the specification was determined from static finite-element analysis and is calibrated to give the effective limit-state stress ranges determined from the spectral analyses. For design, the natural wind gust pressure must be applied to a variety of surfaces with widely varying drag coefficients. Therefore the recommended static design pressure must be multiplied by the appropriate drag coefficient and then may be applied to the surface. Figure 2.28 shows the equivalent static pressure range for design, which has been normalized by the drag coefficient. At the limit-state hourly mean wind velocity of 17 m/s (37 mph), the normalized pressure is 240 Pa (5 psf).

The nonlinearity of the response with respect to the increasing wind velocity is evident in Figure 2.28, indicating that the design static pressure will be very sensitive to the choice of the mean annual wind velocity. In fact, the response increases approximately with the square of the annual mean wind velocity. This fact has been used in the proposed specification commentary to allow adjusting the recommended normalized static pressure range, derived for an annual mean wind speed of 5 m/s (11 mph), for locations with other annual mean wind speeds.

Figure 2.29 shows the response of a truss-type cantilevered sign-support structure #1 which was also analyzed for galloping as described in Section 2.2.2.3. The figure shows the effective stress ranges as a function of the mean hourly wind velocity at (a) the bottom chord of the truss and (b) at the column base. Typically, these are also Category E' details with a CAFL of 18 MPa (2.6 ksi). At the limit-state velocity of 17 m/s (37 mph) the truss chord and column limit-state stress ranges are 65 MPa (9.5 ksi) and 32 MPa (4.6 ksi) respectively which exceed the CAFL and would require redesign. Figure 2.30 shows the equivalent static pressure range for design, which has been normalized by the drag coefficient. At the limit-state hourly mean wind velocity of 17 m/s (37 mph), the normalized pressure is 300 Pa (6.3 psf).

Figure 2.31 shows the response of a luminaire support structure which is 10 m (33 ft) high and carries a single 2.4 m (8 ft) long mast arm. Again, the mast arm and column base details are typically Category E' details. At the limit-state velocity of 17 m/s (37 mph) the mast arm stress range is acceptable but the column base stress range is just slightly above 18 MPa (2.6 ksi). Figure 2.32 shows the normalized equivalent static pressure range for design at the limit-state hourly mean wind velocity of 17 m/s (37 mph) is 170 Pa (3.5 psf).

The last example is a 21 m (70 ft) luminaire pole structure. Figure 2.33 shows the effective stress ranges at the column base (an E' detail) as a function of the mean hourly wind velocity. Results for 1 and 2 percent critical damping are shown, because these structures are often fitted with dampers but the effective damping is unknown. At the limit-state velocity of 17 m/s (37 mph) the column base stress range is about 60 MPa (8.7 ksi) for the case of 2 percent damping, which is much greater than the CAFL.

Figure 2.34 shows the normalized equivalent static pressure range for 2 percent damping for the limit-state hourly mean wind velocity of 17 m/s (37 mph) is 240 Pa (5 psf).

The values of normalized equivalent static pressures for each of the four structures ranged from 170 to 300 Pa (3.6 to 6.3 psf) and are remarkably consistent considering the extremely different types of structures. Considering the numerous uncertainties in this analysis, not enough is known to assign greater or lesser loads to different types of structures. Also, separate loading for different types of structures would unnecessarily complicate the design process. Therefore, these values were averaged and rounded to 250 Pa (5.2 psf), which is recommended in the proposed specification for design.

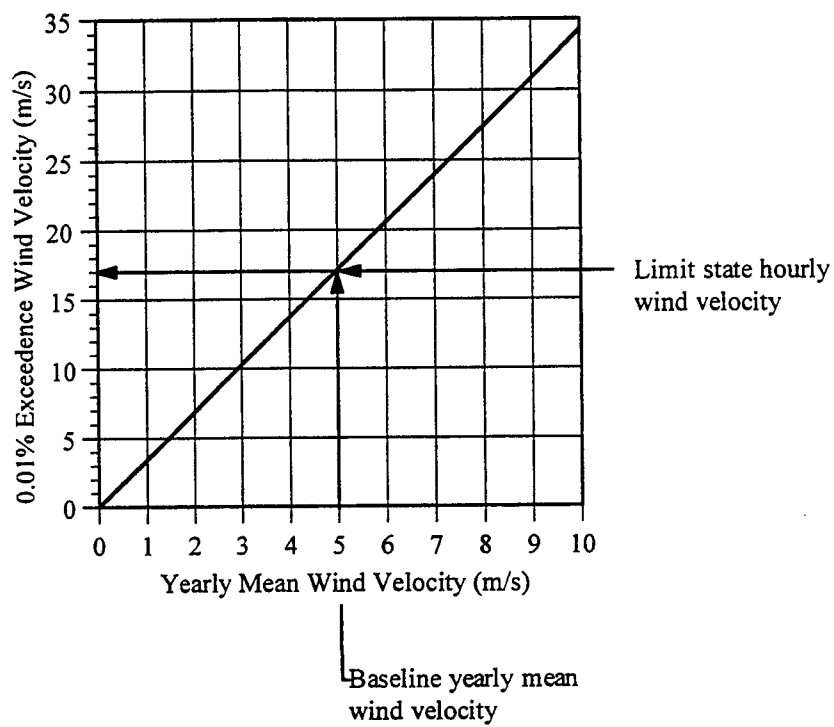
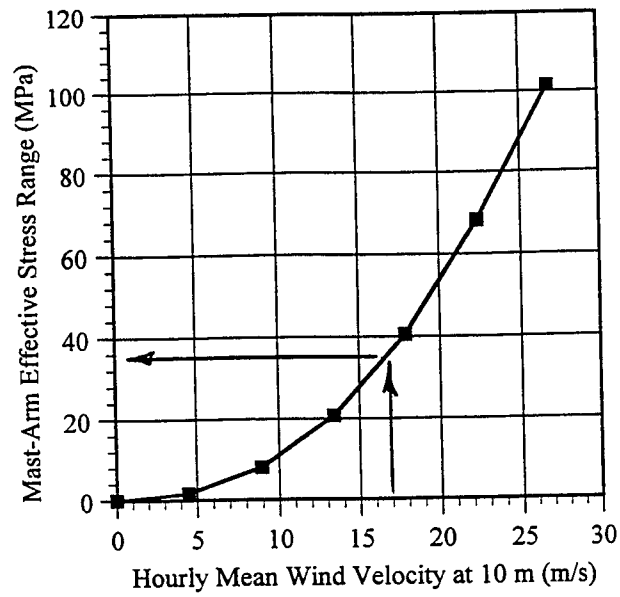
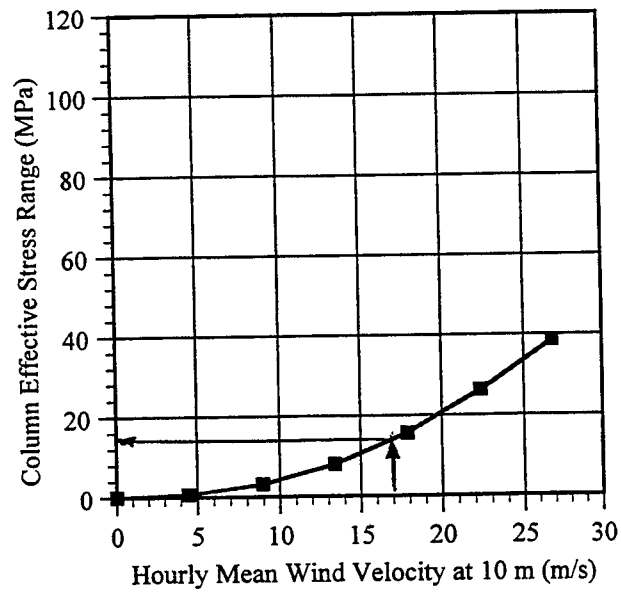


Figure 2.26 - Exceedence (0.01%) Wind Velocities at Various Yearly Mean Wind Speeds



(a)



(b)

Figure 2.27 - Dynamic Response of Cantilevered Signal Structure to Natural Wind Gusts (a) Mast Arm
(b) Column Base

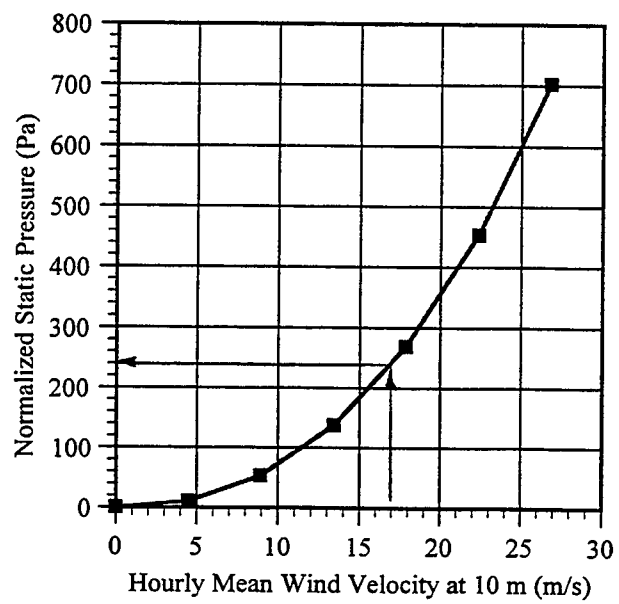
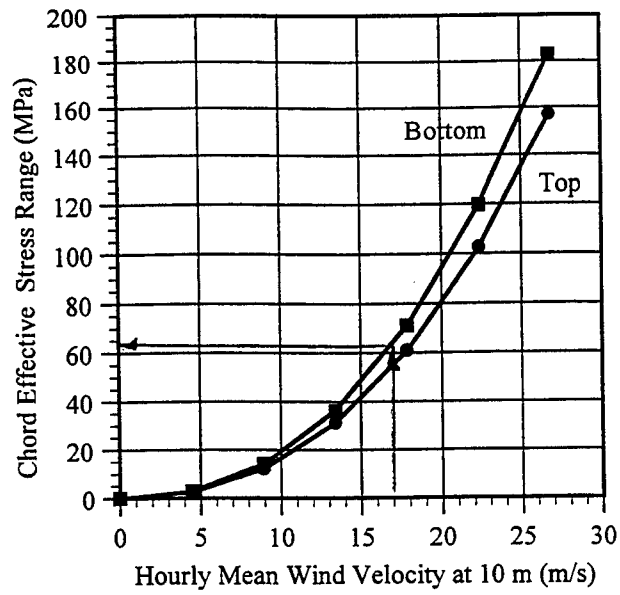
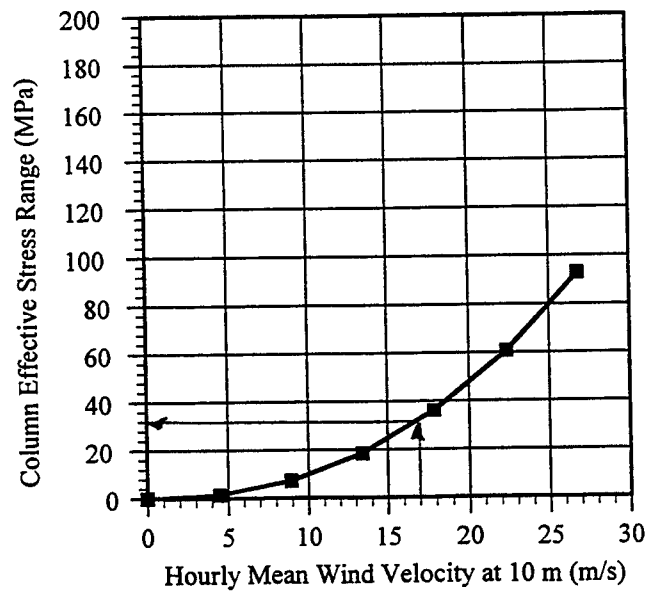


Figure 2.28 - Normalized Natural Wind Gust Static Pressures (Signal Structure)



(a)



(b)

Figure 2.29 - Dynamic Response of Cantilevered Sign Structure to Natural Wind Gusts (a) Mast Arm Chord (b) Column Base

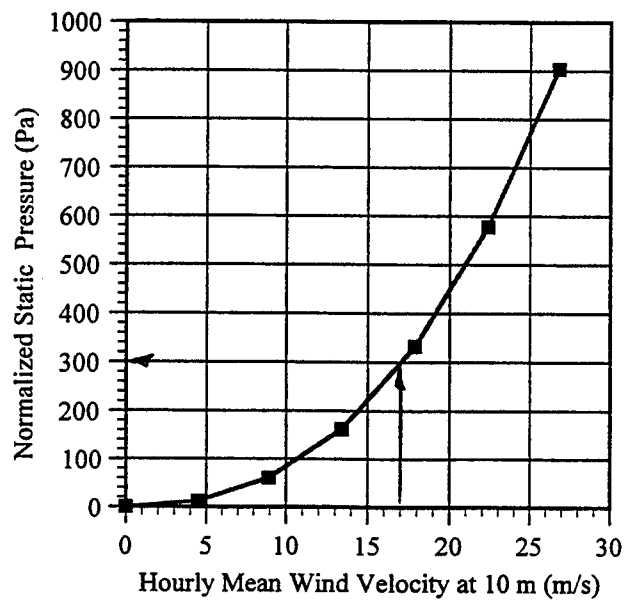
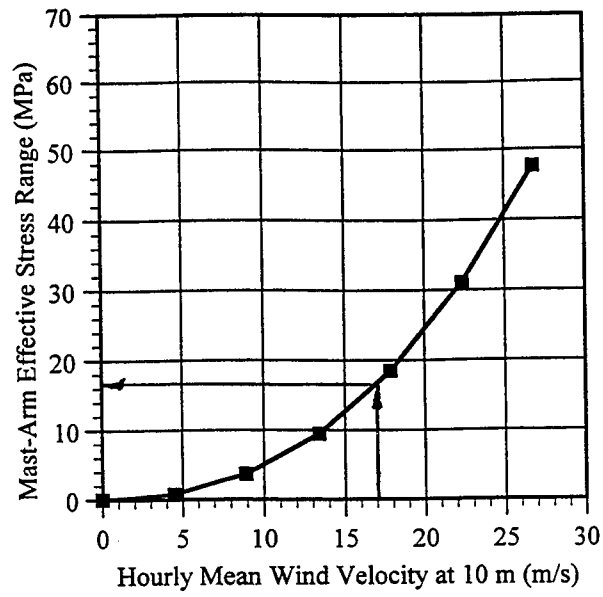
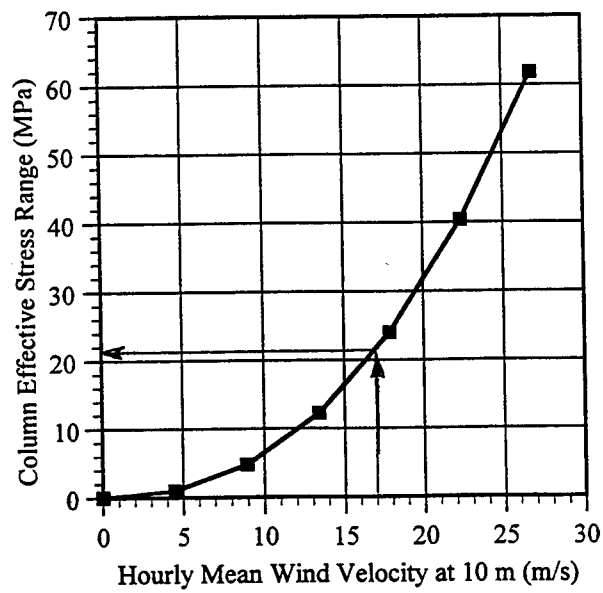


Figure 2.30 - Normalized Natural Wind Gust Static Pressures (Sign Structure)



(a)



(b)

Figure 2.31 - Dynamic Response of Cantilevered Luminaire Structure to Natural Wind Gusts (a) Mast Arm (b) Column Base

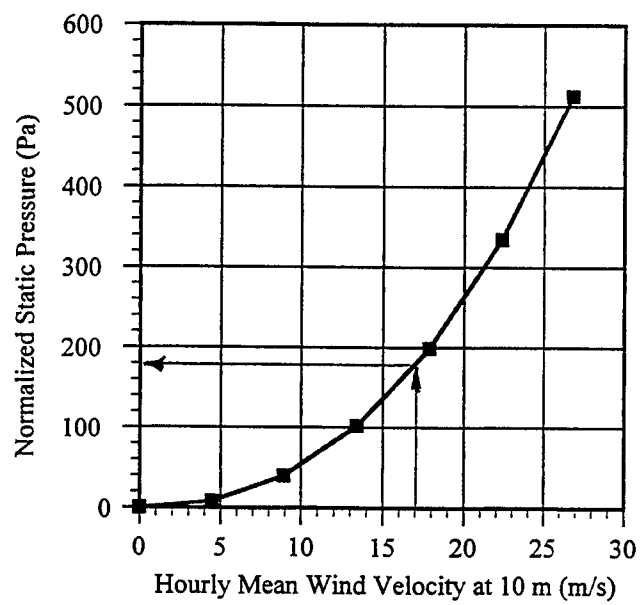


Figure 2.32 - Normalized Natural Wind Gust Static Pressures (Luminaire Structure)

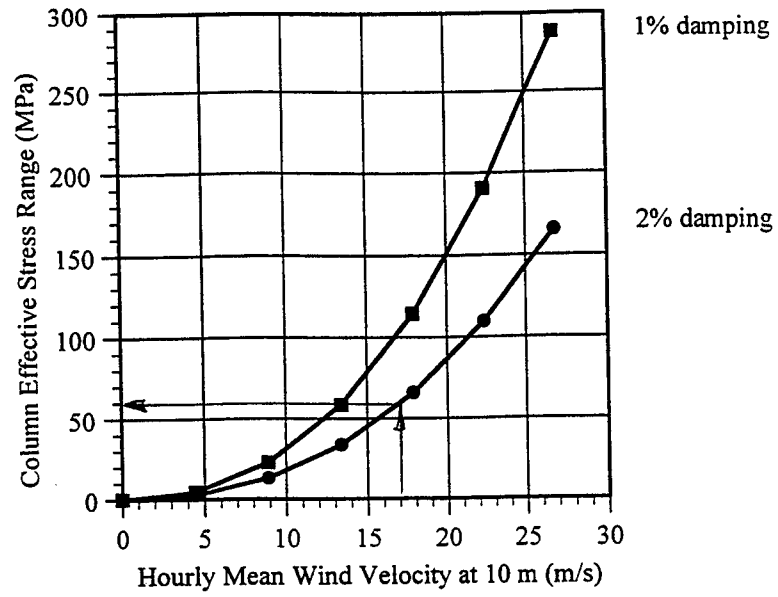


Figure 2.33 - Dynamic Response of 21 m Luminaire Pole to Natural Wind Gusts

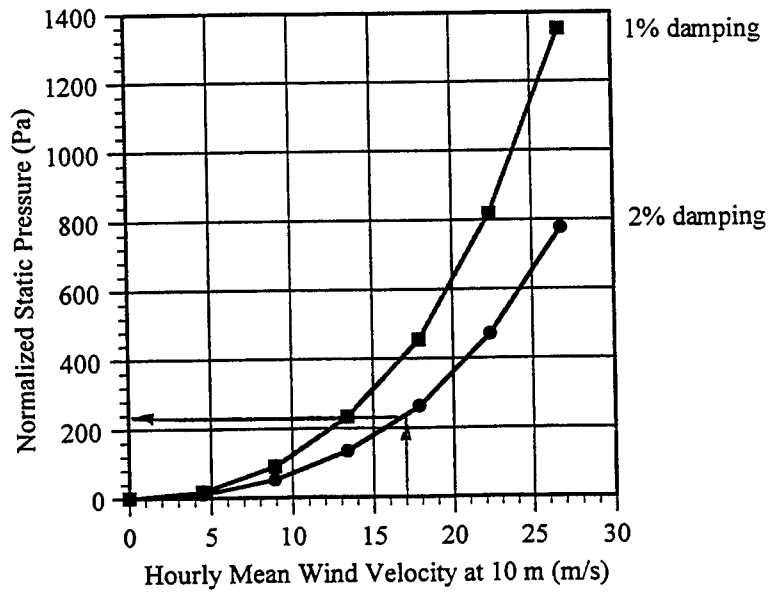


Figure 2.34 - Normalized Natural Wind Gust Static Pressures (21 m Luminaire Pole)

2.2.4 Static Pressure Range for Truck-Induced Gusts

A different type of time-domain dynamic analysis was used to analyze the transient effects of truck gusts. These calculations used the pressure distributions and ramping functions proposed by Creamer et al. [17]. As mentioned in Chapter One, the stress ranges obtained from these field studies were consistently below levels which would lead to fatigue damage. As part of this research, a range of cantilevered sign and signal support structures was analyzed, including fatigue damaged variable-message signs (VMS). The resulting stress ranges caused by loads in both the horizontal and vertical direction were very small and in agreement with previous results, but not consistent with the failures that have occurred. Therefore, it can be concluded that the pressure distribution model proposed by Creamer (at least in the vertical direction) does not accurately represent current truck-induced gust loads.

More recently, an alternative load model for truck gusts was proposed by Desantis [20]. This model is based on the fact that many trucks are now outfitted with deflectors to divert the wind flow upward and minimize the drag created by the trailer. A simple model has been proposed to represent the vertical gust pressure as that imposed by a 105 kph (65 mph) wind to coincide with existing vehicle speed limits. Simply stated, it is assumed that the velocity of the wind in the upward direction is equal to the truck velocity.

The equivalent static truck-gust pressure is determined by utilizing the static wind pressure formula currently in the Specification where $V = 105$ kph (65 mph) and $C_h = 1.0$. To account for an increase in the relative truck speed due to head winds, the gust factor of 1.3 is also included. Since the applied truck gust pressure will lift the mast arm vertically, the pressure obtained above is doubled to represent the entire truck gust pressure range. This doubling of the pressure is based on the assumption that on the first cycle the downward and upward forces are equal. Based on these assumptions, an equivalent static vertical pressure range of 1760 Pa (36.6 psf) can be obtained. This pressure must be multiplied by the appropriate drag coefficient and horizontally projected area to determine the proposed vertical truck-gust load. As discussed in Section 3.2, the pressure should be applied along the length of the sign panel or 3.7 m (12 ft), whichever is greater.

Two variable message sign (VMS) structures which have recently experienced fatigue failures were selected for analysis. One structure was observed vibrating immediately after installation and had developed fatigue cracks after approximately 6 months of service, while the other structure failed after approximately 18 months of service. From analysis, the column-to-base plate connection was identified as the most fatigue sensitive detail on each structure. Stress ranges of 94 MPa (13.6 ksi) and 48 MPa (6.9 ksi) were calculated at these locations using the proposed truck-induced gust loads. As discussed in Section 2.5, these details are typically classified as Category E' with a constant-amplitude fatigue limit of 18 MPa (2.6 ksi). Since the stress ranges for each structure were in excess of the constant-amplitude fatigue limit, fatigue cracking would be expected. Using this information, life prediction calculations were performed for each structure using Equation 6.6.1.2.5-1 in the AASHTO LRFD Bridge Design Specification and the results were consistent with the relative service lives prior to failure. Therefore, the simple static load model described above appears reasonable to use for design purposes.

2.2.5 Recommendations for Fatigue Loads

The results of the analytical research reported herein indicate that:

- The static load model for vortex shedding of simple poles in the AASHTO Standard Specifications for Structural Supports for Highway Signs, Luminaires, and Traffic Signals is adequate and applicable to the vortex-induced vibrations of non-tapered luminaire support structures. All other types of luminaires and cantilevered support structures should not exhibit a significant response to vortex shedding.
- Cantilevered sign and signal support structures should be designed for galloping-induced loads using an equivalent static shear pressure range of 1000 Pa (21 psf) which is applied vertically to the vertically projected area of any sign and/or signal attachments rigidly mounted to the horizontal mast-arm.
- Sign and signal support structures should also be designed for truck-induced gust loads using an equivalent static pressure of 1760 Pa (36.6 psf) times the drag coefficient which is applied vertically to the horizontally projected area of the structural members and any attachments mounted to the horizontal mast arm along a length of the mast arm which is the greater of the length of the sign or 3.7 m (12 ft).
- All types of cantilevered sign, signal, and luminaire support structures should be designed for natural-wind-gust loads using an equivalent static pressure range of 250 Pa (5.2 psf) times the drag coefficient which is applied horizontally to the projected area of any exposed portions of the structure and the attachments.

2.3 ANCHOR BOLT FATIGUE TESTS

As was discussed in Chapter One, previous research [32,33,34] indicates that the fatigue strength of welded details is primarily dependent on two parameters: (1) nominal stress range and (2) notch severity. Notch severity is a function of the stress concentration associated with the detail, local weld geometry, and weld discontinuities. Experience with the behavior of welded components under the application of repeated loading indicates that details which possess similar stress concentrations (e.g. the toe of a weld) and are subjected to similar loading (e.g. nominal stresses normal to the axis of the weld) will behave in a similar manner even though the physical appearance of these details may be significantly different. These similarities in the fatigue cracking mode of various welded details are exploited to associate most of the details in cantilevered support structures with existing details categories in the AASHTO bridge specifications and the AWS D1.1 structural welding code.

The association is less certain for some detail types. Anchor bolts are especially unique with respect to their fatigue behavior. For example, fatigue cracking in anchor bolts initiates at the thread root. The stress concentration and type of discontinuities at the root of a thread are significantly different than the stress concentration and discontinuities associated with the welded details which are the primary emphasis in AASHTO and AWS. Furthermore, being non-welded structural components, the fatigue strength of anchor bolts is influenced by parameters which do not significantly influence the fatigue strength of weldments, e.g. mean stress level and yield strength of the steel. For example, the mean applied stress level typically has no effect on welded details because these details have high tensile residual stresses near the weld, whereas the residual stresses at the root of the threads is less tensile and may even be in compression. Therefore, the effect of mean stress, which may also be referred to as the effect of minimum stress or the effect of maximum stress, is likely to be more pronounced in anchor bolts. As a result, existing knowledge of the fatigue strength of welded details cannot be used to predict anchor bolt fatigue strength.

Several research programs, which will be summarized in Section 2.3.1.1, have been previously conducted to evaluate the fatigue strength of anchor bolts. The results of these research programs indicate that the lower-bound fatigue strength of axially loaded, snug-tight anchor bolts is consistent with the AASHTO Category E' fatigue design curve in the region of finite life (e.g. less than two million cycles). Similarly, the fatigue strength of axially loaded, fully tightened anchor bolts in the region of finite life has been found to be consistent with the AASHTO Category E fatigue design curve. No data, however, had previously been acquired below a stress range of approximately 69 MPa (10 ksi). As a result, the constant-amplitude fatigue limits (CAFL) for snug-tight and fully tightened anchor bolts was unknown.

Just because the lower bound of the finite-life data above 69 MPa (10 ksi) agreed relatively closely with either the E or E' curves, this does not necessarily imply that the CAFL should be the same as the CAFL for Categories E and E'. Categories E and E' were originally derived for welded attachments and cover plates. As discussed above, the residual stress, stress concentration, and discontinuities associated with anchor bolts are different from those for welded attachments and cover

plates. These factors may affect the CAFL in a way that they do not affect the S-N curve in the finite-life region.

In the "infinite-life approach" described in Section 1.3, it is explained that it is the CAFL that is needed for fatigue assessment and that the finite-life portion of the S-N curve is of secondary importance. Therefore, given the importance of the CAFL and the lack of data, a series of fatigue tests were conducted within the scope of the current research program to extend the existing anchor bolt fatigue database into the infinite life region.

Specifically, the objective of these tests was to determine a lower-bound estimate of the CAFL of double-nutted (i.e. anchor bolts configured with one nut on either side of the baseplate), snug-tight anchor bolts subjected to axial tension. In order to accomplish this objective, the test program was arranged so as to evaluate the effects of: (1) maximum stress (or mean stress), (2) yield strength, (3) thread forming method, (4) bolt pretension, and (5) misalignment. The fatigue design recommendations presented in Section 2.3.4 are based upon a worst-case condition so that the effects of these secondary variables need not be explicitly considered in the design process. Material property tests were also performed to ensure that the strength, ductility, and fracture toughness of the specimens obtained for this study were in accordance with existing anchor bolt material property specifications.

The effects of bolt diameter, thread series, and galvanizing were not explicitly considered in the experimental program. A review of previous research (described in Section 2.3.1.1) indicated that these variables do not significantly influence the fatigue strength of anchor bolts. Furthermore, the influence of thread fit on the fatigue strength of anchor bolts was not specifically considered within the scope of the test program. Rather, thread fit was considered a random variable incorporated in the sample of test specimens, which were purchased from two suppliers which used different manufacturing techniques (rolled vs. cut threads).

Section 2.3 is organized into four sub-sections. Sub-Section 2.3.1 provides a summary of the previous research pertaining to anchor bolt fatigue strength and discusses the provisions for the design of bolts for fatigue which are contained in existing design specifications. Sub-Section 2.3.2 summarizes the specimen details, experimental set-up, and test procedures used in this test program. The results of the fatigue tests are presented and discussed in Sub-Section 2.3.3. Finally, recommendations for the design of anchor bolts for fatigue are presented in Sub-Section 2.3.4.

2.3.1 Background

2.3.1.1 Previous Research - Frank [35] performed fatigue tests to evaluate the effects of type of steel, thread series, nominal diameter, galvanizing, thread forming method (i.e. cut vs. rolled), and stress range on the fatigue strength of snug- and fully tightened anchor bolts subjected to axial tension. In Frank's tests, snug was defined by a level of torque equal to 271 N-m (200 ft-lb). Fully tightened was defined as one-third-of-a-turn beyond snug. The tests included anchor bolts fabricated from ASTM A36, ASTM A193 Grade B7, and AISI 4340 (heat treated) steels in nominal diameters ranging from 35 mm to 51 mm (1.375 to 1.5 in). Thread series consisting of 8UN, 6UNC, and 4½UNC were included in the

test program. Single- and double-nutted anchor bolts were also considered. Frank conducted each of the fatigue tests at a maximum stress corresponding to 75 percent of the minimum specified yield strength of the material.

The results of Frank's research indicated that the effects of nominal diameter, thread series, galvanizing, type of steel, and thread forming method were negligible with respect to the fatigue strength of anchor bolts. The results of tests on the fully tightened specimens indicated that tightening of the nuts to one-third-of-a-turn beyond snug resulted in increased fatigue strengths as compared to the double-nutted, snug-tight specimens and the single-nut specimens. Failure of the single-nut specimens was consistently observed to occur at the first engaged thread of the exterior nut. Failure of the double-nutted, snug-tight specimens was observed at either: (1) the first engaged thread of the exterior nut or (2) at multiple threads within the exterior nut. Tightening of the double-nutted anchor bolts to one-third-turn-beyond snug was found to shift the mode of failure to the threaded region outside of the connection (i.e. below the leveling nut).

The shift in failure mode from the first engaged thread of the exterior nut to the threaded region below the leveling nut in fully tightened, double-nutted anchor bolts can be attributed to a variation in the distribution of the applied load which occurs in the fully tightened connection. In double-nutted, snug-tight anchor bolts subjected to axial tension, the entire applied load range is carried by the exterior nut. Furthermore, a majority of the load is transferred to the bolt at the first engaged thread. As a result, the first engaged thread is subjected to the largest stress range and is the critical location with respect to the initiation of fatigue cracks. Tightening of the double-nutted connection to one-third-of-a-turn beyond snug pretensions the short length of bolt between the interior and exterior nuts, creating a clamping force which results in a more even distribution of the applied load between the exterior and interior nuts. This effect was evident in strain gage measurements made by Frank during testing of the fully tightened, double-nutted anchor bolts. These measurements indicated that approximately one-third of the applied load was taken by the interior nut. Furthermore the distribution of load within the nuts of fully tightened, double-nut connections is more uniform (i.e. the transfer of load is not concentrated at the first engaged thread). As a result, the critical location for the initiation of fatigue cracks in fully tightened, double-nutted anchor bolts shifts from the first engaged thread of the exterior nut to the free-length of bolt below the leveling nut which is not subjected to pretensioning.

The beneficial effects of pretension in conventional bolted connections loaded in tension is well known and is described extensively in Reference 36. However, the behavior of conventional bolted connections subjected to axial tension is inherently different from that of fully tightened, double-nutted anchor bolts. In a conventional connection, the entire length of bolt is subjected to the pretension force. In fully tightened, double-nutted anchor bolt connections, the exposed length of bolt below the leveling nut is not subjected to the beneficial effects of pretensioning. As a result, fully tightened, double-nutted anchor bolts are, in general, more susceptible to fatigue cracking at this location.

Dusel et al. [37] conducted a similar test program to evaluate the effects of type of steel, nominal diameter, bolt length, and stress range on the fatigue strength of snug- and fully tightened (i.e. tightened

to one-third-of-a-turn beyond snug) double-nutted anchor bolts subjected to axial tension. The tests included anchor bolts fabricated from ASTM A307 and ASTM A449 steels in nominal diameters ranging from 25 mm to 44 mm (1.0 to 1.75 in). Snug-tight was defined by a level of torque equal to 136 N-m (100 ft-lb). Furthermore, the tests were conducted at maximum stress levels ranging from approximately 10 percent to 100 percent of the yield strength of the material.

Similar to the results of the research performed by Frank, Dusel et al. found that the effects of nominal diameter, type of steel, and bolt length were insignificant. The results of tests on the fully-tightened specimens indicated that tightening of the nuts to one-third-of-a-turn beyond snug resulted in increased fatigue strengths as compared to the snug-tight specimens. Failure of all snug-tight specimens was observed at the first engaged thread of the exterior nut. Failure of fully-tightened specimens was observed at one of three locations: (1) the first engaged thread of the exterior nut; (2) within the threads of the interior nut; or (3) within the threaded region outside of the connection (i.e. below the leveling nut).

The database of fatigue test results generated by Frank and Dusel et al. for single-nutted and double-nutted, snug-tight anchor bolts subjected to axial tension is depicted in Figure 2.35. As will be discussed in Section 2.3.3.3, the magnitude of the maximum stresses to which anchor bolts are subjected significantly influences the fatigue strength. Increases in the magnitude of the maximum stress tend to decrease the fatigue strength. Therefore, the data shown in Figure 2.35 include only those tests conducted at maximum stresses greater than 60 percent of the minimum specified yield strength of the material. A maximum stress equal to 50 percent of the minimum specified yield strength corresponds to the allowable static design stress for anchor bolts [1]. As a result, the data shown in Figure 2.35 represent a worst-case condition in terms of the fatigue strength of snug-tight anchor bolts. Under actual service load conditions, anchor bolts are not expected to be subjected to maximum stresses greater than 50 percent of the material yield strength. For a given applied load range, bolts which are subject to lower maximum stresses would be expected to have longer fatigue lives than are exhibited in Figure 2.35.

The results of a statistical analysis of the data in Figure 2.35 indicates that the lower-bound, corresponding to the mean minus two-times the standard deviation (shown as the lower dashed line), falls between the AASHTO Category E and E' fatigue design curves. Therefore, the fatigue strength of axially-loaded, snug-tight anchor bolts is conservatively rounded down to the nearest AASHTO fatigue design curve, i.e. Category E'. Note that this conclusion is only applicable in the region of finite life (i.e. less than two million cycles).

The database of fatigue test results generated by Frank and Dusel et al. for double-nutted anchor bolts tightened to one-third-of-a-turn beyond snug and subjected to axial tension is depicted in Figure 2.36. Again, the data shown in Figure 2.36 include only those tests conducted at maximum stresses corresponding to greater than 60 percent of the minimum specified yield strength of the material. The results of a statistical analysis of the database indicates that the lower-bound falls between the AASHTO Category D and E fatigue design curves. Therefore, the fatigue strength of axially loaded, fully tightened anchor bolts is conservatively approximated by the AASHTO Category E fatigue design curve in the region of finite life (i.e. less than two million cycles).

2.3.1.2 Review of Existing Design Specifications - The following summarizes the provisions contained in three design specifications (i.e. AISC LRFD [38], BS7608 [39], and Eurocode 3 [40]) known to have provisions for the design of bolts for fatigue. It should be noted that none of the above design specifications specifically address the design of anchor bolts for fatigue. It is useful, however, to compare the provisions contained in these specifications to the available test data related to the fatigue strength of anchor bolts.

In the AISC LRFD Specifications, bolted joints loaded in direct tension are evaluated in terms of the maximum unfactored tensile load attributed to each bolt, including any prying force. Provisions for the calculation of prying loads are provided in Part 11 of the LRFD Manual. The AISC LRFD procedure for the design of bolts for fatigue is identical to the AISC ASD procedure and is based upon a specification developed by the Research Council on Structural Connections (RCSC) [41]. Typically, the AISC provisions are applied to hanger-type or bolted flange connections where the bolts are tensioned against the plies.

The AISC LRFD Specifications for the design of bolts for fatigue are based upon the maximum applied load rather than the applied stress range because the fraction of the externally applied stress range to which fully-tightened, axially-loaded bolts are subjected is highly variable and very difficult to estimate analytically [36]. In the AISC Specifications, the fatigue strength of high strength bolts is given in terms of the nominal unthreaded area of the bolt. The allowable total service load in fatigue for more than 500,000 cycles (i.e. infinite life) is 25 percent of the product of the nominal area of the bolt and the ultimate tensile strength.

In a majority of design specifications, the design of bolts for fatigue is typically based upon the tensile stress area of the bolt. The tensile stress area is defined as:

$$A_T = \frac{\pi}{4} (d - 0.938 P)^2 \quad (mm^2) \quad (2.10)$$

$$A_T = \frac{\pi}{4} \left(d - \frac{0.9743}{n} \right)^2 \quad (in^2)$$

where A_T is the tensile stress area (in^2 or mm^2), d is the nominal diameter of the unthreaded portion of the bolt (in or mm), P is the thread pitch, and n is the number of threads per inch. Generally, the tensile stress area is approximately 75 percent of the nominal area for bolts between 0.75 and 1 inch in diameter. Thus, for the purposes of comparison to other specifications, the allowable service stress for greater than 500,000 cycles permitted in the AISC Specifications is actually about 0.33 times the ultimate tensile strength of the bolt.

In the British Standard Institute's BS7608, a slightly different approach is used for the design of axially-loaded, fully-tightened bolts for fatigue. As in the AISC provisions, the problem of calculating the actual stress range in bolts in fully-tightened connections is deemed to be too difficult. In order to circumvent this problem, BS7608 assumes that the stress range acting on the tensile stress area of the bolt

is 20 percent of the total applied load, regardless of the magnitude of the actual fluctuating portion of the load. This assumption represents a conservative estimation of the actual stress range to which fully tightened bolts are subjected under fatigue loading in a variety of connections. The S-N fatigue design curve is given as a proportion of the tensile strength of the bolt, so that for high-strength bolts with a tensile strength of 785 MPa (115 ksi), the resulting S-N curve falls between the AASHTO Category E and E' design curves for less than 2 million cycles. In BS7608, the tensile strength may not be taken as greater than 785 MPa (115 ksi) even when higher strength bolts are used. The CAFL for bolts is given as 6 percent of the tensile strength, with a slight reduction for bolts larger than 25 mm (1 in) in diameter.

For example, for fully tightened AASHTO Grade 105 anchor bolts with a tensile strength equal to 862 MPa (125 ksi), the tensile strength would be taken as 785 MPa (115 ksi) under the BS7608 provisions, and the S-N design curve for less than 2 million cycles would fall between the AASHTO Category E and E' design curves. For greater than 2 million cycles, the CAFL would be taken as 6 percent of the allowable tensile strength (785 MPa or 115 ksi), or 47 MPa (6.8 ksi) (which is very close to the CAFL for the AASHTO Category D fatigue design curve). For fully-tightened Grade 55 anchor bolts with a tensile strength equal to 517 MPa (75 ksi), the S-N design curve for less than 2 million cycles would fall below the AASHTO Category E' design curve. For greater than 2 million cycles, the CAFL would be taken as 6 percent of the tensile strength (517 MPa or 75 ksi), or 31 MPa (4.5 ksi) (which is very close to the CAFL for the AASHTO Category E fatigue design curve).

If the assumed stress range of 20 percent of the peak load is applied to the AISC provisions, the AISC provisions would imply a CAFL of 20 percent of 0.33 times the ultimate tensile strength (for greater than 500,000 cycles). This is equivalent to 6.6 percent of the tensile strength. Given this assumed stress range, the provisions of the AISC and BS7608 Specifications for the design of bolts for infinite life are approximately in agreement.

In the Eurocode 3, the design S-N curve for axially loaded bolts is specified to be approximately equivalent to the AASHTO Category E' fatigue design. Furthermore, the design S-N curve is independent of the tensile strength of the bolt. The Eurocode S-N curve for bolts is approximately equivalent to the BS7608 S-N curve (and therefore the AISC provisions) for high-strength bolts with yield strengths greater than 785 MPa (115 ksi). AISC and BS7608 would be more conservative than the Eurocode 3 for lower strength bolts. The CAFL in the Eurocode 3 is 23 MPa (3.3 ksi) for all types of bolts, which is significantly more conservative than the CAFL of 47 MPa (6.8 ksi) specified in the BS7608 provisions or the CAFL of 52 MPa (7.5 ksi) implied by the AISC provisions for AASHTO Grade 105 anchor bolts.

The fatigue strength in the Eurocode 3 Specifications is based upon the actual stress range acting on the tensile stress area of the bolt. For snug-tight bolts, this calculation is straightforward (i.e. the stress range within the bolt is equal to the applied load range divided by the tensile stress area of the bolt). For fully-tightened bolts, however, calculation of the actual stress range acting on the tensile stress area is uncertain, and the Eurocode 3 Specifications do not suggest how such calculations are to be performed. However, assuming such a calculation can be performed, the provisions of Eurocode 3 permit a slightly

improved fatigue strength for fully-tightened bolts due to the fact that the reduced stress range acting within the fully-tightened connection would be compared to the S-N fatigue design curve.

Generally, the provisions contained in the above design specifications are consistent with the results of previous research programs [35, 37] which have been performed to determine the fatigue strength of anchor bolts in the region of finite life. As was shown in Figures 2.35 and 2.36, the lower-bound fatigue strengths exhibited by snug- and fully-tightened anchor bolts in the region of finite life are consistent with the AASHTO Category E' and Category E design curves, respectively. These design S-N curves are generally in agreement with the provisions of the AISC LRFD, BS7608, and Eurocode 3 Specifications for the design of bolts for finite life.

There does, however, appear to be disagreement with respect to the magnitudes of the constant-amplitude fatigue limits recommended by the three Specifications. Within each of the design Specifications, the magnitude of the CAFL appears to be arbitrarily set without regard to referenced test data. As a result, significant uncertainty exists with respect to the design of bolts for fatigue in the region of infinite life.

2.3.2 Description of Experiments

2.3.2.1 Test Specimens - A total of 47 specimens were included in the fatigue test program. Table 2.10 summarizes the details of the four types of specimens which were tested. As is shown, the test specimens consisted of 38 mm (1.5 in) diameter AASHTO Grade 55 and AASHTO Grade 105 anchor bolts with a 6UNC thread series. Selection of the diameter and thread series to be tested was based upon a review of state department of transportation standard drawings of cantilevered support structures. Thirty-eight millimeter diameter anchor bolts with a 6UNC thread series were identified as being typical for a majority of cantilevered support structure installations. As is shown in Table 2.10, approximately one-half of the specimens within each material grade were obtained with cut threads. The remaining specimens were obtained with rolled threads.

The basic specimen geometry is depicted in Figure 2.37. As is shown, the specimens were 914 mm (36 in) long with a 203 mm (8 in) long threaded region at each end and were supplied with four washers and four Grade 2H heavy hex nuts. All of the specimens, nuts, and washers were obtained from two independent commercial vendors in order to simulate the thread quality of anchor bolts used in actual construction and to minimize any bias in the test results due to a specific manufacturing process. Furthermore, all of the specimens, nuts, and washers were obtained galvanized in order to simulate the condition of anchor bolts used in typical cantilevered support structure installations. The nuts were re-tapped by the supplier following galvanizing, as is typical.

2.3.2.2 Experimental Set-Up and Procedures - A schematic of the experimental set-up used for the concentrically-loaded tests is depicted in Figure 2.38. As is shown, test fixtures were designed to transfer load directly from a servo-hydraulic actuator directly to the exterior nuts on each end of the

specimen through bearing plates measuring 140 mm (5.5 in) x 146 mm (5.75 in) x 38 mm (1.5 in) thick. Figure 2.39 shows a photograph of a complete test set-up.

As is indicated in Figure 2.40, the effects of misalignment were introduced by fabricating holes in the bearing plates which were offset from the longitudinal axis of the servo-hydraulic actuator. The amount of offset was set so as to subject the misaligned specimens to a 1:40 vertical misalignment, thereby introducing stresses caused by axial tension and non-uniform bending along the longitudinal axis of the specimens.

Selection of the amount of misalignment to which the anchor bolts would be subjected was based upon a review of current state department of transportation specifications for anchor bolt installation, which indicated that the maximum amount of anchor bolt misalignment permitted for cantilevered support structure installations was 1:40 (e.g. Michigan [42]). As a result, misalignments greater than 1:40 were not considered within the scope of the test program. The state of Michigan also specifies the use of bevelled washers on cantilevered support structures in which the anchor bolts are installed at misalignments less than 1:40 [42]. Bevelled washers were used at each end of the misaligned test specimens to minimize any localized bending effects resulting from non-uniform bearing of the nuts against the bearing plate.

In many other states, bevelled washers are not required if the nuts can be brought into firm contact with the base plate by tightening. This technique would create a higher mean tensile stress on one side of the bolt from the bending of the bolt, which could theoretically represent a worse situation than was actually simulated in the experiments. However, if the bevelled washers were not used, a large static moment would push the hydraulic cylinder against one side causing excessive wear. The only significant difference between forcing the nuts into firm contact and using a bevelled washer is a larger maximum stress, i.e. there should be essentially no difference in the resulting dynamic stress ranges. Therefore, this compromise in the tests is not thought to have significantly affected the results.

Each of the specimens was snug-tightened against the bearing plates using a standard torque wrench without the aid of additional lubrication. For the purposes of this research program, snug-tight was defined as tightening of the nuts to a torque of 271 N-m (200 ft-lb). A constant torque value was used to define snug-tight to ensure a reasonable level of consistency between individual tests and to permit a direct comparison with the results obtained by Frank [35]. It should be noted that defining snug-tight by a torque of 271 N-m (200 ft-lb) was arbitrary and does not correspond to any specific level of bolt pretension. However, the definition of snug-tight adopted for the purposes of this research program resulted in levels of bolt pretension below those achieved using the generally accepted definitions of snug-tight (which are discussed in the following paragraphs). As a result, the data obtained from these tests are slightly conservative. For those tests conducted at greater than snug-tight, tightening of the nuts was achieved with the use of a hydraulic wrench. Beeswax was applied to the threaded and bearing surfaces of these specimens to reduce the level of torque required to obtain the desired level of nut tightness.

Several specifications currently contain provisions which specify minimum requirements for obtaining the snug-tight condition. The AISC LRFD Specifications define snug-tight as the "tightness that

exists when all of the plies in a joint are in firm contact." This requirement is generally not applicable to anchor bolt installations because the nuts in a double-nut connection are tightened against a single base plate (i.e. multiple plies do not exist in anchor bolt installations). AASHTO recently issued supplemental specifications for AASHTO M164 (ASTM A325) [43] which define snug-tight as 10 percent of the specified proof load. The proof load is determined from tensile tests and is defined as the "applied load fasteners must resist without evidence of permanent deformation." The level of torque required to achieve the minimum specified bolt tension corresponding to snug-tight is determined from calibrations in a Skidmore-Wilhelm Calibrator. For galvanized bolts, all tests in the AASHTO supplemental specifications are to be performed following galvanizing. The application of these provisions to the installation of anchor bolts, however, is uncertain. For example, double-nutted anchor bolts are subject to pretensioning in the short length of bolt between the double nuts. Such a short length of bolt cannot be calibrated in a Skidmore-Wilhelm Calibrator. As a result, the level of torque required to achieve a bolt pretension of 10 percent of the specified proof load would be unknown.

It is recommended that, in actual anchor bolt installations, snug-tight be defined by the level of torque corresponding to the full-strength of a man using an ordinary spud wrench. This represents the definition previously used by AISC to define snug-tight. Based upon the results of the research reported herein, defining snug-tight as the full strength of a man will always result in a level of torque greater than the definition of snug-tight adopted for this research program (i.e. 271 N-m or 200 ft-lb). As a result, anchor bolts tightened in the field will possess a greater level of pretension and will exhibit a slightly higher fatigue strength than specimens tested in this research program.

All specimens were tested in a double-nut configuration, i.e. one nut on each side of the bearing plate, under constant-amplitude, tension-tension loading. A computer-controlled, 245 kN (55 kip) capacity servo-hydraulic actuator was used to subject the test specimens to sinusoidal loading at frequencies between 10 and 25 Hz. The variable controlled during each of the tests was the stress range on the tensile stress area of the bolt. Except where noted, the maximum stress on the tensile stress area for all tests on the Grade 55 anchor bolts was held constant at approximately 60 percent of the minimum specified yield strength of the material. Due to limitations on the capacity of the testing machine used in this experimental program, the maximum stress on the tensile stress area for the Grade 105 bolts was held constant at either 32 percent or 38 percent of the minimum specified yield strength of the material.

The dynamic load range induced in the test specimens during testing was monitored by a load cell mounted between one of test fixtures and the crosshead of the test machine. Prior to the start of the fatigue test program, however, several concentrically loaded test specimens were instrumented with a series of strain gages and statically tested to ensure adequate calibration of the load cell and to evaluate the magnitude of any bending induced in the specimens due to seating. The specimens were instrumented with a series of four strain gages mounted at 90-degree intervals on the unthreaded portion of the bolt midway between the bearing plates. The results of the static tests indicated good correlation between the bolt load indicated by the load cell and the bolt load computed from the average of the four strain gages readings. Furthermore, bending stresses due to seating of the specimens were found to be negligible. As

a result, the load cell was considered an adequate means by which to monitor the dynamic load range induced in the specimens during testing.

Each specimen was tested under load control with failure defined by the propagation of a crack through the entire specimen cross-section. The experimental set-up and specimen geometry permitted two data points to be obtained from each specimen (i.e one data point from each of the two threaded regions). As a result, all specimens which failed at one end with sufficient threads remaining were retested until failure at the opposite end was obtained. This procedure effectively limited the extended period of time required to conduct fatigue testing in the region of infinite life. Inclusion of multiple data from each of the specimens was found not to significantly influence the results of statistical analyses of the data. The lower-bound corresponding to the first observed failure was found to be identical to the lower-bound when failures at both ends of the specimens were included in the statistical analysis.

2.3.3 Results of Experiments

Due to the inherent geometrical configuration of bolted connections, visual inspection for fatigue cracking was not possible during the course of the testing program. However, post-test inspections of the fatigue specimens indicated that failure was caused by the propagation of a single crack which formed in one of two locations, as is indicated in Figure 2.41. The majority of specimen failures occurred at the first fully engaged thread from the loaded face of the exterior nut of the double-nutted connection, identified as failure location 1 in Figure 2.41. In addition, several specimens failed in the threaded region outside of the double-nutted connection, identified as failure location 2 in Figure 2.41. All but one of the specimens which failed outside of the connection were tightened to greater than snug-tight.

Inspection of the failure surfaces of the anchor bolts that were tested indicated that fatigue cracks initiated at multiple points at the thread root then coalesced into a single primary crack. The total fatigue life is often thought of as being comprised of a "crack-initiation life" and a "crack-propagation life." The practical problem with this concept is that crack formation and coalescence is a complex continuous process and the cutoff in this process, i.e. the criterion for the point at which the propagation life is supposed to begin and the initiation life ends, is arbitrary. Typically, the initiation life is defined to be over when the crack becomes detectable with dye penetrant or other non-destructive evaluation (NDE) technique. In the case of the anchor bolts, this approximately corresponds to the point at which the multiple small cracks coalesce. Note that there is actually a great deal of crack propagation included in the so-called "initiation-life."

In the case of welded joints, the initiation life is a relatively small part of the total life and can be ignored in practice. In the case of anchor bolts, the initiation life is a much greater proportion of the total life. Among reasons for this difference are: 1) weldments have more significant microdefects than bolts; and, 2) weldments have high tensile residual stresses perpendicular to the microdefects whereas bolts may in some cases have a favorable compressive residual stress at the root of the thread. The relatively long initiation life is apparent from the anchor bolt fatigue tests, which typically failed within hours after crack detection. The initiation life is significantly affected by yield strength and mean stress, whereas the

propagation life is not. In weldments, where the total life is dominated by the propagation life, the effect of yield strength and mean stress can be ignored. However, because a greater proportion of the total life is attributed to initiation life in the anchor bolts, the effect of yield strength and mean stress is more significant in anchor bolt fatigue. Compared to the overall scatter in fatigue lives, these effects of yield strength and mean stress are not that significant and are ignored in the proposed fatigue-design specifications. However, these effects will be discussed in explaining the trends in the experimental results.

Generally, the primary crack propagated along a straight-line front towards the center of the cross-section of the specimen. In all cases, the primary crack propagated through approximately 65% to 75% of the specimen cross-section prior to fracture. Figure 2.42 shows photographs of typical fatigue crack surfaces.

Sections 2.3.3.1 through 2.3.3.6 summarize the fatigue test results in terms of S-N curves. Notations used on the S-N curves presented in Figures 2.43 to 2.55 include dotted lines to designate the mean and mean minus two standard deviations of the data. The solid lines are the AASHTO S-N design curves and the horizontal dashed lines indicate the CAFL of each AASHTO design curve.

2.3.3.1 Fatigue Strength of Snug-Tight Specimens - Figure 2.43 summarizes the fatigue test results for the concentrically-loaded, snug-tight specimens in the form of an S-N curve. The data includes tests conducted on both Grade 55 and Grade 105 specimens with rolled and cut threads. As is indicated in Figure 2.43, the lower-bound to the test data is approximately equal to the AASHTO Category E fatigue design curve. Furthermore, inspection of the data in the region of infinite life indicates no failures were obtained below a stress range of 62 MPa (9 ksi). The next lower CAFL would be the fatigue limit corresponding to the AASHTO Category D fatigue design curve (48 MPa or 7 ksi). Thus, the constant-amplitude fatigue limit of axially loaded, snug-tight anchor bolts is conservatively approximated by the fatigue limit corresponding to the AASHTO Category D fatigue design curve (48 MPa or 7 ksi).

Figure 2.44 compares the results of the present research program with the results obtained by previous researchers [35, 37]. The current data falls within the range of scatter exhibited by the previous data. Statistical analysis of the entire database indicates that the lower-bound to the test data falls between the AASHTO Category E and E' fatigue design curves. As a result, the lower-bound S-N design curve representative of the fatigue strength of axially loaded, snug-tight anchor bolts is a unique curve given by the AASHTO Category E' fatigue design curve with a constant-amplitude fatigue limit corresponding to the AASHTO Category D fatigue design curve (48 MPa).

Comparison of the lower-bound estimates of the anchor bolt fatigue test data with the recommendations of other design specifications (as was discussed in Section 2.3.1.2) indicates that the recommended fatigue design strengths for anchor bolts and the provisions contained in these other design specifications are generally consistent for Grade 105 anchor bolts but slightly liberal with respect to the design of Grade 55 anchor bolts. This can generally be expected, since the design Specifications discussed in Section 2.3.1.2 are oriented towards the design of high-strength structural bolts for fatigue.

2.3.3.2 Effects of Maximum Stress - Figures 2.45 through 2.48 summarize the results of tests conducted to determine the effects of maximum stress on the fatigue strength of anchor bolts. The data in these figures are from tests conducted on Grade 55 anchor bolts with both rolled and cut threads at stress ranges varying from 138 MPa (20 ksi) to 69 MPa (10 ksi). At each stress range, longer fatigue lives were obtained for tests conducted at lower magnitudes of maximum stress. This behavior is common in non-welded structural components, which have small residual stresses, and has been observed in fatigue testing of other types of non-welded steels [44].

The maximum stress effect (another way of referring to the mean stress effect) can be attributed to the fact that fatigue life in non-welded structural steels is strongly dependent upon the initiation of fatigue cracks. Fatigue crack initiation (and thus the fatigue life corresponding to the initiation period) is strongly dependent upon the magnitude of the maximum stress. As explained previously, the maximum stress is not as significant in welded details for two reasons: 1) welded details are subject to a pre-existing tensile residual stress on the order of the yield strength of the steel; and, 2) weldments generally possess crack-like defects. Figures 2.45 through 2.48 show that, at lower values of maximum stress, the initiation life increases, resulting in a longer total fatigue life.

The bolts which are subjected to the largest stress range (i.e. the bolts that will govern the fatigue design of all the anchor bolts) will typically be in tension from the static gravity moments and/or the mean wind load. For the purposes of design, a high maximum tensile stress can be assumed. Therefore, the worst-case effect of maximum stress is taken into account in the proposed specifications by basing the design S-N curve on tests conducted at worst-case (highest) maximum stress levels. Any variation of the maximum stress from the worst-case levels in the tests would be favorable. For example, anchor bolts which are subjected to a lower value of maximum stress in service will exhibit fatigue lives greater than that predicted by the design S-N curve. Therefore, the effect of variation in the maximum stress need not be taken into explicit consideration in the proposed specifications. This is fortunate because existing fatigue design codes for metal structures are primarily concerned with welded details and therefore do not account for the effect of maximum stress. Taking maximum stress levels into account would unnecessarily complicate the fatigue design provisions.

As discussed in Section 2.3.2.2, limitations on the capacity of the actuator prevented the Grade 55 and Grade 105 specimens from being tested at magnitudes of maximum stress which were similar in terms of percentage of material yield strength. Thus, the absolute worst-case maximum load effects were not simulated in the tests of the Grade 105 specimens. However, based on the previous experimental studies of Frank [35] and Dusel [37], it is believed that this limitation did not significantly affect the results, i.e. the maximum stress level for the Grade 105 specimens (32 to 38 percent of the yield strength) was considered to be high enough. The results of the previous research suggest that the fatigue strength of higher strength bolts is strongly affected by maximum stress up to a certain level but that as the maximum stress increased to very high levels the effect becomes saturated. The rationale for the diminishing effect of increasing maximum stress could be that: 1) a threshold amount of maximum stress is required to overcome favorable residual stress in the root of the threads; and, 2) that further increases

in maximum stress do not further enhance fatigue. Frank [35] tested high-strength bolts at maximum stress levels equal to 75 percent of the minimum specified yield strength of the material. The results of these tests did not indicate that there was a significant decrease in fatigue strength in comparison to the lower strength anchor bolts tested at the same percentage of yield. Frank's results for high strength anchor bolts at worst-case maximum stress levels are also not any lower than the results in the present study.

2.3.3.3 Effects of Thread Forming Method - Figures 2.49 and 2.50 summarize the effects of thread forming method (cut vs rolled) for the Grade 55 and Grade 105 specimens, respectively. As is shown in Figure 2.49, thread forming did not significantly influence the fatigue strength exhibited by the Grade 55 specimens.

Thread forming, however, did influence the fatigue strength exhibited by the Grade 105 specimens. As is shown in Figure 2.50, Grade 105 specimens with rolled threads consistently exhibited longer fatigue lives at each of the stress ranges considered. The difference in fatigue strengths between the cut and rolled specimens may be attributed to two factors. First, anchor bolts fabricated with cut threads generally possess a smaller thread root radius than anchor bolts fabricated with rolled threads. The stress concentration associated with the cut thread, therefore, is more severe. As a result, anchor bolts fabricated with rolled threads would be expected to exhibit a slightly greater fatigue strength than anchor bolts fabricated with cut threads. Second, anchor bolts fabricated with rolled threads possess compressive residual stresses at the thread root resulting from the rolling process. The compressive residual stresses tend to shield the critical thread root area from part of the applied tensile stress range, resulting in an increase in fatigue strength in comparison to anchor bolts fabricated with cut threads.

The effects of thread forming method are observed in the Grade 105 specimens and not in the Grade 55 specimens for two reasons. First, the magnitude of the compressive residual stresses resulting from the rolling process are proportional to the material yield strength. For the Grade 105 specimens (with a higher yield strength), the compressive residual stresses are larger in magnitude than the magnitude of the compressive residual stresses in the Grade 55 specimens (which have a lower yield strength). Therefore, for a given stress range, the magnitude of the residual stresses in the Grade 105 specimens provide a greater benefit with respect to fatigue strength (i.e. the greater compressive residual stresses in the Grade 105 specimens negate a greater portion of the applied tensile stress range than in the Grade 55 specimens).

Second, the effects of thread forming method are also more apparent in the Grade 105 specimens because limitations on the capacity of the hydraulic actuator used in this test program prevented the Grade 105 specimens from being tested at a maximum stress greater than approximately 38 percent of the minimum specified yield strength of the material. At lower values of maximum stress, the effect of stress concentration on fatigue strength is more apparent (i.e. the effects of stress concentration decrease with increasing maximum stress). At higher values of maximum stress, fatigue damage occurs regardless of the severity of the stress concentration. As a result, no significant variations in fatigue strength were

observed in the Grade 55 specimens (which were tested at 60 percent of the material yield strength) with cut and rolled tests. In addition, the relatively low maximum stress to which the Grade 105 specimens were subjected was not large enough to fully negate the beneficial effects of the compressive residual stresses at the thread root. On the other hand, the Grade 55 specimens, which were tested at a maximum stress corresponding to approximately 60 percent of the minimum specified yield strength of the material, did not exhibit a significant variation in fatigue strength between the cut and rolled specimens (as is shown in Figure 2.49). It can be reasonably theorized that the beneficial effects of the compressive residual stress induced by the rolling process were effectively negated by the high applied tensile load.

In other words, when the magnitude of the minimum tensile stress exceeds the maximum value of the compressive residual stress at the thread root, the applied stress range will be fully tensile. Under these conditions, the beneficial effects of the compressive residual stresses at the root of a rolled thread would not be apparent. As a result, the Grade 105 specimens with rolled threads exhibited slightly longer fatigue lives when compared to the Grade 105 specimens with cut threads. Based upon the results of these tests, it is not clear if this benefit would still be obtained if the Grade 105 bolts had been tested at a maximum stress corresponding to 60 percent of the yield strength of the material.

The results of tests conducted by Frank [35] suggest that the higher fatigue strengths exhibited by the Grade 105 bolts would not have been observed at higher levels of maximum stress. As may be recalled from the discussion in Section 2.3.1.1, the maximum stress in each of the tests conducted by Frank was held constant at 75 percent of the minimum specified yield strength of the material. Frank observed from the results of these tests that the effects of thread forming method were insignificant. Therefore, it appears that the effects of thread forming were minimized in Frank's experiments due to the application of a high maximum tensile stress.

2.3.3.4 Effects of Yield Strength - Fatigue tests of small smooth specimens at zero mean stress or some constant mean or maximum stress typically show that the fatigue strength increases with increasing yield strength. This effect is substantially reduced in the presence of a notch as in a bolt or a welded detail, hence is not taken into account in fatigue design of structural details. Also, there is a competing effect that must be taken into account for practical design applications, i.e. higher-strength anchor bolts have a higher allowable stress and therefore tend to be used at higher maximum stress levels. As explained below, the detrimental effect of higher maximum stress in the higher-strength anchor bolts may cancel out or even exceed the beneficial effect of yield strength.

The effect of yield strength, while holding the absolute maximum stress constant, can be seen in Figures 2.51 and 2.52 for the specimens with cut and rolled threads, respectively. The data in each of these figures were obtained from tests conducted at approximately equivalent absolute magnitudes of maximum stress. Based on the appearance of the data in Figure 2.51, yield strength does not appear to significantly influence the fatigue strength of anchor bolts fabricated with cut threads under these conditions. For reasons discussed in the previous section, the Grade 105 rolled threads exhibit a slightly greater fatigue strength as shown in Figure 2.52. Notwithstanding this small effect, the results show that

yield strength did not have a significant effect on the fatigue strength, even at constant levels of absolute maximum stress. This conclusion is consistent with the results of both Frank [35] and Dusel [37], which also show that yield strength did not have a significant effect on the fatigue strength.

As discussed previously, the approach adopted with respect to the design of anchor bolts for fatigue is to represent the behavior of all types of anchor bolts and loading conditions. In this way, the effects of secondary variables such as maximum stress, yield strength, and thread forming method need not be explicitly considered in the design process. These potentially beneficial effects are small, therefore the proposed lower-bound S-N curve is not excessively conservative, even under the more favorable circumstances.

As was discussed in Section 2.3.3.2, the fatigue strength of anchor bolts is significantly affected by the magnitude of the maximum stress, i.e. larger values of maximum stress decrease the apparent fatigue strength of anchor bolts. Consider Grade 55 anchor bolts and Grade 105 anchor bolts in optimally designed structures, i.e. the bolts are loaded to the same percentage of the respective yield strengths by gravity loads and static mean wind loads. For the purposes of design, a worst-case S-N curve is proposed which is based on the highest allowable maximum stress. The highest value of the maximum stress associated with Grade 55 anchor bolts will be approximately half the highest maximum stress value associated with Grade 105 anchor bolts. The beneficial effect of lower absolute maximum stress in the Grade 55 anchor bolts more than compensates for the lower basic fatigue strength of the material. In fact, for the case where the maximum stresses in Grade 55 and Grade 105 anchor bolts are a similar percentage of the respective yield strengths, Grade 55 anchor bolts exhibit slightly higher fatigue strength than Grade 105 anchor bolts.

Up to this point, the comparison of Grade 55 to Grade 105 fatigue resistance has been in terms of the S-N data which shows differences in the relative fatigue life for the same stress ranges. There is one further factor to consider in the effect of yield strength. Consider a specific support structure subjected to given fatigue load ranges and static design loads. If Grade 105 bolts are used instead of Grade 55 bolts to resist the static design loads, smaller diameter bolts will be allowed. In this case, the fatigue stress ranges will increase as the bolt size decreases because the fatigue load range is constant. Therefore, there is a slightly greater margin of safety or reliability level for the lower-strength anchor bolts. A specific fatigue design check will assure that the stress ranges in the Grade 105 anchor bolts are not any greater than allowable which is the same for both types of anchor bolts. Therefore, the fatigue design would govern the size of the anchor bolts and there would be no benefit allowed for using higher-strength anchor bolts. In fact, the fatigue requirements will effectively discourage the use of the Grade 105 anchor bolts.

2.3.3.5 Effects of Misalignment - Figure 2.53 shows data from tests conducted on the misaligned test specimens under snug-tight conditions with beveled washers. As explained in Section 2.3.2.2, the bevelled washers were used to prevent a large static moment from wearing the test machine. If bevelled washers had not been used, the nuts would have to be tightened until they were in firm contact with the base

plate. The only difference in this case would have been a larger constant mean bending moment between the double nuts. It is believed that this difference would not significantly affect the fatigue strength, therefore the results would not have been substantially different had the bevelled washers not been used. This contention is confirmed by the results of the two tests on full-scale foundations with 1:20 misalignment where bevelled washers were not used. The results of these tests, which will be described in Section 2.4.1.2, are within the scatterband of the data from the single bolt tests, indicating no additional effect from not having the bevelled washers.

Figure 2.53 includes data from Grade 55 and Grade 105 specimens with rolled and cut threads obtained under snug-tight conditions. Figure 2.53 shows a comparison of the misaligned test results with the test data obtained from the concentrically loaded test specimens. The data are presented in terms of the nominal axial stress range acting on the tensile stress area. The bending stress range resulting from the misaligned configuration is not included in the stress calculation. The bending is "built-into" the S-N curve and is reflected by the lower apparent fatigue strength relative to the concentrically loaded test specimens. It appears that, even with the inclusion of the misaligned test data, the AASHTO Category E' design curve still represents a reasonable lower-bound to both the misaligned and concentric test data.

As is shown in Figure 2.53, no failures were obtained in the misaligned specimens below a stress range of 55 MPa (8 ksi). Therefore, the constant-amplitude fatigue limit corresponding to the AASHTO Category D design curve (48 MPa or 7 ksi) can also be used to design anchor bolts for infinite life with misalignments up to 1:40 (provided that bevelled washers are used during installation) without explicit consideration of the bending stresses created by the misaligned configuration. It should be noted that, without bevelled washers, misaligned anchor bolts may be subject to additional localized bending stresses due to non-uniform bearing of the nut against the base plate. Under these conditions, the apparent constant-amplitude fatigue limit may be lower than the AASHTO Category D fatigue limit.

2.3.3.6 Effects of Bolt Preload - Figure 2.54 depicts the fatigue lives exhibited by anchor bolts subjected to varying levels of bolt pretension (one-third-of-a-turn beyond snug, one-sixth-of-a-turn beyond snug, and one-twelfth-of-a-turn beyond snug) at a 138 MPa (20 ksi) nominal stress range. No attempt was made to calculate the actual stress range between the double-nuts. Specimens tested at one-third and one-sixth-of-a-turn beyond snug did not exhibit failures during the testing program. Specimens tested at one-twelfth-of-a-turn beyond snug failed at a number of cycles significantly greater than the snug-tight specimens tested at an identical stress range (see Figure 2.43). Furthermore, two of the three failures observed in the specimens tightened to one-twelfth-of-a-turn beyond snug occurred outside of the connection (i.e. failure location 2 as identified in Figure 2.41).

The limited number of tests conducted at greater than snug-tight prevents any definitive conclusions to be made regarding the effect of this parameter on the fatigue strength of anchor bolts in the infinite life region. However, an evaluation of the existing database of fatigue tests conducted at one-third-of-a-turn beyond snug permits several statements to be made concerning the effects of pretensioning.

As was previously discussed, the results of a statistical analysis of the existing database of anchor bolt tests conducted at one-third-of-turn past snug (as is shown in Figure 2.55) indicates that the fatigue strength of fully tightened anchor bolts in the region of finite life is conservatively approximated by the AASHTO Category E fatigue design curve. Furthermore, examination of the data in the region of infinite life indicates that Frank obtained failures at stress ranges as low as 69 MPa (10 ksi). As a result, the constant-amplitude fatigue limit for fully tightened anchor bolts is below the fatigue limit corresponding to the AASHTO Category C fatigue design curve. Furthermore, it is reasonable to conclude that the constant-amplitude fatigue limit for snug-tight anchor bolts (i.e. the fatigue limit defined by AASHTO Category D) is a worst-case condition. Thus, the actual constant-amplitude fatigue limit for fully tightened anchor bolts likely falls between the fatigue limits corresponding to AASHTO Categories C and D. It is therefore recommended that the fatigue limit corresponding to AASHTO Category D (48 MPa or 7 ksi) be utilized for the design of fully tightened anchor bolts for infinite life.

As discussed above, the results of previous research indicate that the fatigue strength of anchor bolts in the finite life region can be improved by one fatigue category (to Category E) by tightening the nuts to one-third-of-a-turn past snug. The improvement in fatigue strength afforded by tightening to one-third-of-a-turn beyond snug can be attributed to a reduction in load carried by the external nut. Frank determined that, under fully tightened conditions, approximately one-third of the externally applied load is taken by the interior nut. In a majority of the fatigue tests on fully tightened anchor bolts, the transfer of load from the exterior to interior nuts shifted the failure mode from the first engaged thread of the exterior nut to the threaded region below the levelling nut. The limited number of tests conducted at greater than snug-tight in the current research program suggest that the shift in failure modes from the first engaged thread of the exterior nut to the threaded region below the levelling nut can be achieved by tightening to as little as one-twelfth-of-a-turn beyond snug.

Although an improvement in the constant-amplitude fatigue limit for fully tightened anchor bolts (above the Category D fatigue limit associated with snug-tight bolts) has not been suggested, it should be stressed that tightening to one-third-of-a-turn beyond snug is the preferred method for anchor bolt installation. Snug-tight bolts may potentially become loose under service-load conditions, altering the distribution of load to each of the remaining anchor bolts in the foundation assembly. The remaining bolts may be subjected to stress ranges greater than those assumed in design. This is, of course, detrimental to the performance of the anchor bolt assembly with respect to fatigue. Tightening to one-third-of-a-turn beyond snug eliminates the possibility of anchor bolts becoming loose under service conditions. As a result, it is the preferred method for anchor bolt installation.

2.3.3.7 Material Property Tests - A series of material property tests were performed to ensure that strength, ductility, and fracture toughness of the anchor bolt test specimens were in accordance with existing anchor bolt material property specifications. One anchor bolt was randomly selected from each of the four specimen series summarized in Table 2.10 and subjected to a series of material property tests.

Three standard 13 mm (0.5 in) diameter tensile specimens (50 mm or 2 in gage length) and three standard Charpy V-Notch impact specimens were fabricated from each of the four randomly selected anchor bolts.

Two specifications currently specify minimum material property requirements for anchor bolts. The first, AASHTO M314-90, specifies minimum tensile properties for Grade 36, Grade 55, and Grade 105 anchor bolts. The second, ASTM F1554-94, specifies minimum tensile properties for Grade 36, Grade 55, and Grade 105 anchor bolts along with supplemental requirements specifying minimum fracture toughness for Grade 55 and Grade 105 anchor bolts.

The tensile property requirements for the AASHTO and ASTM specifications are identical for each anchor bolt grade. In addition ASTM F1554-94 also specifies two supplemental fracture toughness requirements denoted as S4 and S5. The first supplemental requirement, S4, is applicable to both Grade 55 and Grade 105 anchor bolts and requires a minimum Charpy impact energy at 5 degrees Celsius (41° F). The second supplemental requirement, S5, is applicable only to Grade 105 anchor bolts and requires a minimum Charpy impact energy at -29 degree Celsius (-20° F). Table 2.11 summarizes the tensile and fracture toughness requirements for Grade 55 and Grade 105 anchor bolts. Note that the Grade 55 Charpy V-Notch specimens were tested in accordance with supplemental S4 while the Grade 105 Charpy V-Notch specimens were tested in accordance with the more stringent supplemental S5.

The material property test results are summarized in Table 2.12. As is indicated, the tensile and fracture toughness properties of each of the anchor bolts selected from the four specimen series surpassed the minimum requirements specified in AASHTO M314-90 and ASTM F1554-94.

2.3.4 Recommendations for Fatigue Design of Anchor Bolts

The results of the experimental program reported herein indicate that:

- The AASHTO Category E' design curve should be used to design axially loaded, snug-tight anchor bolts in the region of finite life,
- The AASHTO Category E design curve should be used to design axially loaded, fully tightened anchor bolts in the region of finite life,
- The constant-amplitude fatigue limit corresponding to AASHTO Category D (48 MPa or 7 ksi) should be used to design axially loaded, snug- and fully tightened anchor bolts in the region of infinite life,

- Whenever practical, anchor bolts should be installed in the fully tightened condition (i.e. tightened to one-third-of-a-turn beyond snug for many anchor bolt sizes). Although no benefit is recommended when designing fully tightened anchor bolts for infinite life, it should be noted that the fully tightened condition precludes the possibility of anchor bolts becoming loose under service-load conditions. As a result, the fully tightened condition is inherently better with respect to the fatigue performance of anchor bolts. It should also be noted that, in general, large diameter bolts will require the use of a hydraulic wrench or other proven method of tightening and external lubrication of the threaded and bearing surfaces in order to achieve a fully tightened condition. Tightening anchor bolts greater than 51 mm (2 in) in diameter with coarse pitch threads to one-third-of-a-turn beyond snug will most likely yield the anchor bolt material.
- The bending stress range resulting from misalignments up to 1:40 need not be explicitly considered in stress calculations when designing anchor bolts for infinite life provided that firm contact exists between the anchor bolt nuts and base plate. Where appropriate, beveled washers may be used to obtain a uniform bearing area. Anchor bolts may be subject to prying forces resulting from localized distortion of the base plate. The increase in stress range associated with prying is, of course, detrimental with respect to the behavior of anchor bolts under fatigue loading. As a result, the effects of prying should be minimized in actual anchor bolt installations through the use of base plates with adequate thickness.

In addition to the above design recommendations, the results of this research indicate that:

- The magnitude of the maximum stress to which anchor bolts are subjected significantly influences the fatigue strength. A worst-case assumption, i.e. maximum stress levels of about 60 percent of the minimum specified yield strength of the material, is implicit in the above recommendations. Test results indicate that decreases in the magnitude of the maximum stress below 60 percent of the yield strength can significantly increase the apparent fatigue strength and CAFL.
- In cases where the magnitude of the maximum stress is relatively low (i.e. less than approximately 30 percent of the minimum specified yield strength of the material), anchor bolts fabricated with rolled threads exhibit greater fatigue resistance than anchor bolts fabricated with cut threads. The effect is particularly apparent in higher strength bolts. At larger magnitudes of maximum stress, the effects of thread forming method become negligible as the larger values of applied minimum tensile stress overcome the compressive residual stresses at the root of rolled threads induced by the rolling process. Additional tests should be performed to fully quantify the potential advantages of using anchor bolts fabricated with rolled threads.

- For a given magnitude of maximum stress (in terms of absolute stress), Grade 55 and Grade 105 anchor bolts exhibit approximately identical fatigue strengths. However, for the case where maximum stresses are a similar percentage of the material yield strengths, Grade 55 anchor bolts exhibit slightly higher fatigue strength than Grade 105 anchor bolts. Furthermore, in actual structural applications, when higher strength bolts are proportioned for strength only, the result will be smaller diameter (or fewer) bolts than would be needed for lower strength bolts. This reduction in size will have the effect of increasing the magnitude of the stress ranges for a given load range. Therefore, it is critical that higher strength anchor bolts be designed for fatigue. The constraints of the fatigue requirements, which are equal for both anchor bolt strength levels, may preclude any benefit (with respect to smaller bolt diameters) obtained from using the higher strength bolts.

The above design recommendations are based upon the worst-case stress conditions (i.e. only data consisting of fatigue tests conducted at maximum stresses greater than 60 percent of the minimum specified yield strength of the material were included in the regression analyses to determine the lower-bounds to the snug- and fully tightened databases). In typical structural applications, the maximum stresses to which anchor bolts will be subjected will be significantly less than 60 percent of the yield strength of the material (i.e. at typical service loads, the maximum stresses in anchor bolts due to dead load plus fatigue loads will be less than 60 percent of the material yield strength). Furthermore, the design recommendations assume worst-case conditions with respect to parameters such as yield strength and thread forming method. As a result, these secondary parameters need not be considered in the design of anchor bolts for fatigue. Generally, the recommended fatigue design provisions provide a conservative approximation of anchor bolt fatigue strength.

As a further indication of the validity of these findings, it is noted that the proposed bolt fatigue design recommendations are generally consistent with the provisions of other recommendations for the design of bolts for fatigue. The fatigue design recommendations for bolts in various U.S. and international codes were discussed in Section 2.3.1.2. Although the various codes appear to be very different (e.g. AISC provisions limit the maximum stress while other codes limit the stress range), given a set of common assumptions, the result of the design from these codes is relatively consistent. The proposed recommendations derived from this research program will lead to a result which is consistent with the results from these various design specifications.

Specimen Series	Material Grade¹	Yield Strength² (MPa)	Nominal Diameter (mm)	Thread Series	Thread Type
H55	55	379	38	6UNC	cut
F55	55	379	38	6UNC	rolled
H105	105	724	38	6UNC	cut
F105	105	724	38	6UNC	rolled

¹AASHTO Specification M314-90 (ASTM F1554-94)

²Minimum specified

Table 2.10 - Specimen Details.

Tensile Property*	Grade 55	Grade 105
Tensile Strength (MPa)	517 - 655	862 - 1034
Yield Strength**, min (MPa)	380	724
Elongation in 50 mm, min (%)	21	15
Reduction in Area, min (%)	30	45

*AASHTO M314-90 (ASTM F1554-94)

**0.2% Offset

(a)

Material	Minimum Energy, (J)		Test Temperature (deg. C)
	Ave. 3 Tests	One Test	
Grades 55 & 105	20	16	5*
Grade 105	20	16	-29**

*ASTM F1554-94 S4

**ASTM F1554-94 S5

(b)

Table 2.11 - ASTM F1554-94 (a) Tensile and (b) Charpy Impact Requirements for Anchor Bolts.

Tensile Property	Grade 55**		Grade 105**	
	H55	F55	H105	F105
Tensile Strength (MPa)	580	596	964	1048
Yield Strength*, min (MPa)	421	420	823	930
Elongation in 50 mm, min (%)	32.8	30.9	19.3	18.4
Reduction in Area, min (%)	67.9	62.2	52.0	56.1

*0.2% Offset

**Average of Three Tests

(a)

Material	Impact Energy, (J)		Test Temperature (deg. C)
	Ave. 3 Tests	Lowest Test	
H55	44	37	5
H105	52	47	-29
F55	71	65	5
F105	52	38	-29

(b)

Table 2.12 - (a) Tensile and (b) Charpy Impact Test Results.

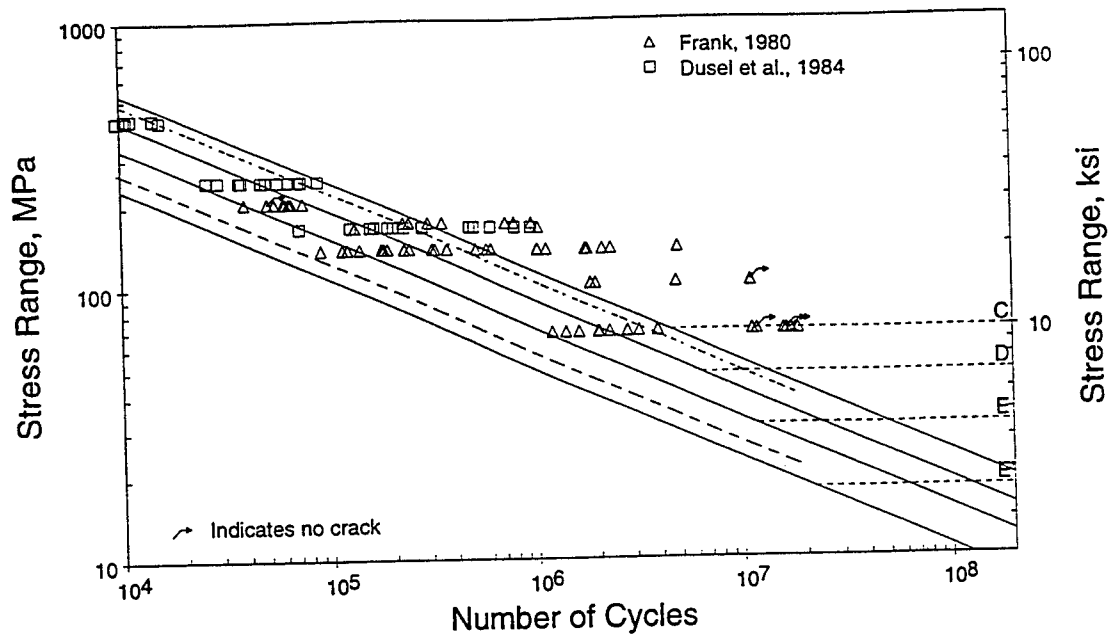


Figure 2.35 - Previous Database of Snug-Tight Anchor Bolt Fatigue Tests (Includes only those data obtained from tests conducted at maximum stresses corresponding to greater than $0.6F_y$). Dotted lines are mean and mean minus two standard deviations of the data. Solid lines are the AASHTO S-N design curves. Horizontal dashed lines indicate CAFL of each AASHTO design curve.

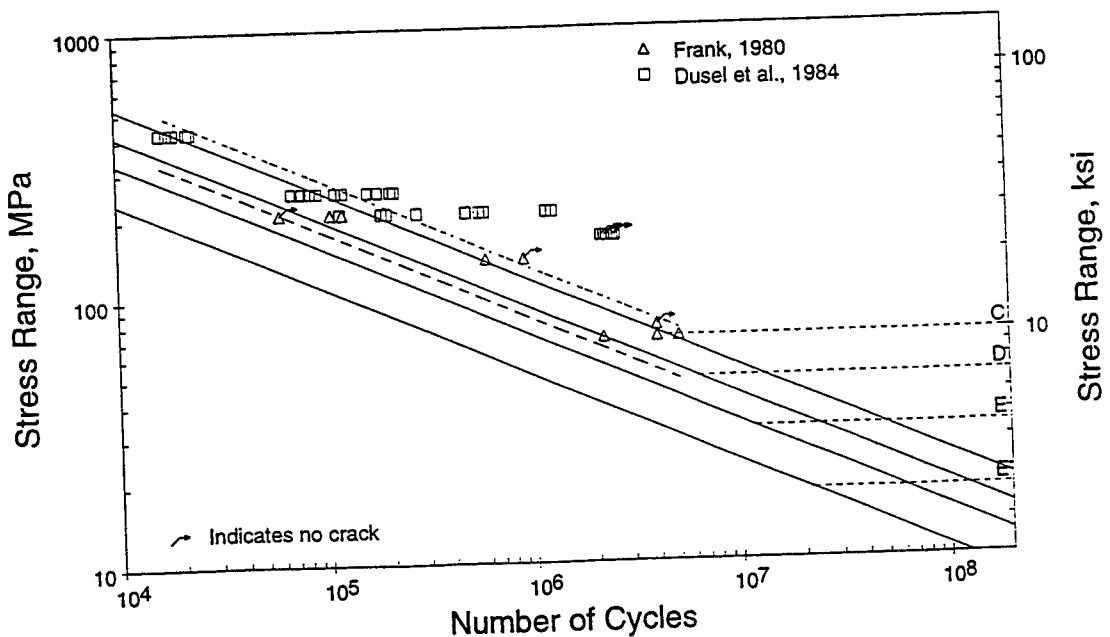


Figure 2.36 - Previous Database of Fully-Tightened Anchor Bolt Fatigue Tests (Includes only those data obtained from tests conducted at maximum stresses corresponding to greater than $0.6F_y$) (Notation similar to Figure 2.35).

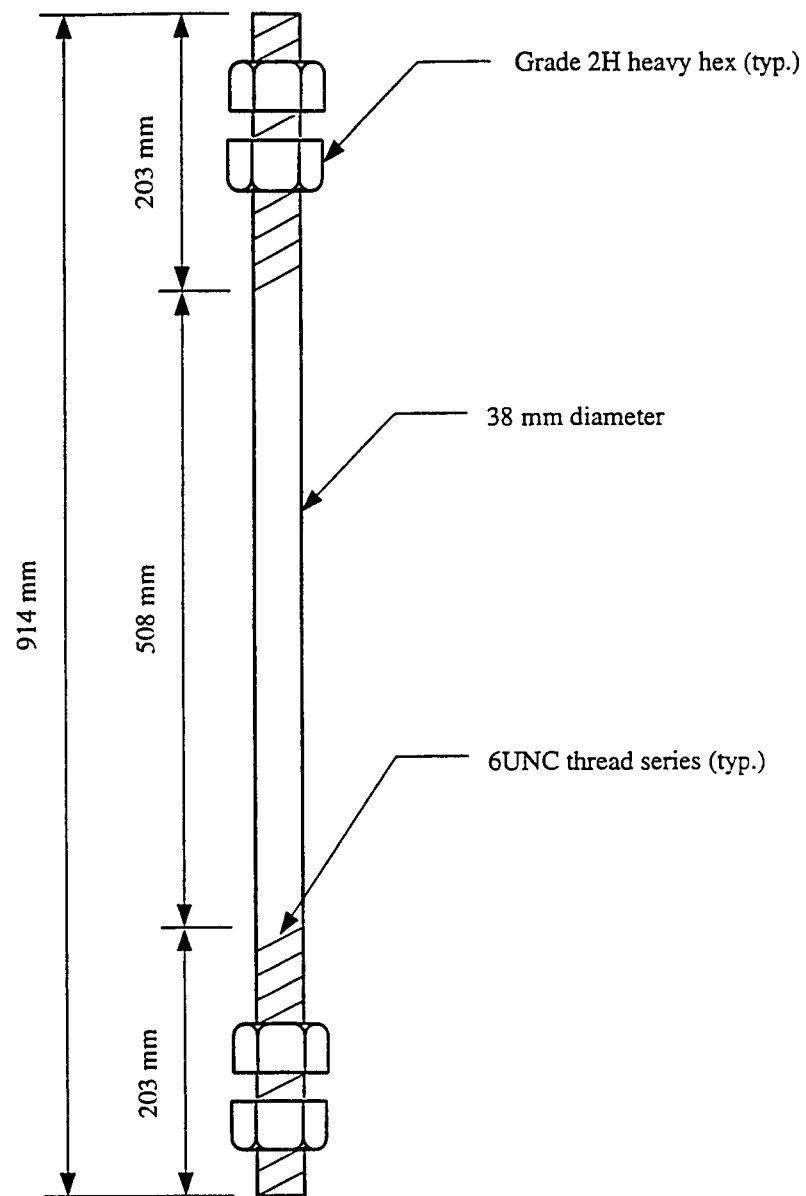


Figure 2.37 - Specimen Geometry.

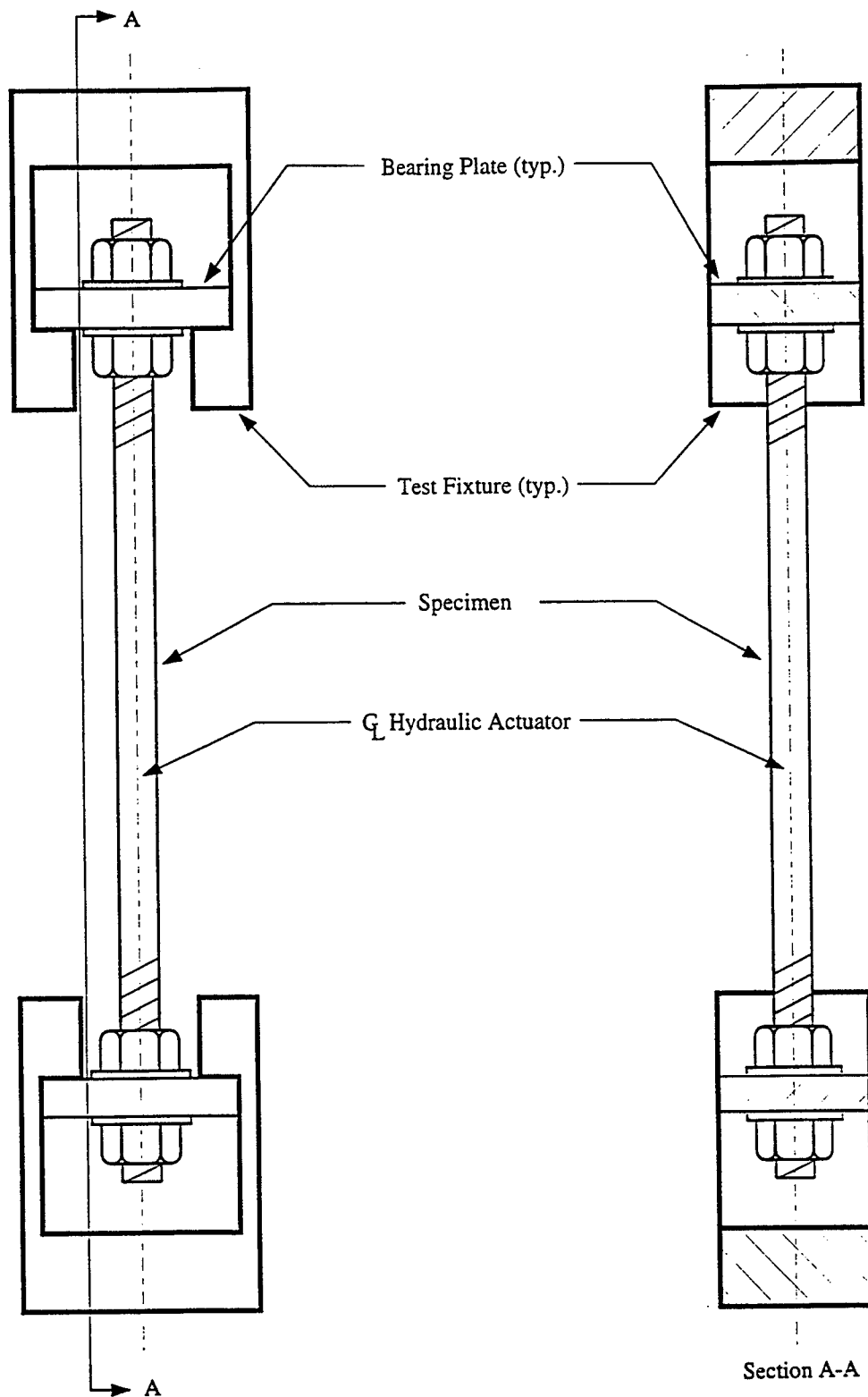


Figure 2.38 - Experimental Set-Up for Concentrically-Loaded Tests.

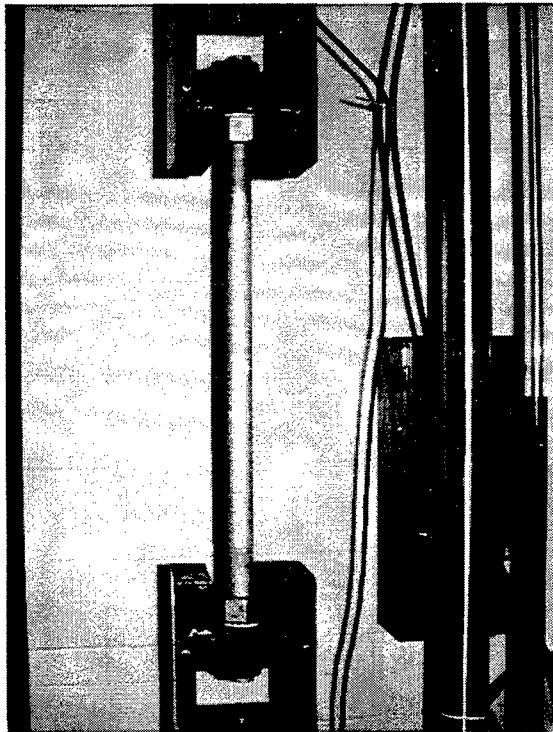


Figure 2.39 - Photograph Showing Test Set-Up for Concentrically-Loaded Tests.

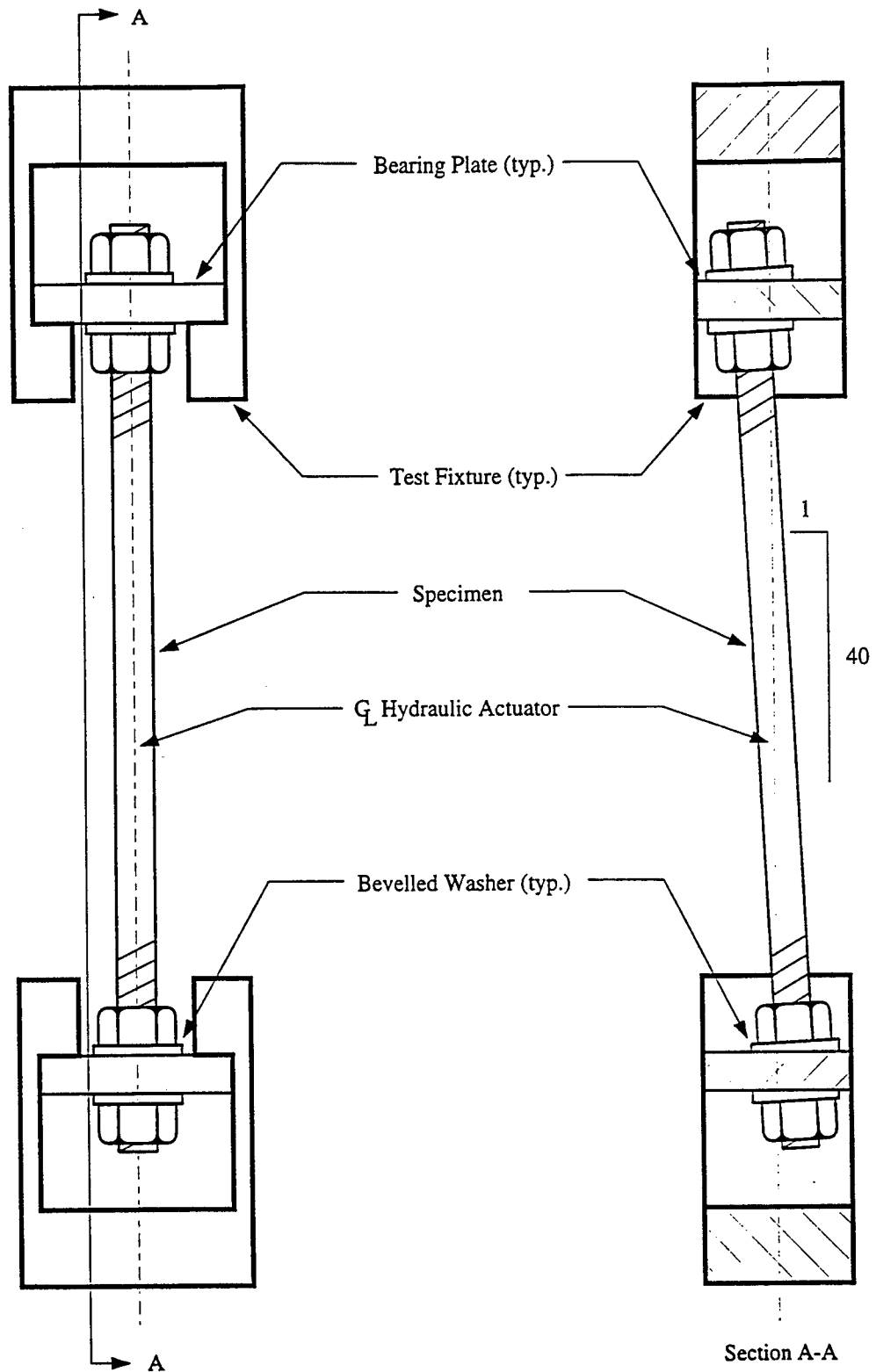
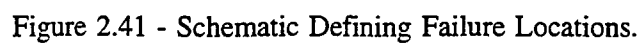
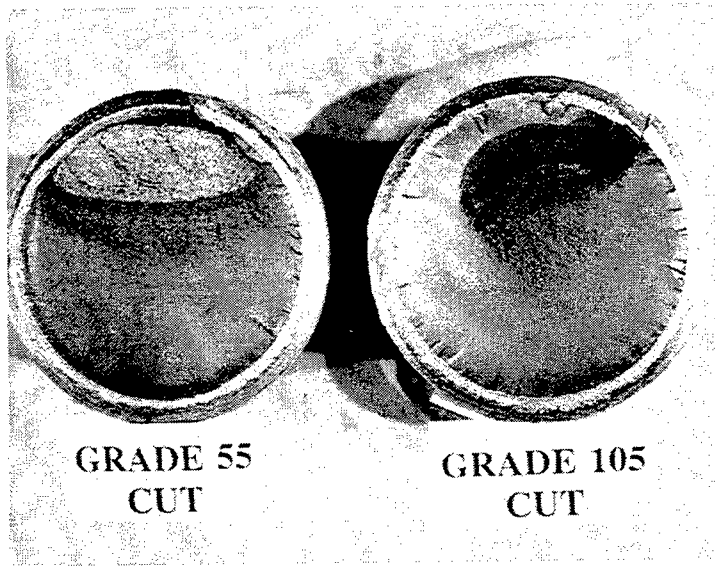
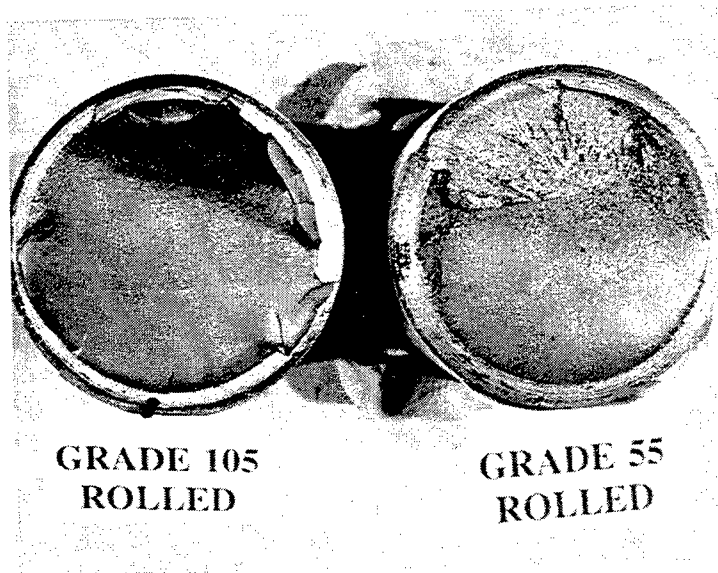


Figure 2.40 - Experimental Set-Up for Misaligned Tests.





**Fatigue Crack
Initiation (typ.)**



Fracture Surface

**Fatigue Crack
Surface**

Figure 2.42 - Photographs Showing Typical Cracked Specimens.

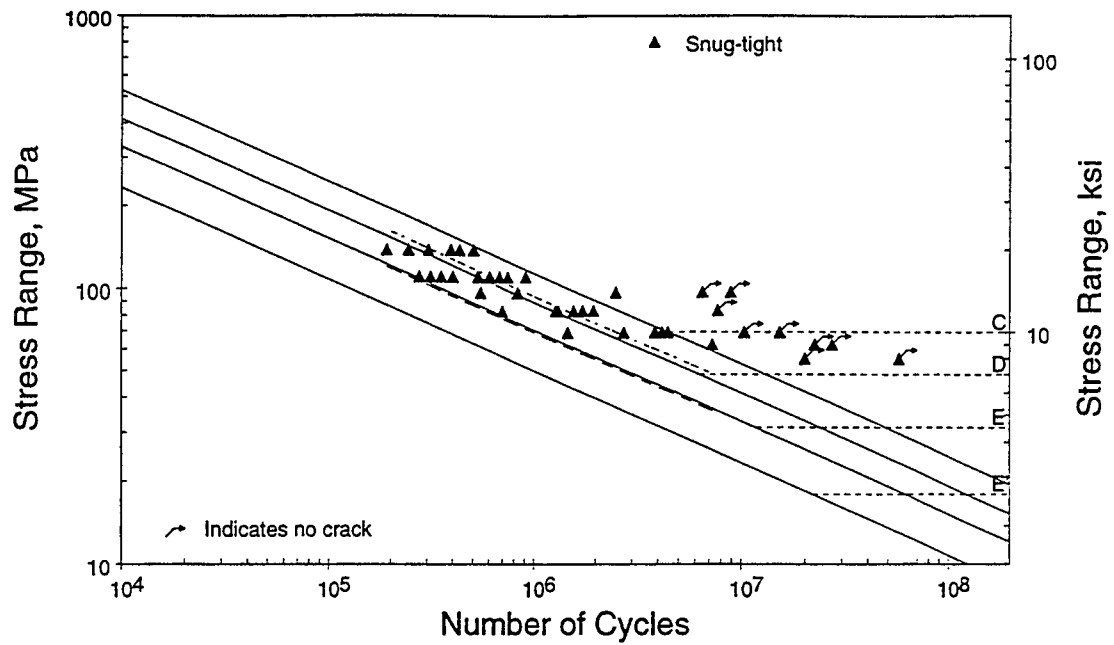


Figure 2.43 - S-N Curve Showing Concentrically-Loaded, Snug-Tight Test Data.

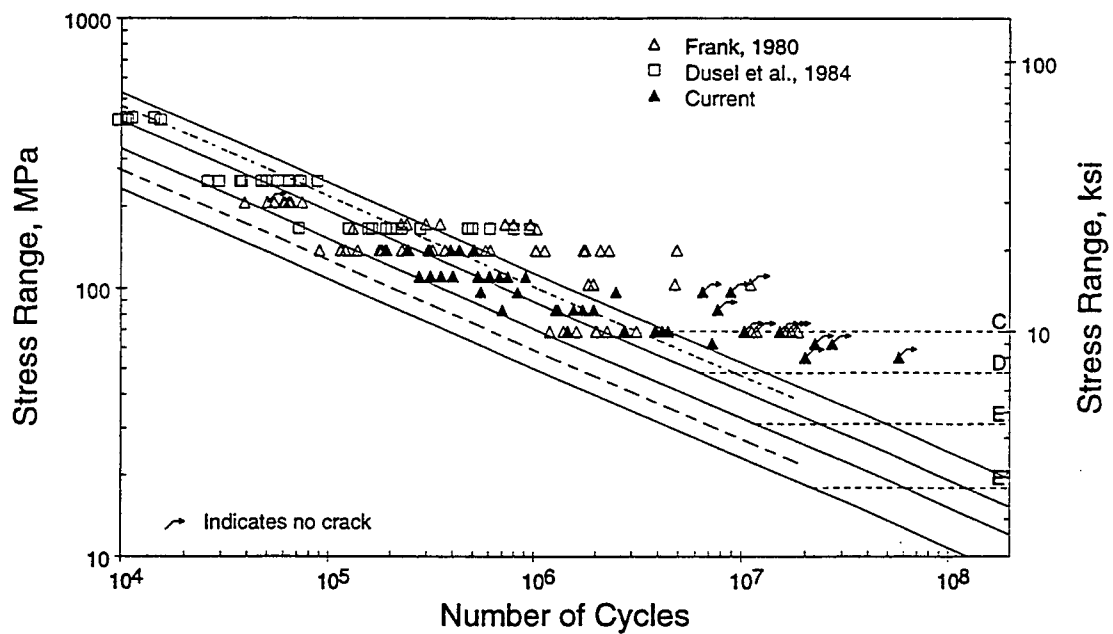


Figure 2.44 - S-N Curve Comparing Concentrically-Loaded, Snug-Tight Test Data with Previous Database.

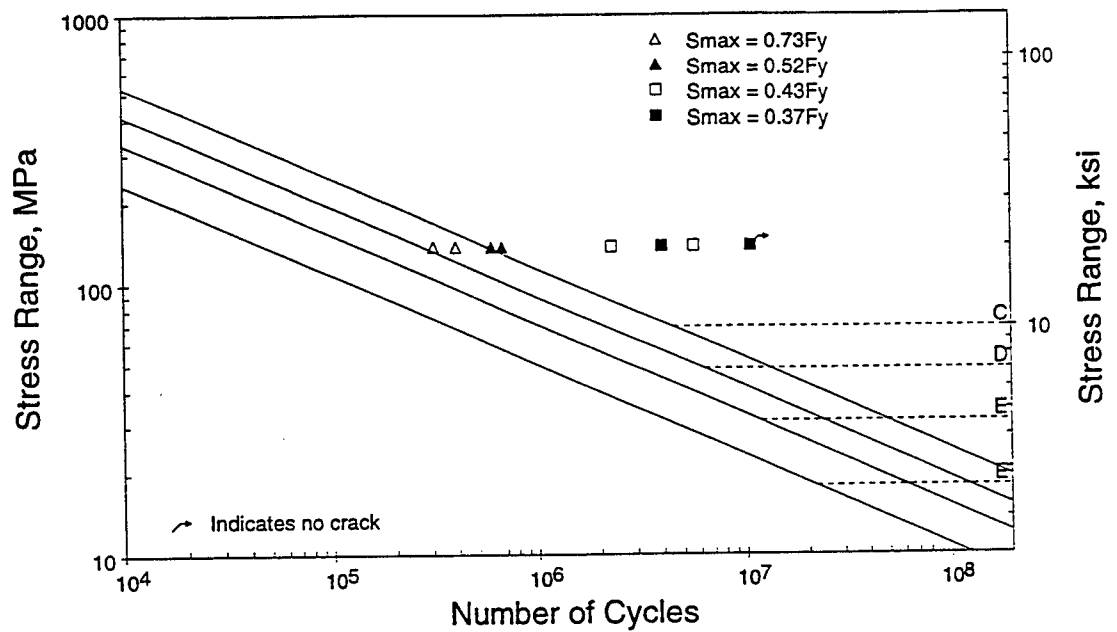


Figure 2.45 - S-N Curve Showing Effects of Maximum Stress for Grade 55 Specimens with Rolled Threads at 138 MPa Stress Range.

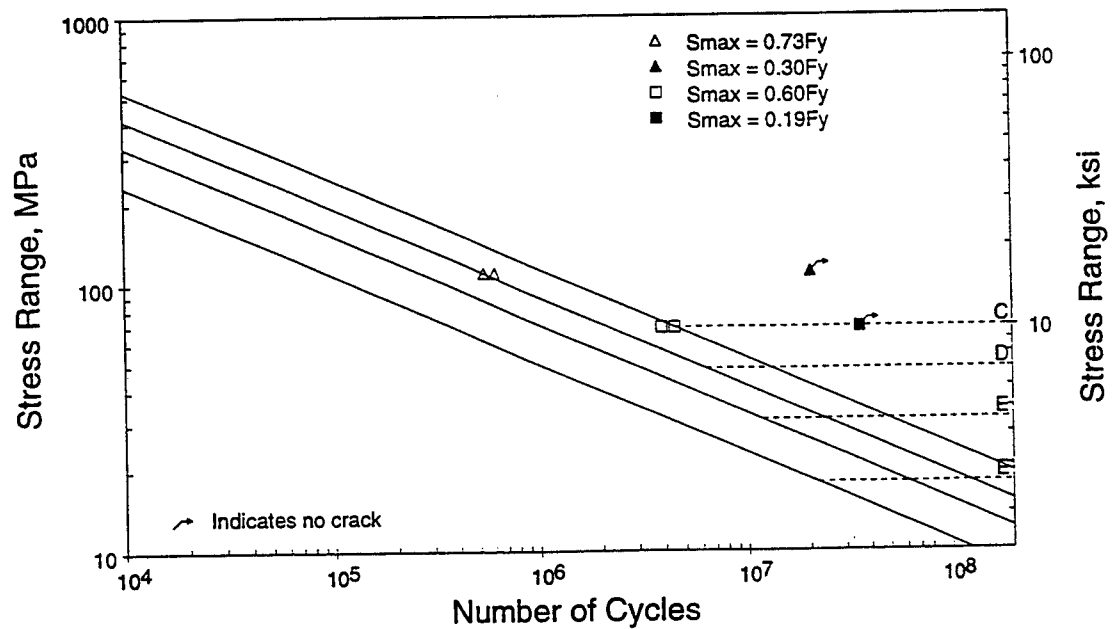


Figure 2.46 - S-N Curve Showing Effects of Maximum Stress for Grade 55 Specimens with Rolled Threads at 110 MPa and 69 MPa Stress Ranges.

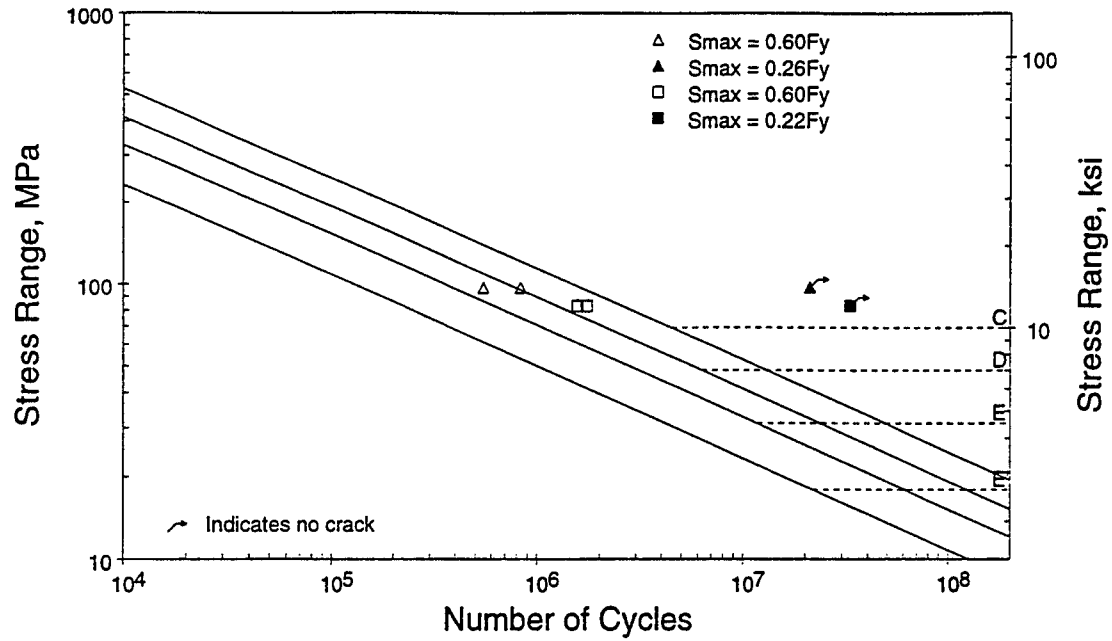


Figure 2.47 - S-N Curve Showing Effects of Maximum Stress for Grade 55 Specimens with Cut Threads at 97 MPa and 83 MPa Stress Ranges.

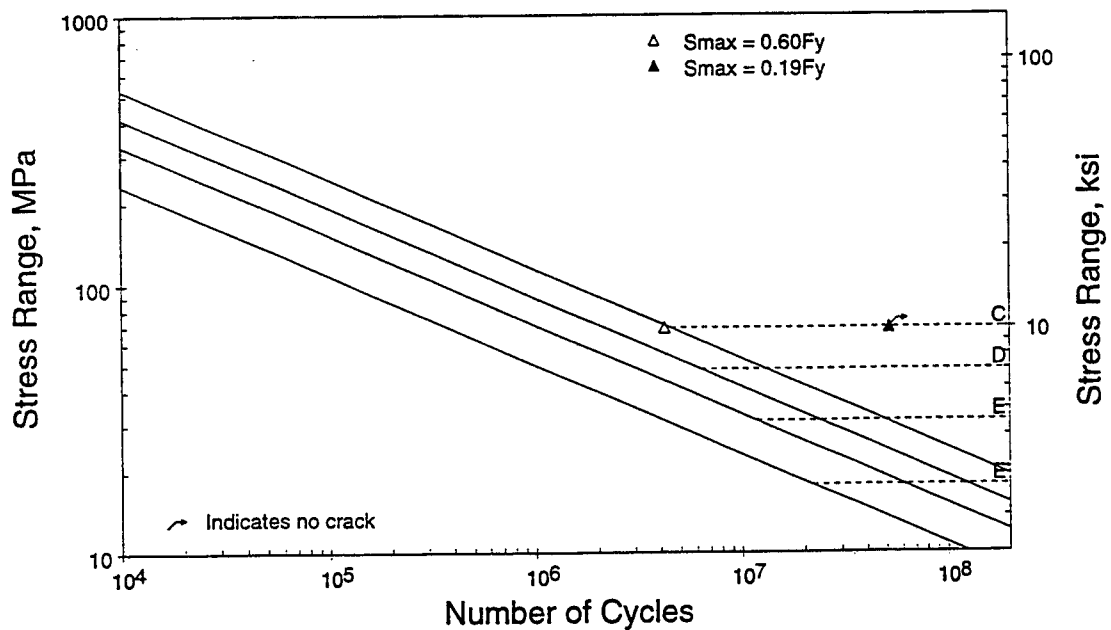


Figure 2.48 - S-N Curve Showing Effects of Maximum Stress for Grade 55 Specimens with Cut Threads at 69 MPa Stress Range.

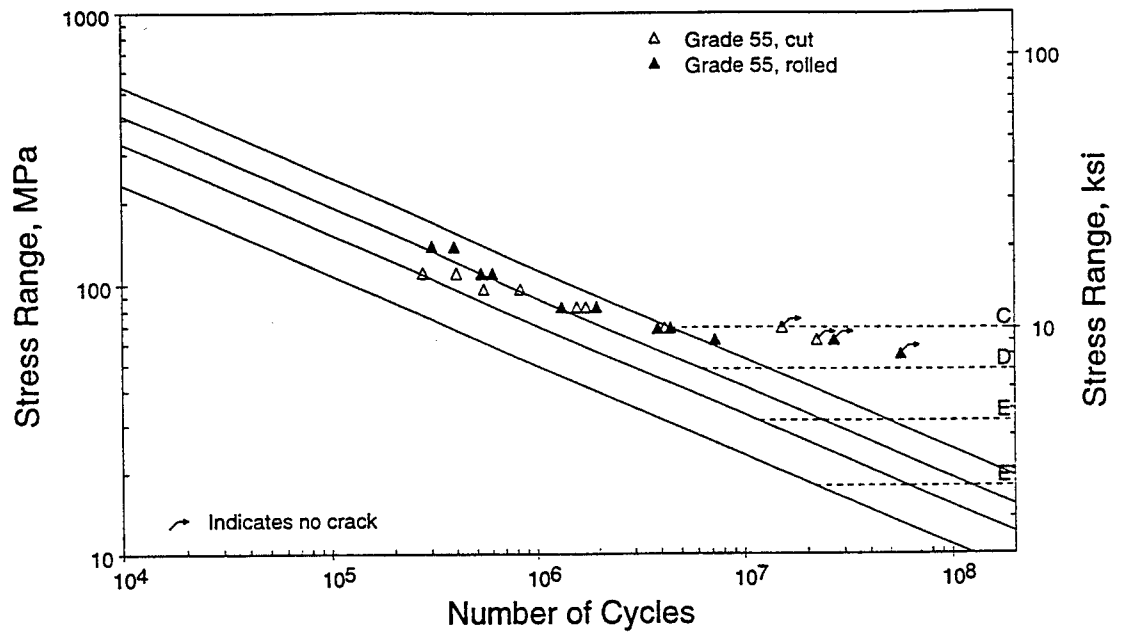


Figure 2.49 - S-N Curve Showing Effects of Thread Forming Method for Grade 55 Specimens.

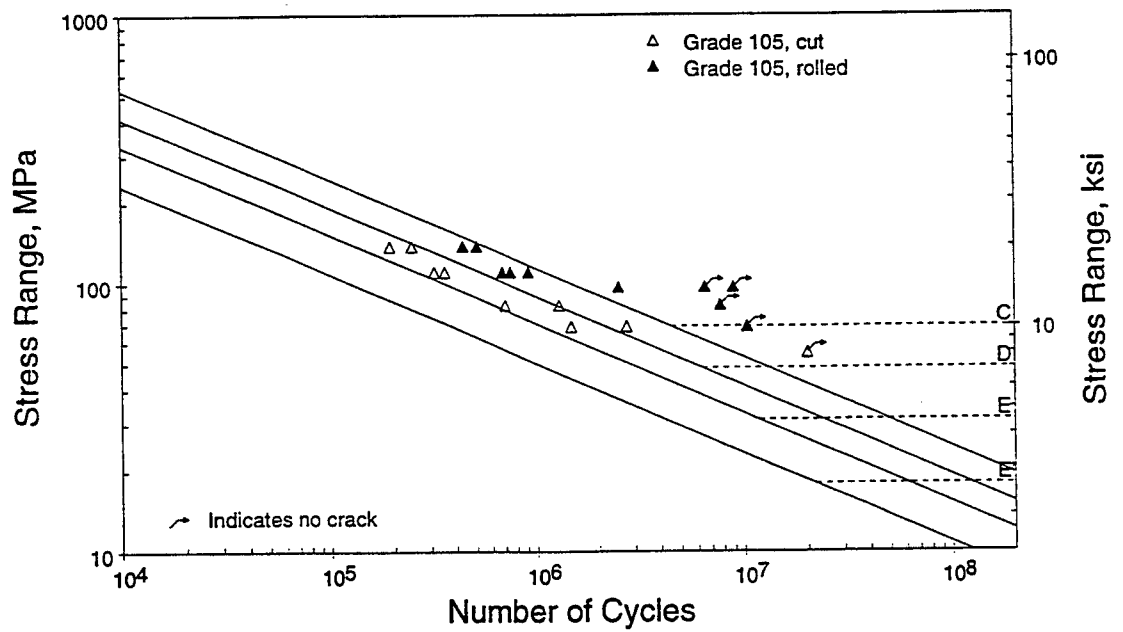


Figure 2.50 - S-N Curve Showing Effects of Thread Forming Method for Grade 105 Specimens.

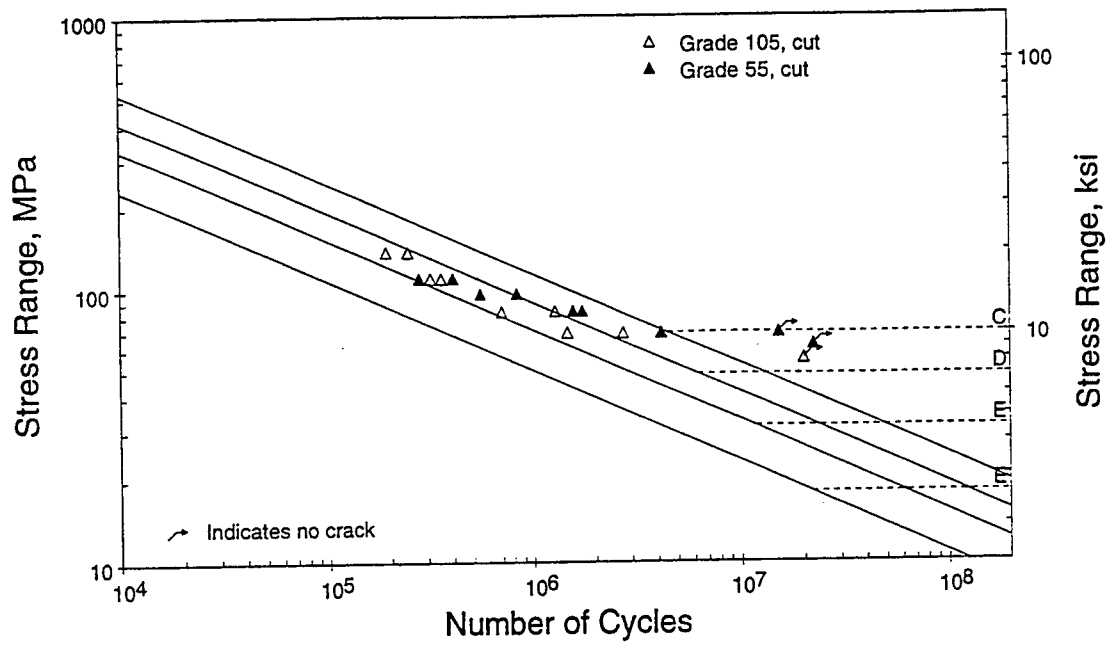


Figure 2.51 - S-N Curve Showing Effects of Material Grade For Specimens with Cut Threads (Tests conducted at approximately same absolute maximum stress).

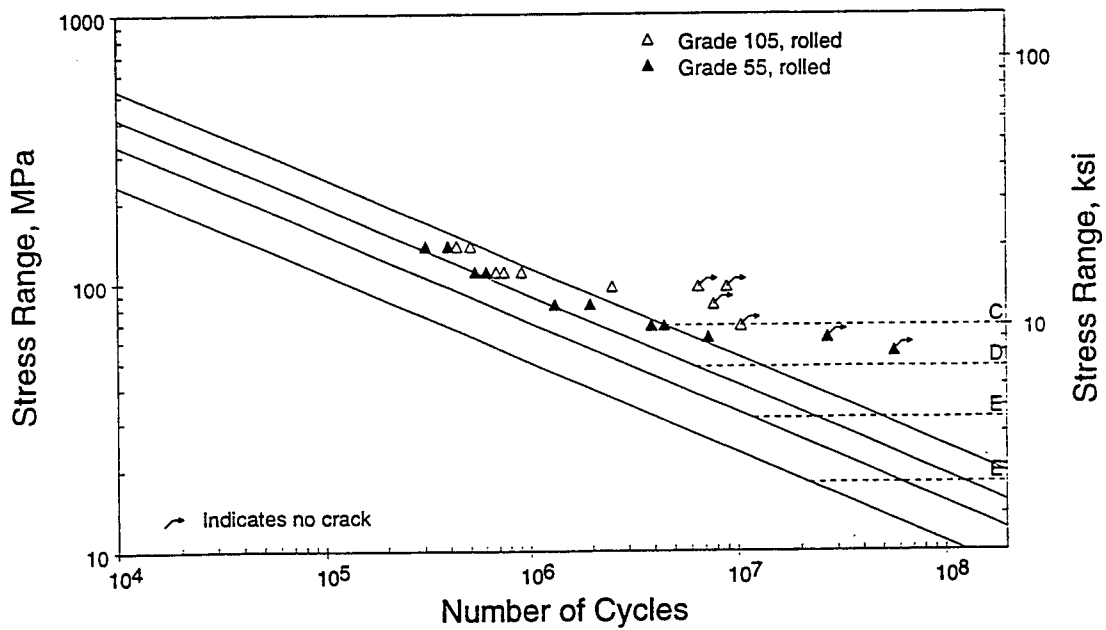


Figure 2.52 - S-N Curve Showing Effects of Material Grade For Specimens with Rolled Threads (Tests conducted at approximately same absolute maximum stress).

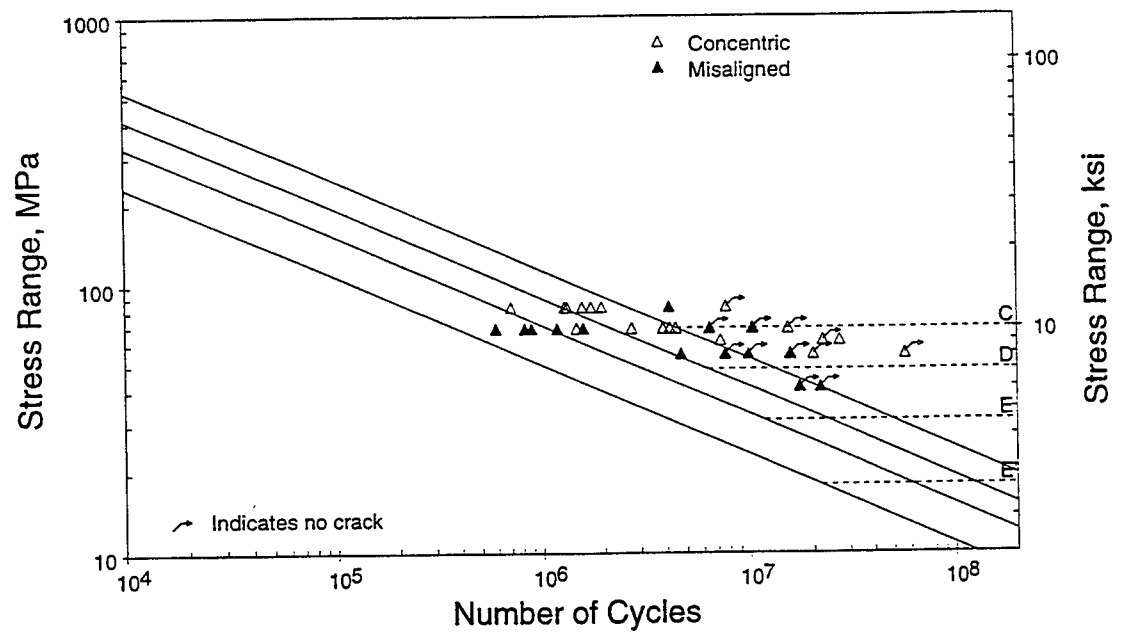


Figure 2.53 - S-N Curve Comparing Snug-Tight Misaligned and Concentrically-Loaded Specimens

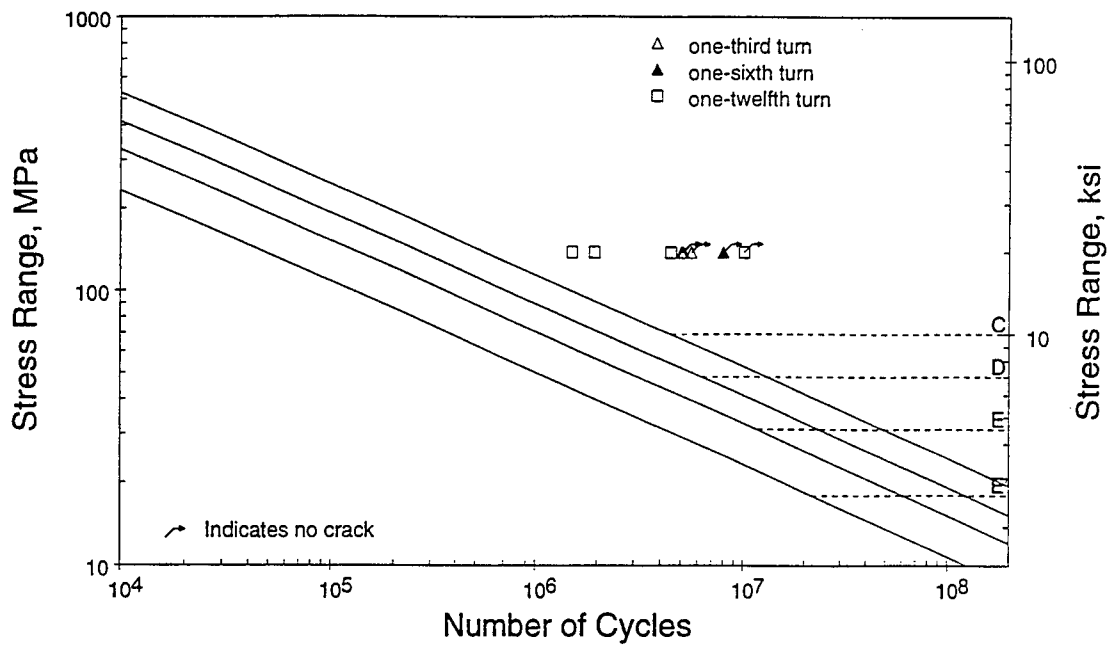


Figure 2.54 - S-N Curve Showing Effects of Bolt Pretension

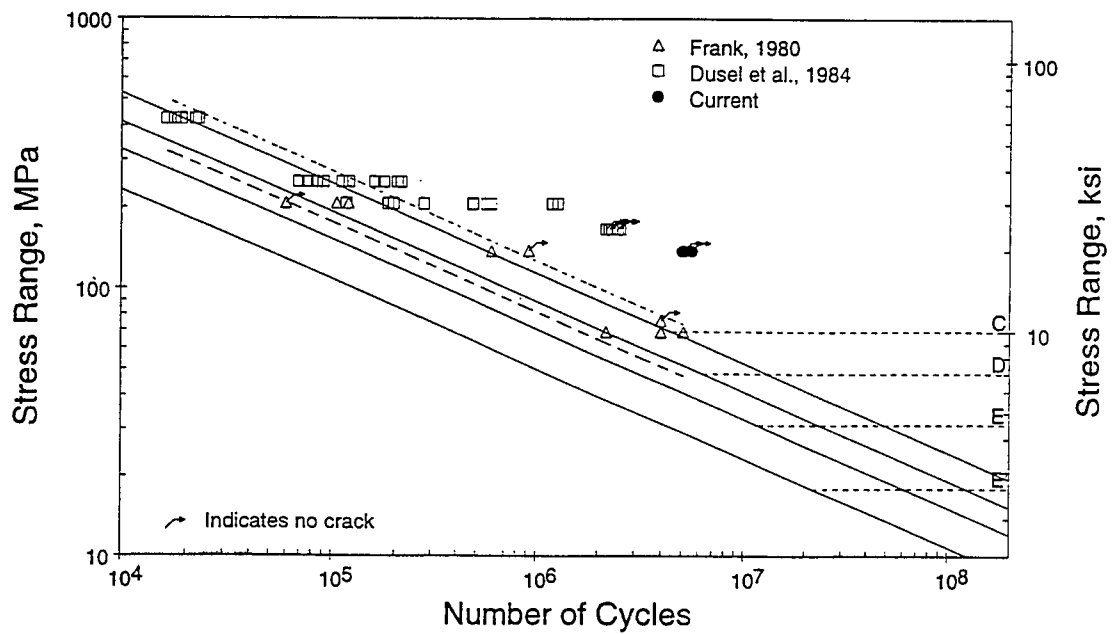


Figure 2.55 - S-N Curve Showing Previous Database of Fully-Tightened Anchor Bolt Fatigue Tests. Includes only those data obtained from tests conducted at maximum stresses corresponding to greater than $0.6F_y$.

2.4 RELATIONSHIP BETWEEN SUPPORT-STRUCTURE FORCES AND ANCHOR-BOLT STRESSES

Although the theoretical relationship between anchor-bolt stresses and support-structure forces (i.e. base moments and torsion and base shears) is relatively straight forward, variations in numerous site-specific parameters can significantly alter the distribution of stress between bolts within a bolt group and within any single bolt. The most significant of these parameters include misalignment, exposed length of the bolts, and tightness of the nuts. Misalignment of the anchor bolt group (a fixture typically keeps them mutually parallel) relative to the vertical axis tends to influence the stress distribution within the anchorage assembly in two distinct ways. First, misalignment of the bolts produces a bending moment in each bolt from the eccentricity of the axial forces in each of the bolts. Second, misaligned bolts which are not installed with bevelled washers will add additional localized bending stresses due to non-uniform bearing of the nut against the base plate (prying). Increasing the length of bolt exposed between the bottom of the lower leveling nut and the top of concrete increases the moment arm for the bending in the bolts from the shear forces applied through the column base plate. Increasing the exposed length also reduces the torsional stiffness of the anchorage assembly. Finally, nut looseness results in a redistribution of the anchor-bolt stresses due to the inability of one or more loose bolts to effectively carry loads applied to the support structure. Also, as explained in the previous section, the pretension which occurs between properly tightened nuts reduces the actual stress range felt by the bolts between the nuts. What happens is that more of the nominal applied stress range is carried by the base plate which is made to act monolithically with the bolt by the pretension. This latter effect increases the fatigue strength (in terms of the nominal applied stress range), at least for stress ranges above the CAFL (the finite-life region).

Although the results of field inspections of cantilevered support structures have indicated that the occurrence of loose and misaligned bolts is relatively common, little or no research has been conducted to study the effects of these parameters. Because these parameters are difficult to quantify analytically, an experimental study was conducted to investigate the effect of these factors on the relationship between support-structure forces and anchor-bolt stresses.

2.4.1 Description of Experiments

2.4.1.1 Test Specimens - Each test specimen consisted of two components: a cast-in-place foundation with embedded galvanized anchor bolts, and a fabricated steel column stub with base plate. The anchor bolt size and pattern were selected as representative of small to mid-sized cantilevered sign support structures with mast arm spans from 3 m (10 ft) to 9.1 m (30 ft).

Two concrete foundations and two column stubs were fabricated and combined to make up the four test assemblies described in Table 2.13. The two concrete foundations were detailed with eight 38 mm (1.5 in) diameter anchor bolts placed in a 533 mm (21 in) diameter circular pattern. The anchor bolts were fabricated to AASHTO M314-90 "Standard Specification for Steel Anchor Bolts" (Grade 55) with a 6UNC (rolled) thread series. Each concrete foundation was conservatively designed and detailed to provide a shear and moment capacity in excess of the predicted anchor bolt group ultimate strength. One

concrete foundation was cast without any intentional anchor bolt misalignment (it is recognized that some level of misalignment is inevitable in the construction of these anchorages) and the second was cast with all eight bolts racked at an angle of 1:20 from the vertical. At the time of casting the misaligned concrete foundation, this was the maximum misalignment allowed in the Michigan DoT anchor bolt special provision. Since that time however, the special provision has been revised to allow misalignments of up to only 1:40 from vertical. To our knowledge, no other state DoT qualitatively defines a maximum allowable anchor bolt misalignment.

Each of the anchor bolts in the two concrete foundations was instrumented with four uniaxial strain gages. The four strain gages, laid out at 90-degree intervals around the bolt, were placed on the shank portion of the anchor bolt directly above the concrete foundation. On each of the eight bolts, the gages were oriented with respect to the primary axes (parallel and perpendicular to the direction of the applied load) of the concrete base rather than radially around the anchor bolt pattern. A close-up photograph of the column base and anchor bolt pattern is shown in Figure 2.56. After casting the concrete foundations, several anchor bolts from the "straight" fixture were calibrated to known tension and compression loads. The purpose of these calibrations was to ensure that the strain gage data was not significantly influenced by the close proximity to the applied load from the nut and the concrete base. Results of these calibrations indicated that the expected linear relationship between applied load and average axial bolt strain was achieved.

Two 406 mm (16 in) diameter by 3 m (10 ft) long steel column stubs were fabricated with a socket-type connection between the column and base plate by a national supplier of cantilevered support structures. Each specimen was detailed identically with the exception of the base plate thickness. The 38 mm (1.5 in) thick base plate is representative of typical support structure base plates which are typically chosen such that their thickness is greater than or equal to the bolt diameter. This 38 mm thick base plate structure was tested with Assemblies 1 and 3. Assemblies 2 and 4 used a column-stub specimen with a 25 mm (1 in) thick base plate. The base plate thickness on these specimens was intentionally undersized to investigate the possible effect of base plate thickness (stiffness) on load distribution. Strain gages were also placed on the column stub to verify the overturning moment at the column base. Uniaxial strain gages, as well as biaxial rosettes, were positioned at 90 degree intervals around the column stub at 51 mm (2 in) and 102 mm (4 in) above the base plate. The results were consistent with analytical predictions, however calculation of longitudinal bending stresses in the column at 51 mm (2 in) above the base plate required the use of biaxial stress/strain relationships. Restraint provided by the socket connection weld generated significant transverse (i.e. hoop) strains at this lower location.

2.4.1.2 Experimental Setup and Procedures - Column stubs were attached to the concrete foundations following standard construction practices for ungrouted, double-nut anchor bolt installations. Initially, each anchor bolt in the group was tightened in an iterative sequence to one-third of a turn beyond the snug-tight condition. Tightening to one-third of a turn required the use of a hydraulic wrench and

therefore became quite time consuming. It was decided that for static tests, fully tightened anchor bolts may not be necessary to obtain reliable strain gage data. To prove this assumption, the first test was repeated with the anchor bolts tightened using conventional hand-tightening procedures to a rotation of approximately 1/6 of a turn beyond snug. Based on consistent results between this experiment and the experiment with fully tightened bolts, the remaining tests were conducted with the anchor bolts tightened by hand.

As shown in the test matrix in Table 2.13, each of the four assemblies was tested statically under six load conditions to study the effect of various parameters (i.e. misalignment, exposed length, etc.). For each load condition, the specimen was monotonically loaded in tension and compression to loads slightly below the current static design allowable for anchor bolts (i.e. $0.5 F_y$). All 32 strain gages on the bolts, strain gages on the column stub, and the applied load were continuously monitored by a computer-controlled data acquisition system. Data were saved at discrete load increments on both the loading and unloading portion of the test.

A reusable test fixture was designed to easily attach to the top of both column stubs. A schematic of the entire test setup is shown in Figures 2.57. Loads were applied with a 130 kN (30 kip) servo-hydraulically controlled actuator with a load cell. The test fixture was designed to allow static tests to be performed at four different moment:torsion:shear (M:T:V) ratios by applying loads to the test fixture at four different locations.

The actuator positions were selected following an evaluation of the magnitudes of the loads for which cantilevered sign support structures are designed. This evaluation revealed that the M:T:V ratios are sensitive to structural configuration and total sign area. The typical M:T:V ratios for small to mid-sized cantilevered sign structures are in the range of 30:2:1 (for high mast luminaires for example) to 14:17:1 (for structures with long mast arms).

The first two test positions required that the actuator be mounted horizontally at a height of 6.9 m (22.5 ft) above the lab floor and positioned with and without an eccentricity of 1.5 m (5.0 ft) from the vertical axis of the column stub. These two tests investigated the relationship of support-structure forces and anchor-bolt stresses at M:T:V ratios of 19.5:0:1 and 19.5:5:1 respectively (these ratios are in feet). The other two test positions required that the actuator be mounted 5.3 m (17.5 ft) above the lab floor with and without an eccentricity of 3.0 m (10.0 ft); which gives M:T:V ratios of 14.5:0:1 and 14.5:10:1 respectively.

Two additional tests were conducted on each assembly with the actuator located in the first two positions (M:T:V ratios of 19.5:0:1 and 19.5:5:1). The first test studied the effect of loose, or failed, nuts by sequentially loosening and then retightening one bolt from the eight bolt group. The bolt selected for loosening was located furthest from the neutral axis of the bolt group. Finally, one test on each assembly evaluated the effect of variations in the exposed length of anchor bolts above the foundation. All tests were first conducted with approximately 25 mm (1 in) of bolt exposed between the top of the concrete foundation and the bottom of the leveling nut. This configuration was selected for testing because it is commonly specified by state DoT's in cantilevered support structure standard drawings. The results are

compared to those obtained when approximately 76 mm (3 in) of bolt is exposed above the concrete foundation.

At the conclusion of the 32 static tests on the column-anchor bolt assemblies, four full-scale proof-of-principle fatigue tests were conducted to verify results of the anchor bolt fatigue tests described in Section 2.3.

2.4.2 Results of Experiments

2.4.2.1 Static Test Results - Raw strain-gage data were examined and any obviously erroneous readings were removed from the analysis. Then the strains from the four gages per bolt were averaged together to obtain an axial strain in each bolt. This averaging was done to reduce the error in the measurements and to eliminate (for the time being) the effect of bending of each bolt. This bending effect is examined later. As illustrated in Figure 2.57, bolts #1 and #5 were located along the axis of loading at a distance of 267 mm (10.5 in) from the neutral axis and are therefore the highest stressed bolts in the pattern. The other bolts were numbered counterclockwise from bolt #1 around the anchor bolt pattern.

A plot of axial strain in each of the eight bolts at incrementally applied loads is presented in Figure 2.58. These data are from a test conducted on Assembly #1 (i.e. 38 mm thick base plate on a straight anchor bolt pattern) with 25 mm (1 in) exposed bolt length and the actuator positioned at a Moment:Torsion:Shear ratio of 19.5:0:1. As expected, the axial strain in bolts #1 and #5 are the highest of the bolt group and the data are symmetric for applied loads in both tension and compression. As expected, the magnitude of axial strain in bolts #2, #4, #6, and #8 is consistently lower than the strain in bolts #1 and #5 by approximately 60 to 80 percent. Finally, because of bolts #3 and #7 placement on the neutral axis of bending, measured strains in these components were negligible. Similar results were obtained for tests conducted with the 25 mm (1 in) base plate, 75 mm (3 in) exposed bolt length, and misaligned anchor bolt pattern.

A statistical study was conducted to evaluate average axial bolt strains at the maximum applied tension and compression loads. The actual average bolt strains were normalized by the predicted average bolt strains for a known maximum applied column load. Predicted axial bolt strains were calculated from the flexure formula (M/I) where I is the moment of inertia of the entire bolt group (0.0002577 m^4 or 621 in^4). Given an accurate model to predict anchor-bolt stresses, normalized strains (i.e. measured strains divided by predicted strains) at all bolt locations would be expected to equal 1.0. Because predicted and measured strains are near zero in bolts #3 and #7, the data from these bolts are excluded from the statistical analysis.

It was not clear if the results from bolts #2, #4, #6, and #8 (closer to the neutral axis) would be different from the results from bolts #1 and #5 where the average axial strains were higher. The mean and variance for each set of data (for tests conducted with a 38 mm (1.5 in) base plate with no applied torsion) were compared to see if there were any significant differences. The mean is simply the arithmetic average of the data set while the variance measures how closely the data are clustered about the mean value. For bolts #1 and #5 only, the mean and variance were 1.09 and 0.029 respectively. When these

data are included in the data set with bolts #2, #4, #6, and #8, the mean and variance of the data were 1.054 and 0.024 respectively. A "t test" was conducted on the mean and an "F test" was conducted on the variance and these tests concluded that the means and variances from these two data sets were not significantly different (with greater than 95 percent confidence). (These tests are explained in standard statistical references [45].) In the other tests with misalignment and torsion, similar close agreement was found between the data set for bolts #1 and #5 and the data set for all six bolts. Therefore, it was concluded that the data from all six of these bolts could be considered as one consistent data set or "population." In addition, the exposed length of the anchor bolt was found to have no influence on the distribution of axial stresses in the bolt group as would be expected. Therefore, data from the tests with a 75 mm (3 in) exposed length are included in the same data set as the data from the tests with a 25 mm (1 in) exposed length.

Table 2.14 is a summary of statistic data (i.e. mean and variance) for all six bolts from both exposed lengths included in the analyses. The effects of torsion on the distribution of bolt stresses can be seen by comparing the results at M:T:V ratios of 19.5:5:1 and 14.5:10:1 to those at M:T:V ratios of 19.5:0:1 and 14.5:0:1. There is only a random difference in the means of these data sets, meaning the torsion did not increase the magnitude of the axial stresses in the bolts in a systematic way. However, the data sets which included torsion had variances which were approximately three times greater than those without torsion. F tests show that there is greater than 99 percent confidence that the variance of the data with torsion is greater than the variance of the data without torsion. For unexplained reasons, possibly a coincidence, the tests conducted with the 25 mm (1 in) base plate on a misaligned anchor bolt pattern do not show this increase in variance due to torsion.

The increase in variance due to torsion can also be seen in Figure 2.59 which presents histograms of the normalized bolt strains for tests with a 38 mm (1.5 in) base plate and no misalignment, with and without torsion. The normalized bolt strain data for tests with torsion were distributed from a low of 0.4 to a high of 1.6 with approximately 25 percent of strains clustered near 90 percent of the theoretical bolt strain. Normalized bolt strain data for tests without torsion were distributed from a low of 0.6 to a high of 1.3 with approximately 42 percent of the results clustered near 90 percent of the theoretical bolt strain.

The base plate thickness also had a significant effect on the anchor bolt stresses. The data in Table 2.14 seem to suggest that the mean has increased for the case of the 25 mm (1 in) thick base plate without misalignment, although this could not be established with confidence by t tests. However, the F tests showed that the 25 mm (1 in) thick base plate increased the variance, with greater than 97 percent confidence in all cases except the case of misalignment and torsion. For the misaligned test for this case, the variance did not increase with torsion and seems anomalous.

It is believed that an increase in flexibility of the base plate causes localized bending to occur in the anchor bolts. This localized bending, or prying, is caused by a non-uniform distribution of stresses on the anchor bolt nut which would increase scatter in the test data. Based on these findings, only adequately stiffened base plates should be allowed in the design of cantilevered support structures. It

appears that the old design rule-of-thumb for sizing base plates which states that "at a minimum, base plate thicknesses should be equal to the anchor bolt diameter" is reasonable.

Surprisingly, misalignment did not have a statistically significant effect on the results. Based on Table 2.14, it appears that the mean is lower for the misaligned data, although no rational explanation for this bias has been developed. Based on the data for the 38 mm (1.5 in) thick base plate only, it also appears that misalignment increases the variance and exacerbates the increase in variance due to torsion. However, none of these apparent differences could be established with confidence using the statistical tests. Therefore, it was concluded that the misalignment of the anchor bolt pattern (1:20) does not significantly influence the distribution of stresses among the bolt group. Misalignments of less than 1:20, which are more realistic installation conditions, will most likely have an even smaller effect on the distribution of bolt stresses.

At least one test on each assembly was conducted after loosening bolt #1 from the anchor bolt pattern. The objective of these tests was to simulate the effect of a completely loose or fractured bolt. Based on the simple flexure model, it would be expected that strains in anchor bolts #2 and #8 (i.e those adjacent to anchor bolt #1) would increase by 69 percent as the load is transferred to these two bolts. However, the average increase in strain at these two locations was measured as 51 percent for tests conducted on assemblies with a 38 mm (1.5 in) base plate. Therefore, the Mc/I design assumption conservatively overestimates the distribution of strains for this condition. It is believed that with one or more bolts missing from the bolt pattern, flexibility of the base plate affects the distribution of forces to the anchor bolts. A single test was also conducted to simulate the behavior of a four bolt anchor bolt pattern. In addition to the two bolts located on the neutral axis of bending (bolts #3 and #7), bolts #1 and #5 were also completely loosened to produce a four bolt pattern. Unfortunately, the results of this test were inconclusive with respect to determining the distribution of anchor-bolt stresses. Excessive distortion in the 38 mm (1.5 in) base plate caused the plate to bind up on these loosened bolts and effectively transfer axial loads. These observations highlight the importance of a properly sized and detailed base plate in effectively distributing support-structure forces to the anchor bolt assembly.

The use of inadequate base plate thickness will not be allowed in the proposed specification. Therefore, in order to examine the probable distribution of anchor bolt stresses under the proposed specification, only data from the 38 mm (1.5 in) thick base plate should be considered. A histogram of normalized bolt strains for all tests (with and without misaligned anchor bolts) conducted on specimens with a 38 mm (1.5 in) base plate is presented in Figure 2.60. By visual observation, the data presented in Figure 2.60 appear to be normally distributed. The mean and variance of this data set are 0.93 and 0.064 respectively. Since there is no systematic effect on the mean which is approximately 1.0, it appears reasonable to calculate the relationship between anchor-bolt stresses and support-structure forces with the simple flexure formula (Mc/I). The variance of the data will contribute to the overall uncertainty in fatigue resistance. However, on balance, for every bolt with a stress range on the high side there should be a bolt with a stress range on the low side. Furthermore, this uncertainty is far less than the uncertainty in the magnitude of the wind loads. Therefore, it is concluded that no additional factors must be included

in the design procedure to account for the variance in the bolt stresses. Furthermore, the variance in the bolt stresses will have no effect on ultimate strength. Although certain bolts may begin to yield prematurely, the ductility will allow full strength to be obtained from each bolt.

In addition to the axial stresses generated from resisting overturning moments at the cantilevered support structure base, anchor bolts will also be subject to bending stresses. Bending moments in individual anchor bolts are typically generated by the transfer of horizontal base shear forces and torsional moments as individual shear forces applied through the base plate to the anchor bolts and into the concrete foundation. As expected, the bending stresses are most significantly affected by the amount of exposed bolt between the top of the foundation and bottom of the leveling nut. Standard plans for cantilevered support structures typically specify that exposed lengths shall not exceed 25 mm (1 in), which minimizes the moment arm for bending from these shear forces. However, some states like to dry-pack grout under the base plate, which requires a greater exposed length. In addition to increasing the bending stresses, the dry pack has been reported to be a source of corrosion problems as it gets cracked and retains water. For these reasons, grouting between the base plate and the concrete should be discouraged.

The amount of bending in individual anchor bolts was evaluated by closely examining the data for each of the four strain gages placed on a typical anchor bolt. By comparing measurements at two strain gage locations 180 degrees apart on an anchor bolt, the calculation of bending moments about a perpendicular axis was possible. The biaxial moments were then resolved into the principal moments. For example, measurements obtained from a test with a 38 mm (1.5 in) base plate, straight anchor bolt pattern, and a 76 mm (3 in) exposed length resulted in the computation of bending moments of 123 and 88 N-m (1.09 and 0.78 kip-in) at anchor bolts #3 and #7 respectively. (These bolts near the neutral axis of the bolt group had very little axial force and were therefore most suitable for measuring bending stress).

The best model to use to calculate the bending stresses was found to be a beam fixed at the bottom of the leveling nut and fixed at the top of concrete, with the top end free to displace circumferentially around the bolt circle relative to the end in the concrete. Assuming a horizontal shear of 1/8 the applied load and a beam length of 76 mm (3 in), a theoretical bending moment was calculated which is 40 to 90 percent greater than the measured moment. It is recognized that the assumption of a fixed connection at the concrete interface is not consistent with the actual behavior at this location. Some amount of elastic and inelastic deformations will occur along the anchor bolt-to-concrete interface which may cause cracking or spalling at high shear loads. In fact, tests on the misaligned anchor bolt assembly resulted in some limited spalling in this area. However, the use of a greater length (to account for fixity at some point below the top of concrete or to take the point of load application as the mid-thickness plane of the base plate) makes the theoretical moment even greater which makes the result less accurate. Similarly, the use of beam models with one fixed and one free end or one fixed and one pinned end would provide an even more conservative result and were therefore not considered.

Correlation of measured and predicted anchor bolt moments for a similar test configuration with only a 25 mm (1 in) exposed length proved to be even more inaccurate. It is believed that the short length of exposed bolt (less than one diameter) was inadequate to develop bending stresses (the bolt behaved

more like a shear link). Although a comparison could not be made to theoretical bending stresses, the magnitude of these stresses could be evaluated from the test data. For the most critical bolts in axial tension (bolts #1 and #5) the percentage of bending stress was less than 10 percent of the average axial stress. This increase in stress is small and occurs only at one location around the bolt circumference. There is a lower combined stress range at the point 180 degrees away. Therefore, it appears that the bending effect can be ignored for anchor bolts which have an exposed length less than one diameter in height. Exposed heights greater than one bolt diameter, for grouting for example, would require calculation of the bending stress using the conservative fixed-fixed beam model.

2.4.1.2 Full-Scale Foundation Anchor Bolt Fatigue Tests - At the conclusion of the static test program to determine the relationship between support-structure forces and anchor-bolt stresses, four fatigue tests were conducted on the anchor bolts used in the full-scale concrete foundations. These tests were conducted with the actuator positioned such that only horizontal shear and overturning moment were applied to the 8 bolt group (i.e. no torsion). Two tests were conducted on the concrete foundation cast with misaligned anchor bolts (1:20) and similarly, two tests were conducted on the foundation cast without misalignment. Bevelled washers were not used in these full-scale foundation tests. For all tests, the exposed length on the anchor bolts was set at 25 mm (1 in) to reflect typical installation conditions. However, the bolts were only snug-tightened to allow comparison with the anchor bolt fatigue test data described above. The actuator load was applied at a frequency of 1 Hz in only one direction such that a 138 MPa (20 ksi) tension-tension stress range was measured in the critical bolt (bolt #1 or #5). The maximum bolt stress was set at approximately 60 percent of the minimum yield stress to duplicate the conditions used in the individual anchor bolt fatigue tests. After failure of the first bolt on each concrete foundation, the direction of loading was reversed and the other critical bolt was similarly tested. It is possible that the compression cycles that this bolt experienced during the first test in the other direction could limit the fatigue life in the second test, but no such bias was observed in the second test results relative to the first test results.

Fatigue failures in the straight anchor bolts occurred at 263,000 and 397,000 cycles while failures in the misaligned anchor bolts occurred at 240,000 and 488,000 cycles. A plot of the results from these four full-scale foundation tests is presented in Figure 2.61 along with the snug-tight data obtained from the individual anchor bolt fatigue tests described in Section 2.3. In accordance with the above recommendation, bending stresses were not considered in plotting the stress ranges for these four data points in Figure 2.61. These four data points from the foundation tests conducted on bolts with and without misalignment are within the scatter band of results for individual bolts tested without misalignment. Although the data set is not large, it is reasonable to conclude that the results obtained from individual anchor bolt fatigue tests accurately predict the behavior of bolts in a complete assembly. Furthermore, the fact that the four points are within the scatterband also indicates that it is not necessary to include the bending stresses in the stress range for exposed lengths less than one bolt diameter.

In addition, these full-scale foundation tests indicated that misalignment did not significantly affect the fatigue resistance. Although the amount of misalignment was well beyond typical installed conditions (i.e. 1:20), the two misaligned data points were within the level of scatter and one misaligned bolt actually exhibited the longest fatigue life.

As a result of these full-scale anchor bolt assembly fatigue tests, information was also gained on the fatigue resistance of two common column to base plate connection details. As mentioned above, the fatigue test was initiated with a double-fillet welded socket connection. The applied loads necessary to propagate fatigue cracks in the anchor bolts generated stress ranges of 103 MPa (15 ksi) at the column base which led to the development of a fatigue crack at only 24,000 cycles. Note that this data point falls below the Category E' S-N curve which is estimated for socket connection details. To complete the fatigue test program, the socket connection was retrofitted with the addition of eight gusset stiffeners. The stiffeners were fabricated from 13 mm (0.5 in) thick plate and extended 610 mm (24 in) up the column shaft with the outstanding edge of the stiffener plate tapered at a 16 degree angle from the wall of the column. A full-penetration weld with fillet reinforcement was used for 152 mm (6 in) near the termination of the stiffener. The application of stiffeners reduced the stress range at the column base to 34 MPa (3 ksi). With these modifications, approximately 1.4 million additional load cycles were accumulated on the specimen without any fatigue cracks at the socket connection fillet weld or at the termination of the gusset stiffeners.

2.4.3 Recommendations for Calculating Design Stresses in Anchor Bolts

The results of an experimental program conducted to determine the relationship between support-structure forces and anchor-bolt stresses can be summarized by the following:

- Axial stresses in anchor bolts included in an anchor bolt group can be calculated using the common flexure equation - Mc/I . This relationship was valid for both straight and misaligned anchor bolt configurations as well as various Moment:Torsion:Shear ratios when the stiffness of the base plate was sufficient to limit prying effects. Prying is caused by non-uniform bearing on the top or bottom nut as a result of base plate distortions.
- Bending stresses caused by horizontal shear forces and torsional moments can be ignored in the fatigue design of anchor bolts when the exposed length (top of foundation to underside of leveling nut) of the anchor bolt is less than one bolt diameter. Typically, standard plans for cantilevered support structures specify that exposed lengths shall not exceed 25 mm (1 in).
- For anchor bolt installations which have exposed lengths greater than one bolt diameter, use of a fixed-fixed beam model is appropriate for calculating bending stresses.

	Number of Bolts (Pattern)	Bolt Diameter (mm)	Bolt Pattern Diameter (mm)	Base Plate Thickness (mm)	Column Shaft Diameter (mm)	Mis- Aligned Concrete Base
Assembly 1	8 (round)	38	533	38	406	N
Assembly 2	8 (round)	38	533	25	406	N
Assembly 3	8 (round)	38	533	38	406	Y
Assembly 4	8 (round)	38	533	25	406	Y

Notes:

1. A total of 6 load cases will be examined for each assembly.

- Moment:Torsion:Shear ratios of 19.5:0:1
19.5:5:1
14.5:0:1
14.5:10:1

- One load case which loosens the nut on Bolt #1

- One load case which varies the length of the exposed bolt (25 mm and 76 mm)

Table 2.13 - Anchor Bolt Group Test Matrix

Plate Size	M:T:V Ratio	Mean	Variance	Misaligned Bolt Pattern
38 mm	19.5:0:1 and 14.5:0:1	1.05	0.024	N
38 mm	19.5:5:1 and 14.5:10:1	1.01	0.064	N
38 mm	19.5:0:1 and 14.5:0:1	0.83	0.033	Y
38 mm	19.5:5:1 and 14.5:10:1	0.83	0.102	Y
25 mm	19.5:0:1 and 14.5:0:1	1.23	0.055	N
25 mm	19.5:5:1 and 14.5:10:1	1.06	0.174	N
25 mm	19.5:0:1 and 14.5:0:1	0.85	0.058	Y
25 mm	19.5:5:1 and 14.5:10:1	0.76	0.055	Y

Table 2.14 - Statistical Data from Anchor Bolt Tests
(Mean and Variance normalized to Predicted Values)

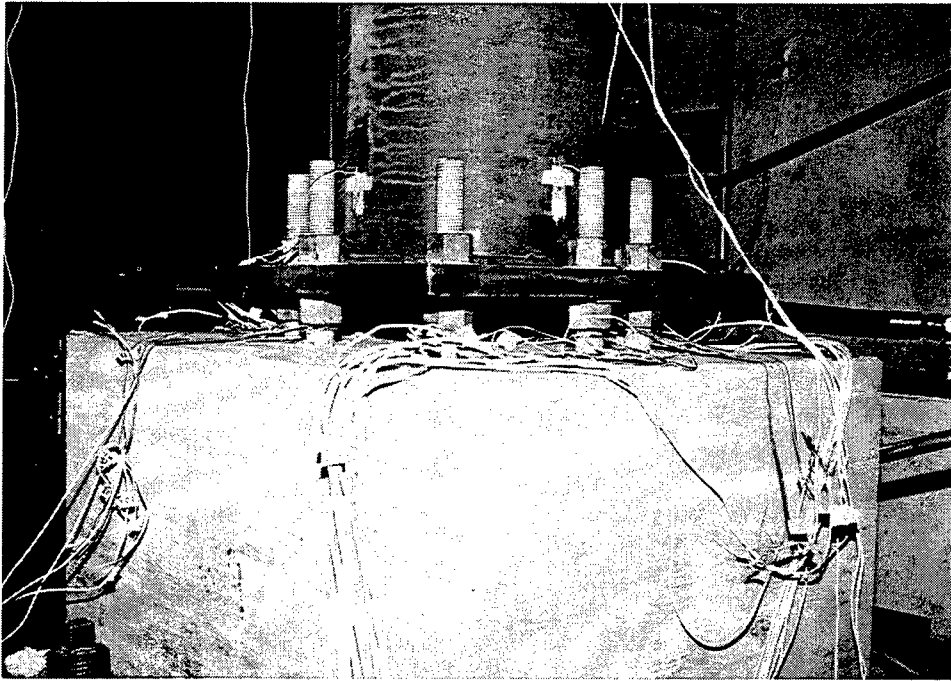


Figure 2.56 - Photograph of Column Base/Anchor Bolt Assembly

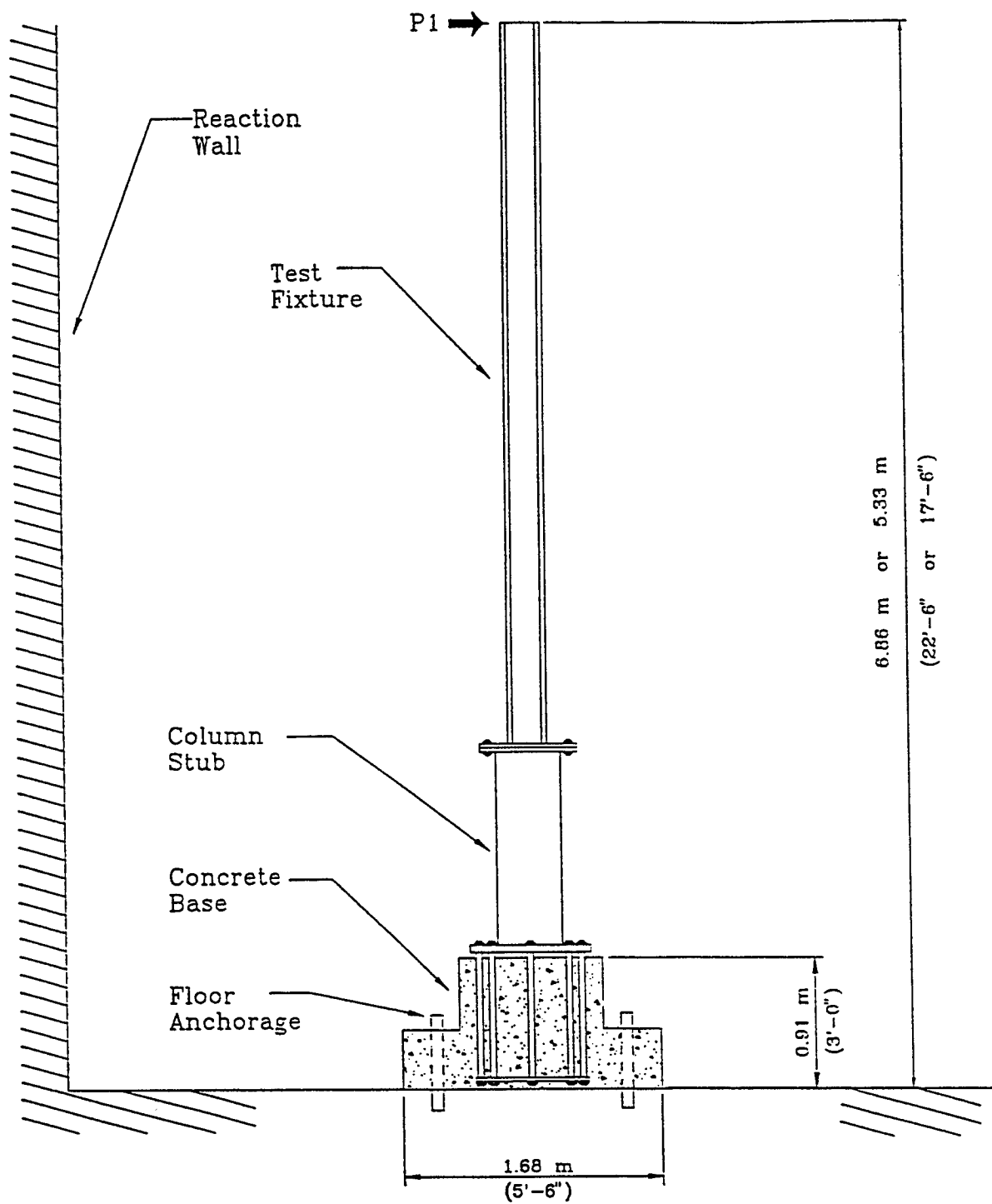


Figure 2.57(a) - Anchor Bolt Group Test Setup (Elevation)

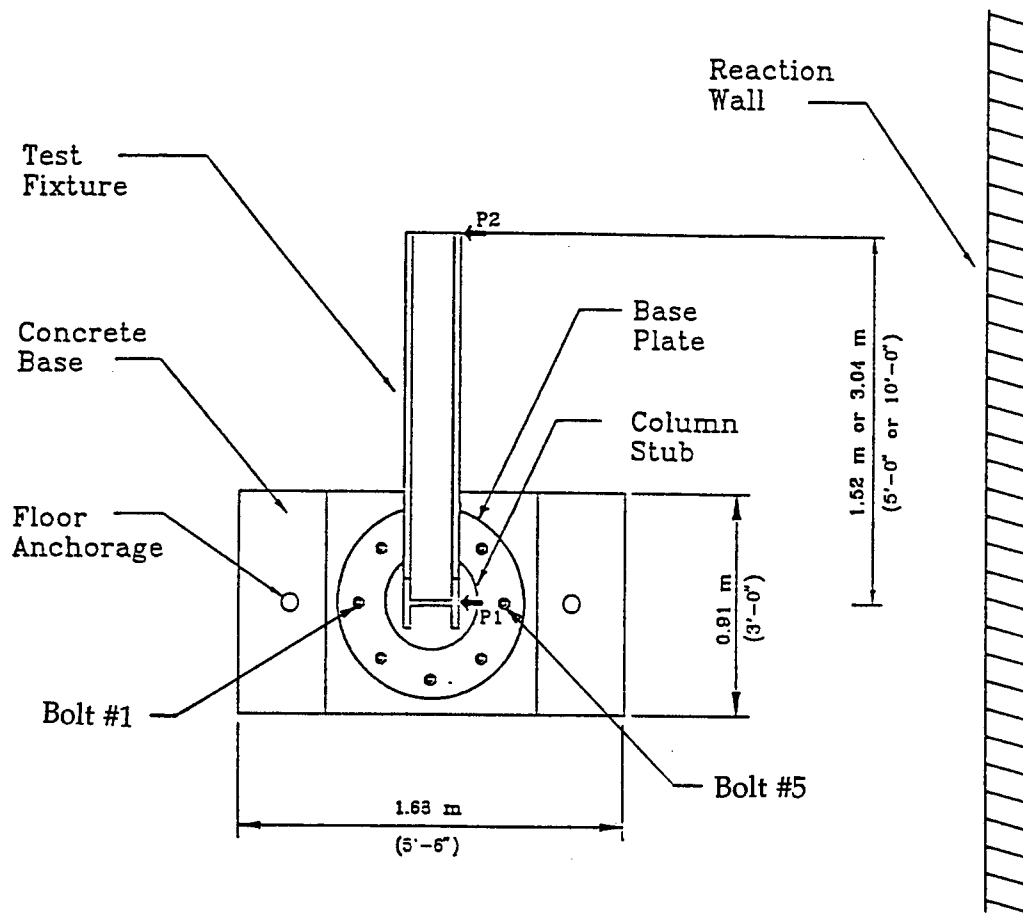


Figure 2.57(b) - Anchor Bolt Group Test Setup (Plan)

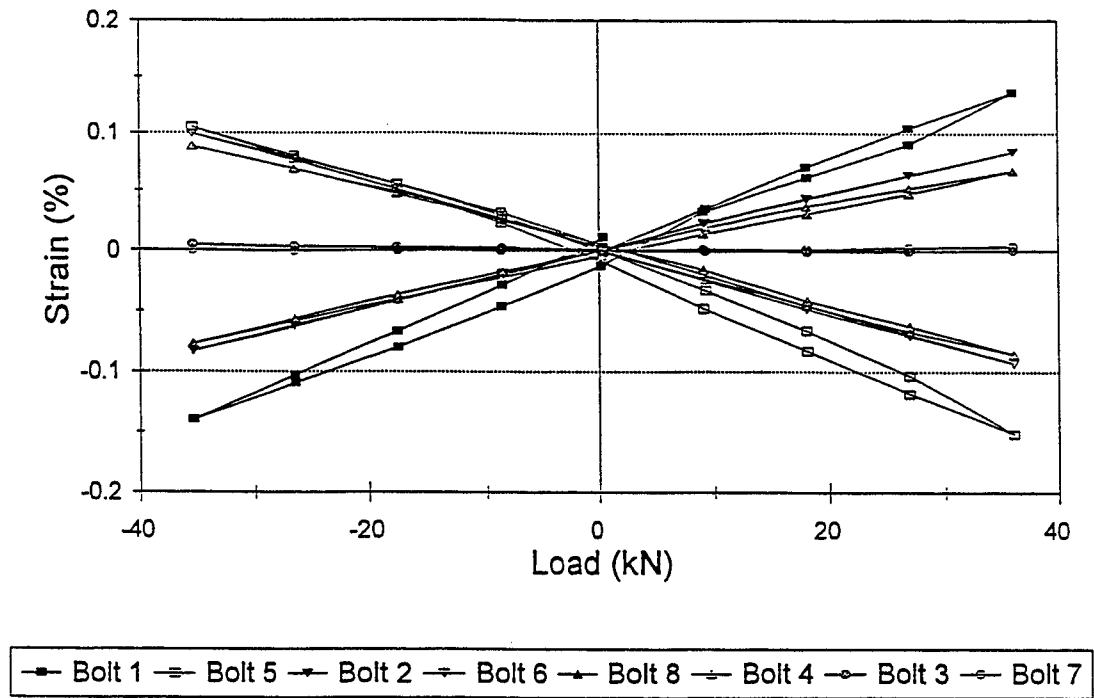


Figure 2.58 - Distribution of Axial Strains in Anchor Bolt Group With 38 mm Base Plate (Tests without Misalignment or Torsion and 25 mm Exposed Length)

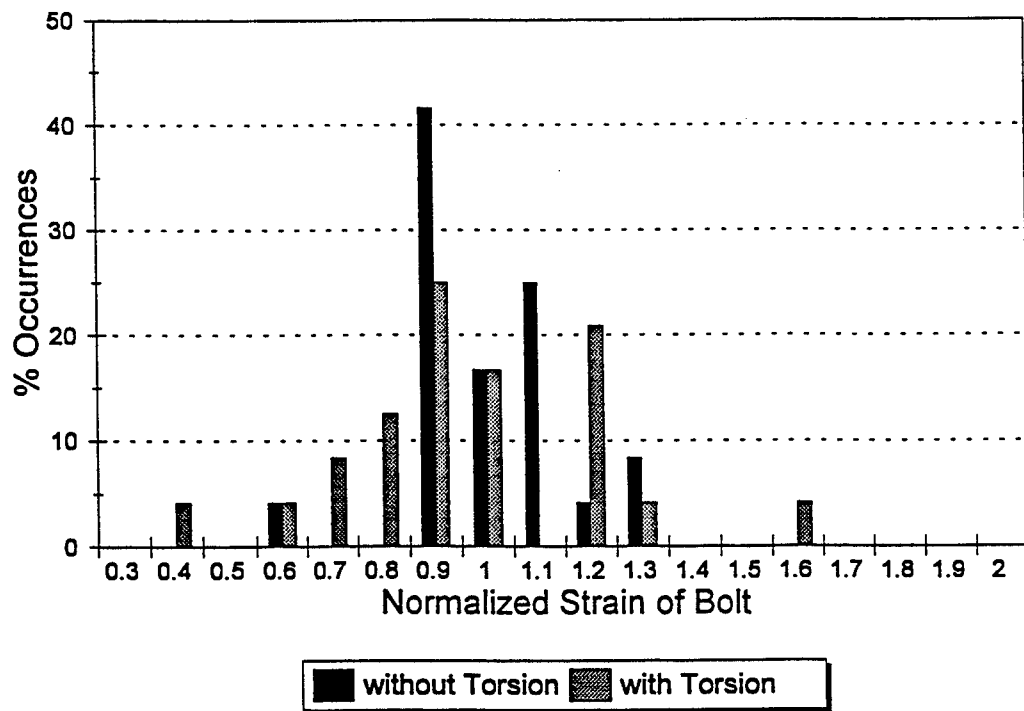


Figure 2.59 - Histogram of Normalized Bolt Strains (No Misalignment)

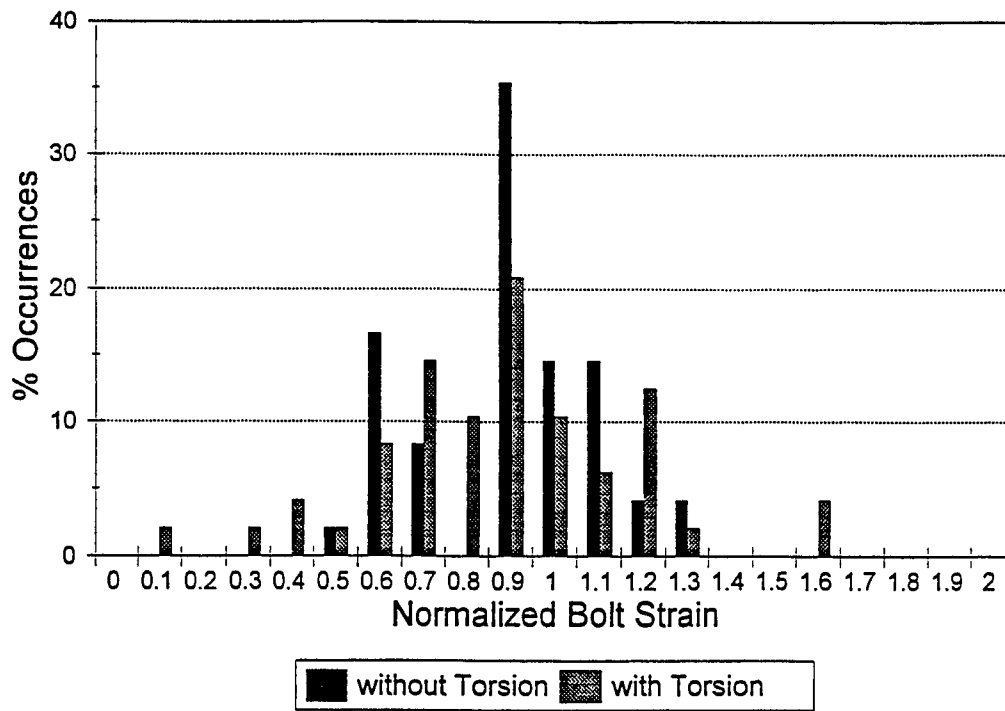


Figure 2.60 - Histogram of Normalized Bolt Strains (All Data with 38 mm Base Plate)

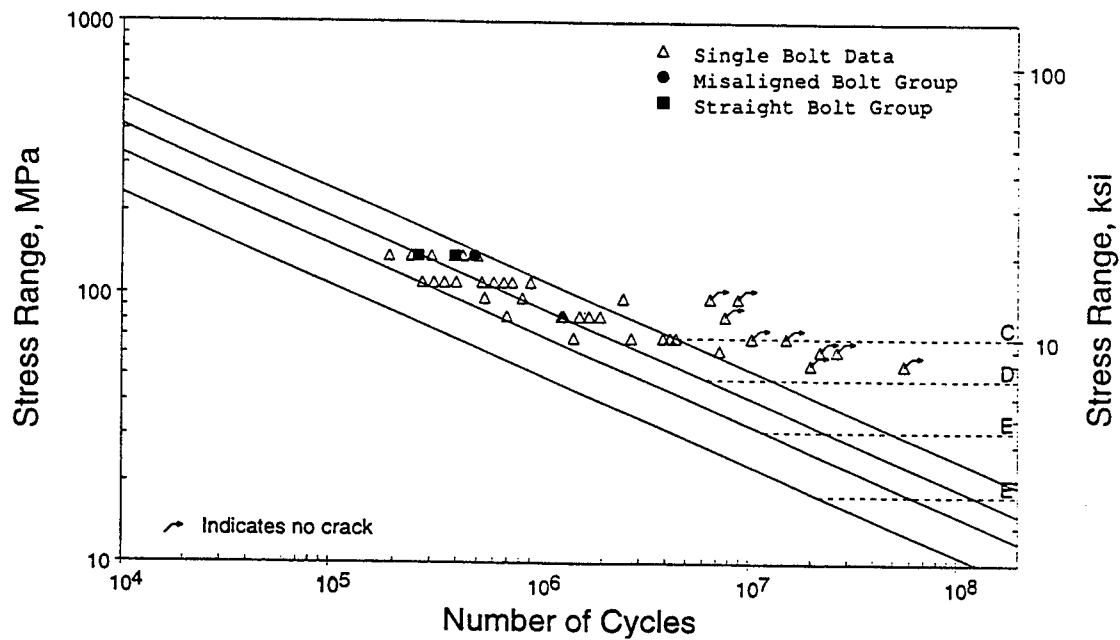


Figure 2.61 - S-N Plot of Anchor Bolt Assembly Test Data and Individual Bolt Test Data (Snug-Tight Condition)

2.5 FATIGUE CATEGORIZATION OF CONNECTION DETAILS

The current AASHTO Standard Specifications for Structural Supports for Highway Signs, Luminaires and Traffic Signals [1] contain provisions which specify that cantilevered support structures should be designed for infinite fatigue life in accordance with the procedures outlined in the AASHTO bridge specifications [46]. The geometrical configuration of typical cantilevered support structure connection details, however, varies significantly from the bridge details found in the AASHTO bridge specifications. As a result, designers are faced with significant uncertainty when attempting to apply the provisions of the AASHTO bridge specifications to the design of cantilevered support structures for fatigue.

This section describes the categorization of typical cantilevered support structure connection details according to the fatigue design curves in the AASHTO Bridge specification and/or AWS "Structural Welding Code - Steel." Section 2.5.1 summarizes the factors which influence the fatigue strength of welded details. Section 2.5.2 describes the methodology which was used to categorize typical cantilevered support structure connection details to the existing AASHTO and/or AWS fatigue design curves. The actual categorization of cantilevered support structure connection details is provided in Appendix A of this report.

2.5.1 Fatigue of Welded Details

Fatigue is a complex phenomenon governed by factors which are highly variable and difficult to quantify. The results of previous research [32,33,34], however, indicate that the fatigue resistance of welded details can be characterized by two primary parameters: (1) nominal stress range and (2) notch severity. The notch severity describes the severity of the stress concentration associated with a welded detail. It includes the effects of the global stress concentration associated with the configuration of the detail and the effects of local stress concentration due to the geometry of the weld and the existence of any weld discontinuities. Previous research has also demonstrated that material yield strength, mean stress levels, and operating temperatures [34] have little, if any, influence on the fatigue resistance of full-scale, welded structural connections.

The provisions of the AASHTO bridge specifications for the design of structures for fatigue are based upon a nominal stress approach in which details are grouped into categories according to their relative fatigue resistance. Each category then corresponds to an S-N Curve. The AASHTO Specifications contain seven design S-N curves labeled A through E' in order of decreasing fatigue strength. There is also an eighth S-N curve, labeled Category F, for the design of fillet welds loaded in shear. Category F rarely controls the design of structures for fatigue and is not applicable to any support structure details. Therefore, Category F will not be discussed further. Each design S-N curve possesses a constant-amplitude fatigue limit (CAFL) below which infinite fatigue life is obtained under constant-amplitude loading.

The AASHTO fatigue design categories were developed from the results of full-scale, constant-amplitude fatigue testing of bridge details. Because fatigue resistance is highly variable, the design categories are based upon a lower-bound 95 percent confidence limit. Thus, the AASHTO S-N design categories implicitly account for variables which are highly variable and difficult to quantify such as local stress concentration associated with weld geometry and weld discontinuities. Details which are grouped within the same design category generally exhibit similar cracking modes and are subject to similar stress concentrations. For example, transverse stiffeners and transverse butt welds with reinforcement are both Category C details. Thus, even though the geometrical configurations of these details are very different, transverse stiffeners and transverse butt welds with reinforcement exhibit similar fatigue resistance because the severity of the stress concentration at the weld toe associated with each of the details is similar.

2.5.2 Categorization of Connection Details

The categorization of cantilevered support structure connection details to the existing AASHTO and/or AWS fatigue design curves is based upon a general understanding of fatigue behavior, knowledge of previous research which has led to the development of the existing fatigue design curves, experience with structural failures which have resulted from fatigue, and engineering judgment. In only a few cases however, are actual fatigue test data available [49]. The fatigue resistance of cantilevered support structure connection details was linked to the existing knowledge base of bridge details which have been subjected to extensive testing. The link was made by comparing the stress concentrations and location at which cracks form (e.g. the toe of a weld). A similar approach has been used previously to categorize the fatigue resistance of ship details to the AASHTO fatigue design curves [47]. In a few cases, however, some uncertainty exists with respect to the proper fatigue design category of a particular detail. In these cases, a conservative judgment was made. Consequently, the fatigue strength of several of the details may actually be higher than is indicated in the fatigue categorization table. It is possible that the fatigue strength of these details could be revised if full-scale tests of these details were performed.

Appendix A of this report contains the categorization of typical cantilevered support structure connection details to the existing AASHTO and/or AWS fatigue design categories. Identification of the typical cantilevered support structure connection details was based upon a review of: (1) state department of transportation standard drawings of cantilevered sign, signal, and luminaire support structures, (2) literature obtained from cantilevered support structure manufacturers, and (3) literature developed by the AASHTO-AGC-ARTBA Task Force No. 13 [48].

The format of the categorization has been divided into two sections, which is similar to the format of the categorization of bridge details found in Reference 46. The first section consists of a tabular summary of the typical fatigue details and their corresponding fatigue design categories. The second section consists of illustrative drawings of the fatigue details described in the tabular summary. The illustrative drawings are included as an aid in the interpretation of some of the details described in the table.

It is intended that the categorization be used for both steel and aluminum structures. Generally, the fatigue categorization of a particular detail will be the same for both steel and aluminum, although different S-N curves correspond to any given category for steel or aluminum. The only detail for which a distinction needs to be made between steel and aluminum is indicated in the section of the table titled "Mechanically Fastened Connections." Following the fatigue categorization table are the values of the constant-amplitude fatigue limits associated with each of the fatigue categories for both steel and aluminum. Fatigue limits for Category A to E aluminum details were obtained from the Aluminum Association Specification - 6th edition. However, fatigue limits for Category B, E', and ET are not included in the specification and were obtained by reducing the fatigue limit for steel components by a factor of 2.6. This factor is the average ratio of the Category A to E fatigue limits for aluminum and steel components and is also very close to the ratio of the modulus of elasticity for the two materials.

The following paragraphs provide a summary of the fatigue categorizations of several cantilevered support structure fatigue details. Emphasis has been placed on those details which are based on conservative judgments or those details which are significantly different from the standard categorizations presented in the AASHTO bridge specification. Expanded definitions and illustrations of referenced details can be found in the categorization of typical cantilevered support structure connection details included in Appendix A.

Plain Members:

The slip-fit splice connection (Detail #2), a detail unique to the fabrication and erection of cantilevered support structures - particularly high mast luminaires, is classified as a Category B fatigue detail because of the possibility of surface irregularities being created during the installation process as well as fretting in service. It is also common for these slip-fit connections to have a hole and set screw or other type of fastener installed at the joint (Detail #4). As explained below, any type of hole is a Category D detail. Also, these slip-fit connections are often sealed with a Category E fillet weld (Detail #13) to prevent corrosion.

Mechanically Fastened Connections:

The baseline fatigue strength of bolted connections (Detail #4) is checked by calculating the stress range in terms of the net area of the section and comparing to the Category D fatigue design curve. However, if a high-strength bolted connection is fully tensioned, the fatigue strength is improved to a Category B Detail. Fully tensioned slip-critical connections are designed based on the gross section, while fully tensioned bearing connections are designed based on the net section (Detail #3). Since it is believed that the inspection effort at typical cantilevered support structure installations is inadequate to ensure slip-critical connections (given that sign erectors do not typically have the equipment or quality assurance to consistently provide slip-critical connections), the use of gross section calculations is not allowed.

Section 2.3 of this report recommends that the Category D design curve is a reasonable lower-bound estimate of the constant-amplitude fatigue limit for axially loaded, snug- and fully tightened anchor

bolts (Detail #5). Bending stress ranges resulting from misalignments up to 1:40 need not be explicitly considered when designing anchor bolts for infinite fatigue life provided that firm contact exists between the anchor bolt nuts and base plate. Where appropriate, beveled washers may be used to obtain a uniform bearing area.

The fatigue resistance of members or miscellaneous signs, signal, etc. which are attached to the structure with mechanical clamps or U-bolts (Detail #6) can be classified as Category D. This classification is based on an extrapolation of the fatigue strength of anchor bolts and other steel mechanically fastened connections which are both listed as Category D details.

Groove-Welded Connections:

The fatigue strength of a basic transverse full-penetration groove-welded splice (Detail #10) is classified as Category E. There are two reasons for this classification: 1) these groove welds almost always involve a change in tube thickness and associated misalignment (eccentricity and bending); and, 2) without removal of the internal backing ring, inspection is nearly impossible. Recent fatigue tests have shown that if defects are not screened out of groove welds, the fatigue strength is as low as Category E. However, if the weld reinforcement is ground smooth (Detail #9), weld toe defects are removed and the effects of a transition in thickness are mitigated, the fatigue strength can be upgraded to Category D. Although removal of the backing ring will improve inspectability, it will not significantly enhance the fatigue performance of the joint.

As indicated in the fatigue categorization table, a full-penetration groove-welded tube-to-transverse plate connection (Detail #12) with backing ring not removed has been classified as Category E' detail. This classification is primarily due to the backing ring, which cannot be completely fused by the one-sided weld. This lack of fusion results in a notch under the backing ring that acts as an initial crack subject to direct tensile stress ranges. Therefore, the thickness of the backing ring should be minimized to reduce the initial crack size. The constant-amplitude fatigue limit, and hence the fatigue category, was calculated for this and other similar notches using fracture mechanics and the threshold value of the range in stress intensity factor for fatigue crack growth. Attachment of the backing ring to the transverse plate with a full-penetration weld (Detail #11) will improve the fatigue strength to at least Category E because of the removal of the lack of fusion defect. This improvement may actually be greater if tests are conducted to quantify the fatigue resistance of this configuration.

Fillet-Welded Connections:

As mentioned previously, fillet-welded column or mast-arm lap splices (Detail #13) are classified as Category E. Note that slotted tubes which are connected to gussets (Detail #15) have a notch area at the end of the slot which is subjected to tensile stress ranges and is therefore classified as Category E' (for tubes with wall thicknesses less than 10 mm or 0.375 in). If the notch is removed by cutting a cope hole at the top of the slot, this detail can be upgraded to Category E (Detail #14). Similarly, because of a notch-like lack-of-fusion area, most one-sided fillet welds (Detail #17) and lap-welded angle to gusset

connections which are welded to the end of the gusset or wrapped around the gusset (Detail #15) are also classified as Category E'.

Fillet-welded socket connections (Detail #16) are classified as Category E' details. This classification is based upon the results of full-scale tests conducted by Fisher [49] on the fatigue strength of fillet-welded socket connections with various weld profiles (i.e. variations in the inclination of the fillet). The results of Fisher's tests indicated that the fatigue strength of this connection is best described by the Category E' fatigue design curve. Although the results indicated that connections with unequal leg fillet welds (long leg on the tubular member) had slightly higher fatigue strengths than connections with 45° fillet welds, the magnitude of this improvement is not sufficient to upgrade the fatigue classification of this detail.

The fit-up of components in all fillet welded connections shall meet the assembly requirements in Section 3.3 of the AWS Structural Welding Code [24]. In particular, the root opening at fillet-welded socket joints shall not exceed 8 mm (0.315 in). At joints which have separations greater than 2 mm (0.06 in), the leg of the fillet weld shall be increased by the amount of the root opening. Close adherence to this requirement is recommended for socket connections with multi-sided column sections.

The classification for fillet-welded tubular joints (Detail #19) is taken from the AWS Structural Welding Code. A special category, Category ET, which is actually much worse than Category E' was established for these connections. Because of the influence of localized deformations in the main tubular member, the Category ET classification was established for connections with main member radius to thickness ratios (r/t) below 24. The fatigue strength of tubular members with r/t ratios greater than 24 is further reduced by the equation presented in the proposed specification.

Attachments:

The provisions for load bearing and non-load bearing attachments is similar to the AASHTO bridge specifications. Upgrades are allowed for attachments longer than 102 mm (4 in) when the weld termination embodies a transition radius or taper (Details #21 and #22). Guidelines for the fatigue strength of these connections with tapered transitions were obtained from the Eurocode 3 [40] Specification for design of steel chimneys (Part 3.2). It should be emphasized that the use of gusset stiffeners at column-to-plate or mast-arm-to-plate connections can significantly improve the fatigue resistance of these connections. For example, gusset stiffeners can be designed to reduce the stress range at Category E' socket joint connections below the fatigue limit. This reduction in stress, will relocate the critical fatigue detail to the weld toe at the termination of the stiffener where the fatigue strength can be improved to Category C with proper detailing.

In non-load-bearing attachments, the only significant stress range is the primary stress in the main member. Load-bearing attachments are those where there is a transverse load range in the attachment itself in addition to the primary stress range in the main member, i.e. the critical point at the weld toe is subjected to a biaxial stress ranges. An example of a load-bearing attachment (Detail #24) is a longitudinal gusset connected to a non-tubular main member. Both the stress range in the main member

and the transverse stress range are considered separately, but the simplified approach does not require consideration of the combined principal stress.

Another type of load bearing attachment is the box in the box-type mast-arm to column connection. In this case, based on provisions for tubular connections in the AWS D1.1, the allowable stress range in the box itself is even lower (Category ET) because of the special fit-up requirements in tube-to-tube, and transverse-plate to tube connections (Detail #19). The cracks caused by the transverse stress range could appear in either the box itself or in the main member; in either case the solution to the cracking is to lower the transverse stress range by increasing the depth of the box or the box plate thickness. The mast-arm moment may also require increasing the section properties of the main member. The main member is proportioned according to Category E. The design stress range in the main member is found from the section modulus of the main member and moment just below the box connection, which is equal to the mast-arm end moment (unless there is an additional moment from a luminaire above the mast arm).

A special case of the load-bearing attachment is when the main member has minimal bending or axial stresses (Detail #23, which is commonly referred to as the cruciform). This detail can be classified as a Category C detail when the load bearing plate is less than 13 mm (0.5 in) in thickness. Similar to the AASHTO bridge specification, a reduction in fatigue strength is required for fillet-welded attachments when the plate thickness is greater than 13 mm (0.5 in). This reduction in fatigue strength results from the increased width of the lack-of-fusion region between the fillet welds which results with increases in attachment thickness above 13 mm (0.5 in). An equation developed by Frank and Fisher is included in the specification and can be used to quantify this reduction for various geometric configurations.

Chapter Three

INTERPRETATION, APPRAISAL AND APPLICATIONS

3.1 REVIEW OF EXISTING SPECIFICATION

Cantilevered sign, signal, and luminaire support structures are currently designed in accordance with the AASHTO Standard Specifications for Structural Supports for Highway Signs, Luminaires, and Traffic Signals [1]. As discussed in Chapter One, several recent fatigue failures and complaints from engineers highlight the fact that the specification and accompanying commentary are vague and insufficient regarding the design of cantilevered support structures for vibration and fatigue. Provisions contained in the existing specification which addressed wind-induced fatigue loads, allowable deflection limits, and fatigue resistance of cantilevered support structure connection details were reviewed. To serve as a comparison, design provisions contained in the Ontario Highway Bridge Design Code [30] and state department of transportation standards are also discussed where appropriate.

3.1.1 Wind-Induced Limit State Fatigue Loads

Current specifications used for the design of cantilevered support structures for vibration and fatigue [1,30] do not recognize or contain provisions pertaining to galloping, natural wind gusts and truck-induced wind gusts. As a result, designers are provided no guidance regarding the design of cantilevered support structures for these phenomena.

Both specifications however, contain provisions for the design of structures for vortex-induced vibrations. The following paragraphs summarize the provisions contained within the two specifications and compare the magnitudes of the across-wind forces specified in each.

The current AASHTO Specifications for the design of cantilevered sign, signal, and luminaire support structures contain provisions for the design of simple cantilever poles for vortex shedding. The provisions are based upon research conducted by Brockenbrough [50]. The methodology of the AASHTO design provisions are as follows: The natural frequency is estimated using an analytical solution for the natural frequency corresponding to the first mode of vibration of a simple pole. The critical wind velocity, V_{cr} , associated with vortex-shedding lock-in is computed using the Strouhal relation (i.e. Equation 1.2). The transverse pressure, P_t , acting on the pole is given by:

$$P_t = \frac{P}{2\beta} \quad (3.1)$$

where P is calculated from the standard AASHTO wind pressure formula (without the 1.3 gust factor) and β is the damping ratio (conservatively estimated in the Specifications as 0.005). This transverse pressure, P_t , is then used to compute stresses for the design of the pole for fatigue.

Tapered poles are accounted for in the Specifications in a similar manner. Equations are provided to compute equivalent lengths and diameters for estimation of the natural frequencies of tapered poles. The critical wind velocity is computed using the Strouhal relation (i.e. Equation 1.2), evaluated using the diameter of the pole at a distance $3L/4$ (where L is the length of the pole) from the base. The transverse pressure, P_t , acting on the pole is then calculated by Equation 3.1.

As mentioned previously, the provisions contained in the current Specifications for vortex shedding are based upon research conducted on simple cantilever poles. Thus, the applicability of these provisions to the design of cantilevered support structures for vortex shedding is questionable. Furthermore, the provisions do not contain adequate guidance concerning application of the transverse loading. Specifically, the provisions do not specify whether the transverse loading, P_t , represents a pressure range or a pressure amplitude. It is assumed herein that P_t is a pressure range.

The Ontario Highway Bridge Design Code, Third Edition, also contains provisions for the design of support structures for vortex shedding. The provisions require that a structure be designed based upon the results of a dynamic modal analysis to solve for the amplitude of the steady-state response due to an applied force per unit length in the transverse direction, $F_s(x,t)$, defined as:

$$F_s(x,t) = \frac{1}{2} \rho V_{cr}^2 C_s D \sin[2 \pi n_e t] \quad (3.2)$$

where ρ is the density of air, V_{cr} is the critical wind velocity computed from the Strouhal relation, C_s is the transverse force coefficient, D is the across-wind dimension of the structural element, n_e is the natural frequency of the structure, x is the coordinate describing the length or height along the structure, and t is time. For circular elements subjected to flow in the subcritical flow region, the transverse force coefficient C_s is specified as 0.71. Furthermore, the loading is an amplitude applied to the structure in accordance with mode shape being considered in the analysis and is assumed to act in phase along the entire length of the element.

The design of tapered elements is accounted for in the Ontario Code in a manner similar to that in the AASHTO specification. As was previously discussed, however, vortex shedding lock-in in a tapered structural element is a condition of localized resonance in which the vortex shedding forces remain correlated over a limited length of the element at each discrete increment in critical wind velocity. The Ontario Code specifies that, in a tapered element, the across-wind load, $F_s(x,t)$, be assumed to act over a length equal to ± 10 percent of the diameter $D(x)$ at which the critical wind velocity is calculated. The length of the structural element over which the transverse load is applied represents an estimate of the length over which the vortex shedding forces remain perfectly correlated. As a result, the design of structures with tapered elements requires a series of modal analyses in which the transverse load is incrementally moved along the tapered member to solve for the maximum amplitude of the steady-state response of the structure. At each increment, the load is assumed to act in the direction of the natural mode of vibration at the location being considered.

For the design of simple cantilever poles for vortex shedding, the Ontario Code permits the use of a simplified analysis using an equivalent static load per unit length, F_s , applied transverse to the direction of the free-stream wind velocity to estimate the amplitude of the steady-state, dynamic response:

$$F_s = \frac{0.3}{\xi} C_s D V_{cr}^2 \quad (3.3)$$

where ξ is the damping ratio (assumed to equal 0.0075 for steel and aluminum poles), and C_s , D , and V_{cr} are as described above.

Comparison of the AASHTO Specification and Ontario Code indicates that the provisions for the design of simple cantilevered poles are reasonably consistent. Consider, for example, a simple prismatic cantilever pole with a diameter equal to 305 mm (12 in) and a natural frequency equal to 5 Hz. Using the Strouhal relation (with a Strouhal number equal to 0.18, which is specified in each of the design codes), the critical wind velocity, V_{cr} , for lock-in is equal to 8.5 m/s (28 ft/s).

Based upon the AASHTO Specifications, the equivalent static transverse pressure (assuming a drag force coefficient equal to 1.10 and a height coefficient equal to 1.00) would equal 4870 Pa (102 psf). The equivalent static transverse force range per unit length, F_v , would therefore equal 1490 N/m (i.e. 4870 Pa \times 0.305 m) or 0.102 k/ft. Based upon the provisions of the Ontario Code, the amplitude of the equivalent static transverse force amplitude per unit length can be calculated as 630 N/m (13 psf) from Equation 3.3. The amplitude should be doubled to obtain the force range 1260 N/m (0.086 k/ft) which is reasonably close to the value of 1490 N/m (0.102 k/ft) from the AASHTO equation.

3.1.2 Allowable Deflection Limits

Over the years, as design methods have become more refined, cantilevered support structures have become increasingly lighter and presumably less expensive. An undesirable consequence of this refinement is an increased level of flexibility. Another factor contributing to the increased level of flexibility of these structures is an increase in length of the cantilever arms. Unfortunately, the existing Specifications allow this increased level of flexibility because the only displacement limitation is on the dead-load deflection at the top of the vertical support. There is no limit on the deflections due to wind and other live load and there are no limits on the deflection of the mast arm at all.

In view of this lack of deflection criteria, several states have included limitations on mast arm deflections in standard drawings for cantilevered support structures. For example, the state of Oregon indicates that the allowable amplitudes of live-load displacement of the pole is four percent of the height of the pole, i.e. the total range could be up to eight percent. The Oregon drawings also limit the total range of displacement of the tip of the mast arm due to wind-induced vibration to 1.5 percent of the mast arm length. For a 14 m (45 ft) mast arm length, this displacement range limit is 203 mm (8 in). However, the standard drawings specifically state that this limit does not include displacements resulting from rotations of the pole top. Thus the total displacement at the mast arm tip could be much greater than 1.5 percent of the mast arm length.

A much more stringent deflection requirement is included in the Texas standards. Mast arm tip displacement ranges are limited to 203 mm (8 in), including the effect of rotation at the top of the pole. Nevertheless, 203 mm (8 in) is still quite a large displacement range.

3.1.3 Fatigue Resistance of Connection Details

Provisions are included in the existing AASHTO Specifications which address the fatigue design of cantilevered support structures. These provisions, however, are vague regarding the loads which are used to determine fatigue resistance. For all structures except signs and single-pole luminaires, it is implied in the specification that the wind loads for static strength design shall be used. Although it is recognized that these critical stresses occur infrequently, it is suggested that stress ranges from these loads be kept below the constant amplitude fatigue limit. Specifically, Section 1.9.6 of the AASHTO specification states on page 45: *"Critical stress levels may be reached due to the design wind load, but the recurrence of such is expected to be low. Nevertheless, even with the uncertainty involved, it is suggested that sound practice in designing luminaire and traffic signal supports should be based on the infinite life (endurance limit) of the materials."*

For single pole structures, the specification clearly recommends the use of transverse wind pressures from vortex shedding for fatigue design.

In addition to the ambiguity regarding fatigue design wind loads, no assistance is given to the designer on the fatigue resistance of typical cantilevered support structure connection details. The importance of welded base plate to column and mast arm to column connections is mentioned, however, no quantitative design information is provided.

3.2 DEVELOPMENT OF THE PROPOSED SPECIFICATION

3.2.1 Fatigue Limit State Loads and Importance Factors

The results of research presented in Chapter Two have identified galloping, vortex shedding, natural wind gusts and truck-induced gusts as wind-loading mechanisms which can induce large-amplitude vibrations and/or fatigue damage in cantilevered signal, sign and light support structures. The amplitude of vibration and resulting stress ranges are enhanced by the low levels of stiffness and damping possessed by many of these structures. Galloping and vortex shedding are aeroelastic instabilities which, when they occur, will typically induce nearly constant-amplitude vibrations at the natural frequency of the structure (resonance). These conditions can lead to fatigue failures in a short period of time after installation. On the other hand, natural wind and truck-induced wind gusts induce variable-amplitude vibrations which are randomly distributed. Over the life of the structure, the cumulative effects of these gust loads can produce fatigue damage at critical connection details. This section includes a summary of recommended fatigue limit-state loads for the four wind-loading phenomena, as well as a discussion concerning the use of importance factors to adjust the level of reliability of cantilevered support structures.

Wind speed values are presented in units of m/s and mph in the proposed specification to remain consistent with the supporting data presented in Chapters 1 and 2 of this report. It should be noted however, that the use of kmph appears to be more common in metric wind load specifications.

3.2.1.1 Galloping - The results of previously discussed wind tunnel [25] and water tank [13] testing, as well as the oscillations observed on cantilevered support structures in the field, are consistent with the characteristics of the galloping phenomena. These characteristics include the sudden onset of large-amplitude, across-wind vibrations which increase with wind velocity. It is important to note however, that galloping is not caused by support structure members, but rather by the attachments to the horizontal mast arm (i.e. signs and signals).

The geometry and orientation of these attachments, as well as the wind direction, directly influence the susceptibility of cantilevered support structures to galloping. In particular, signal attachments configured with or without a backplate are more susceptible to galloping when subject to flow from the rear and signs are more susceptible to galloping when configured with a backplate. Galloping of sign attachments is independent of aspect ratio and is more prevalent with wind flows from the front of the structure.

As discussed in Section 2.2.2, finite-element simulations of the wind tunnel experiments indicated that the attachments to the model support structures were subjected to equivalent static shear force ranges between 1150 and 1770 Pa (24 and 37 psf) during the occurrence of galloping. These values are slightly more conservative but are consistent with the equivalent static shear force ranges between 775 to 1292 Pa (16.2 to 27.0 psf) obtained from finite-element analyses of full-scale support structures which were observed to vibrate in the field. Based upon these results, it is recommended that an equivalent static lift-pressure (shear force) range equal to 1000 Pa (21 psf) be used in the design of cantilevered sign and signal support structures for galloping-induced fatigue. This shear force range should be applied vertically to the surface area of all sign and/or signal attachments rigidly mounted to the horizontal mast arm as seen in the normal elevation.

Although this design shear force range is at the low end of the apparent loads from the wind-tunnel tests, it is near the average of the apparent loads from the field observations. However, it is already a rare occurrence for structures to start galloping, and it was concluded that it would be too conservative to design for anything greater. Also, as discussed in Section 3.3, many structures will have to be stiffened and/or designed with improved fatigue strength details in order to resist the limit-state wind loads. If the structure is stiffened by any amount, which is likely, then the susceptibility to galloping and vortex shedding induced vibrations may be diminished.

Because of the previously demonstrated success [13] in mitigating galloping-induced vibrations on a cantilevered support structure, designers and fabricators will have the option of specifying a proven mitigation device in lieu of designing for this galloping shear force range.

3.2.1.2 Vortex Shedding - Structural elements exposed to steady, uniform wind flows will shed vortices in the wake behind the element in a pattern commonly referred to as a von Karmen vortex street. When the frequency of vortex shedding approaches one of the natural frequencies of the structure, significant amplitudes of vibration can be caused by a condition termed lock-in. The critical velocity at which lock-in will occur is defined by the Strouhal relationship ($V_{CR} = f_n d/S$) which is discussed in detail in Section 1.2.2.

A lower bound wind speed can be established for signal and sign structures. Although vortices are shed at low wind velocities, for wind speeds less than 5 m/s (16 ft/s) the vortices do not impart sufficient energy to excite most structures. Typical natural frequencies and member diameters for sign and signal support structures result in critical wind velocities well below the 5 m/s (16 ft/s) threshold for the occurrence of vortex shedding. However, because of extremely low levels of damping inherent in luminaire support structures, vortex shedding at wind speeds less than 5 m/s (16 ft/s) may excite resonant vibration. Also, an upper bound wind speed can be established for all types of cantilevered support structures. At wind speeds greater than 20 m/s (66 ft/s), enough natural turbulence is generated to disturb the formation of vortices.

As discussed in Section 2.2.2, the results of finite-element simulations of the wind tunnel experiments indicated equivalent static pressure ranges that were consistent with the existing load models in the AASHTO and Ontario specifications. Therefore, the vortex shedding load provisions contained in the present AASHTO Standard Specifications for Structural Supports for Highway Signs, Luminaires, and Traffic Signals are adequate for the design of luminaire support structures. The equivalent static pressure range to be used for the design of vortex shedding induced loads is:

$$P_{VS} = \frac{0.613 V_{CR}^2 C_d}{2\beta} \quad (Pa) \quad (3.4)$$

$$P_{VS} = \frac{0.00118 V_{CR}^2 C_d}{2\beta} \quad (psf)$$

where V_{CR} is expressed in m/sec (ft/sec), C_d is the drag coefficient of the structural member, and β is the damping ratio which is conservatively estimated as 0.005. This equation is a slightly modified version of the equation currently in the code to eliminate ambiguity regarding units for the critical velocity. The existing standards calculate a critical wind velocity in units of m/s (ft/s) from the Strouhal relationship and then require units of kmph (mph) when determining the transverse pressure. The calculated equivalent static pressure range (P_{VS}) shall be applied transversely along the length of the luminaire column.

Unlike the present specification, the mass of the luminaire attachments shall be included in the analysis to determine the first mode of vibration transverse to the wind direction. Luminaires which may not have the attachments installed immediately should be designed for this worst-case condition. Because the natural frequency of a structure without an applied mass is typically higher than those with a luminaire attachment, the resulting critical wind speed and vortex shedding pressure range will also be higher.

Although the formation of vortices from sign and signal attachments is possible, wind tunnel tests described in Section 2.1 have indicated that significant vibrations do not occur from vortex shedding from attachments to cantilevered sign and signal support structures. This is probably because these attachments are more susceptible to galloping-induced vibrations. Finally, support structures composed of uniformly tapered members do not appear susceptible to vortex-induced vibrations when tapered at least 0.0117 mm/mm (0.14 in/ft). The dimensions of most tapered members result in critical wind velocities below the threshold velocity (5 m/s or 16 ft/s), and furthermore, any vortices which may form are correlated over a short length of the member and therefore generate insignificant vortex shedding forces. For example, calculations conducted on several tapered luminaire support structures with heights ranging from 6.4 m (21 ft) to 21.3 m (70 ft) resulted in stress ranges at fatigue sensitive connection details of less than 7 MPa (1 ksi).

3.2.1.3 Natural Wind Gusts - The equivalent static natural wind gust pressure range specified for design was based on an analytical study of the response of several cantilevered support structures subject to random gust loads. A detailed discussion of this investigation is included in Section 2.2.3. The analyses were based on a limit-state wind velocity of 17 m/s (37 mph) which was identified as the 0.01 percent exceedence for a yearly mean wind velocity of 5 m/s (11 mph). A collection of yearly mean wind speed data from 59 weather stations (many at airports with relatively open terrain typical of highways) across the U.S. showed that 81 percent of the cities had yearly mean wind speeds below 5 m/s (11 mph) and 98 percent of the cities had mean wind speeds below 5.8 m/s (13 mph). Therefore, it was decided to use a 5 m/s (11 mph) yearly mean wind speed to develop an equivalent static design pressure for natural gust loads. (The recommended static load range can be easily adjusted to suit other choices of mean wind speed.)

From the analyses of many characteristic signal, sign, and luminaire structures, equivalent static "normalized" pressure ranges from 170 to 300 Pa (3.6 to 6.3 psf) were obtained. These equivalent static pressure ranges on each surface are normalized by the associated drag coefficient to take into account the varying types of surfaces on each structure. The values of the equivalent static normalized pressure ranges were averaged and rounded to 250 Pa (5.2 psf) for use in the following design equation:

$$P_{NW} = 250 C_d \text{ (Pa)} \quad (3.5)$$

$$P_{NW} = 5.2 C_d \text{ (psf)}$$

where C_d is the drag coefficient of the exposed component. The calculated natural wind gust pressure range should be applied in the horizontal direction to the projected area of all exposed support structure members, signs, signals, and/or miscellaneous attachments.

Although support structures at most locations can safely be designed using the pressure range obtained in Equation 3.5, support structure installations at sites with yearly mean wind speeds in excess

of 5 m/s (11 mph) would be inadequately designed to achieve infinite fatigue life. Conversely, structures which are installed at locations with known yearly mean wind speeds significantly below 5 m/s (11 mph) would be overdesigned to resist natural wind gusts. To accommodate the design of structures at locations where the yearly mean wind velocity is known (particularly sites with higher wind speeds), the following equivalent static natural wind gust pressure can be used for design.

$$P_{NW} = 250 C_d \left(\frac{V_{mean}^2}{25} \right) \quad (Pa) \quad (3.6)$$

$$P_{NW} = 5.2 C_d \left(\frac{V_{mean}^2}{125} \right) \quad (psf)$$

The analysis of luminaires subject to natural wind gusts is particularly important because if the luminaire column is tapered and therefore vortex shedding does not have to be checked, natural wind gusts are the only possible dynamic wind loading. The vibration and fatigue design of signal and sign support structures, however, will typically be controlled by other wind-loading phenomena.

These static pressure ranges are not as high as the maximum static design wind loads for strength. If the present specification implies that for signals and luminaires the stress range resulting from the maximum static design wind load should be below the CAFL, then these proposed specifications will be less conservative. However, design examples in Appendix B show that many existing structures are underdesigned for these natural wind gust loads. Therefore, it is concluded that designers do not interpret the specification the way it was interpreted above. When high-mast luminaires are analyzed for these proposed loads, the stress ranges are very high. It could be argued that it is unreasonable to expect that the natural wind gusts will be correlated (in phase) all along a high mast column. It may be reasonable to apply the natural wind gusts only along part of the height. However, because there was no basis for such a partial length loading, it was not adopted as part of the proposed specification.

3.2.1.4 Truck Gusts - The passage of trucks beneath cantilevered sign and signal support structures induce gust loads on the attachments mounted to the mast arms of these structures. Finite element analyses (discussed in Section 2.2.4) using previously published pressure distributions and ramping functions produced very small stress ranges in both the horizontal and vertical direction of sign and signal structures.

However, recent vibration problems on sign structures with large horizontally projected areas (along the direction of traffic), e.g. variable message signs, has focussed attention on vertical gust pressures created by the passage of trucks beneath the sign. To improve fuel economy, many trucks are now outfitted with deflectors to divert the wind flow upward and minimize the drag created by the trailer. A simple model has been proposed to represent the vertical gust pressure induced by a passing truck as

that imposed by a 65 mph (105 kmph) wind to coincide with existing vehicle speed limits [20]. Simply stated, it is assumed that the velocity of the wind in the upward direction is equal to the truck velocity.

The equivalent static truck-gust pressure amplitude is determined by utilizing the static wind pressure formula currently in the Specification where $V = 105$ kmph (65 mph) and $C_h = 1.0$. The gust factor of 1.3 is also included to account for an increase in the relative truck speed due to possible head winds. Since the applied truck gust pressure amplitude will lift the mast arm vertically, the pressure obtained above is doubled to represent the entire truck gust pressure range. Based on these assumptions, an equivalent static pressure range to be used for the design of truck-induced gust loads is:

$$P_{TG} = 1760 C_d \text{ (Pa)} \quad (3.7)$$

$$P_{TG} = 36.6 C_d \text{ (psf)}$$

where C_d is the appropriate drag coefficient. This pressure range shall be applied in the vertical direction to the area of the underside of all signs, walkways, and/or lighting fixtures projected on a horizontal plane. For structures with large sign panels, pressures should be applied along the entire length of the horizontal areas to recognize the possibility of passage of two trucks side-by-side. For smaller signs and all signal support structures the equivalent static truck gust pressure range should be applied along 3.7 m (12 ft) of the mast arm. Although somewhat arbitrary, this either/or length requirement was included to ensure adequate fatigue resistance in larger, and potentially more dangerous, sign structures. Finally, for structures installed at locations where the posted speed limit is much less than 105 kmph (65 mph) the equivalent static design pressure range may be recalculated based on this lower wind velocity.

3.2.1.5 Importance Factors - Importance factors are introduced into the proposed design recommendations to adjust the level of structural reliability of cantilevered support structures. Recognizing that most structures designed by the current Specifications, which include little guidance for vibration and fatigue design, have performed satisfactorily over the years it would seem irrational to suggest that all structures be significantly redesigned. Recent failures however, underscore the need for more rigorous design requirements for certain structural configurations and/or site locations.

Table 3.1 lists the importance factors for Category I, II, and III structure types. The table is further subdivided to provide importance factors for the design of cantilevered signal, sign, and luminaire structures when considering galloping, vortex shedding, natural wind, and truck-induced wind gusts. These importance factors should be applied to the limit-state wind loads prior to determining the fatigue resistance and/or maximum mast-arm displacement of cantilevered support structures.

Definitions of the three importance categories are provide below:

- I - Critical cantilevered support structures installed on major highways.
- II - Other cantilevered support structures installed on major highways and all cantilevered support structures installed on secondary highways.
- III - Cantilevered support structures installed at all other locations.

Structures classified as Category I present a high hazard in the event of failure and will be designed to resist rarely occurring wind loading and vibration phenomena described above. Structures classified as Category III will be designed to the same level of reliability, on average, as those structures designed prior to development of the proposed specifications. The Category III importance factors shown in Table 3.1 are a result of design calibrations conducted on several typical cantilevered sign, signal, and luminaire support structures. Eighteen representative support structures (i.e. six of each type) were analyzed using the limit-state wind loads proposed above to determine stress ranges at fatigue sensitive connection details. Ratios of the detail's constant-amplitude fatigue limit stress range and stress range obtained using the proposed specification were then calculated and averaged for each of the four proposed limit-state wind loads (where applicable). As stated, these ratios represent, on average, the reduction in load required to reduce the stress range at fatigue critical connection details below the constant-amplitude fatigue limit. The use of six samples of each structure type for calibration purposes was considered sufficient to obtain reliable results. The ratios which were obtained were consistent for similar wind loads and scatter of the data typically varied by no more than ± 50 percent of the mean value. Finally, importance factors for Category II were defined as the average of Category I and III importance factors.

It is intended that only the most critical cantilevered support structures be classified as Category I. Some examples of structures which should be considered for Category I classification include large sign structures (including variable message signs), signals with long mast-arms, and high mast towers in excess of 30 m (100 ft) which are installed on highways where the vehicle speed is such that the consequences of excessive displacement of a sign or signal or a collision with a fallen structure is intolerable.

The probability of experiencing the full fatigue design wind loads in the proposed specifications is not any less for the Category II and III structures. Therefore, if these Category II and III structures do experience the full fatigue design wind loads, they are only designed for a fraction of these loads and therefore fatigue cracking or excessive deflection would eventually be expected. The rationale is that for Category II and III structures, the consequences of a failure are not as serious. Obviously, sound engineering judgement shall be used in the classification process.

3.2.2 Resistance to Fatigue Damage and Excessive Mast Arm Deflections

3.2.2.1 Fatigue Resistance - Because of the inherent variability in frequency and duration of wind-induced vibrations, designing cantilevered signal, sign, and luminaire structures for a finite fatigue life using cycle counting and Miner's rule for cumulative damage is impractical. Not only does the possibility exist for a large number of cycles to be accumulated in a short period of time when resonant vibrations are induced by galloping or vortex shedding, but the long-term cumulative effects of natural wind and truck-induced wind gusts can also result in the development of fatigue damage. Therefore, an infinite life approach is specified for the fatigue design of cantilevered support structures. Fatigue critical details shall be designed with nominal stress ranges near the detail which are below the appropriate constant-amplitude fatigue limit.

To assist designers, a categorization of typical cantilevered support structure details to the existing AASHTO and AWS fatigue design categories was provided in Section 2.5. The table and figures associated with this categorization are included in Appendix A of this report. The details included in this categorization were obtained from a review of state department of transportation standard drawings and manufacturer literature. This list should not be considered as a complete set of all possible connection details, but rather it is intended to remove the uncertainty associated with applying the provisions of the AASHTO Bridge specification to the fatigue design of cantilevered support structures.

In addition to considering the fatigue resistance of anchor bolts in the previously discussed fatigue categorization, details regarding the fabrication and installation of anchor bolts are also included in the proposed specification. To ensure that the materials and manufacturing processes used in the fabrication of anchor bolts will not degrade the fatigue resistance of these components, all anchor bolts used in the construction of cantilevered sign, signal, and luminaire support structures should conform to the provisions in the AASHTO M314-90 Standard Specification for Steel Anchor Bolts.

Similarly, additional provisions regarding the installation of anchor bolts are necessary because several of these conditions can directly influence fatigue strength. Most importantly, all anchor bolts should be installed in the fully tightened condition (i.e. 70 percent of minimum tensile strength) to eliminate the possibility of bolts becoming loose under service load conditions. Bolts which become loose, or bolts which were only snug tightened, are more susceptible to fatigue damage. The most common method of tightening anchor bolts is the turn-of-nut method. For most small diameter bolts, this method specifies that the nut should be rotated 1/3 turn beyond the snug-tight condition to ensure adequate pretension. Turning large diameter anchor bolts with coarse pitch threads 1/3 turn beyond snug may yield the bolt material. In general, most large diameter anchor bolts will require the use of a hydraulic wrench or other proven method of tightening and external lubrication of the threaded and bearing surfaces in order to achieve a fully tightened condition. For double-nutted anchor bolt installations, snug-tight should be defined as the full strength of one nut and until the base plate is in firm contact with the top and bottom nut.

Misalignment is another common installation condition which can influence the fatigue strength of anchor bolts. However, the results of research discussed in Section 2.3 indicate that bending stresses

resulting from misalignments up to 1:40 do not need to be considered in stress calculations provided that firm contact exists between the anchor bolt nuts and base plate. Where appropriate, a beveled washer can be used to obtain a uniform bearing area.

Experiments to determine the relationship between column forces and anchor bolt stresses clearly showed that inadequate column base-plate thickness can cause unusually high anchor bolt stresses. Therefore, a recommendation is made in the commentary to keep the minimum thickness of the base plate equal to or greater than the bolt diameter. These experiments also showed that bending stresses in the individual bolts become significant as the standoff distance between the top of concrete and the bottom of the levelling nut increases. Some states have a large standoff distance to facilitate grouting under the base plate. The experiments showed that the bending stresses were small and could be ignored for a standoff distance of less than the diameter of the bolts. For greater standoff distances, a fixed-fixed beam bending model was shown to be conservative.

3.2.2.2 Deflection Limits - Because of the low levels of stiffness and damping inherent in cantilevered signal and single mast-arm sign support structures, even structures which are adequately designed to resist fatigue damage may experience excessive deflections at the free end of horizontal mast-arms. Therefore, static deflection ranges at the free end of the mast-arm should not exceed 200 mm (8 in) in the vertical direction when the galloping and truck gust limit-state fatigue loads described above are applied to these structures. There is no requirement for the maximum displacement in the horizontal direction.

The primary objectives of this requirement are to minimize: 1) difficulty in seeing the signs and signals; 2) vibration damage to signal/sign attachments; and, 3) the number of motorist complaints. Luminaries are excluded from this requirement because of an apparent tolerance for large deflections in those structures, while trussed or double mast-arm sign structures are excluded because of inherently stiff mast-arm members.

Category		Importance Factor			
		Galloping	Vortex Shedding	Natural Wind	Truck Gusts
I	Sign	1.0	x	1.0	1.0
	Signal	1.0	x	1.0	1.0
	Luminaire	x	1.0	1.0	x
II	Sign	0.65	x	0.75	0.89
	Signal	0.65	x	0.80	0.84
	Luminaire	x	0.65	0.72	x
III	Sign	0.31	x	0.49	0.77
	Signal	0.30	x	0.59	0.68
	Luminaire	x	0.30	0.44	x

Note: x - Structure is not susceptible to this type of loading.

Table 3.1 - Importance Factors for Vibration and Fatigue Design

3.3 IMPACT OF THE PROPOSED SPECIFICATION

The implementation of proposed modifications to the present AASHTO Standard Specifications for Structural Supports for Highway Signs, Luminaires, and Traffic Signals will have a major impact on the safety and reliability of structures designed according to these provisions. Although the existing Specifications have in most cases produced reliable structural designs, recent fatigue failures and complaints from designers underscore the need for major modifications to Section 1.9.6 - Vibration and Fatigue. The results of research reported in Chapter Two have produced fatigue limit-state wind loads to be used in design as well as guidelines to assess the fatigue resistance of various cantilevered support structure connection details.

The initial impact caused by the implementation of these provisions will be an increase in the computational requirements necessary to design cantilevered support structures. In addition to adding several steps to the design of custom cantilevered support structures, all standard drawings provided by state DoT's as well as support structure manufacturers will require reevaluation. Examples of the computational effort required to design structures for the proposed vibration and fatigue provisions are included in Appendix B of the report. Design examples are included for a cantilevered signal and sign support structure, as well as a simple post luminaire.

The impact of the proposed specifications on the selection of individual member sizes and member-to-member connection requirements can be assessed by examining the data contained in the Importance Factor table (Table 3.1) discussed above. As discussed in Section 3.2.1, this table was obtained by conducting analyses of several support structures from each group (i.e. signs, signals, and luminaires) using the proposed design provisions. These importance factors represent the ratio of allowable fatigue design stress ranges (i.e. constant-amplitude fatigue limit) to calculated limit-state wind load stress ranges at fatigue sensitive connections. Stated more directly, the inverse of the importance factors for Category II and III structures actually represent the increase in structural capacity required, on average, for Category II and I structures respectively to resist the fatigue limit-state design wind loads. This increase in structural capacity can be obtained by simply increasing the section properties of the connected members and/or more efficiently by detailing the connections with more fatigue resistant connections. As discussed in Section 2.5, the fatigue resistance of most typical cantilevered support structures is controlled primarily by AASHTO Category E and E' details. Therefore, an upgrade of only one or two fatigue categories can make a significant change in the allowable stress range. For example, by utilizing a full-penetration groove welded tube-to-plate connection with the backing ring also attached to the plate with a full-penetration weld, the fatigue resistance can be increased to Category E from Category E'. This improvement represents a 73 percent increase in allowable stress range at the connection.

An examination of the importance factors listed in Table 3.1 indicate that galloping-induced wind loads will control the design of Category I and II sign and signal support structures. On average, Category I and Category II structures designed for galloping will require 230 and 54 percent increases in fatigue

resistance respectively. As discussed above, and illustrated in Design Example #1 presented in Appendix B, the fatigue resistance can be improved by increasing section properties and/or using more fatigue resistant details. Although not identified in the table, Category I and II signal structures which were analyzed without the attachment of backplates (and therefore had a smaller tributary area on which to apply the galloping-induced loads) required 35 and 22 percent increases in fatigue resistance respectively.

Sign and signal structures which are installed with approved vibration mitigation devices no longer must be designed for galloping-induced fatigue limit-state loads. The vibration and fatigue design of these structures will then be controlled by natural wind gusts. Category I sign and signal structures will require fatigue improvements of 104 and 69 percent respectively. For Category II structures, the fatigue resistance must be increased by 33 percent for sign supports and 25 percent for signal supports. It should be noted that these values for natural wind gust loads can be altered significantly by designing structures for the yearly mean wind speed at the actual installation site. For example, at a location where the mean yearly wind speed is only 1 m/s (2.2 mph) less than the design assumption of 5 m/s (11 mph), natural wind gust pressures will be reduced by 64 percent.

With the exception of signal structures without backplates or with vibration mitigation devices, truck induced wind gusts will rarely control the design of these cantilevered support structures. Likewise, only sign structures which possess large horizontally projected areas (e.g. variable message signs) will typically be controlled by truck-induced gust loads.

In most of the signal and single mast-arm sign support structures analyzed, the mast-arm-to-column connection was consistently the most susceptible to fatigue damage. However, in trussed or double mast-arm sign support structures the column-to-base plate connection would typically control fatigue design. As discussed in Section 2.2, static analyses typically overestimate the mast-arm moments by 30 to 50 percent when the inertial effects inherent in dynamic analysis are ignored. Because of the variability of measured lift pressures and the added computational effort necessary to conduct dynamic finite element analysis however, the use of an equivalent static load model and its built-in safety factor is reasonable. Based on these calibration analyses, the most fatigue resistant major connection detail on cantilevered signal and sign support structures was the anchor bolt assembly. This finding was surprising because of the number of documented anchor bolt fatigue failures. It is believed, however, that many of these failures were actually fractures with little fatigue crack growth caused by brittle materials and/or inadequately installed bolts which led to unusually high stress ranges. The proposed specification will tighten requirements for the fabrication and installation of anchor bolts used in cantilever support structures. Compliance with these requirements may create the need for a more detailed inspection program during construction of Category I and II structures.

Vortex shedding induced fatigue limit-state loads will only control the design of non-tapered luminaire support structures. Most likely few, if any, of these structures would be classified as Category I or II installations. However, if they were, they would require a 230 percent or 54 percent increase in fatigue resistance for Category I and II respectively. The design of all tapered-member luminaire support structures would be controlled by natural-wind-induced gust loads. To satisfy the proposed vibration and

fatigue provisions, luminaire support structures classified as Category I would require a 127 percent increase in fatigue resistance while those classified as Category II would require a 39 percent increase.

By definition, those structures classified as Category III will, on average, require little fatigue improvement to meet the proposed requirements. It would be expected, however, for a limited number of particularly poor fatigue details on cantilevered signal, sign, and luminaire support structures to require small improvements in fatigue strength.

If the structure's member sizes are increased to resist the fatigue limit-state wind loads, it is not likely that the displacement limits would govern the design. However, if the increased fatigue strength is achieved primarily by upgrading the details without increasing member sizes, then additional stiffening may be required to meet the proposed mast-arm deflection criteria.

Chapter Four

CONCLUSIONS AND SUGGESTED RESEARCH

4.1 CONCLUSIONS

Experimental and analytical research was performed on wind loading, dynamic response, and fatigue of cantilevered sign, signal, and luminaire support structures. The findings of this research are the basis for proposed modifications to the vibration and fatigue provisions of the AASHTO Standard Specifications for Structural Supports for Highway Signs, Luminaires, and Traffic Signals. General conclusions from this research can be summarized as follows:

- Static tests on a full-scale, eight bolt anchor bolt group proved that the distribution of axial anchor bolt forces can be predicted using the flexure formula with the moment of inertia of the bolt group. Bending stresses caused by horizontal shear forces and torsional moments can be ignored in the design of anchor bolts when the exposed length of the anchor bolt does not exceed one bolt diameter.
- The constant-amplitude fatigue limit corresponding to the AASHTO Category D design curve (i.e. 48 MPa or 7 ksi) is a reasonable lower-bound estimate for axially loaded, snug- and fully tightened anchor bolts.
- The fatigue resistance of most other cantilevered support structure connection details are classified as Category E or E' with constant-amplitude fatigue limits of 31 or 18 MPa (4.5 or 2.6 ksi). These low levels of fatigue resistance require low stress ranges and inefficient structural designs.
- There are at least four wind-loading phenomena which can produce significant displacement and stress ranges in these structures, i.e. galloping, vortex shedding, natural wind gusts, and truck-induced wind gusts.
- "Equivalent" static load ranges are recommended which are applied from zero load in a simple structural frame analysis. The computed static stress ranges are conservative and reasonably close to the stress ranges from the dynamic finite-element analyses.

- Equivalent static load ranges were developed for each of the four types of loading and for each general type of structure. When the structure is designed for these recommended static load ranges, the structure should remain resistant to excessive displacements and fatigue cracking for a 25 year or greater lifetime. These static load ranges should be used to design critical structures on high speed high volume roads.
- Based on an analysis of existing designs of cantilevered sign, signal, and luminaire support structures using the recommended static load ranges, the resulting applied stress ranges are on average 2.3 times higher than the fatigue strength of the details (typically Category E') which control the design. Therefore, either: 1) the section modulus at the location of this detail must be increased by a factor of 2.3; 2) details with Category D fatigue strength (rather than E') must be chosen; or, 3) some combination of stiffer structure and improved fatigue strength must be used. Structures designed in accordance with these proposed specifications will be much safer, on average, than present structures. However, there remains a possibility that the proposed specifications may not be sufficiently conservative. For example, the galloping load was not the largest that was observed in the field or in the wind tunnel, and this galloping load continues to increase as the wind velocity increases. The proposed specifications must attempt to strike a balance between safety and excessive conservatism.
- Based on these analyses of existing structures, importance factors were derived for each type of load and each type of structure. The importance factors are reduction factors for the recommended static load ranges. When the importance factor for non-critical structures is used, the resulting designs should have approximately the same degree of risk as existing structures. The importance factors allow engineering judgment and flexibility in applying the proposed specifications.

4.2 SUGGESTED RESEARCH

Based on findings of the current research program, the following topics are suggested for future research.

1. Fatigue Testing - Conduct fatigue tests on several of the most common fatigue-critical connection details which have been categorized in this report without the benefit of full-scale test data. Several candidate details include: 1) the full-penetration tube-to-transverse plate connection with various backing ring details, 2) the socket-type tube-to-transverse plate connection with various weld profiles and fit-ups, and 3) the built-up box type mast-arm to column connection. The proposed tests will verify the fatigue

resistance of these details, provide qualitative comparisons between the fatigue resistance details with similar function, and investigate the effects of variables such as dimensional tolerance.

2. Field Tests - Conduct full-scale tests on cantilevered sign-support structures to refine the proposed natural wind and truck-induced wind load models, which were developed without the benefit of wind-tunnel or field data. At least one conventional sign-support structure and one variable-message sign-support structure should be instrumented to measure gust velocity, applied pressure, strain, acceleration and displacement due to truck-induced vertical pressure and natural-wind-gust horizontal pressure. Some of the variable message signs have power and two-way communication through fiber-optic cable which could facilitate long-term monitoring.

3. Mitigation of Wind-Induced Vibrations - Perform full-scale field tests and analyses on modified new designs for cantilevered support-structures and retrofit existing structures which are prone to wind-induced vibrations. Possible wind-load mitigation techniques include the use of a sign blank placed horizontally to prevent galloping, louvered signs and signal backplates, the installation of dampers, and the use of a diagonal tension cable between luminaires above mast arms and mast arm tips. The application of dampers in practice is based primarily on trial and error experience. Some thorough analysis should be done to design and fine tune dampers in a more rational manner.

4. Gathering of Data on Susceptible Structures - Conduct field site visits to determine the characteristics of the structures and foundations, including natural frequency and damping, the soil, the wind environment and obstructions, and other relevant factors for structures which have been reported to vibrate excessively or have experienced cracking. Similar data should also be gathered for structures that have not exhibited vibration problems. The comparison of these data sets may lead to a better understanding of the conditions necessary for the occurrence of large-amplitude vibrations.

5. Analysis of Overhead Structures - Research the literature and other design codes and conduct dynamic and static analyses to estimate equivalent static load ranges for vortex shedding, natural wind gusts, and truck-induced gusts on overhead sign and signal bridges. (It is supposed that overhead structures are not susceptible to galloping.)

REFERENCES

1. American Association of State Highway & Transportation Officials, Standard Specifications for Structural Supports for Highway Signs, Luminaires and Traffic Signals, AASHTO, 1994.
2. Kaczinski, M.R., et al., Fatigue Resistant Design of Cantilevered Signal, Sign and Light Supports, National Cooperative Highway Research Program, Interim Report - NCHRP Project 10-38, Transportation Research Board, Washington, D.C., 1994.
3. Fisher, J.W., et al., Fatigue Cracking in Highway Sign Anchor Rods, Proceedings of the Ninth Structures Congress, Indianapolis, IN, 1991.
4. Novak, M., "Aeroelastic Galloping of Prismatic Bodies," Journal of the Engineering Mechanics Division, ASCE, Vol. 95, No. EM1, 1969.
5. Van Dien, J.P., Fatigue Resistant Design of Cantilevered Sign, Signal, and Luminaire Support Structures, Master's Thesis, Lehigh University, 1995.
6. Blevins, R.D., Flow-Induced Vibration, Second Edition, Van Nostrand Reinhold, New York, NY, 1990.
7. Davenport, A.G., et al., "Vibration of Structures Induced by Wind," Shock and Vibration Handbook, Third Edition (Harris, C.R. - Ed), McGraw-Hill, New York, NY.
8. Kolousek, V., et al., Wind Effects on Civil Engineering Structures, Elsevier, New York, NY, 1984.
9. Simiu E., et al., Wind Effects on Structures: An Introduction to Wind Engineering, John Wiley & Sons, NY, 1978.
10. Den Hartog, J.P., Mechanical Vibrations, Fourth Edition, McGraw-Hill, New York, NY, 1956.
11. Novak, M., "Galloping Oscillations of Prismatic Structures," Journal of the Engineering Mechanics Division, ASCE, Vol. 98, No. EM1, 1972.
12. Parkinson, G.V., et al., "On the Aeroelastic Instability of Bluff Cylinders," Transactions ASME, Journal of Applied Mechanics, Vol. 83, 1961.
13. McDonald, J.R., et al., Wind Load Effects on Signals, Luminaires and Traffic Signal Structures, Report 1303-1F, Wind Engineering Research Center, Texas Tech University, Lubbock, TX, 1995.
14. Havranek, D.D., Valmont Industries, Personal Communication to W. Henneberger of the Texas Department of Transportation, 1984.
15. Liu, H., Wind Engineering - A Handbook for Structural Engineers, Prentice-Hall, Englewood Cliffs, NJ, 1991.

16. Edwards, J.A., et al., Deflection Criteria for Wind-Induced Vibrations in Cantilever Highway Sign Structures, Report 110-79-2, Center for Transportation Engineering Studies, North Carolina State University at Raleigh, Raleigh, NC, 1984.
17. Creamer, B.M., Frank, K.H. and Klingner, R.E., Fatigue Loading of Cantilever Sign Structures from Truck Wind Gusts, Report No. FHWA/tx-79/10+209-1f, Center for Highway Research, University of Texas, Austin, 1979.
18. Edwards, J.A. and Bingham, W.L., Wind Engineering: A Handbook for Structural Engineers, Prentice Hall, Englewood Cliffs, NJ, 1991.
19. McCrum, R.L. (Michigan DoT), Letter report to M. Kaczinski of Lehigh University dated December 22, 1993.
20. DeSantis, P.V. and Haig, P., "Unanticipated Loading Causes Highway Sign Failure," Proceedings of ANSYS Convention, 1996.
21. "Winds Blow I-15 Sign Down," Engineering News Record, December 11, 1995.
22. American Association of State Highway and Transportation Officials, "Guide Specification for Fatigue Design of Steel Bridges," 1989.
23. Fisher, J.W., Nussbaumer, A., Keating, P.B., and Yen, B.T., "Resistance of Welded Details Under Variable Amplitude Long-Life Fatigue Loading," NCHRP Report 354, National Cooperative Highway Research Program, Transportation Research Board, National Research Council, Washington, DC, 1993.
24. American Welding Society, D1.1, Structural Welding Code, 1992.
25. Covert, E.E., et al., Static and Dynamic Wind Tunnel Tests on Selected Stoplight and Signs and Their Supports, Wright Brothers Facility Report 1306, Massachusetts Institute of Technology, Cambridge, MA, 1995.
26. Clough, R.W., et al., Dynamics of Structures, Second Edition, McGraw-Hill, Inc., New York, NY, 1993.
27. Fung, Y.C., An Introduction to the Theory of Aeroelasticity, Dover Publications, Inc., Mineola, NY, 1993.
28. Davenport, A.G., The Spectrum of Horizontal Gustiness Near the Ground in High Winds, Quarterly Journal, Royal Meteorological Society, Vol. 87, London, 1961.
29. ABAQUS, Version 5.3, Hibbitt, Karlsson & Sorensen, Inc., Pawtucket, RI, 1993.
30. Ontario Ministry of Transportation, Ontario Highway Bridge Design Code, Third Edition, Ontario Ministry of Transportation, 1992.

31. Lundquist, R.C., et al., Aerodynamically Induced Stresses in Traffic Signals and Luminaire Supports, Mechanics Research Report MRI-TR-2430-1, Bridge Department, California Division of Highways, 1972.
32. Fisher, J.W., et al., "Effect of Weldments on the Fatigue Strength of Steel Beams," NCHRP Report 102, National Cooperative Highway Research Program, Transportation Research Board, National Research Council, Washington, DC, 1970.
33. Fisher, J.W., et al., "Fatigue Strength of Steel Beams with Welded Stiffeners and Attachments," NCHRP Report 147, National Cooperative Highway Research Program, Transportation Research Board, National Research Council, Washington, DC, 1974.
34. Keating, P.B., and Fisher, J. W., "Evaluation of Fatigue Tests and Design Criteria on Welded Details," NCHRP Report 286, National Cooperative Highway Research Program, Transportation Research Board, National Research Council, Washington, DC, 1986.
35. Frank, K.H., "Fatigue Strength of Anchor Bolts," Journal of the Structural Division, ASCE, Vol. 106, No. ST6, 1980.
36. Kulak, G.L., et al., Guide to Design Criteria for Bolted and Riveted Joints, Second Edition, John Wiley & Sons, New York, NY, 1987.
37. Dusel, J.P., et al., Determination of Fatigue Characteristics of Hot-Dipped Galvanized A307 and A449 Anchor Bars and A325 Cap Screws, State of California, Department of Transportation, Division of Engineering Services, Sacramento, CA, 1984.
38. American Institute of Steel Construction, Manual of Steel Construction, LRFD, Second Edition, Volumes I & II, AISC, Chicago, IL, 1994.
39. British Standards Institute, Code of Practice for Fatigue Design and Assessment of Steel Structures, BS7608, 1993.
40. European Prestandard, Eurocode 3: Design of Steel Structures, European Committee for Standardization, 1992.
41. Research Council on Structural Connections (RCSC), Specification for Structural Joints Using ASTM A325 or A490 Bolts, RCSC, 1988.
42. Cook, S., Michigan Department of Transportation, Personal Communication, 1995.
43. Verma, K.K., et al., "High-Strength Bolts for Bridges," Engineering Journal, American Institute of Steel Construction, Vol. 29, No. 1, 1992.
44. Barsom, J.M., et al., Fracture & Fatigue Control in Structures, Second Edition, Prentice-Hall, Inc., Englewood Cliffs, NJ, 1987.
45. Kennedy, J.B. and Neville, A.M., Basic Statistical Methods for Engineers and Scientists, Second Edition, Harper & Row, Inc., New York, NY, 1974.

46. American Association of State Highway & Transportation Officials, AASHTO LRFD Bridge Design Specifications, SI Units, First Edition, AASHTO, 1994.
47. Fisher, J.W., et al., Structural Failure Modes of Advanced Double-Hull, Fatigue and Fracture Failure Modes, TDL 91-01, Vol. 3a, Lehigh University, Bethlehem, PA, 1992.
48. AASHTO-AGC-ARTBA Task Force 13, A Guide to Standardized Highway Lighting Pole Hardware, ARTBA Technical Bulletin No. 270, AGC Standard Form No. 133, 1980.
49. Fisher, J.W., et al., Fatigue Behavior of Steel Light Poles, Report No. FHWA/CA/SD-81/82, California Department of Transportation, Sacramento, CA, 1981.
50. Brockenbrough, R.L., Suggested Structural Design Criteria for Steel Lighting Standards, U.S. Steel Report 57 019-450(6), 1970.

Appendix A

Fatigue Categorization of Cantilevered Support Structure Connection Details

CONSTRUCTION	DETAIL	STRESS CATEGORY	APPLICATION	EXAMPLE
Plain Members	1. With Rolled or cleaned surfaces. Flame-cut edges with ANSI/AASHTO/AWS D5.1 (Section 3.2.2) smoothness of 1,000 micro-in. or less.	A	-	-
	2. Slip-joint splice where L is greater than 1.5 diameters.	B	High mast towers.	1
Mechanically Fastened Connections	3. Net section of fully-tightened high- strength (ASTM A325, A490) bolted connections.	B	Bolted joints.	2
	4. Net section of other mechanically fastened connections: Steel: Aluminum:	D E	-	3
	5. Anchor bolts or other fasteners in tension; stress range based on the tensile stress area. Misalignments of less than 1:40 with full contact.	D	Anchor bolts. Bolted mast-arm-to-column connections.	8
Holes and Cutouts	6. Connection of members or attachment of miscellaneous signs, signals, etc. with clamps or U-bolts.	D	-	-
	7. Net section of holes and cutouts.	D	Wire outlet holes. Drainage holes. Unreinforced handholes.	5

CONSTRUCTION	DETAIL	STRESS CATEGORY	APPLICATION	EXAMPLE
Groove-Welded Connections	8. Tubes with continuous full- or partial-penetration groove welds parallel to the direction of the applied stress.	B'	Longitudinal seam welds.	6
	9. Full-penetration groove-welded splices with welds ground to provide a smooth transition between members. (With or without backing ring removed)	D	Column or mast-arm butt-splices.	4
	10. Full-penetration groove-welded splices with weld reinforcement not removed. (With or without backing ring removed)	E	Column or mast-arm butt-splices.	4
	11. Full-penetration groove-welded tube-to-transverse plate connections with the backing ring attached to the plate with a full-penetration weld.	E	Column-to-base-plate connections. Mast-arm-to-flange-plate connections.	5
	12. Full-penetration groove-welded tube-to-transverse plate connections (backing ring not removed).	E'	Column-to-base-plate connections. Mast-arm-to-flange-plate connections.	5

CONSTRUCTION	DETAIL	STRESS CATEGORY	APPLICATION	EXAMPLE
Fillet-Welded Connections	13. Fillet-welded lap splices.	E	Column or mast-arm lap splices	3
	14. Members with axial and bending loads with fillet-welded end connections without notches perpendicular to the applied stress. Welds distributed around the axis of the member so as to balance weld stresses.	E	Angle-to-gusset connections with welds terminated short of plate edge. Slotted tube-to-gusset connections with coped holes.	2,6
	15. Members with axial and bending loads with fillet-welded end connections without notches perpendicular to the applied stress. Welds distributed around the axis of the member so as to balance weld stresses.	E'	Angle-to-gusset connections. Slotted tube-to-gusset connections without coped holes.	2,6
	16. Fillet-welded tube-to-transverse plate connections.	E'	Column-to-base-plate or mast-arm-to-flange-plate socket connections.	7,8
	17. Fillet-welded connections with one-sided welds normal to the direction of the applied stress.	E'	Built-up box mast-arm-to-column connections.	8
	18. Fillet-welded mast-arm-to-column pass-through connections.	E'	Mast-arm-to-column pass-through connections.	9
	19. Fillet welded T-, Y-, and K-tube-to-tube, angle-to-tube, or plate-to-tube connections.	see a	Chord-to-vertical or chord-to-diagonal truss connections. Mast-arm directly welded to column. Built-up box connection.	8,10,11

CONSTRUCTION	DETAIL	STRESS CATEGORY	APPLICATION	EXAMPLE
Attachments	20. Non-load bearing longitudinal attachments with partial- or full-penetration groove welds, or fillet welds, in which the main member is subjected to longitudinal loading:		Weld terminations at ends of longitudinal stiffeners. Reinforcement at handholes.	12, 13
	L ≤ 51 mm:	C		
	51 mm < L ≤ 102 mm:	D		
	L > 102 mm when t ≤ 25 mm:	E		
	21. Non-load bearing longitudinal attachments with L > 102 mm and full-penetration groove welds. The main member is subjected to longitudinal loading and the weld termination embodies a transition radius or taper with the weld termination ground smooth:		Weld terminations at ends of longitudinal stiffeners.	14
	R > 152 mm or α ≤ 15°:	C		
	152 > R > 51 mm or 15° < α ≤ 60°:	D		
	R ≤ 51 mm or α > 60°:	E		
	22. Non-load bearing longitudinal attachments with L > 102 mm and fillet or partial-penetration groove welds. The main member is subjected to longitudinal loading and the weld termination embodies a transition radius or taper with the weld termination ground smooth:		Weld terminations at ends of longitudinal stiffeners.	14
	R > 51 mm or 15° < α ≤ 60°:	D		
	R ≤ 51 mm or α > 60°:	E		

CONSTRUCTION	DETAIL	STRESS CATEGORY	APPLICATION	EXAMPLE
Attachments (Con't)				
	23. Transverse load-bearing fillet-welded attachments where $t \leq 13$ mm and the main member is subjected to minimal axial and/or flexural loads. (When $t > 13$ mm see Note c)	C	Longitudinal stiffeners welded to baseplates.	12,14
	24. Transverse load-bearing longitudinal attachments with partial-or full-penetration groove welds or fillet welds, in which the non-tubular main member is subjected to longitudinal loading and the weld termination embodies a transition radius which is ground smooth: $R > 51$ mm or $15^\circ < \alpha \leq 60^\circ$: $R \leq 51$ mm or $\alpha > 60^\circ$:	D E see b	Gusset-plate-to-chord attachments.	15

Notes:

- a) Category ET with respect to stress in branching member provided that $r/t \leq 24$ for the chord member. When $r/t > 24$ then the fatigue strength equals:

$$(F)_n = (\Delta F)_n^{ET} \times \left(\frac{24}{r/t}\right)^{0.7}$$

Where $(\Delta F)_n^{ET}$ is the CAFL for category ET.

Category E with respect to stress in chord.

h) First check with respect to the longitudinal stress range in the main member per the requirements for non-load bearing longitudinal attachments. The attachment must then be separately checked with respect to the transverse stress range in the attachment per the requirements for transverse load-bearing longitudinal attachments.

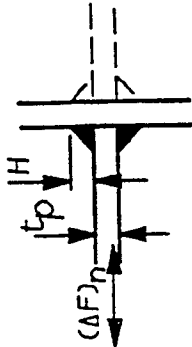
c) When $t > 13$ mm, the fatigue strength shall be the lesser of Category C or the following:

$$(\Delta F)_n^C = (\Delta F)_n^C \times \frac{0.094 + 1.23 \frac{H}{t_p}}{\frac{1}{t_p^6}}$$

Where $(\Delta F)_n^C$ is the CAFL for category C, H is the effective weld throat (mm), and t_p is the plate thickness (mm) as defined in Detail A.

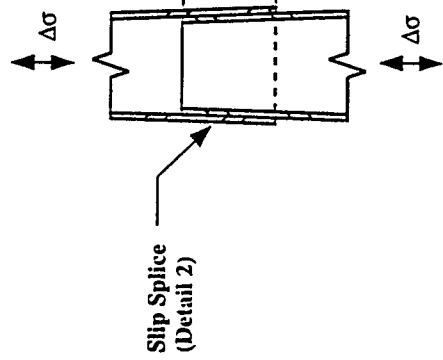
Constant Amplitude Fatigue Thresholds

Detail Category	Steel	Aluminum
	Threshold (MPa)	Threshold (MPa)
A	165	70
B	110	41
B'	83	32
C	69	28
D	48	17
E	31	13
E'	18	7
ET	8	3

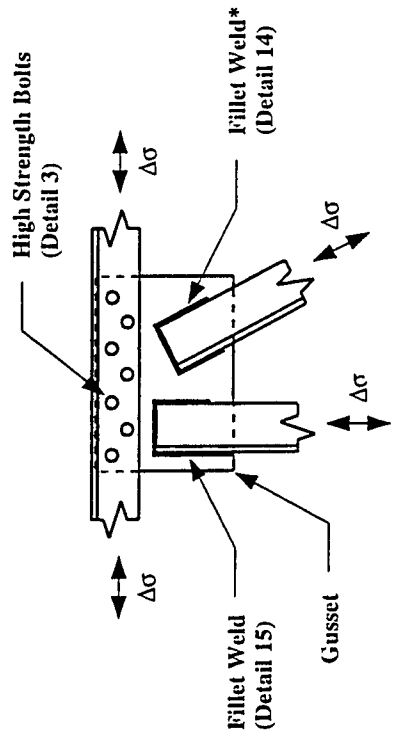


Detail A

Note: 1 MPa = 0.145 ksi

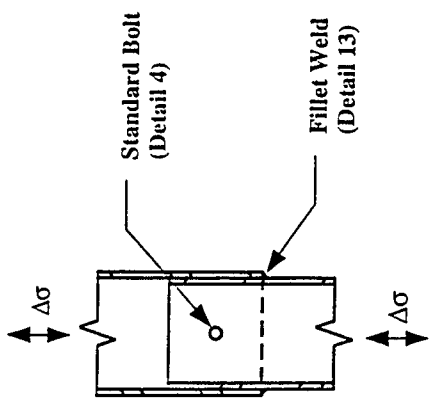


Slip-Joint Splice
Example 1

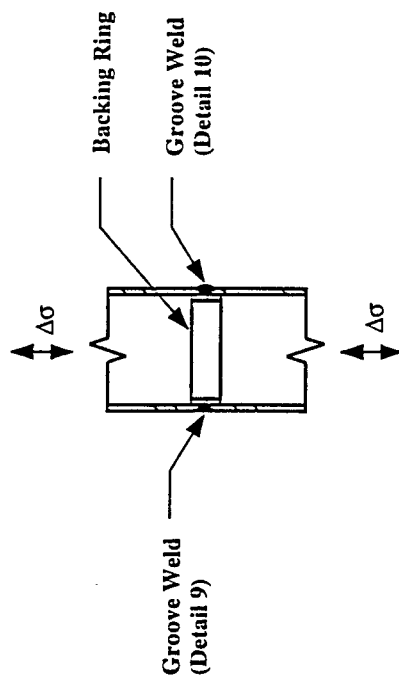


Double-Angle Truss Gusset
Example 2

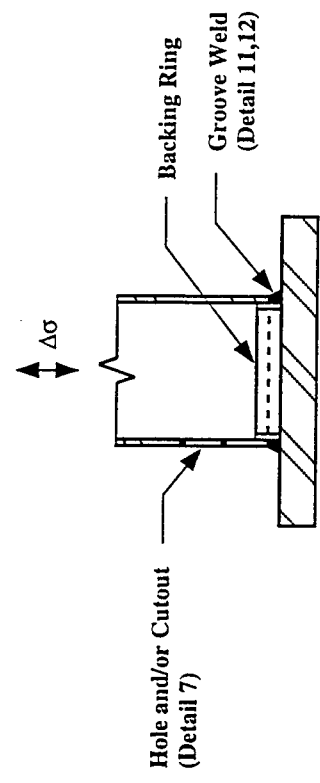
*Weld stopped short of gusset edge.



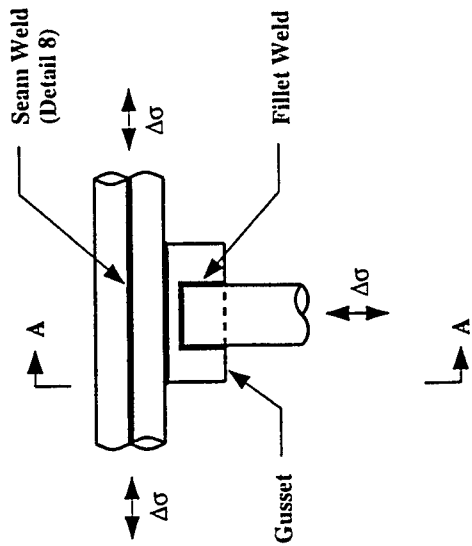
Fillet-Welded Lap-Splice
Example 3



Groove-Welded Butt-Splice
Example 4

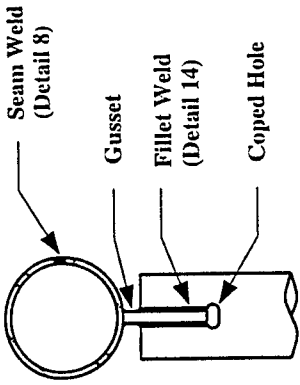


Groove-Welded Tube-to-Transverse Plate Connection
Example 5



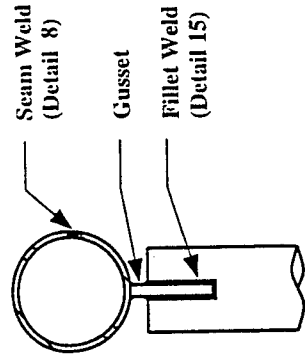
Slotted Tube-to-Gusset Connection
Example 6

A-8



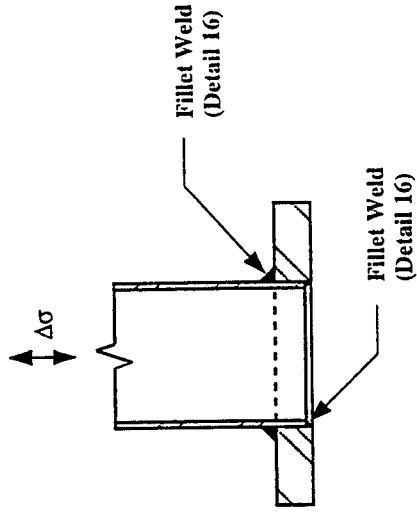
Section A-A

Slotted Tube-to-Gusset Connection
Example 6



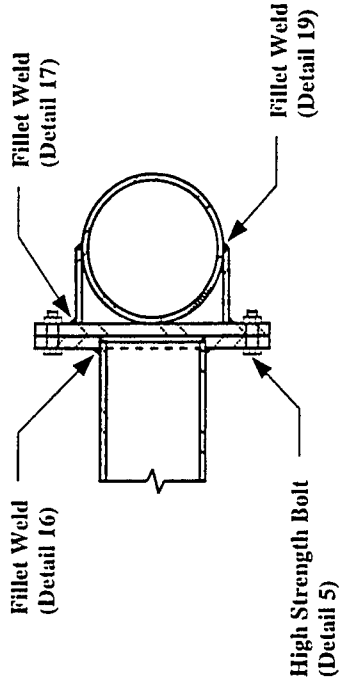
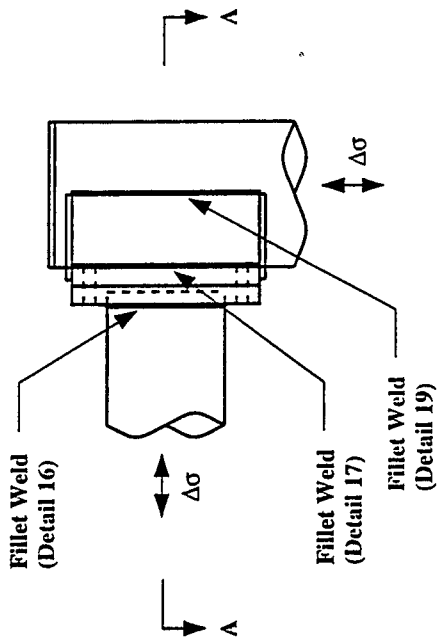
Section A-A

Slotted Tube-to-Gusset Connection
Example 6



Fillet-Welded Socket Connection
Example 7

Illustrative Examples (2 of 5)



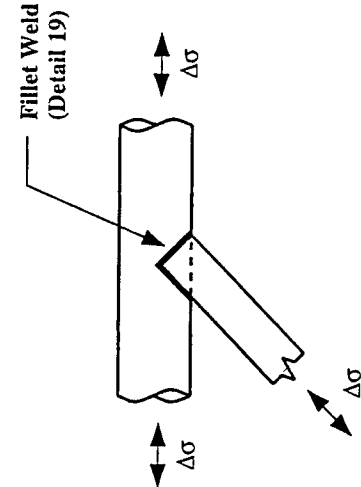
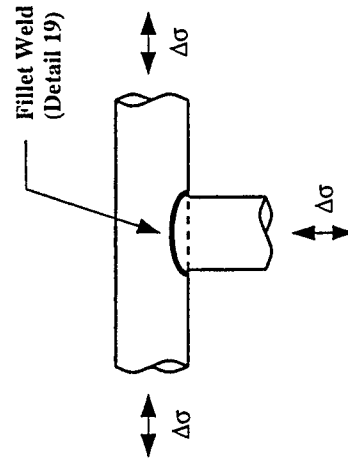
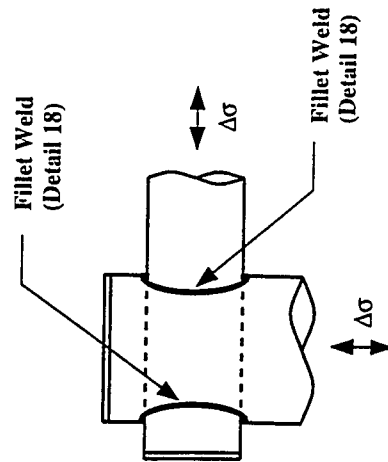
Section A-A

**Fillet-Welded Mast-Arm-to-Column Connection
(Built-Up Box)**

**Fillet-Welded Mast-Arm-to-Column Connection
(Built-Up Box)**

Example 8

Example 8



**Fillet-Welded Tube-to-Tube Column
Pass-Through Connection**

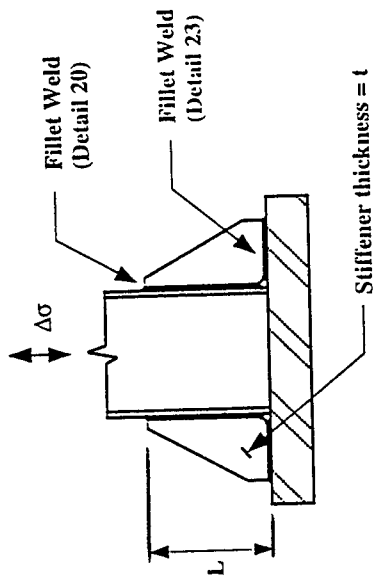
Example 9

Fillet-Welded Tube-to-Tube Connection

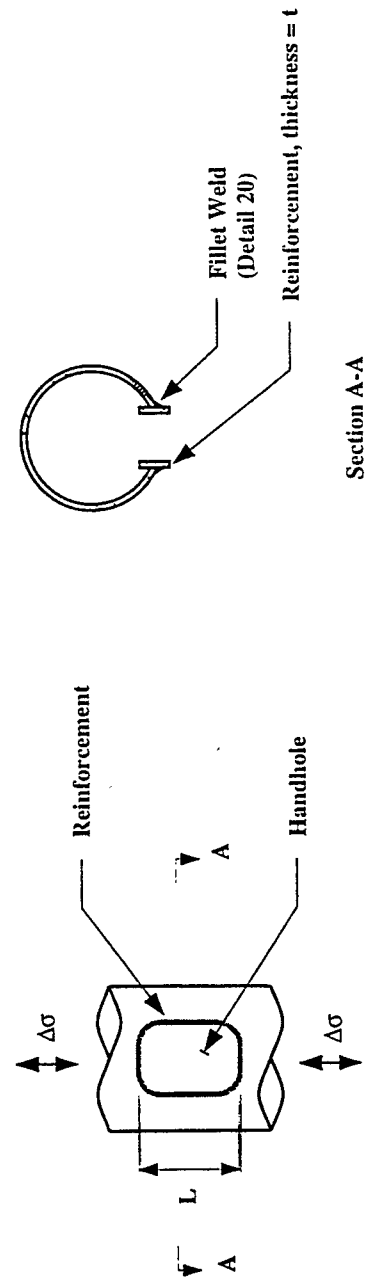
Fillet-Welded Angle-to-Tube Connection

Example 10
Illustrative Examples (3 of 5)

Example 11

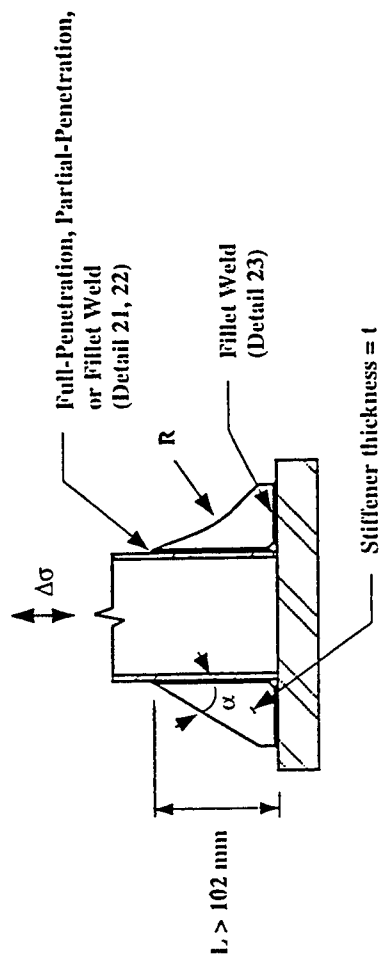


Non-Load Bearing Longitudinal Attachment
Example 12



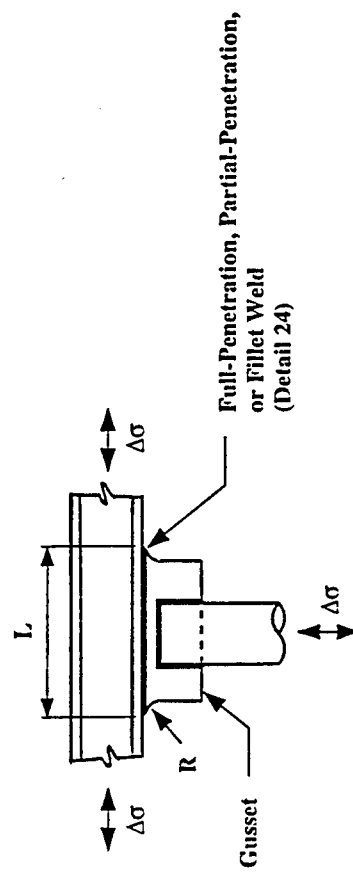
Reinforced Handhole
Example 13

Reinforced Handhole
Example 13



Non-Load Bearing Longitudinal Attachment

Example 14



Transverse Load-Bearing Longitudinal Attachment

Example 15

Illustrative Examples (5 of 5)

Appendix B

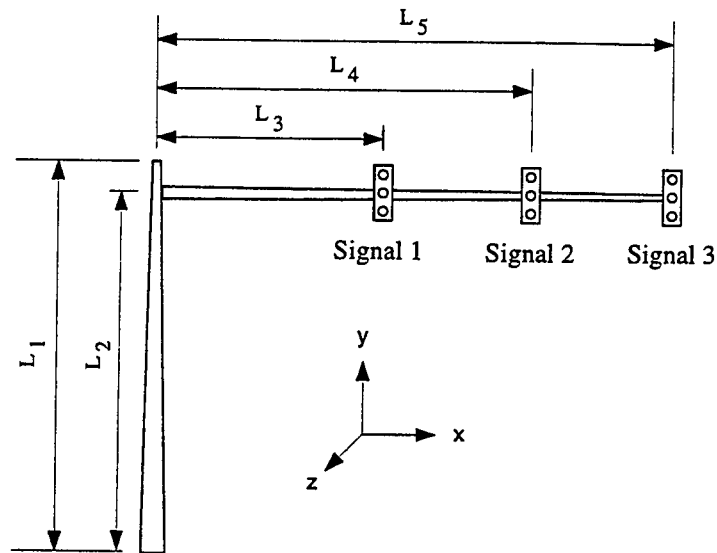
Fatigue Design Examples

EXAMPLE 1

1. GENERAL

1.1 Description

The structure is a cantilevered signal support structure (steel) composed of uniformly tapered structural elements. The signal is to be designed for vibration and fatigue in accordance with Section 1.9.6 of the AASHTO Specifications. It is assumed that the signal will be installed on a secondary highway and is therefore checked per the requirements for a Category II structure. Furthermore, it is assumed that the structure will be erected without approved vibration mitigation devices. All calculations are performed using U.S. Customary units.



1.2 Dimensions

Column:

Column length = $L_1 = 22$ ft
Length to mast-arm = $L_2 = 18$ ft
Diameter at base = $d_b = 13$ in
Diameter at tip = $d_t = 10$ in
Thickness = $t = 0.2391$ in

Signal:

Area projected on a vertical plane:
(w/ backplate): $(A_{sig})_v = 9$ ft²
Area projected on a horizontal plane:
(w/ backplate): $(A_{sig})_h = 1$ ft²

Mast-Arm:

Length to signal 1 = $L_3 = 25$ ft
Length to signal 2 = $L_4 = 37$ ft
Length to signal 3 = $L_5 = 49$ ft
Diameter at base = $d_b = 10.5$ in
Diameter at tip = $d_t = 4$ in
Thickness = $t = 0.2391$ in

Anchor Bolts:

Nominal bolt diameter = $d_b = 1.5$ in
Thread series = 6 UNC
Number of bolts = 4
Bolt circle diameter = $d_{bc} = 19$ in

1.3 Critical Fatigue Details

The structure contains the following details which must be designed for fatigue:

1. Anchor Bolts (Detail 5 in Table 1.9.6.2)
2. Column-to-baseplate fillet-welded socket connection (Detail 16 in Table 1.9.6.2)
3. Mast-arm-to-column connection (built-up box) (Details 5, 16, 17, and 20 in Table 1.9.6.2)

2. CALCULATION OF LIMIT STATES FATIGUE LOADS

2.1 Galloping

The equivalent static shear range to be applied to each of the signal attachments is calculated in accordance with Equation 1.9.6 - 1:

$$P_G = 21.0I_F = (21.0)(0.65) = 13.65 \text{ psf}$$

where $I_F = 0.65$ (Table 1.9.6.1) is the importance factor used in the design of a Category II signal support structure for galloping.

The equivalent static shear load range to be applied to each of the signal attachments is calculated by:

$$F_G = P_G(A_{sig})_v = (13.65 \text{ psf})(9 \text{ ft}^2) = 122.85 \text{ lbs}$$

where $(A_{sig})_v = 9 \text{ ft}^2$ is the area of each of the signal attachments projected on a vertical plane.

2.2 Vortex Shedding

As per the requirements of Section 1.9.6A-b, vortex shedding need not be considered in the design of cantilevered signal support structures for vibration and fatigue.

2.3 Natural Wind Gusts

It is assumed that the signal will be erected at a location where the yearly mean wind velocity is 11 mph. Therefore, Equation 1.9.6 - 4 is applied without modification.

The equivalent static pressure range to be applied to the structure is calculated in accordance with Equation 1.9.6 - 4:

$$P_{NW} = 5.2C_dI_F = 5.2C_d(0.80) = 4.16C_d \text{ psf}$$

where $I_F = 0.80$ (Table 1.9.6.1) is the importance factor used in the design of a Category II signal support structure for natural wind.

The equivalent static load range to be applied to the column is calculated by:

$$(F_G)_{col} = P_{NW}(A_{col})_v = P_{NW}[L_1d_{ave}] = [(4.16)(1.10)][(22 \text{ ft})(11.5 \text{ in})(1 \text{ ft}/12 \text{ in})] = 96.48 \text{ lbs}$$

where $(A_{col})_v$ is the area of the column projected on a vertical plane, L_1 is the length of the column, d_{ave} is the average diameter of the column, and $C_d = 1.10$ is a conservative estimate of the drag coefficient for a circular cylinder (Table 1.2.5C).

The equivalent static load range to be applied to the mast-arm is calculated by:

$$(F_G)_{arm}^* = P_{NW}(A_{arm})_v = P_{NW}[L_5 d_{ave}] = [(4.16)(1.10)][(49 \text{ ft})(7.25 \text{ in})(1 \text{ ft}/12 \text{ in})] = 135.47 \text{ lbs}$$

where $(A_{arm})_v$ is the area of the mast-arm projected on a vertical plane, L_5 is the length of the mast-arm, d_{ave} is the average diameter of the mast-arm, and $C_d = 1.10$ is a conservative estimate of the drag coefficient for a circular cylinder (Table 1.2.5C).

The equivalent static load range to be applied to each of the signal attachments is calculated by:

$$(F_G)_{sig} = P_{NW}(A_{sig})_v = [(4.16)(1.20)][(9 \text{ ft}^2)] = 44.93 \text{ lbs}$$

where $(A_{sig})_v = 9 \text{ ft}^2$ is the area of the signal projected on a vertical plane and $C_d = 1.20$ is the drag coefficient for a signal (Table 1.2.5C).

Note:

*The area of the mast-arm behind each of the signal attachments has been conservatively included in the calculation of the equivalent load range.

2.4 Truck Gusts

It is assumed that the support structure will be erected at a location where the posted speed limit is not significantly less than 65 mph. Therefore, Equation 1.9.6 - 5 is applied without modification.

The equivalent static pressure range to be applied to the structure is calculated in accordance with Equation 1.9.6 - 5:

$$P_{TG} = 36.6C_d I_F = 36.6C_d(0.84) = 30.74C_d \text{ psf}$$

where $I_F = 0.84$ (Table 1.9.6.1) is the importance factor used in the design of a Category II signal support structure for truck gusts.

As per the requirements of Section 1.9.6A - d, the equivalent static pressure is to be applied along the outer 12 ft length of the mast-arm. Therefore, the equivalent static load range to be applied to the mast-arm is calculated by:

$$(F_{TG})_{arm} = P_{TG}(A_{arm})_h = P_{TG}[(12 \text{ ft})d_{ave}] = [(30.74)(1.10)][(12 \text{ ft})(4.80 \text{ in})(1 \text{ ft}/12 \text{ in})] = 162.31 \text{ lbs}$$

where $(A_{arm})_h$ is the area of the outer 12 ft length of the mast-arm projected on a horizontal plane, d_{ave} is the average diameter of the mast-arm over the outer 12 ft length, and $C_d = 1.10$ is a conservative estimate of the drag coefficient for a circular cylinder (Table 1.2.5C).

The equivalent static load range to be applied to Signal 2 and Signal 3 is calculated by:

$$(F_{TG})_{sig} = P_{TG}(A_{sig})_h = [(30.74)(1.20)][(1 \text{ ft}^2)] = 36.89 \text{ lbs}$$

where $(A_{sig})_h = 1 \text{ ft}^2$ is the area of the signal projected on a horizontal plane and $C_d^* = 1.20$ is the drag coefficient for a signal (Table 1.2.5C).

Note:

* $C_d = 1.20$ is the drag coefficient for flow normal to the plane of a signal. It is assumed that this drag coefficient is also valid for flow parallel to the plane of the signal.

3. CALCULATION OF BENDING MOMENTS

3.1 Moment Due to Galloping

The bending moment at the centerline of the column (about the z - axis) is calculated by:

$$(M_z)_G = F_G [L_3 + L_4 + L_5] = (122.85 \text{ lbs})[(25 \text{ ft}) + (37 \text{ ft}) + (49 \text{ ft})]$$
$$(M_z)_G = 13636 \text{ lb-ft (163.63 k-in)}$$

3.2 Moment Due to Natural Wind Gusts

The bending moment at the base of the column (about the x - axis) is calculated by:

$$(M_x)_{NW} = (F_{NW})_{col}(L_1/2)^* + (F_{NW})_{arm}L_2 + 3(F_{NW})_{sig}L_2 = (96.48 \text{ lbs})(11 \text{ ft}) + (135.47 \text{ lbs})(18 \text{ ft}) + (3)(44.93 \text{ lbs})(18 \text{ ft})$$
$$(M_x)_{NW} = 5926 \text{ lb-ft (71.11 k-in)}$$

Note:

*It is conservatively assumed that the load on the column $[(F_{NW})_{col}]$ acts at the mid-height of the column.

The bending moment at the centerline of the column (about the y - axis) is calculated by:

$$(M_y)_{NW} = (F_{NW})_{arm}(L_5/2)^* + (F_{NW})_{sig}(L_3 + L_4 + L_5) = (135.47 \text{ lbs})(24.5 \text{ ft}) + (44.93 \text{ lbs})(25 \text{ ft} + 37 \text{ ft} + 49 \text{ ft})$$
$$(M_y)_{NW} = 8306 \text{ lb-ft (99.67 k-in)}$$

Note:

*It is conservatively assumed that the load on the mast-arm $[(F_{NW})_{arm}]$ acts at the mid-point of the mast-arm.

3.2 Moment Due to Truck Gusts

The bending moment at the centerline of the column (about the z - axis) is calculated by:

$$(M_z)_{TG} = (F_{TG})_{arm}(L_5 - 6 \text{ ft})^* + (F_{TG})_{sig}(L_4 + L_5) = (162.31 \text{ lbs})(43 \text{ ft}) + (36.89 \text{ lbs})(37 \text{ ft} + 49 \text{ ft})$$
$$(M_z)_{TG} = 10152 \text{ lb-ft (121.82 k-in)}$$

Note:

*It is conservatively assumed that the load on the mast-arm $[(F_{TG})_{arm}]$ acts at the mid-point between Signal 2 and Signal 3.

4. STRESS RANGE CALCULATIONS

4.1 Anchor Bolts

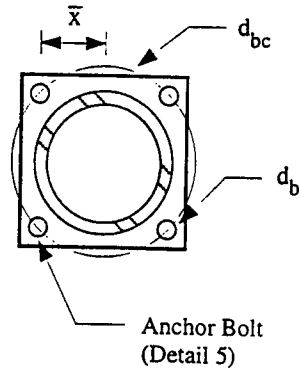
Details of the anchor bolt group are provided below:

Nominal bolt diameter = $d_b = 1.5$ in

Thread series = 6 UNC

Number of bolts = 4

Bolt circle diameter = $d_{bc} = 19$ in



4.1.1 Moment of Inertia of the Bolt Group

The centroidal distance to each of the anchor bolts is calculated by:

$$\bar{x} = \frac{d_{bc}}{2} \cos 45^\circ = \frac{19 \text{ in}}{2} \cos 45^\circ = 6.718 \text{ in}$$

where \bar{x} is the centroidal distance to each of the anchor bolts and d_{bc} is the diameter of the bolt circle.

The tensile stress area of each of the anchor bolts is calculated by:

$$A_T = \frac{\pi}{4} \left[d_b - \frac{0.9743}{n} \right]^2 = \frac{\pi}{4} \left[1.5 \text{ in} - \frac{0.9743}{6} \right]^2 = 1.405 \text{ in}^2$$

where A_T is the tensile stress area of each anchor bolt (Section 1.3.4A), d_b is the nominal bolt diameter, and n is the number of threads per inch.

The moment of inertia of the bolt group is calculated by:

$$I_b = \sum A_T \bar{x}^2 = 4[(1.405 \text{ in}^2)(6.718 \text{ in})^2] = 253.64 \text{ in}^4$$

where $A_T = 1.405 \text{ in}^2$ is the tensile stress area of each bolt and $\bar{x} = 6.718 \text{ in}$ is the centroidal distance to each of the bolts.

4.1.2 Anchor Bolt Stress Range

Based upon the calculations of Section 3, galloping controls the design of the anchor bolt group for fatigue. Therefore, the axial stress range in each of the anchor bolts is calculated by:

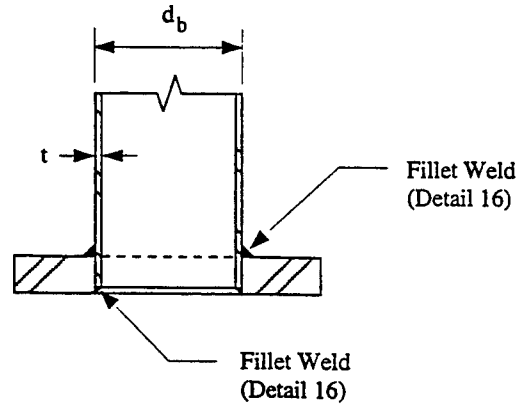
$$(S_R)_{bolt} = \frac{(M_z)_G c}{I_b} = \frac{(163.63 \text{ k-in})(6.718 \text{ in})}{253.64 \text{ in}^4} = 4.3 \text{ ksi}$$

Anchor bolts are classified as Category D fatigue details (Detail 5 in Table 1.9.6.2). The constant amplitude fatigue limit corresponding to Category D is 7 ksi (Table 1.9.6.2). Since the calculated stress range (4.3 ksi) is less than the constant amplitude fatigue limit (7 ksi), the anchor bolt group is adequately designed for fatigue.

4.2 Column-to-Base Plate Connection

Details of the column-to-base plate socket connection are provided below:

Diameter at base = $d_b = 13 \text{ in}$
Thickness = $t = 0.2391 \text{ in}$



4.2.1 Moment of Inertia

The moment of inertia of the column is calculated by:

$$I_{col} = \frac{\pi}{64} [d_b^4 - (d_b - 2t)^4] = \frac{\pi}{64} [(13 \text{ in})^4 - (13 \text{ in} - 0.4782 \text{ in})^4] = 195.18 \text{ in}^4$$

4.2.2 Column Stress Range

Based upon the calculations of Section 3, galloping controls the design of the column-to-base plate connection for fatigue. Therefore, the stress range at the column base is calculated by:

$$(S_R)_{col} = \frac{(M_z)_G c}{I_{col}} = \frac{(163.63 \text{ k-in})(6.5 \text{ in})}{195.18 \text{ in}^4} = 5.4 \text{ ksi}$$

The column-to-base-plate socket connection is classified as a Category E' fatigue detail (Detail 16 in Table 1.9.6.2).

The constant amplitude fatigue limit corresponding to Category E' is 2.6 ksi (Table 1.9.6.2). Since the calculated stress range (5.4 ksi) is greater than the constant amplitude fatigue limit (2.6 ksi), the socket connection is inadequately designed for fatigue.

Potential Redesigns:

1. Assuming: (1) the fatigue resistance of the connection is not improved (i.e. a Category E' socket connection (Detail 16 in Table 1.9.6.2) is used) and (2) the thickness of the column is not increased (i.e. $t = 0.2391$ inches), the connection will be adequately designed for fatigue using a 19 inch column diameter.
2. Assuming: (1) the fatigue resistance of the connection is improved to Category E (i.e. a Category E full-penetration connection (Detail 11 in Table 1.9.6.2) is used) and (2) the thickness of the column is not increased (i.e. $t = 0.2391$ in), the connection will be adequately designed for fatigue using a 15 inch column diameter.
3. Assuming: (1) the fatigue resistance of the connection is improved to Category E (i.e. a Category E full-penetration connection (Detail 11 in Table 1.9.6.2) is used) and (2) the diameter of the column is not increased (i.e. $d_b = 13$ in), the connection will be adequately designed for fatigue using a column thickness equal to 0.3125 in.
4. Assuming (1) the fatigue resistance of the connection is improved to Category C (i.e. the column-to-base-plate connection is fabricated with properly detailed stiffeners (Detail 21 in Table 1.9.6.2), and (2) the thickness of the column is not increased (i.e. $t = 0.2391$ inches), the connection will be adequately designed for fatigue using a 13 inch column diameter.

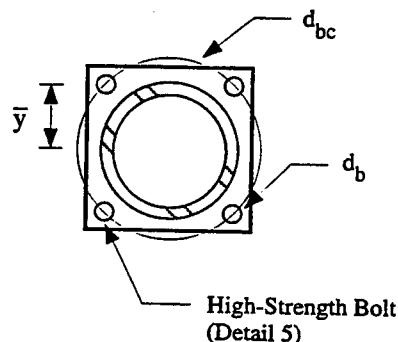
4.3 Mast-Arm-to-Column Connection

The mast-arm-to-column connection (built-up box) is composed of three components which must be checked for fatigue: (1) flange-plate bolt group, (2) mast-arm-to-flange-plate socket connection, and (3) built-up box. Each of these components will be considered individually in the following:

4.3.1 Flange Plate Bolt Group

Details of the flange plate bolt group are provided below:

Nominal bolt diameter = $d_b = 1.25$ in
 Thread series = 7 UNC
 Number of bolts = 4
 Bolt circle diameter = $d_{bc} = 20$ in



4.3.1.1 Moment of Inertia

The centroidal distance to each of the bolts is calculated by:

$$\bar{y} = \frac{d_{bc}}{2} \cos 45^\circ = \frac{20 \text{ in}}{2} \cos 45^\circ = 7.071 \text{ in}$$

where \bar{y} is the centroidal distance to each of the bolts and d_{bc} is the diameter of the bolt circle.

The tensile stress area of each of the bolts is calculated by:

$$A_T = \frac{\pi}{4} \left[d_b - \frac{0.9743}{n} \right]^2 = \frac{\pi}{4} \left[1.25 \text{ in} - \frac{0.9743}{7} \right]^2 = 0.969 \text{ in}^2$$

where A_T is the tensile stress area of each bolt (Section 1.3.4A), d_b is the nominal bolt diameter, and n is the number of threads per inch.

The moment of inertia of the bolt group is calculated by:

$$I_b = \sum A_T \bar{y}^2 = 4[(0.969 \text{ in}^2)(7.071 \text{ in})^2] = 193.80 \text{ in}^4$$

where $A_T = 0.969 \text{ in}^2$ is the tensile stress area of each bolt and $\bar{y} = 7.071 \text{ in}$ is the centroidal distance to each of the bolts.

4.3.1.2 Flange Plate Bolt Stress Range

Based upon the calculations of Section 3, galloping controls the design of the flange plate bolt group for fatigue. Therefore, the bolt stress range is calculated by:

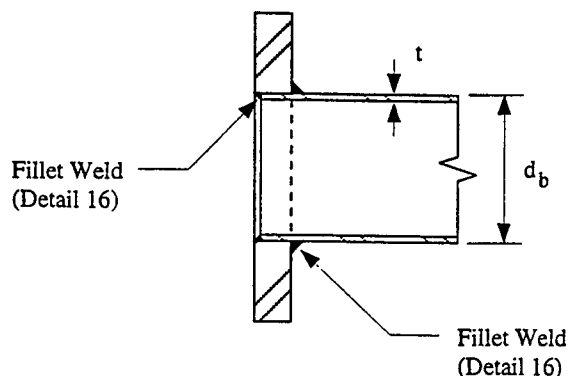
$$(S_R)_{bolt} = \frac{(M_z)_G^c}{I_b} = \frac{(163.63 \text{ k-in})(7.071 \text{ in})}{193.80 \text{ in}^4} = 6.0 \text{ ksi}$$

Properly tightened high-strength bolts are classified as Category D fatigue details (Detail 5 in Table 1.9.6.2). The constant amplitude fatigue limit corresponding to Category D is 7 ksi (Table 1.9.6.2). Since the calculated stress range (6.0 ksi) is less than the constant amplitude fatigue limit (7 ksi), the flange-plate bolt group is adequately designed for fatigue.

4.3.2 Mast-Arm to Flange Plate Socket Connection

Details of the mast-arm-to-flange-plate socket connection are provided below:

Diameter at base = $d_b = 10.5$ in
Thickness = $t = 0.2391$ in



4.3.2.1 Moment of Inertia

The moment of inertia of the mast-arm is calculated by:

$$I_{arm} = \frac{\pi}{64} [d_b^4 - (d_b - 2t)^4] = \frac{\pi}{64} [(10.5 \text{ in})^4 - (10.5 \text{ in} - 0.4782 \text{ in})^4] = 101.49 \text{ in}^4$$

4.3.2.2 Mast-Arm Stress Range

Based upon the calculations of Section 3, galloping controls the design of the mast-arm-to-flange-plate socket connection for fatigue. Therefore, the mast-arm stress range is calculated by:

$$(S_R)_{arm} = \frac{(M_z)_G c}{I_{arm}} = \frac{(163.63 \text{ k-in})(5.25 \text{ in})}{101.49 \text{ in}^4} = 8.5 \text{ ksi}$$

The mast-arm-to-flange-plate socket connection is classified as a Category E' fatigue detail (Detail 16 in Table 1.9.6.2). The constant amplitude fatigue limit corresponding to Category E' is 2.6 ksi (Table 1.9.6.2). Since the calculated stress range (8.5 ksi) is greater than the constant amplitude fatigue limit (2.6 ksi), the socket connection is inadequately designed for fatigue.

Potential Redesigns:

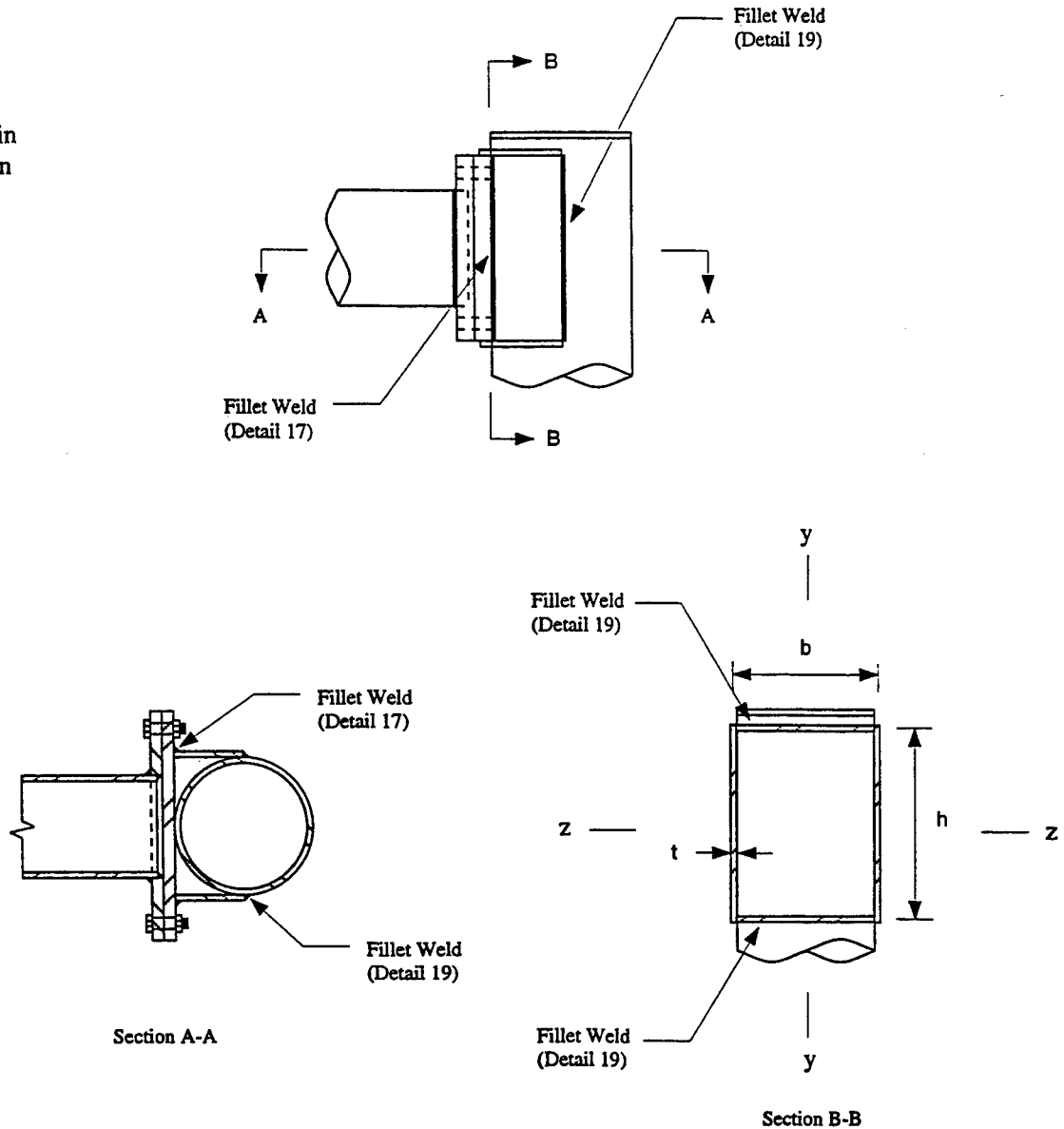
1. Assuming: (1) the fatigue resistance of the connection is not improved (i.e. a Category E' socket connection (Detail 16 in Table 1.9.6.2) is used) and (2) the thickness of the mast-arm is not increased (i.e. $t = 0.2391$ inches), the connection will be adequately designed for fatigue using a 19 inch mast-arm diameter.
2. Assuming: (1) the fatigue resistance of the connection is improved to Category E (i.e. a Category E full-penetration connection (Detail 11 in Table 1.9.6.2) is used) and (2) the thickness of the mast-arm is not increased (i.e. $t = 0.2391$ inches), the connection will be adequately designed for fatigue using a 15 inch mast-arm diameter.
3. Assuming: (1) the fatigue resistance of the connection is improved to Category E (i.e. a Category E full-

penetration connection (Detail 11 in Table 1.9.6.2) is used) and (2) the diameter of the mast-arm is increased to 13 inches (i.e. $d_b = 13$ in), the connection will be adequately designed for fatigue using a mast-arm thickness equal to 0.3125 in.

4.3.3 Built-Up Box

Details of the built-up box are provided below:

$h = 19$ in
 $b = 10.5$ in
 $t = 0.25$ in



4.3.3.1 Moment of Inertia

The moment of inertia of the built-up box is calculated by:

$$(I_z)_{box} = \sum \frac{1}{12} t h^3 + \sum A \bar{z}^2 = 2 \left[\frac{1}{12} (0.25 \text{ in})(19 \text{ in})^3 \right] + 2 [(10.5 \text{ in})(0.25 \text{ in})(9.5 \text{ in})^2] = 759.60 \text{ in}^4$$

$$(I_y)_{box} = \sum \frac{1}{12} t b^3 + \sum A \bar{y}^2 = 2 \left[\frac{1}{12} (0.25 \text{ in})(10.5 \text{ in})^3 \right] + 2 [(19 \text{ in})(0.25 \text{ in})(5.25 \text{ in})^2] = 310.08 \text{ in}^4$$

4.3.3.2 Built-Up Box Stress Range

Based upon the calculations of Section 3, the built-up box must be checked with respect to galloping and natural wind. The stress range in the built-up box due to galloping is calculated by:

$$(S_R)_{box} = \frac{(M_z)_{GC}}{(I_z)_{box}} = \frac{(163.63 \text{ k-in})(9.5 \text{ in})}{759.60 \text{ in}^4} = 2.0 \text{ ksi}$$

The stress range in the built-up box due to natural wind gusts is calculated by:

$$(S_R)_{box} = \frac{(M_y)_{NWC}}{(I_y)_{box}} = \frac{(99.67 \text{ k-in})(5.25 \text{ in})}{310.08 \text{ in}^4} = 1.7 \text{ ksi}$$

Based upon the above calculations, galloping controls the design of the built-up box for fatigue.

The built-up-box-to-flange-plate connection is classified as a Category E' fatigue detail (Detail 17 in Table 1.9.6.2). The constant amplitude fatigue limit corresponding to Category E' is 2.6 ksi (Table 1.9.6.2). Since the calculated stress range (2.0 ksi) is less than the constant amplitude fatigue limit (2.6 ksi), the connection is adequately designed for fatigue.

The built-up-box-to-column connection is classified as a Category ET fatigue detail (Detail 19 in Table 1.9.6.2). The constant amplitude fatigue limit corresponding to Category ET is 1.2 ksi (Table 1.9.6.2). No reduction in the fatigue resistance is necessary because the r/t ratio of the column at the location of the mast-arm is less than 24. Since the calculated stress range (2.0 ksi) is greater than the constant amplitude fatigue limit (1.2 ksi), the connection is inadequately designed for infinite fatigue life.

Potential Redesigns:

1. Assuming: (1) the fatigue resistance of the connection is not improved (i.e. a Category ET connection (Detail 19 in Table 1.9.6.2) is used to attach the built-up box to the column) and (2) the column diameter at the location of the mast-arm is 13 inches with a 0.3125 inch wall thickness, the connection will be adequately designed for fatigue using a box height, h, equal to 22 inches, a box width, b, equal to 13 inches, and a plate thickness, t, equal to 0.3125 inches.

5. DEFLECTION

Section 1.9.6C limits the vertical-plane mast-arm displacement range to 8 inches under application of the limit states fatigue design load. Based upon the calculations of Section 3, galloping controls the design of the structure with respect to the deflection limit state.

5.1 Vertical-Plane Displacement Range of the Original Structure

5.1.1 Assumptions

(1) The displacement range at the tip of the mast-arm is calculated using the superposition of the following displacement components:

Δ_1 : Displacement range at the tip of the mast-arm due to the rotation of the column (assuming a cantilever beam fixed at the base of the column) under application of the moment $(M_x)_G = 163.63$ k-in.

Δ_2 : Displacement range at the tip of the mast-arm due to the deflection of the mast-arm (assuming a cantilever beam fixed at the base of the mast-arm) under the application of $F_G = 122.85$ lbs to Signal 1.

Δ_3 : Displacement range at the tip of the mast-arm due to the deflection of the mast-arm (assuming a cantilever beam fixed at the base of the mast-arm) under the application of $F_G = 122.85$ lbs to Signal 2.

Δ_4 : Displacement range at the tip of the mast-arm due to the deflection of the mast-arm (assuming a cantilever beam fixed at the base of the mast-arm) under the application of $F_G = 122.85$ lbs to Signal 3.

(2) Calculation of each of the displacement quantities noted above is based upon the average moment of inertia of each of the components.

5.1.2 Average Moment of Inertia of Column

From previous calculations, the moment of inertia at the base of the column is:

$$(I_{col})_{base} = 195.18 \text{ in}^4$$

The moment of inertia at the location of the mast-arm is:

$$(I_{col})_{top} = \frac{\pi}{64} [d_t^4 - (d_t - 2t)^4] = \frac{\pi}{64} [(10.5 \text{ in})^4 - (10.5 \text{ in} - 0.4782 \text{ in})^4] = 101.49 \text{ in}^4$$

The average moment of inertia of the column is:

$$(I_{col})_{ave} = \frac{(I_{col})_{base} + (I_{col})_{top}}{2} = \frac{195.18 \text{ in}^4 + 101.49 \text{ in}^4}{2} = 148.34 \text{ in}^4$$

5.1.3 Average Moment of Inertia of Mast-Arm

From previous calculations, the moment of inertia at the base of the mast-arm is:

$$(I_{arm})_{bot} = 101.49 \text{ in}^4$$

The moment of inertia at the tip of the mast-arm is:

$$(I_{arm})_{tip} = \frac{\pi}{64} [d_t^4 - (d_t - 2t)^4] = \frac{\pi}{64} [(4 \text{ in})^4 - (4 \text{ in} - 0.4782 \text{ in})^4] = 5.01 \text{ in}^4$$

The average moment of inertia of the mast-arm is:

$$(I_{arm})_{ave} = \frac{(I_{arm})_{bot} + (I_{arm})_{tip}}{2} = \frac{101.49 \text{ in}^4 + 5.01 \text{ in}^4}{2} = 53.25 \text{ in}^4$$

5.1.4 Mast-Arm Displacement Range Δ_1

The rotation of the column at the location of the mast-arm is calculated by:

$$\theta_{col} = \frac{(M_z)_G L_2}{E(I_{col})_{ave}} = \frac{(163.63 \text{ k-in})(18 \text{ ft})(12 \text{ in/ft})}{(29000 \text{ ksi})(148.34 \text{ in}^4)} = 0.00822 \text{ rad}$$

The displacement range at the tip of the mast-arm due to the rotation of the column is calculated by:

$$\Delta_1 = \theta_{col} L_5 = (0.00822 \text{ rad})(49 \text{ ft})(12 \text{ in/ft}) = 4.83 \text{ in}$$

5.1.5 Mast-Arm Deflection Displacement Δ_2

The displacement range at the tip of the mast-arm due to the galloping load applied to signal 1 is calculated by:

$$\Delta_2 = \frac{(F_G)_{sig} L_3^2}{6E(I_{arm})_{ave}} [3L_5 - L_3] = \frac{(122.85 \text{ lbs})(25 \text{ ft})^2}{6(29 \times 10^6 \text{ psi})(53.25 \text{ in}^4)} [3(49 \text{ ft}) - (25 \text{ ft})](12 \text{ in/ft})^3$$

$$\Delta_2 = 1.75 \text{ in}$$

5.1.6 Mast-Arm Displacement Range Δ_3

The displacement range at the tip of the mast-arm due to the galloping load applied to signal 2 is calculated by:

$$\Delta_3 = \frac{(F_G)_{sig} L_4^2}{6E(I_{arm})_{ave}} [3L_5 - L_4] = \frac{(122.85 \text{ lbs})(37 \text{ ft})^2}{6(29 \times 10^6 \text{ psi})(53.25 \text{ in}^4)} [3(49 \text{ ft}) - (37 \text{ ft})](12 \text{ in/ft})^3$$

$$\Delta_3 = 3.45 \text{ in}$$

5.1.7 Mast-Arm Displacement Range Δ_4

The displacement range at the tip of the mast-arm due to the galloping load applied to signal 3 is calculated by:

$$\Delta_4 = \frac{(F_G)_{sig} L_5^3}{3E(I_{arm})_{ave}} = \frac{(122.85 \text{ lbs})(49 \text{ ft})^3 (12 \text{ in/ft})^3}{3(29 \times 10^6 \text{ psi})(53.25 \text{ in}^4)}$$

$$\Delta_4 = 5.39 \text{ in}$$

5.1.8 Total Mast-Arm Deflection Range Δ_{total}

The total displacement range at the tip of the mast-arm is obtained by the superposition of each of the deflection quantities:

$$\Delta_{total} = \Delta_1 + \Delta_2 + \Delta_3 + \Delta_4 = (4.83 \text{ in}) + (1.75 \text{ in}) + (3.45 \text{ in}) + (5.39 \text{ in})$$

$$\Delta_{total} = 15.42 \text{ in}$$

The allowable vertical-plane mast-arm displacement range is 8 inches (Section 1.9.6C). The computed deflection range at the tip of the mast-arm (15.42 in) exceeds the allowable deflection range (8 in). Therefore, the structure is inadequately designed with respect to the deflection limit state.

5.2 Vertical-Plane Displacement Range of the Redesigned Structure

5.2.1 Assumptions

(1) It is assumed that the structure is redesigned as follows:

Column

d = 13 in (prismatic)

t = 0.3125 in

Mast-Arm

d_b = 13 in

d_t = 6.5 in

t = 0.3125 in

(2) The assumption used in the calculations shown in Section 5.1 is also used in the calculations which follow.

5.2.2 Moment of Inertia of Column

The moment of inertia of the column is:

$$I_{col} = \frac{\pi}{64} [d_t^4 - (d_t - 2t)^4] = \frac{\pi}{64} [(13 \text{ in})^4 - (13 \text{ in} - 0.625 \text{ in})^4] = 250.78 \text{ in}^4$$

5.2.3 Average Moment of Inertia of Mast-Arm

From the above calculation, the moment of inertia at the base of the mast-arm is:

$$(I_{arm})_{base} = 250.78 \text{ in}^4$$

The moment of inertia at the tip of the mast-arm is:

$$(I_{arm})_{tip} = \frac{\pi}{64} [d_t^4 - (d_t - 2t)^4] = \frac{\pi}{64} [(6.5 \text{ in})^4 - (6.5 \text{ in} - 0.625 \text{ in})^4] = 29.14 \text{ in}^4$$

The average moment of inertia of the mast-arm is:

$$(I_{arm})_{ave} = \frac{(I_{arm})_{base} + (I_{arm})_{tip}}{2} = \frac{250.78 \text{ in}^4 + 29.14 \text{ in}^4}{2} = 139.96 \text{ in}^4$$

5.2.4 Mast-Arm Deflection Range Δ_1

The rotation of the column at the location of the mast-arm is calculated by:

$$\theta_{col} = \frac{(M_z)_G L_2}{E(I_{col})_{ave}} = \frac{(163.63 \text{ k-in})(18 \text{ ft})(12 \text{ in/ft})}{(29000 \text{ ksi})(250.78 \text{ in}^4)} = 0.00486 \text{ rad}$$

The displacement range at the tip of the mast-arm due to the rotation of the column is calculated by:

$$\Delta_1 = \theta_{col} L_5 = (0.00486 \text{ rad})(49 \text{ ft})(12 \text{ in/ft}) = 2.86 \text{ in}$$

5.2.5 Mast-Arm Deflection Range Δ_2

The displacement range at the tip of the mast-arm due to the galloping load applied to signal 1 is calculated by:

$$\Delta_2 = \frac{(F_G)_{sig} L_3^2}{6E(I_{arm})_{ave}} [3L_5 - L_3] = \frac{(122.85 \text{ lbs})(25 \text{ ft})^2}{6(29 \times 10^6 \text{ psi})(139.96 \text{ in}^4)} [3(49 \text{ ft}) - (25 \text{ ft})](12 \text{ in/ft})^3$$

$$\Delta_2 = 0.66 \text{ in}$$

5.2.6 Mast-Arm Deflection Range Δ_3

The displacement range at the tip of the mast-arm due to the galloping load applied to signal 2 is calculated by:

$$\Delta_3 = \frac{(F_G)_{sig} L_4^2}{6E(I_{arm})_{ave}} [3L_5 - L_4] = \frac{(122.85 \text{ lbs})(37 \text{ ft})^2}{6(29 \times 10^6 \text{ psi})(139.96 \text{ in}^4)} [3(49 \text{ ft}) - (37 \text{ ft})](12 \text{ in/ft})^3$$

$$\Delta_3 = 1.31 \text{ in}$$

5.2.7 Mast-Arm Deflection Range Δ_4

The displacement range at the tip of the mast-arm due to the galloping load applied to signal 3 is calculated by:

$$\Delta_4 = \frac{(F_G)_{sig} L_5^3}{3E(I_{arm})_{ave}} = \frac{(122.85 \text{ lbs})(49 \text{ ft})^3(12 \text{ in/ft})^3}{3(29 \times 10^6 \text{ psi})(139.96 \text{ in}^4)}$$

$$\Delta_4 = 2.05 \text{ in}$$

5.2.7 Total Mast-Arm Deflection Range Δ_{total}

The total displacement range at the tip of the mast-arm is obtained by the superposition of each of the deflection quantities:

$$\Delta_{total} = \Delta_1 + \Delta_2 + \Delta_3 + \Delta_4 = (2.86 \text{ in}) + (0.66 \text{ in}) + (1.31 \text{ in}) + (2.05 \text{ in})$$

$$\Delta_{total} = 6.88 \text{ in}$$

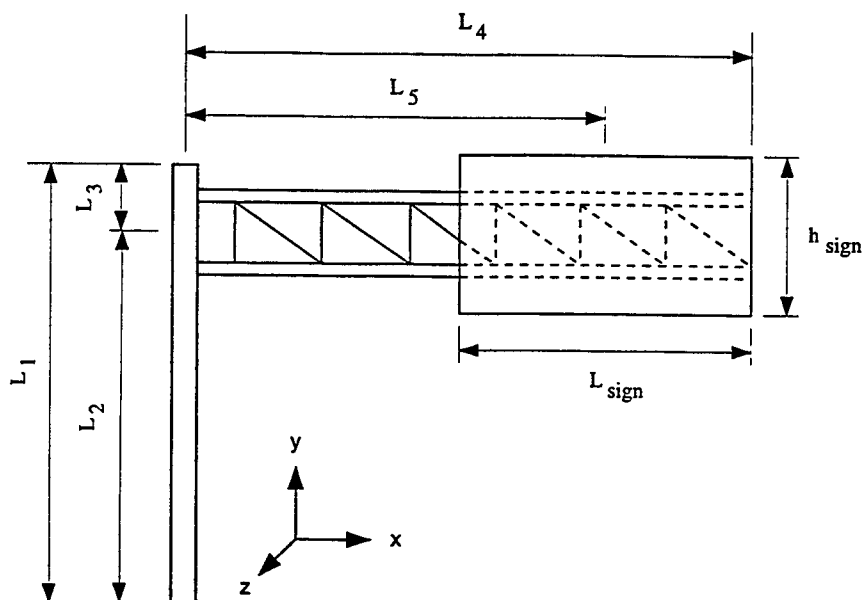
The allowable vertical-plane mast-arm displacement range is 8 inches (Section 1.9.6C). The computed deflection range at the tip of the mast-arm (6.88 in) is less than the allowable deflection range (8 in). Therefore, the structure is adequately designed with respect to the deflection limit state.

EXAMPLE 2

1. GENERAL

1.1 Description

The structure is a two-chord truss cantilevered sign support structure (steel) composed of prismatic structural elements. The sign is to be designed for vibration and fatigue in accordance with Section 1.9.6 of the AASHTO Specifications. It is assumed that the sign will be installed on a major highway and is therefore checked per the requirements for a Category I structure. Furthermore, it is assumed that the structure will be erected without approved vibration mitigation devices. All calculations are performed using S.I. units.



1.2 Dimensions

Column:

Column length = $L_1 = 10.2108$ m
 Length to mid-depth of truss = $L_2 = 8.9916$ m
 Length from mid-depth of truss to
 end of column = $L_3 = 1.2192$ m
 Diameter = $d_{col} = 0.6096$ m
 Thickness = $t_{col} = 0.009525$ m

Sign:

Length = $L_{sign} = 7.3152$ m
 Height = $h_{sign} = 3.048$ m
 Depth = $d_{sign} = 0.0762$ m

Mast-Arm:

Mast-arm length = $L_4 = 13.716$ m
 Length to centroid of sign = $L_5 = 10.0584$ m
 Truss depth = $d_{truss} = 1.524$ m
 Chord diameter = $d_{chord} = 0.3048$ m
 Chord thickness = $t_{chord} = 0.01113$ m
 Brace diameter = $d_{brace} = 0.1016$ m
 Brace thickness = $t_{brace} = 0.00602$ m

Anchor Bolts:

Nominal bolt diameter = $d_b = 0.070$ m
 Thread series = 4 UNC
 Number of bolts = 8
 Bolt circle diameter = $d_{bc} = 0.7874$ m

1.3 Critical Fatigue Details

1. Anchor Bolts (Detail 5 in Table 1.9.6.2)
2. Column-to-baseplate groove-welded connection with backing ring not removed (Detail 12 in Table 1.9.6.2)
3. Fillet-welded stiffener at column base (Details 22 and 23 in Table 1.9.6.2)

Other fatigue details within the structure (e.g. mast-arm-to-column connection) are not checked in this design example.

2. CALCULATION OF LIMIT STATES FATIGUE LOADS

2.1 Galloping

The equivalent static shear range to be applied to the sign attachment is calculated in accordance with Equation 1.9.6-1:

$$P_G = 1000I_F = (1000)(1.0) = 1000 \text{ Pa}$$

where $I_F = 1.0$ (Table 1.9.6.1) is the importance factor used in the design of a Category I sign support structure for galloping.

The area of the sign projected on a vertical plane is calculated by:

$$(A_{\text{sign}})_v = L_{\text{sign}}h_{\text{sign}} = (7.3152 \text{ m})(3.048 \text{ m}) = 22.3 \text{ m}^2$$

where $L_{\text{sign}} = 7.3152 \text{ m}$ is the length of the sign and $h_{\text{sign}} = 3.048 \text{ m}$ is the height of the sign.

The equivalent static shear load range to be applied to the sign attachment is calculated by:

$$F_G = P_G(A_{\text{sign}})_v = (1000 \text{ Pa})(22.3 \text{ m}^2) = 22300 \text{ N}$$

where $(A_{\text{sign}})_v = 22.3 \text{ m}^2$ is the area of the sign projected on a vertical plane.

2.2 Vortex Shedding

As per the requirements of Section 1.9.6A-b, vortex shedding need not be considered in the design of cantilevered sign support structures for vibration and fatigue.

2.3 Natural Wind Gusts

It is assumed that the support structure will be erected at a location where the annual mean wind velocity is 6 m/s. Since this annual mean wind velocity is greater than 5 m/s, the equivalent static pressure range to be applied to the structure is calculated in accordance with Equation 1.9.6 - C3:

$$P_{NW} = 250 C_d \left[\frac{V_{\text{mean}}^2}{25} \right] I_F = (250) C_d \left[\frac{(6 \text{ m/s})^2}{(25)} \right] (1.0) = 360 C_d \text{ Pa}$$

where $I_F = 1.0$ (Table 1.9.6.1) is the importance factor used in the design of a Category I sign support structure for natural wind.

The equivalent static load range to be applied to the column is calculated by:

$$(F_{NW})_{col} = P_{NW}(A_{col})_v = P_{NW}[L_1 d_{col}] = [(360)(1.10)][(10.2108 \text{ m})(0.6096 \text{ m})] = 2465 \text{ N}$$

where $(A_{col})_v$ is the area of the column projected on a vertical plane, $L_1 = 10.2108 \text{ m}$ is the length of the column, $d_{col} = 0.6096 \text{ m}$ is the diameter of the column, and $C_d = 1.10$ is a conservative estimate of the drag coefficient for a circular cylinder (Table 1.2.5C).

The equivalent static load range to be applied to each of the chords is calculated by:

$$(F_{NW})_{chord}^* = P_{NW}(A_{chord})_v = P_{NW}[(L_4 - L_{sign})d_{chord}] = [(360)(1.10)][(13.716 \text{ m} - 7.3152 \text{ m})(0.3048 \text{ m})] = 773 \text{ N}$$

where $(A_{chord})_v$ is the area of the chord projected on a vertical plane, $(L_4 - L_{sign}) = 6.4008 \text{ m}$ is the length of the chord exposed to the wind, $d_{chord} = 0.3048 \text{ m}$ is the diameter of the chord, and $C_d = 1.10$ is a conservative estimate of the drag coefficient for a circular cylinder (Table 1.2.5C).

Note:

*The area of the chord behind the sign attachment is excluded from the calculation of the equivalent load range.

The equivalent static load range acting on each of the brace members in the truss is neglected in this design example.

The equivalent static load range to be applied to the sign attachment is calculated by:

$$(F_{NW})_{sign} = P_{NW}(A_{sign})_v = [(360)(1.19)][(22.3 \text{ m}^2)] = 9553 \text{ N}$$

where $(A_{sign})_v = 22.3 \text{ m}^2$ is the area of the sign projected on a vertical plane and $C_d = 1.19$ is the drag coefficient for a sign with a 2.4:1 length-to-width ratio (Table 1.2.5C).

2.4 Truck Gusts

It is assumed that the support structure will be erected at a location where the posted speed limit is not significantly less than 65 mph. Therefore, Equation 1.9.6 - 5 is applied without modification.

The equivalent static pressure range to be applied to the structure is calculated in accordance with Equation 1.9.6 - 5:

$$P_{TG} = 1760C_dI_F = 1760C_d(1.0) = 1760C_d \text{ Pa}$$

where $I_F = 1.0$ (Table 1.9.6.1) is the importance factor used in the design of a Category I sign support structure for truck gusts.

As per the requirements of Section 1.9.6A - d, the equivalent static pressure is to be applied along the full length of the sign attachment.

The equivalent static load range to be applied to the sign attachment is calculated by:

$$(F_{TG})_{sign} = P_{TG}(A_{sign})_h = P_{TG}[L_{sign}d_{sign}] = [(1760)(1.45)][(7.3152 \text{ m})(0.0762 \text{ m})] = 1423 \text{ N}$$

where $(A_{sign})_h$ is the area of the sign projected on a horizontal plane, $L_{sign} = 7.3152 \text{ m}$ is the length of the sign, and d_{sign}

= 0.0762 is the depth of the sign in the direction of traffic (it is assumed that this depth includes any miscellaneous lights, walkways, etc. which may be mounted to the structure), and $C_d^* = 1.45$ is the drag coefficient for a square section (Table 1.2.5C).

Note:

* $C_d = 1.45$ is the drag coefficient for flow normal to the side of a square section. It is assumed that this drag coefficient is representative of the drag coefficient to which a sign attachment would be subjected under flow normal to the depth of the sign in the direction of traffic.

The equivalent static load range to be applied to the bottom chord is calculated by:

$$(F_{TG})_{\text{chord}} = P_{TG}(A_{\text{chord}})_h = P_{TG}[L_{\text{sign}}d_{\text{chord}}] = [(1760)(1.10)][(7.3152 \text{ m})(0.3048 \text{ m})] = 4317 \text{ N}$$

where $(A_{\text{chord}})_h$ is the area of the bottom chord projected on a horizontal plane, $L_{\text{sign}} = 7.3152 \text{ m}$ is the length of the sign, $d_{\text{chord}} = 0.3048 \text{ m}$ is the diameter of the chord, and $C_d = 1.10$ is the drag coefficient for a circular cylinder (Table 1.2.5C).

3. CALCULATION OF BENDING MOMENTS

3.1 Moment Due to Galloping

The bending moment at the centerline of the column (about the z - axis) is calculated by:

$$(M_z)_G = F_G L_5 = (22300 \text{ N})(10.0584 \text{ m})$$

$$(M_z)_G = 224302 \text{ N-m} \Rightarrow \text{Controls}$$

3.2 Moment Due to Natural Wind Gusts

The bending moment at the base of the column (about the x - axis) is calculated by:

$$(M_x)_{NW} = (F_{NW})_{\text{col}}(L_1/2) + 2(F_{NW})_{\text{chord}}(L_2) + (F_{NW})_{\text{sign}}(L_2)$$

$$(M_x)_{NW} = (2465 \text{ N})(5.1054 \text{ m}) + 2(773 \text{ N})(8.9916 \text{ m}) + (9553 \text{ N})(8.9916 \text{ m})$$

$$(M_x)_{NW} = 112383 \text{ N-m}$$

The bending moment at the centerline of the column (about the y - axis) is calculated by:

$$(M_y)_{NW} = 2(F_{NW})_{\text{chord}}[(L_4 - L_{\text{sign}})/2] + (F_{NW})_{\text{sign}}(L_5) = 2(773 \text{ N})(3.2004 \text{ m}) + (9553 \text{ N})(10.0584 \text{ m})$$

$$(M_y)_{NW} = 101036 \text{ N-m}$$

3.2 Moment Due to Truck Gusts

The bending moment at the centerline of the column (about the z - axis) is calculated by:

$$(M_z)_{TG} = (F_{TG})_{sign}(L_5) + (F_{TG})_{chord}(L_5) = (1423 \text{ N})(10.0584 \text{ m}) + (4317 \text{ N})(10.0584 \text{ m})$$

$$(M_z)_{TG} = 57735 \text{ N-m}$$

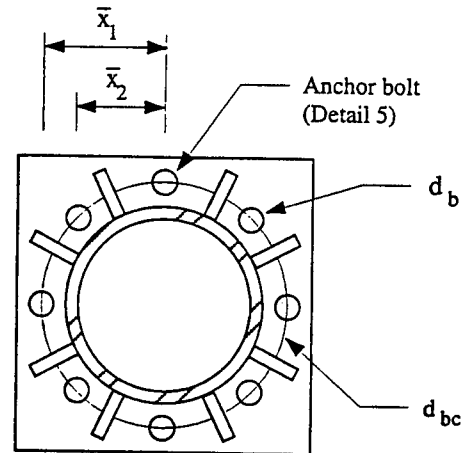
4. STRESS RANGE CALCULATIONS

Note: In this design example only the details at the column base will be checked for fatigue. In an actual design, all of the details within the structure should be checked for fatigue.

4.1 Anchor Bolts

Details of the anchor bolt group are provided below:

Nominal bolt diameter = $d_b = 70 \text{ mm}$ (0.070 m)
Thread series = 4 UNC
Thread pitch = 6.35 mm
Number of bolts = 8
Bolt circle diameter = $d_{bc} = 0.7874 \text{ m}$



4.1.1 Moment of Inertia of the Bolt Group

The centroidal distance to each of the anchor bolts is calculated by:

$$\bar{x}_1 = \frac{d_{bc}}{2} = \frac{0.7874 \text{ m}}{2} = 0.3937 \text{ m}$$

$$\bar{x}_2 = \frac{d_{bc}}{2} \cos 45^\circ = \frac{0.7874 \text{ m}}{2} \cos 45^\circ = 0.2784 \text{ m}$$

where \bar{x} is the centroidal distance to each of the anchor bolts and $d_{bc} = 0.7874 \text{ m}$ is the diameter of the bolt circle.

The tensile stress area of each of the anchor bolts is calculated by:

$$A_T = \frac{\pi}{4} [d_b - 0.938 P]^2 = \frac{\pi}{4} [70 \text{ mm} - 0.938 (6.35 \text{ mm})]^2 = 3221 \text{ mm}^2$$

where A_T is the tensile stress area of each anchor bolt (Section 1.3.4A), $d_b = 70 \text{ mm}$ is the nominal bolt diameter, and $P = 6.35 \text{ mm}$ is the thread pitch.

The moment of inertia of the bolt group is calculated by:

$$I_b = \sum A_T \bar{x}^2 = 2[(3.221 \times 10^{-3} \text{ m}^2)(0.3937 \text{ m})^2] + 4[(3.221 \times 10^{-3} \text{ m}^2)(0.2874 \text{ m})^2] = 2.063 \times 10^{-3} \text{ m}^4$$

where $A_T = 3.221 \times 10^{-3} \text{ m}^2$ is the tensile stress area of each bolt and \bar{x} is the centroidal distance to each of the bolts.

4.1.2 Anchor Bolt Stress Range

Based upon the calculations of Section 3, galloping controls the design of the anchor bolt group for fatigue. Therefore, the axial stress range in each of the anchor bolts is calculated by:

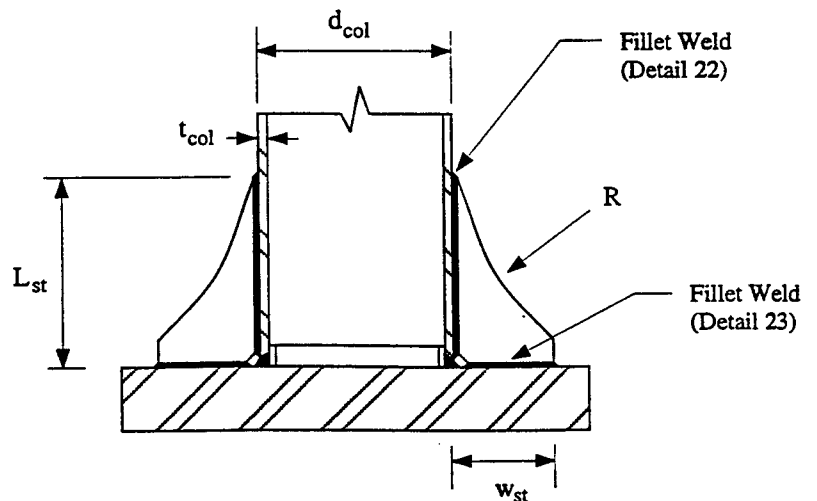
$$(S_R)_{bolt} = \frac{(M_z)_G^c}{I_b} = \frac{(224302 \text{ N-m})(0.3937 \text{ m})}{2.063 \times 10^{-3} \text{ m}^4} = 42.8 \times 10^6 \text{ Pa (42.8 MPa)}$$

Anchor bolts are classified as Category D fatigue details (Detail 5 in Table 1.9.6.2). The constant amplitude fatigue limit corresponding to Category D is 48 MPa (Table 1.9.6.2). Since the calculated stress range (42.8 MPa) is less than the constant amplitude fatigue limit (48 MPa), the anchor bolt group is considered adequately designed for fatigue.

4.2 Column-to-Base Plate Connection

Details of the column-to-base plate groove-welded connection are provided below:

Column diameter = $d_{col} = 0.6096 \text{ m}$
 Column thickness = $t_{col} = 0.009525$
 Stiffener length = $L_{st} = 0.4572 \text{ m}$
 Stiffener width = $w_{st} = 0.1588 \text{ m}$
 Stiffener thickness = $t_{st} = 0.01905 \text{ m}$
 Number of stiffeners = 8
 Stiffener radius = $R > 0.6096 \text{ m}$



4.2.1 Moment of Inertia

The moment of inertia of the column is calculated by:

$$I_{col} = \frac{\pi}{64} [d_{col}^4 - (d_{col} - 2t_{col})^4] = \frac{\pi}{64} [(0.6096 \text{ m})^4 - (0.6096 \text{ m} - 0.01905 \text{ m})^4] = 8.084 \times 10^{-4} \text{ m}^4$$

where $d_{col} = 0.6096 \text{ m}$ is the column diameter and $t_{col} = 0.009525$ is the column thickness.

The area of each of the stiffeners at the column base is calculated by:

$$A_{st} = w_{st} t_{st} = (0.1588 \text{ m})(0.01905 \text{ m}) = 3.025 \times 10^{-3} \text{ m}^2$$

where $w_{st} = 0.1588 \text{ m}$ is the width of the stiffener at the column base and $t_{st} = 0.01905 \text{ m}$ is the thickness of the stiffener at the column base.

The radius to the centroid of the stiffener circle is calculated by:

$$r_{st} = \frac{d_{col}}{2} + \frac{w_{st}}{2} = \frac{0.6096 \text{ m}}{2} + \frac{0.1588 \text{ m}}{2} = 0.3842 \text{ m}$$

where r_{st} is the radius to the centroid of the stiffener circle, $d_{col} = 0.6096 \text{ m}$ is the diameter of the column, and $w_{st} = 0.1588 \text{ m}$ is the width of the stiffener at the column base.

The centroidal distance to each of the stiffeners is calculated by:

$$\bar{x}_1 = r_{st} \sin 22.5^\circ = (0.3842 \text{ m}) \sin 22.5^\circ = 0.1470 \text{ m}$$

$$\bar{x}_2 = r_{st} \cos 22.5^\circ = (0.3842 \text{ m}) \cos 22.5^\circ = 0.3550 \text{ m}$$

The moment of inertia at the column base is calculated by:

$$I_{cb} = I_{col} + \sum A_{st} \bar{x}^2$$

$$I_{cb} = (8.084 \times 10^{-4} \text{ m}^4) + [4(3.025 \times 10^{-3} \text{ m}^2)(0.1470 \text{ m})^2 + 4(3.025 \times 10^{-3} \text{ m}^2)(0.3550 \text{ m})^2]$$

$$I_{cb} = 2.595 \times 10^{-3} \text{ m}^4$$

Note that the individual moments of inertia of each of the stiffeners is neglected in the calculation of the moment of inertia of the column base.

4.2.2 Stress Range at Column-to-Baseplate Connection

Based upon the calculations of Section 3, galloping controls the design of the groove-welded column-to-baseplate connection for fatigue. Therefore, the stress range at the groove-welded column-to-baseplate connection is calculated by:

$$(S_R)_{col} = \frac{(M_z)_{G^c}}{I_{cb}} = \frac{(224302 \text{ N-m})(0.3048 \text{ m})}{2.595 \times 10^{-3} \text{ m}^4} = 26.3 \times 10^6 \text{ Pa (26.3 MPa)}$$

The groove-welded column-to-base-plate connection (without the backing ring fully-fused) is classified as a Category E' fatigue detail (Detail 12 in Table 1.9.6.2). The constant amplitude fatigue limit corresponding to Category E' is 18 MPa (Table 1.9.6.2). Since the calculated stress range (26.3 MPa) is greater than the constant amplitude fatigue limit (18 MPa), the groove-welded column-to-baseplate connection is inadequately designed for fatigue.

Potential Redesigns:

1. The groove-welded column-to-baseplate connection can be improved by fusing the backing ring to the baseplate with a full-penetration groove weld (i.e. a full-penetration groove-weld is used on the inside diameter of the backing ring). Under this condition, the fatigue resistance of the connection would be improved to Category E (Detail 11 in Table 1.9.6.2). The constant amplitude fatigue limit corresponding to Category E is 31 MPa (Table 1.9.6.2). Since the calculated stress range (26.3 MPa) is less than the constant amplitude fatigue limit (31 MPa), the column-to-baseplate connection would be adequately designed for fatigue.
2. The allowable fatigue strength of the Category E' groove-welded column-to-baseplate connection can be met by increasing the thickness of the stiffeners to 31.75 mm. This modification will reduce the calculated stress range to 18 MPa. As illustrated below, the fatigue strength of the stiffener-to-baseplate connection should be checked for these conditions.

4.2.3 Stress Range at Stiffener-to-Baseplate Connection

Based upon the calculations of Section 3, galloping controls the design of the stiffener-to-baseplate connection for fatigue. Therefore, the stress range at the stiffener-to-baseplate connection is calculated by:

$$(S_R)_{col} = \frac{(M_z)_{G^c}}{I_{cb}} = \frac{(224302 \text{ N-m})(0.46355 \text{ m})}{2.595 \times 10^{-3} \text{ m}^4} = 40.1 \times 10^6 \text{ Pa (40.1 MPa)}$$

The stiffener-to-baseplate connection is a transverse load-bearing fillet-welded attachment with a thickness greater than 0.013 m (Detail 23 in Table 1.9.6.2). Therefore, the constant amplitude fatigue limit of this detail must be reduced in accordance with the following relationship:

$$\Delta F = (\Delta F)_n^c \times \frac{0.094 + 1.23 \frac{H}{t_p}}{t_p^{\frac{1}{6}}} = (69 \text{ MPa}) \times \frac{0.094 + 1.23 [\frac{16 \text{ mm}}{19 \text{ mm}}]}{(19 \text{ mm})^{\frac{1}{6}}} = 47.6 \text{ MPa}$$

where $H = 16 \text{ mm}$ is the effective throat of the stiffener-to-baseplate fillet weld, and $t_p = 19 \text{ mm}$ is the thickness of the stiffener plate.

Since the calculated stress range (40.1 MPa) is less than the constant amplitude fatigue limit (47.6 MPa), the stiffener-to-baseplate connection is adequately designed for fatigue.

4.2.4 Stress Range at Termination of Stiffener

Based upon the calculations of Section 3, galloping controls the design of the stiffener-to-column connection for fatigue. Therefore, the stress range at the termination of the stiffener is calculated by:

$$(S_R)_{col} = \frac{(M_z)_G c}{I_{col}} = \frac{(224302 \text{ N-m})(0.3048 \text{ m})}{8.084 \times 10^{-4} \text{ m}^4} = 84.6 \times 10^6 \text{ Pa (84.6 MPa)}$$

The weld termination at the end of the stiffener is classified as a Category D fatigue detail (Detail 22 in Table 1.9.6.2). The constant amplitude fatigue limit corresponding to Category D is 48 MPa (Table 1.9.6.2). Since, the calculated stress range (84.6 MPa) is greater than the constant amplitude fatigue limit (48 MPa), the weld termination at the end of the stiffener is inadequately designed for fatigue.

Potential Redesign:

1. Assuming: (1) the fatigue resistance of the weld termination is improved to Category C by using a full-penetration weld with the stiffener radiused to greater than 0.6096 m (i.e. Detail 21 in Table 1.9.6.2) and (2) the diameter of the column is not increased (i.e. $d = 0.6096 \text{ m}$), the weld termination at the end of the stiffener will be adequately designed for fatigue using a column thickness equal to 0.0127 m.

Note: Although not specifically shown in this example problem, the remaining connection details in the structure (e.g. mast-arm-to-column connection) should also be checked for fatigue.

5. DEFLECTION

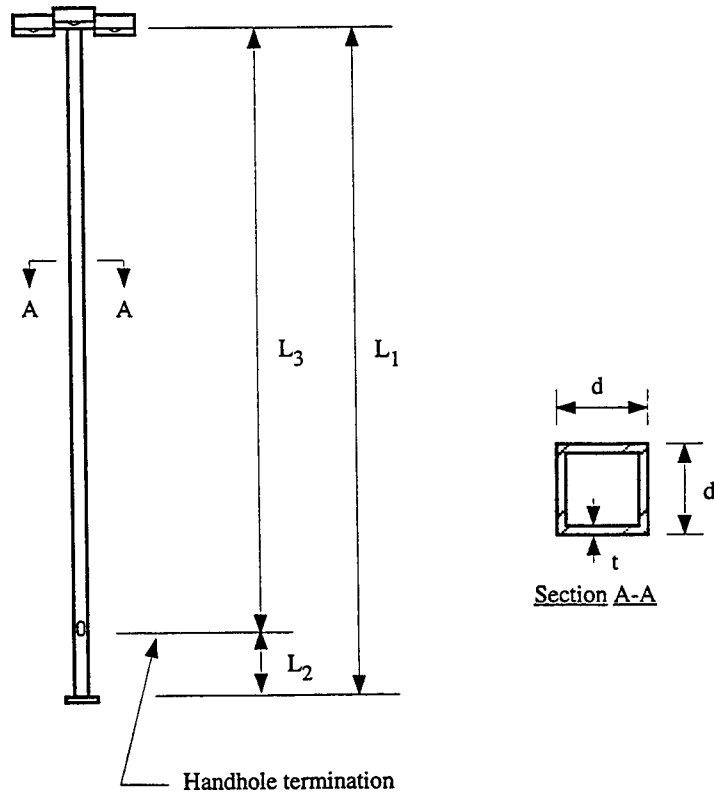
As per the requirements of Section 1.9.6C, cantilevered sign support structures with trussed mast-arms need not be designed to satisfy the deflection limit state.

EXAMPLE 3

1. GENERAL

1.1 Description

The structure is a pole-top luminaire (steel) composed of a prismatic structural support. The luminaire is to be designed for vibration and fatigue in accordance with Section 1.9.6 of the AASHTO Specifications. It is assumed that the luminaire will be installed at a location other than a major or secondary highway and is therefore checked per the requirements for a Category III structure. Furthermore, it is assumed that the structure will be erected without approved vibration mitigation devices. All calculations are performed using S.I. units.



1.2 Dimensions

Column:

Column length = $L_1 = 11.890$ m
Length from column base to termination
of handhole = $L_2 = 0.381$ m
Length from termination of handhole
to top of column = $L_3 = 11.509$ m
Width = $d = 0.1524$ m
Thickness = $t = 0.004554$ m

Anchor Bolts:

Nominal bolt diameter = $d_b = 0.0254$ m
Thread series = 8 UNC
Number of bolts = 4
Bolt circle diameter = $d_{bc} = 0.3175$ m

Luminaire:

Area projected on a vertical plane = $(A_{lum})_v = 0.434$ m²
Weight = $W = 667$ N

1.3 Critical Fatigue Details

The structure contains the following details which must be designed for fatigue:

1. Anchor bolts (Detail 5 in Table 1.9.6.2)
2. Column-to-baseplate fillet-welded socket connection (Detail 16 in Table 1.9.6.2)
3. Partial-penetration column seam weld (Detail 8 in Table 1.9.6.2)
4. Weld termination at reinforced handhole (Detail 20 in Table 1.9.6.2)

2. CALCULATION OF LIMIT STATES FATIGUE LOADS

2.1 Galloping

As per the requirements of Section 1.9.6A-2a, galloping need not be considered in the design of luminaire support structures for vibration and fatigue.

2.2 Vortex Shedding

The moment of inertia of the column, I_{col} , is calculated by:

$$I_{col} = \frac{1}{12} [d^4 - (d - 2t)^4] = \frac{1}{12} [(0.1524 \text{ m})^4 - (0.1524 \text{ m} - 0.009108 \text{ m})^4] = 9.821 \times 10^{-6} \text{ m}^4$$

where $d = 0.1524 \text{ m}$ is the width of the column and $t = 0.004554 \text{ m}$ is the thickness of the column.

The cross-sectional area of the column, A_{col} , is calculated by:

$$A_{col} = [d^2 - (d - 2t)^2] = [(0.1524 \text{ m})^2 - (0.1524 \text{ m} - 0.009108 \text{ m})^2] = 2.693 \times 10^{-3} \text{ m}^2$$

where $d = 0.1524 \text{ m}$ is the width of the column and $t = 0.004554 \text{ m}$ is the thickness of the column.

The weight per unit length of the column, w , is calculated by:

$$w = \gamma A_{col} = (77100 \text{ N/m}^3)(2.693 \times 10^{-3} \text{ m}^2) = 207.63 \text{ N/m}$$

where $\gamma = 77100 \text{ N/m}^3$ is the unit weight of steel and $A_{col} = 2.693 \times 10^{-3} \text{ m}^2$ is the cross-sectional area of the column.

The first mode natural frequency of the structure, f_{n1} , is approximated in accordance with Equation 1.9.6 - C2:

$$f_{n1} = \frac{1.732}{2\pi} \sqrt{\frac{EI_{col}g}{WL_1^3 + 0.236wL_1^4}} = \frac{1.732}{2\pi} \sqrt{\frac{(200 \times 10^9 \text{ Pa})(9.821 \times 10^{-6} \text{ m}^4)(9.81 \text{ m/s}^2)}{(667 \text{ N})(11.890 \text{ m})^3 + 0.236(207.63 \text{ N/m})(11.890 \text{ m})^4}}$$

$$f_{n1} = 0.83 \text{ Hz}$$

where $E = 200 \times 10^9 \text{ Pa}$ is the modulus of elasticity of steel, $I_{col} = 9.821 \times 10^{-6} \text{ m}^4$ is the moment of inertia of the column, $g = 9.81 \text{ m/s}^2$ is the acceleration of gravity, $W = 667 \text{ N}$ is the weight of the luminaire, $L_1 = 11.890 \text{ m}$ is the

length of the column, and $w = 207.63 \text{ N/m}$ is the weight per unit length of the column.

The critical wind velocity, V_c , at which vortex shedding lock-in occurs is calculated in accordance with Equation 1.9.6 - 2:

$$V_c = \frac{f_{n1} d}{S} = \frac{(0.83 \text{ Hz})(0.1524 \text{ m})}{0.11} = 1.15 \text{ m/s}$$

where $f_{n1} = 0.83 \text{ Hz}$ is the natural frequency corresponding to the first mode of vibration, $d = 0.1524 \text{ m}$ is the across-wind dimension of the column, and $S = 0.11$ is the Strouhal number for a square section.

The equivalent static pressure range, P_{vs} , to be applied to the column is calculated in accordance with Equation 1.9.6-3:

$$P_{vs} = \frac{0.613 V_c^2 C_d I_F}{2 \beta} = \frac{0.613 (1.15 \text{ m/s})^2 (1.45) (0.30)}{2 (0.005)} = 35.27 \text{ Pa}$$

where $V_c = 1.15 \text{ m/s}$ is the critical wind velocity associated with vortex shedding lock-in (Equation 1.9.6 - 2), $C_d = 1.45$ is the drag coefficient for a square section (Table 1.2.5C), $I_F = 0.30$ is the importance factor used in the design of a Category III luminaire support structure for vortex shedding (Table 1.9.6.1), and $\beta = 0.005$ is a conservative estimate of the damping ratio.

The equivalent static load range, F_{vs} , to be applied to the column is calculated by:

$$F_{vs} = P_{vs}(A_{col})_v = P_{vs}[L_1 d] = [35.27 \text{ Pa}][(11.890 \text{ m})(0.1524 \text{ m})] = 63.91 \text{ N}$$

where $(A_{col})_v$ is the area of the column projected on a vertical plane, $L_1 = 11.890 \text{ m}$ is the length of the column, and $d = 0.1524 \text{ m}$ is the width of the column.

2.3 Natural Wind Gusts

It is assumed that the luminaire will be erected at a location where the yearly mean wind velocity is 5 m/s . Therefore, Equation 1.9.6 - 4 is applied without modification.

The equivalent static pressure range, P_{NW} , to be applied to the structure is calculated in accordance with Equation 1.9.6 - 4:

$$P_{NW} = 250 C_d I_F = 250 C_d (0.44) = 110 C_d \text{ Pa}$$

where $I_F = 0.44$ (Table 1.9.6.1) is the importance factor used in the design of a Category III luminaire support structure for natural wind.

The equivalent static load range to be applied to the column, $(F_{NW})_{col}$, is calculated by:

$$(F_{NW})_{col} = P_{NW}(A_{col})_v = P_{NW}[L_1 d] = [(110)(1.45)][(11.890 \text{ m})(0.1524 \text{ m})] = 289.02 \text{ N}$$

where $(A_{col})_v$ is the area of the column projected on a vertical plane, $L_1 = 11.890 \text{ m}$ is the length of the column, $d = 0.1524 \text{ m}$ is the width of the column, and $C_d = 1.45$ is the drag coefficient for a square section (Table 1.2.5C).

The equivalent static load range to be applied to the luminaire, $(F_{NW})_{lum}$, is calculated by:

$$(F_{NW})_{lum} = P_{NW}(A_{lum})_v = [(110)(1.20)][(0.434 \text{ m}^2)] = 57.29 \text{ N}$$

where $(A_{lum})_v = 0.434 \text{ m}^2$ is the area of the luminaire projected on a vertical plane and $C_d = 1.20$ is the drag coefficient for a luminaire with a rectangular flat side shape (Table 1.2.5C).

2.4 Truck Gusts

As per the requirements of Section 1.9.6A-d, truck gusts need not be considered in the design of luminaire support structures for vibration and fatigue.

3. CALCULATION OF BENDING MOMENTS

3.1 Moment Due to Vortex Shedding

The bending moment at the base of the column is calculated by:

$$M_{VS} = (F_{VS})_{col}(L_1/2) = (63.91 \text{ N})(5.945 \text{ m})$$

$$M_{VS} = 380 \text{ N-m}$$

3.2 Moment Due to Natural Wind Gusts

The bending moment at the base of the column is calculated by:

$$M_{NW} = (F_{NW})_{col}(L_1/2) + (F_{NW})_{lum}L_1 = (289.02 \text{ N})(5.945 \text{ m}) + (57.29 \text{ N})(11.890 \text{ m})$$

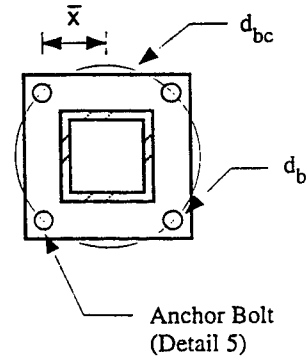
$$M_{NW} = 2399 \text{ N-m} \Rightarrow \underline{\text{Controls}}$$

4. STRESS RANGE CALCULATIONS

4.1 Anchor Bolts

Details of the anchor bolt group are provided below:

Nominal bolt diameter = $d_b = 25.4 \text{ mm}$ (0.0254 m)
 Thread series = 8 UNC
 Thread pitch = 3.175 mm
 Number of bolts = 4
 Bolt circle diameter = $d_{bc} = 0.3175 \text{ m}$



4.1.1 Moment of Inertia of the Bolt Group

The centroidal distance to each of the anchor bolts, \bar{x} , is calculated by:

$$\bar{x} = \frac{d_{bc}}{2} \cos 45^\circ = \frac{0.3175 \text{ m}}{2} \cos 45^\circ = 0.1123 \text{ m}$$

where $d_{bc} = 0.3175 \text{ m}$ is the diameter of the bolt circle.

The tensile stress area of each of the anchor bolts is calculated by:

$$A_T = \frac{\pi}{4} [d_b - 0.938 P]^2 = \frac{\pi}{4} [25.4 \text{ mm} - 0.938(3.175 \text{ mm})]^2 = 391 \text{ mm}^2 (3.91 \times 10^{-4} \text{ m}^2)$$

where A_T is the tensile stress area of each anchor bolt (Section 1.3.4A), $d_b = 25.4 \text{ mm}$ is the nominal bolt diameter, and $P = 3.175 \text{ mm}$ is the thread pitch.

The moment of inertia of the bolt group is calculated by:

$$I_b = \sum A_T \bar{x}^2 = 4[(3.91 \times 10^{-4} \text{ m}^2)(0.1123 \text{ m})^2] = 1.971 \times 10^{-5} \text{ m}^4$$

where $A_T = 3.91 \times 10^{-4} \text{ m}^2$ is the tensile stress area of each bolt and $\bar{x} = 0.1123 \text{ m}$ is the centroidal distance to each of the bolts.

4.1.2 Anchor Bolt Stress Range

Based upon the calculations of Section 3, natural wind gusts control the design of the anchor bolt group for fatigue. Therefore, the axial stress range in each of the anchor bolts is calculated by:

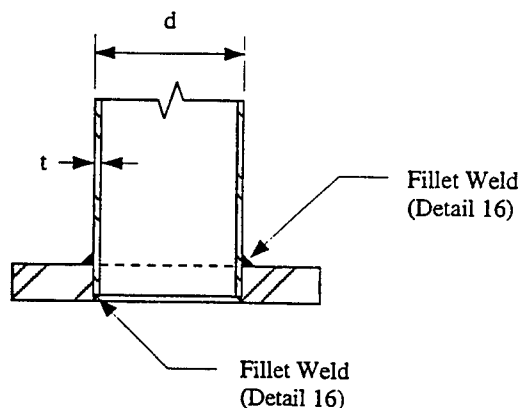
$$(S_R)_{bolt} = \frac{M_{NW}c}{I_b} = \frac{(2399 \text{ N-m})(0.1123 \text{ m})}{1.971 \times 10^{-5} \text{ m}^4} = 13.67 \times 10^6 \text{ Pa (13.67 MPa)}$$

Anchor bolts are classified as Category D fatigue details (Detail 5 in Table 1.9.6.2). The constant amplitude fatigue limit corresponding to Category D is 48 MPa (Table 1.9.6.2). Since the calculated stress range (13.67 MPa) is less than the constant amplitude fatigue limit (48 MPa), the anchor bolt group is adequately designed for fatigue.

4.2 Column-to-Base Plate Connection

Details of the column-to-base-plate socket connection are provided below:

Width = $d = 0.1524 \text{ m}$
Thickness = $t = 0.004554 \text{ m}$



4.2.1 Moment of Inertia

From previous calculations, the moment of inertia of the column is:

$$I_{col} = 9.821 \times 10^{-6} \text{ m}^4$$

4.2.2 Column Stress Range

Based upon the calculations of Section 3, natural wind gusts control the design of the column-to-base plate connection for fatigue. Therefore, the stress range at the column base is calculated by:

$$(S_R)_{col} = \frac{M_{NW}c}{I_{col}} = \frac{(2399 \text{ N-m})(0.0762 \text{ m})}{9.821 \times 10^{-6} \text{ m}^4} = 18.61 \times 10^6 \text{ Pa (18.61 MPa)}$$

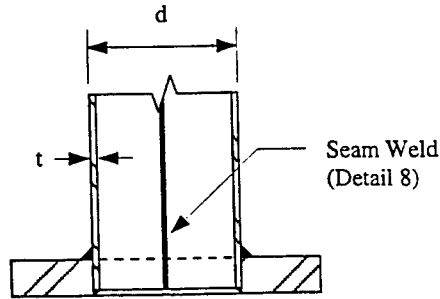
The column-to-base-plate socket connection is classified as a Category E' fatigue detail (Detail 16 in Table 1.9.6.2).

The constant amplitude fatigue limit corresponding to Category E' is 18 MPa (Table 1.9.6.2). Although the calculated stress range (18.61 MPa) is slightly greater than the constant amplitude fatigue limit (18 MPa), the socket connection is considered adequately designed for fatigue

4.3 Seam Weld

Details of the partial-penetration column seam weld are provided below:

Width = $d = 0.1524$ m
Thickness = $t = 0.004554$ m



4.3.1 Moment of Inertia

From previous calculations, the moment of inertia of the column is:

$$I_{col} = 9.821 \times 10^{-6} \text{ m}^4$$

4.3.2 Column Stress Range

Based upon the calculations of Section 3, natural wind gusts control the design of the column seam weld for fatigue. Therefore, the stress range at the column base is calculated by:

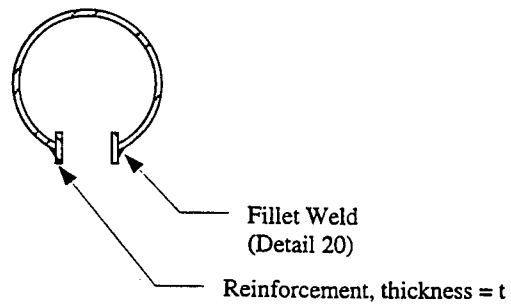
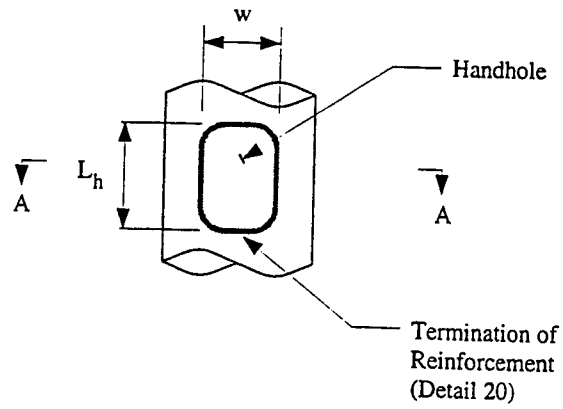
$$(S_R)_{col} = \frac{M_{NW}^C}{I_{col}} = \frac{(2399 \text{ N-m})(0.0762 \text{ m})}{9.821 \times 10^{-6} \text{ m}^4} = 18.61 \times 10^6 \text{ Pa (18.61 MPa)}$$

The partial-penetration column seam weld is classified as a Category B' fatigue detail (Detail 8 in Table 1.9.6.2). The constant amplitude fatigue limit corresponding to Category B' is 83 MPa (Table 1.9.6.2). Since the calculated stress range (18.61 MPa) is less than the constant amplitude fatigue limit (83 MPa), the partial-penetration column seam weld is considered adequately designed for fatigue.

4.4 Handhole

Details of the handhole are provided below:

$$\begin{aligned}L_h &= 0.1524 \text{ m} \\w &= 0.1016 \text{ m} \\t &= 0.00635 \text{ m}\end{aligned}$$



Section A-A

4.4.1 Moment of Inertia

From previous calculations, the moment of inertia of the column is:

$$I_{col} = 9.821 \times 10^{-6} \text{ m}^4$$

4.4.2 Handhole Stress Range

Based upon the calculations of Section 3, natural wind gusts control the design of the handhole for fatigue. The bending moment at the termination of the handhole due to natural wind is computed by:

$$M_{NW} = (F_{NW})_{col} \left[\frac{L_1}{2} - L_2 \right] + (F_{NW})_{lum} [L_3]$$

$$M_{NW} = (289.02 \text{ N})[5.945 \text{ m} - 0.381 \text{ m}] + (57.29 \text{ m})[11.509 \text{ m}] = 2267 \text{ N-m}$$

The stress range at the termination of the handhole is calculated by:

$$S_R = \frac{M_{NW} c}{I_{col}} = \frac{(2267 \text{ N-m})(0.0762 \text{ m})}{9.821 \times 10^{-6} \text{ m}^4} = 17.59 \times 10^6 \text{ Pa} \text{ (17.59 MPa)}$$

The handhole termination is classified as a Category E fatigue detail (Detail 20 in Table 1.9.6.2). The E categorization arises from the fact that the length of the reinforcement is greater than 0.102 m. The constant amplitude fatigue limit corresponding to Category E is 31 MPa (Table 1.9.6.2). The calculated stress range (17.59 MPa) is less than the constant amplitude fatigue limit (31 MPa). Therefore, the handhole termination is adequately designed for fatigue.

5. DEFLECTION

As per the requirements of Section 1.9.6C, luminaire support structures need not be designed to satisfy the deflection limit state.

Appendix C

Proposed Specification and Commentary

**1994 Standard Specifications for Structural Supports
for Highway Signs, Luminaires and Traffic Signals**

Item 1

Revise Section 1.9.6 to the following:

1.9.6 - VIBRATION AND FATIGUE OF CANTILEVERED SUPPORT STRUCTURES

The following section shall be applied for the design of cantilevered sign, signal and luminaire support structures. These provisions are not directly applicable for the design of strain poles or overhead sign bridges.

(A) Wind Loads for Fatigue and Deflection Design

(1) Importance Factors (I_F)

An importance factor which accounts for the degree of hazard to traffic and damage to property shall be applied to the limit-state wind loads specified in Section 1.9.6(A)(2). Importance Factors for cantilevered signal, sign, and luminaire support structures exposed to the four wind loads are presented in Table 1.9.6.1. For combined structures (e.g., signal and luminaire combined structure) use of more conservative importance factor is recommended.

Category		Importance Factor			
		Galloping	Vortex Shedding	Natural Wind	Truck Gusts
I	Sign	1.0	x	1.0	1.0
	Signal	1.0	x	1.0	1.0
	Luminaire	x	1.0	1.0	x
II	Sign	0.65	x	0.75	0.89
	Signal	0.65	x	0.80	0.84
	Luminaire	x	0.65	0.72	x
III	Sign	0.31	x	0.49	0.77
	Signal	0.30	x	0.59	0.68
	Luminaire	x	0.30	0.44	x

Note: x - Structure is not susceptible to this type of loading.

Table 1.9.6.1 - Importance Factors for Vibration and Fatigue Design

Category Descriptions:

- I - Critical cantilevered support structures installed on major highways.
- II - Other cantilevered support structures installed on major highways and all cantilevered support structures installed on secondary highways.
- III - Cantilevered support structures installed at all other locations.

(2) Wind Loads

Cantilevered support structures are exposed to several wind phenomena which can produce cyclic loads. Vibrations associated with these cyclic forces can become significant because of the low levels of stiffness and damping inherent in cantilevered support structures. To avoid large-amplitude vibrations and to preclude the development of fatigue cracks in various connection details, cantilevered support structure shall be designed for fatigue to resist each of the following limit-state wind forces acting separately. These loads are then used to calculate nominal stress ranges at fatigue sensitive connection details as described in Section 1.9.6(B).

In lieu of using the equivalent static pressures provided in this specification, a dynamic analysis of the structure may be performed using appropriate dynamic load functions derived from reliable data.

(a) Galloping Induced Wind Load (P_G)

Galloping, or Den Hartog instability, results in large-amplitude, resonant oscillations in a plane normal to the direction of wind flow. It is limited to structures with non-symmetrical cross sections, such as sign and signal structures with attachments to the horizontal mast-arm. Structures without attachments to the mast arm are not susceptible to galloping induced wind loads.

Cantilevered sign and signal support structures shall be designed for galloping-induced cyclic loads by applying an equivalent static shear pressure vertically to the surface area of all sign panels and/or signal heads rigidly mounted to the horizontal mast-arm as seen in the normal elevation. The magnitude of this vertical shear pressure range shall be equal to the following:

$$P_G = 21.0 \cdot I_F \quad (\text{psf}) \quad (1.9.6-1)$$

$$P_G = 1000 \cdot I_F \quad (\text{Pa})$$

In lieu of designing to resist periodic galloping forces, cantilevered sign and signal structures may be erected with approved vibration mitigation devices.

(b) Vortex Shedding Induced Wind Load (P_{VS})

The shedding of vortices on alternate sides of a member may result in resonant oscillations in a plane normal to the direction of flow. Typical natural frequencies and member dimensions preclude the possibility of most cantilevered sign and signal support structures from being susceptible to vortex

shedding induced vibrations. However, non-tapered luminaire support structures shall be designed to resist vortex shedding induced loads.

Vortex shedding lock-in can occur at a critical wind velocity, V_c , (ft/sec or m/sec) of:

$$\begin{aligned} V_c &= f_n d / S_n \quad (\text{for circular sections}) \\ \text{and} \quad V_c &= f_n b / S_n \quad (\text{for multi-sided sections}). \end{aligned} \quad (1.9.6-2)$$

Where f_n is the first natural frequency of the structure (cps), d and b are the diameter and flat-to-flat dimension of the horizontal mast arm for circular and multi-sided sections respectively (ft or m), and S_n is the Strouhal number. The Strouhal number shall be taken as 0.18 for circular sections, 0.15 for multi-sided sections, and 0.11 for square sections.

The equivalent static pressure range to be used for the design of vortex shedding induced loads is:

$$P_{VS} = \frac{0.00118 V_c^2 C_d I_F}{2\beta} \quad (psf) \quad (1.9.6-3)$$

$$P_{VS} = \frac{0.613 V_c^2 C_d I_F}{2\beta} \quad (Pa)$$

where V_c is expressed in ft/sec (m/sec), C_d is the drag coefficient specified in Section 1.2.5, and β is the damping ratio which is conservatively estimated as 0.005.

The equivalent static pressure range (P_{VS}) shall be applied transversely to luminaire posts (i.e., horizontal direction) and horizontal mast arms (i.e., vertical direction). In lieu of designing to resist periodic vortex shedding forces, cantilevered luminaire support structures may be erected with approved vibration mitigation devices.

(c) Natural Wind Gust Load (P_{NW})

Due to the inherent variability in the velocity and direction of air flow, natural wind gusts are the most basic wind phenomena which induce vibrations in wind-loaded structures. Therefore, all cantilevered sign, signal, and luminaire support structures shall be designed to resist an equivalent static natural wind gust pressure range of:

$$P_{NW} = 5.2 C_d I_F \quad (psf) \quad (1.9.6-4)$$

$$P_{NW} = 250 C_d I_F \quad (Pa)$$

where C_d is the appropriate drag coefficient specified in Section 1.2.5. This natural wind gust pressure range shall be applied in the horizontal direction to the exposed area of all support structure members, signs, signals, and/or miscellaneous attachments. The design natural wind gust pressure range is based on a yearly mean wind speed of 11 mph (5 m/s). For locations with more detailed wind records (particularly sites with higher wind speeds), refer to the commentary of Section 1.9.6.

(d) Truck Induced Gust Load (P_{TG})

The passage of trucks beneath cantilevered support structures induce gust loads on the attachments mounted to the mast arms of these structures. Although loads are applied in both the horizontal and vertical direction, mast arm vibrations caused by forces in the vertical direction are most critical. Therefore, truck gust pressures are applied only to the exposed horizontal surface of the attachment and mast arm.

Sign and signal support structures shall be designed to resist an equivalent static truck gust pressure range of:

$$P_{TG} = 36.6 C_d I_F \text{ (psf)} \quad (1.9.6-5)$$

$$P_{TG} = 1760 C_d I_F \text{ (Pa)}$$

where C_d is the worst case drag coefficient from Section 1.2.5. This pressure range shall be applied in the vertical direction to the mast arm as well as the area of all signs, walkways, and/or lighting fixtures projected on a horizontal plane. Apply this pressure range along the full length of any attached sign panels or the outer 12 ft. (3.7 m), whichever is greater.

(3) Requirements for Individual Truss Members

Vibration in truss structures can also occur in individual members. Slender tension members and redundant diagonals are particularly susceptible to vibration and the preventative cure consists of increasing member stiffness, thereby reducing flexural deflection and raising vibration response frequencies. Present specification requirements for maximum L/r ratios should be adequate to prevent excessive vibration.

(B) Fatigue Design Criteria

Cantilevered support structures shall be designed for fatigue to resist each of the equivalent static wind loads acting separately (modified by the appropriate importance factors) specified in Section 1.9.6(A). All components, mechanical fasteners, and weld details shall be designed to satisfy the requirements of their respective detail categories for infinite fatigue life. A summary of typical cantilevered support structure connection details is presented in Table 1.9.6.2 and is illustrated in Figure 1.9.6.1.

(C) Deflection Design Criteria

The horizontal mast arms of cantilevered signal and single mast-arm sign support structures shall be designed to minimize deflections due to galloping and truck-gust wind-induced vibrations. Static deflection ranges at the free end of horizontal mast arms shall not exceed 8 inches (200 mm) vertically when the equivalent static wind loads (modified by the appropriate importance factors) specified in Section 1.9.6(A) are applied to the structure. Luminaires and other sign support structures (i.e double member or truss type mast-arms) need not satisfy these deflection requirements.

CONSTRUCTION	DETAIL	STRESS CATEGORY	APPLICATION	EXAMPLE
Plain Members	1. With Rolled or cleaned surfaces. Flame-cut edges with ANSI/AASHTO/AWS D5.1 (Section 3.2.2) smoothness of 1,000 micro-in. or less.	A	-	-
	2. Slip-joint splice where L is greater than 1.5 diameters.	B	High mast towers.	1
	3. Net section of fully-tightened high-strength (ASTM A325, A490) bolted connections.	B	Bolted joints.	2
	4. Net section of other mechanically fastened connections: Steel: Aluminum:	D E	-	3
Mechanically Fastened Connections	5. Anchor bolts or other fasteners in tension; stress range based on the tensile stress area. Misalignments of less than 1:40 with beveled washers.	D	Anchor bolts. Bolted mast-arm-to-column connections.	8
	6. Connection of members or attachment of miscellaneous signs, signals, etc. with clamps or U-bolts.	D	-	-
Holes and Cutouts	7. Net section of holes and cutouts.	D	Wire outlet holes. Drainage holes. Unreinforced handholes.	5

Table 1.9.6.2 - Fatigue Details of Cantilevered Support Structures (1 of 6)

CONSTRUCTION	DETAIL	STRESS CATEGORY	APPLICATION	EXAMPLE
Groove-Welded Connections	8. Tubes with continuous full- or partial-penetration groove welds parallel to the direction of the applied stress.	B'	Longitudinal seam welds.	6
	9. Full-penetration groove-welded splices with welds ground to provide a smooth transition between members. (With or without backing ring removed)	D	Column or mast-arm butt-splices.	4
	10. Full-penetration groove-welded splices with weld reinforcement not removed. (With or without backing ring removed)	E	Column or mast-arm butt-splices.	4
	11. Full-penetration groove-welded tube-to-transverse plate connections with the backing ring attached to the plate with a full-penetration weld.	E	Column-to-base-plate connections. Mast-arm-to-flange-plate connections.	5
	12. Full-penetration groove-welded tube-to-transverse plate connections (backing ring not removed).	E'	Column-to-base-plate connections. Mast-arm-to-flange-plate connections.	5

Table 1.9.6.2 - Fatigue Details of Cantilevered Support Structures (2 of 6)

CONSTRUCTION	DETAIL	STRESS CATEGORY	APPLICATION	EXAMPLE
Fillet-Welded Connections	13. Fillet-welded lap splices.	E	Column or mast-arm lap splices	3
	14. Members with axial and bending loads with fillet-welded end connections without notches perpendicular to the applied stress. Welds distributed around the axis of the member so as to balance weld stresses.	E	Angle-to-gusset connections with welds terminated short of plate edge. Slotted tube-to-gusset connections with coped holes.	2,6
	15. Members with axial and bending loads with fillet-welded end connections without notches perpendicular to the applied stress. Welds distributed around the axis of the member so as to balance weld stresses.	E'	Angle-to-gusset connections. Slotted tube-to-gusset connections without coped holes.	2,6
	16. Fillet-welded tube-to-transverse plate connections.	E'	Column-to-base-plate or mast-arm-to-flange-plate socket connections.	7,8
	17. Fillet-welded connections with one-sided welds normal to the direction of the applied stress.	E'	Built-up box mast-arm-to-column connections.	8
	18. Fillet-welded mast-arm-to-column pass-through connections.	E'	Mast-arm-to-column pass-through connections.	9
	19. Fillet welded T-, Y-, and K-tube-to-tube, angle-to-tube, or plate-to-tube connections.	see a	Chord-to-vertical or chord-to-diagonal truss connections. Mast-arm directly welded to column. Built-up box connection.	8,10,11

Table 1.9.6.2 - Fatigue Details of Cantilevered Support Structures (3 of 6)

CONSTRUCTION	DETAIL	STRESS CATEGORY	APPLICATION	EXAMPLE
Attachments	20. Non-load bearing longitudinal attachments with partial- or full-penetration groove welds, or fillet welds, in which the main member is subjected to longitudinal loading: L ≤ 51 mm: 51 mm < L ≤ 12t or 102 mm: L > 12t or 102 mm when t ≤ 25 mm:	C D E	Weld terminations at ends of longitudinal stiffeners. Reinforcement at handholes.	12,13
	21. Non-load bearing longitudinal attachments with L > 102 mm and full-penetration groove welds. The main member is subjected to longitudinal loading and the weld termination embodies a transition radius or taper with the weld termination ground smooth: R > 152 mm or α ≤ 15°; 152 > R > 51 mm or 15° < α ≤ 60°; R ≤ 51 mm or α > 60°;	C D E	Weld terminations at ends of longitudinal stiffeners.	14
	22. Non-load bearing longitudinal attachments with L > 102 mm and fillet or partial-penetration groove welds. The main member is subjected to longitudinal loading and the weld termination embodies a transition radius or taper with the weld termination ground smooth: R > 51 mm or 15° < α ≤ 60°; R ≤ 51 mm or α > 60°;	C D E	Weld terminations at ends of longitudinal stiffeners.	14

Table 1.9.6.2 - Fatigue Details of Cantilevered Support Structures (4 of 6)

CONSTRUCTION	DETAIL	STRESS CATEGORY	APPLICATION	EXAMPLE
Attachments (Con't)				
	23. Transverse load-bearing fillet-welded attachments where $t \leq 13$ mm and the main member is subjected to minimal axial and/or flexural loads. (When $t > 13$ mm see Note c)	C	Longitudinal stiffeners welded to baseplates.	12,14
	24. Transverse load-bearing longitudinal attachments with partial-or full-penetration groove welds or fillet welds, in which the non-tubular main member is subjected to longitudinal loading and the weld termination embodies a transition radius which is ground smooth: $R > 51$ mm or $15^\circ < \alpha \leq 60^\circ$; $R \leq 51$ mm or $\alpha > 60^\circ$;	D E see b	Gusset-plate-to-chord attachments.	15

Notes:

- a) Category ET with respect to stress in branching member provided that $r/t \leq 24$ for the chord member. When $r/t > 24$ then the fatigue strength equals:

$$(F)_n = (\Delta F)_n^{ET} \times \left(\frac{24}{r/t}\right)^{0.7}$$

Where $(\Delta F)_n^{ET}$ is the CAFIL for category ET.

Category E with respect to stress in chord.

Table 1.9.6.2 - Fatigue Details of Cantilevered Support Structures (5 of 6)

b) First check with respect to the longitudinal stress range in the main member per the requirements for non-load bearing longitudinal attachments. The attachment must then be separately checked with respect to the transverse stress range in the attachment per the requirements for transverse load-bearing longitudinal attachments.

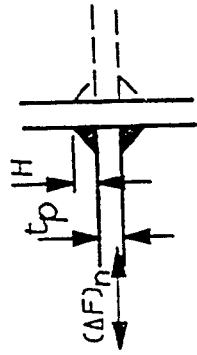
c) When $t > 13$ mm, the fatigue strength shall be the lesser of Category C or the following:

$$(\Delta F) = (\Delta F)_n^C \times \frac{0.094 + 1.23 \frac{H}{t_p}}{\frac{1}{t_p^{\frac{1}{6}}}}$$

Where $(\Delta F)_n^C$ is the CAFL for category C, H is the effective weld throat (mm), and t_p is the plate thickness (mm) as defined in Detail A.

Constant Amplitude Fatigue Thresholds

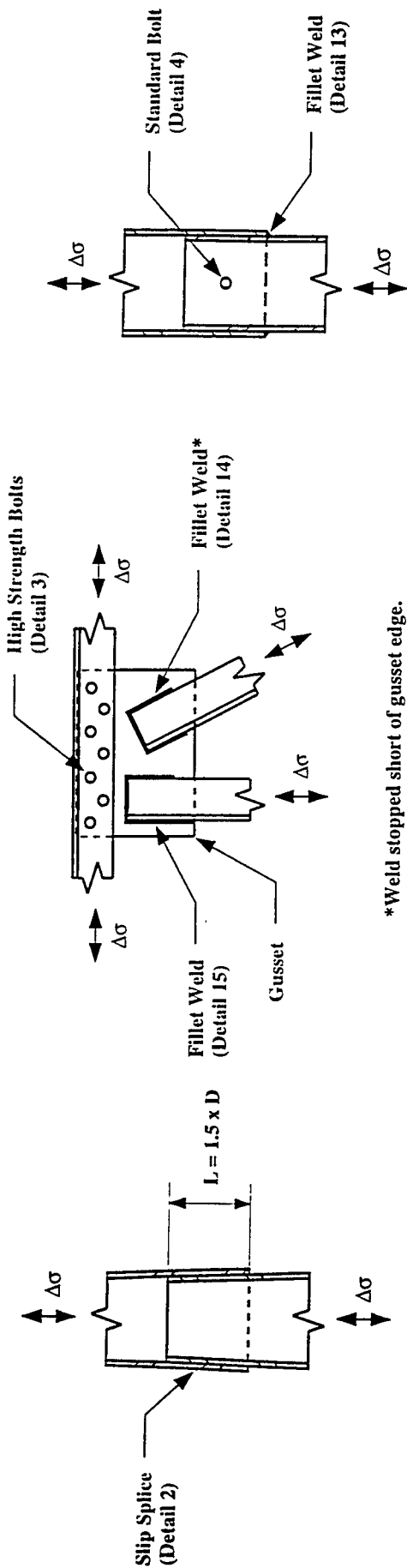
Detail Category	Steel	Aluminum
	Threshold (MPa)	Threshold (MPa)
A	165	70
B	110	41
B'	83	32
C	69	28
D	48	17
E	31	13
E'	18	7
ET	8	3



Detail A

Note: 1 MPa = 0.145 ksi

Table 1.9.6.2 - Fatigue Details of Cantilevered Support Structures (6 of 6)

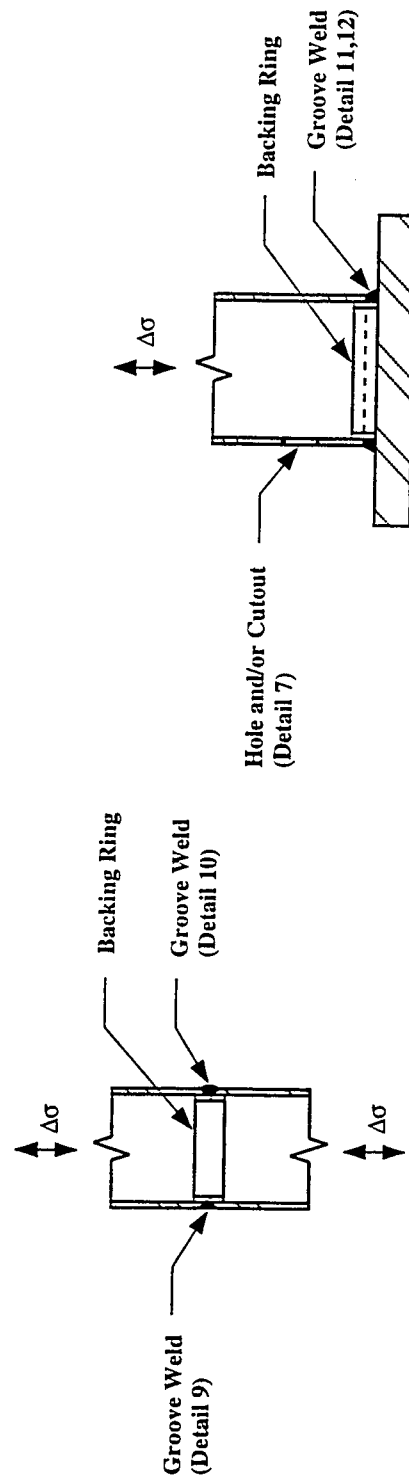


Slip-Joint Splice
Example 1

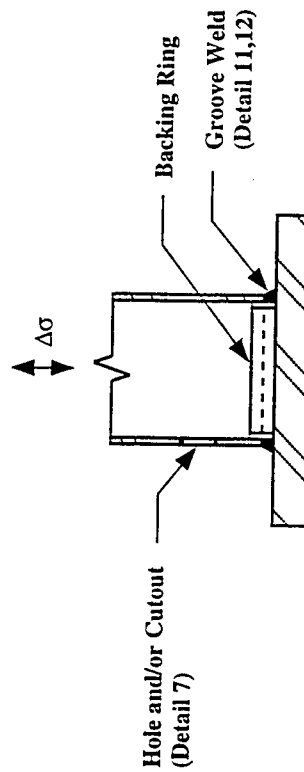
Double-Angle Truss Gusset
Example 2

*Weld stopped short of gusset edge.

Fillet-Welded Lap-Splice
Example 3

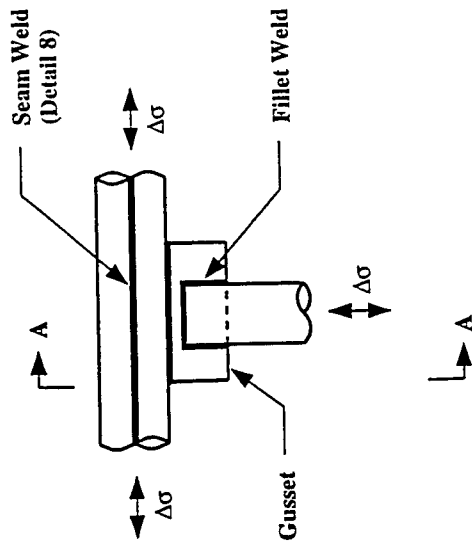


Groove-Welded Butt-Splice
Example 4



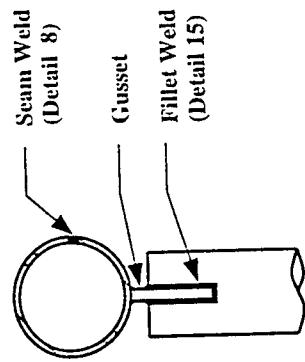
Groove-Welded Tube-to-Transverse Plate Connection
Example 5

Figure 1.9.6.1 - Illustrative Examples (1 of 5)

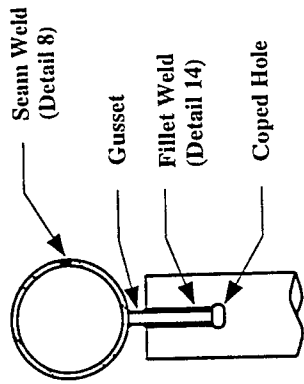


Slotted Tube-to-Gusset Connection
Example 6

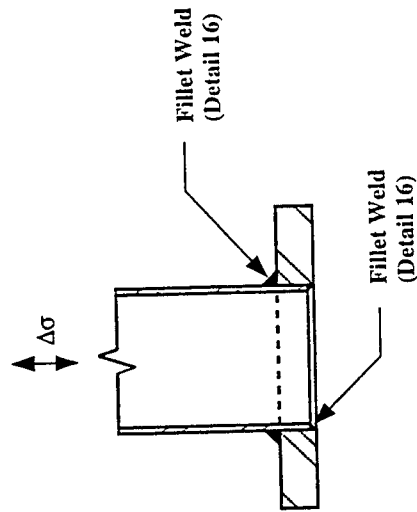
C-12



Section A-A
Slotted Tube-to-Gusset Connection
Example 6

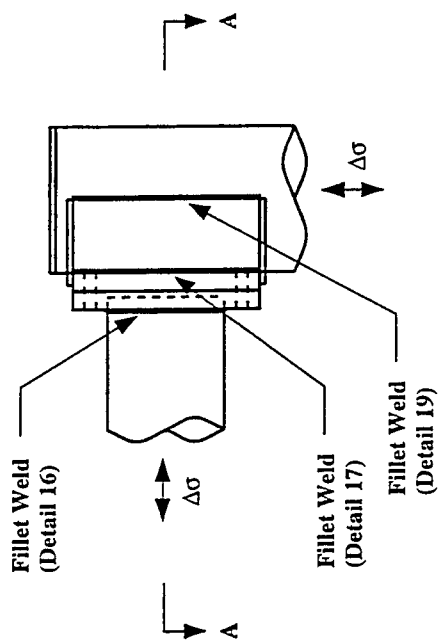


Section A-A
Slotted Tube-to-Gusset Connection
Example 6



Fillet-Welded Socket Connection
Example 7

Figure 1.9.6.1 - Illustrative Examples (2 of 5)



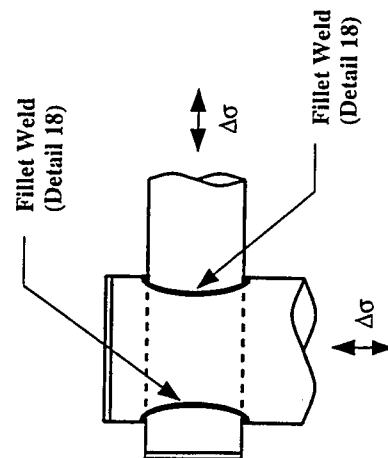
Section A-A

**Fillet-Welded Mast-Arm-to-Column Connection
(Built-Up Box)**

Example 8

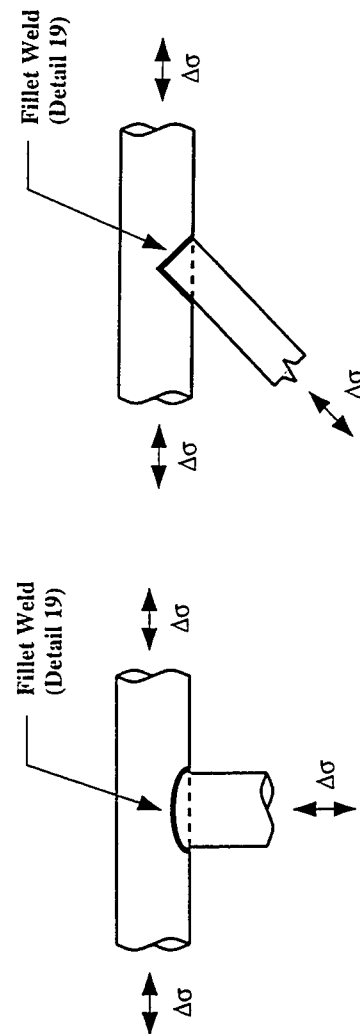
**Fillet-Welded Mast-Arm-to-Column Connection
(Built-Up Box)**

Example 8



**Fillet-Welded Tube-to-Tube Column
Pass-Through Connection**

Example 9



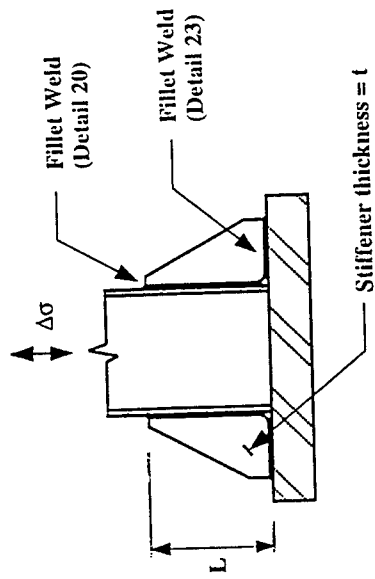
Fillet-Welded Tube-to-Tube Connection

Example 10

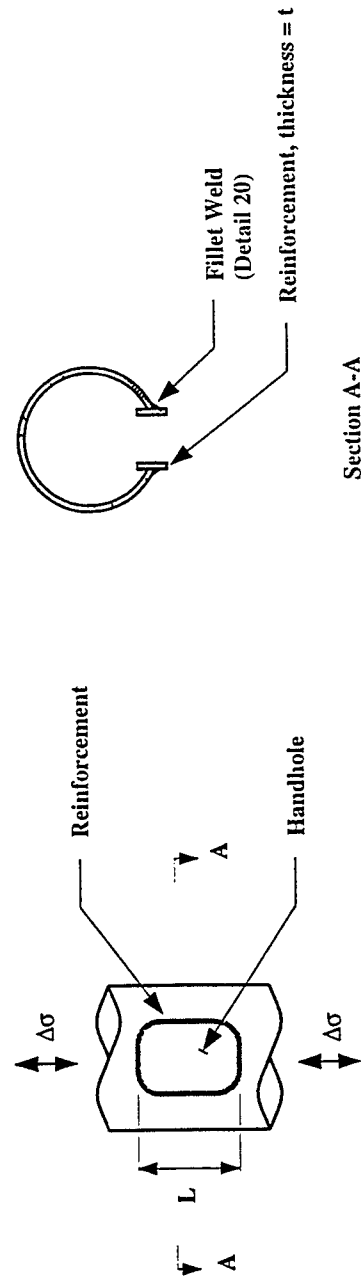
Fillet-Welded Angle-to-Tube Connection

Example 11

Figure 1.9.6.1 - Illustrative Examples (3 of 5)



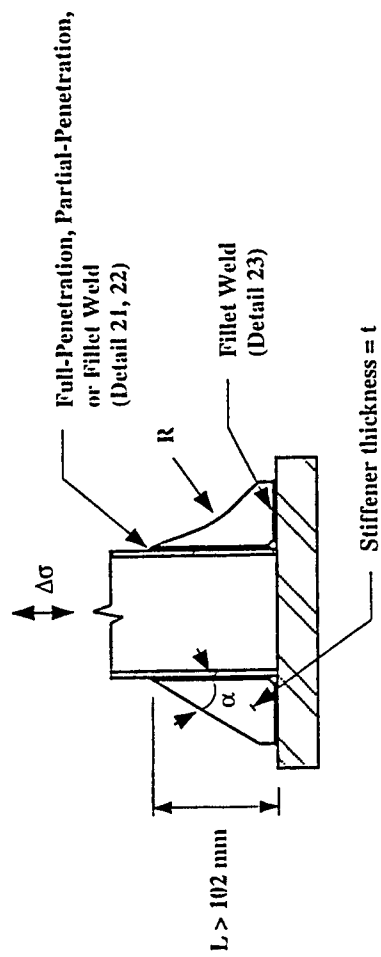
Non-Load Bearing Longitudinal Attachment
Example 12



Reinforced Handhole
Example 13

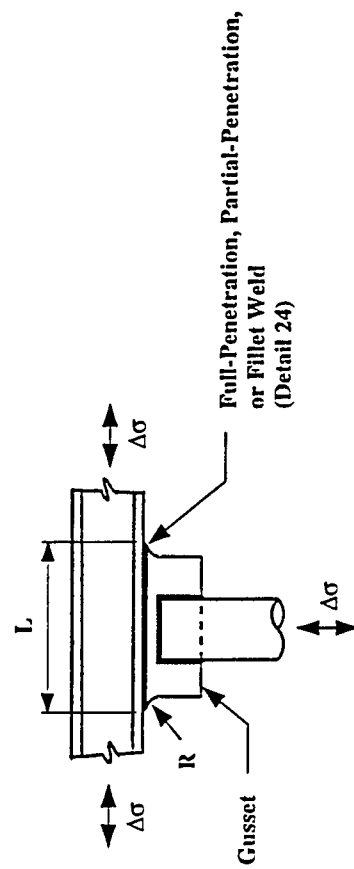
Reinforced Handhole
Example 13

Figure 1.9.6.1 - Illustrative Examples (4 of 5)



Non-Load Bearing Longitudinal Attachment

Example 14



Transverse Load-Bearing Longitudinal Attachment

Example 15

Figure 1.9.6.1 - Illustrative Examples (5 of 5)

Other Affected Areas:

I. The commentary to Section 1.9.6 shall be revised to the following:

1.9.6 - VIBRATION AND FATIGUE OF CANTILEVERED SUPPORT STRUCTURES

(A) Vibration due to Fatigue Wind Loads

(1) Importance Factors

Importance factors are introduced into the specification to adjust the level of structural reliability of cantilevered support structures. The importance factors given in Table 1.9.6.1 shall be applied to the limit-state wind loads prior to determining the fatigue resistance and/or maximum mast-arm displacement in signal support structures.

Structures classified as Category I present a high hazard in the event of failure and will be designed to resist rarely occurring wind loading and vibration phenomena, while structures classified as Category III will be designed to the same level of reliability, on average, as those structures designed prior to modification of Section 1.9.6 of the specification. Category II is an average of Category I and III. It is intended that only the most critical cantilevered support structures be classified as Category I. Some examples of structures which should be considered for Category I classification include large sign structures (including variable message signs), signals with long mast-arms, and high mast towers in excess of 100 ft (30 m) which are installed on highways where the vehicle speed is such that the consequences of excessive deflection or a collision with a fallen structure is intolerable. Category II and III structures are not less likely to experience the full limit-state wind loads associated with Category I. If Category II or III cantilevered support structures do experience the limit state loads over a period of time, they would be expected to experience excessive deflections and/or fatigue damage. Sound engineering judgement shall be used in the classification process.

(2) Recent research [1] has identified galloping, vortex shedding, natural wind gusts and truck-induced gusts as wind-loading mechanisms which can induce large-amplitude vibrations and/or fatigue damage in cantilevered signal, sign and light support structures. The amplitude of vibration and resulting stress ranges are increased by the low levels of stiffness and damping possessed by many of these structures. In some cases, the vibration is only a serviceability problem because motorists cannot clearly see the mast arm attachments or are concerned about passing under the structures. In other cases, where deflections may or may not be considered excessive, the magnitudes of stress ranges induced in these structures have resulted in the development of fatigue cracks at various connection details including the anchor bolts.

The wind-loading phenomena specified in Section 1.9.6(A)(2) possess the greatest potential for creating large-amplitude vibrations in cantilevered support structures. In particular, galloping and vortex shedding are aeroelastic instabilities which will typically induce vibrations at the natural frequency of the structure (resonance). These conditions can lead to fatigue failures in a short period of time after installation.

Design pressures for each of the four possible fatigue wind-loading mechanisms are presented as an equivalent static wind pressure range (or a shear stress range in the case of galloping). These pressure (or shear stress) ranges should be applied to the structure as prescribed by the specification in a simple static analysis to determine stress ranges at fatigue sensitive details and maximum mast-arm deflections for all signal and some sign support structures. In lieu of designing for galloping or vortex shedding limit-state fatigue wind loads, approved mitigation devices may be specified and are discussed below.

(a) Galloping

The results of wind tunnel [1] and water tank [2] testing, as well as the oscillations observed on cantilevered support structures in the field are consistent with the characteristics of the galloping phenomena. These characteristics include the sudden onset of large-amplitude, across-wind vibrations which increase with wind velocity. It is important to note however, that galloping is typically not caused by support structure members, but rather by the attachments to the horizontal mast arm (i.e. signs and signals).

The geometry and orientation of these attachments, as well as the wind direction, directly influence the susceptibility of cantilevered support structures to galloping. In particular, signal attachments configured with or without a backplate are more susceptible to galloping when subject to flow from the rear and signals are more susceptible to galloping when configured with a backplate. Galloping of sign attachments is independent of aspect ratio and is more prevalent with wind flows from the front of the structure.

By conducting wind tunnel tests and analytical calibrations to field and forensic test data, an equivalent static vertical shear of 21 psf (1000 Pa) was determined for the galloping phenomena. This vertical shear range should be applied to the entire frontal area of each of the sign/signal attachments in a static analysis to determine stress ranges at critical connection details. For example, if an 8 ft. by 10 ft. sign panel is mounted to a horizontal mast arm, a static force of 1.7 kips (e.g. 21 psf \times 8' \times 10') should be applied vertically to the structure at the center of gravity of the sign panel.

Mitigation of galloping-induced vibrations is possible by altering the aerodynamic properties of rigidly attached sign/signal attachments. For example, this can be accomplished on signal structures by first removing any back plates which are attached to the signal heads and/or by providing an articulated joint between the signal head and mast arm. The next method involves providing positive aerodynamic damping to the structure by installing sign blanks mounted horizontally directly above the signal attachment closest to the tip of the mast arm. This method has been shown to be effective in mitigating galloping induced vibrations on signal support structures with horizontally-mounted signal attachments [2]. However, the installation of sign blanks may influence the design of these structures for truck-induced wind gusts.

(b) Vortex Shedding

Structural elements exposed to steady, uniform wind flows will shed vortices in the wake behind the element in a pattern commonly referred to as a von Karmen vortex street. When the frequency of vortex shedding approaches one of the natural frequencies of the structure, significant amplitudes of vibration can be caused by a condition termed lock-in. The critical velocity at which lock-in will occur is defined by the Strouhal relationship ($V_c = f_n d/S$).

A lower bound wind speed can be established for sign and signal structures. Although vortices are shed at low wind velocities, for wind speeds less than 16 fps (5 m/s) the vortices do not impart sufficient energy to excite most structures. Typical natural frequencies and member diameters for sign and signal support structures result in critical wind velocities well below the 16 fps (5 m/s) threshold for the occurrence of vortex shedding. However, because of extremely low levels of damping inherent in luminaire support structures, vortex shedding at wind speeds less than 16 fps (5 m/s) may excite resonant vibration. Also, an upper bound wind speed can be established for all types of cantilevered support structures. At wind speeds greater than 66 fps (20 m/s) enough natural turbulence is generated to disturb the formation of vortices.

Although possible, recent tests [1,2] have indicated that the occurrence of vortex shedding from attachments to cantilevered sign and signal support structures is not critical. In fact, these attachments are

more susceptible to galloping-induced vibrations. Finally, support structures composed of uniformly tapered members do not appear susceptible to vortex-induced vibrations when tapered at least 0.14 in/ft (0.0117 mm/mm). The dimensions of most tapered members result in critical wind velocities below the threshold velocity (16 fps), and furthermore, any vortices which may form are correlated over a short length of the member and therefore generate insignificant vortex shedding forces.

Calculation of the first modal frequency for simple pole luminaire structures (without mast arms) can be accomplished using the following equations.

$$f_{n1} = \frac{1.75}{\pi} \sqrt{\frac{EIg}{wl^4}} \quad (\text{Without luminaire mass}) \quad (1.9.6-C1)$$

$$f_{n1} = \frac{1.732}{2\pi} \sqrt{\frac{EIg}{Wl^3 + 0.236wl^4}} \quad (\text{With luminaire mass}) \quad (1.9.6-C2)$$

Where W is the weight of the luminaire, w is the weight of the pole per unit length, g is the acceleration of gravity, l is the length of the pole, and I is the moment of inertia of the pole.

However, determining the first modal frequency for luminaires with mast arms is best accomplished by a finite element based modal analysis. The mass of the luminaire attachments shall be included in the analysis to determine the first mode of vibration transverse to the wind direction. Luminaires which may not have the attachments installed immediately shall be designed for this worst-case condition. Because the natural frequency of a structure without an applied mass is typically higher than those with a luminaire attachment, the resulting critical wind speed and vortex shedding pressure range will also be higher.

(c) Natural Wind Gusts

The equivalent static natural wind gust pressure range specified for design was developed with data obtained from an analytical study of the response of cantilevered support structures subject to random gust loads [1]. This parametric study was based on the 0.01 percent exceedance for a yearly mean wind velocity of 11 mph (5 m/s), which is a reasonable upper-bound of yearly mean wind velocities for most locations in the country. There are locations however, where the yearly mean wind velocity is larger than 11 mph (5 m/s). For installation sites with more detailed information regarding yearly mean wind speeds (particularly sites with higher wind speeds), the following equivalent static natural wind gust pressure range shall be used for design.

$$P_{NW} = 5.2 C_d \left(\frac{V_{mean}^2}{125} \right) \quad (psf) \quad (1.9.6-C3)$$

$$P_{NW} = 250 C_d \left(\frac{V_{mean}^2}{25} \right) \quad (Pa)$$

(d) Truck Gusts

Recent vibration problems on sign structures with large projected areas in the horizontal plane (along the direction of traffic), e.g. variable message signs, has focussed attention on vertical gust pressures created by the passage of trucks beneath the sign. To improve fuel economy, many trucks are outfitted with deflectors to divert the wind flow upward and minimize the drag created by the trailer. It has been proposed to represent this gust pressure as that imposed by a 65 mph (30 m/s) wind to coincide with existing vehicle speed limits [3].

The equivalent static truck gust pressure is determined by utilizing the wind pressure formula in Section 1.2.5 where $V = 65$ mph (30 m/s) and $C_h = 1.0$. To account for an increase in the relative truck speed due to head winds, the gust factor of 1.3 is also included. For structures installed at locations where the posted speed limit is much less than 65 mph (30 m/s), the design pressure may be recalculated based on this lower wind velocity. Since the applied truck gust pressure will lift the mast arm vertically, the pressure obtained above is doubled to represent the entire truck gust pressure range. This doubling of the pressure is based on the assumption that on the first cycle the downward and upward forces are equal. Utilizing appropriate drag coefficients (C_d), the truck gust pressure range can then be applied to all horizontally projected areas (i.e. both the mast arm and any mast arm attachments). For structures with large sign panels, pressures shall be applied along the entire length of the horizontal areas to recognize the possibility of passage of two trucks side-by-side. The equivalent static truck gust pressure shall be applied along the outer 12 ft (3.7 m) of the mast arm on structures without large sign panels.

(B) Fatigue

Because of the inherent variability in frequency and duration of wind-induced vibrations, designing cantilevered signal, sign, and luminaire support structures for finite fatigue life is impractical. Not only does the possibility exist for a large number of cycles to be accumulated in a short period of time when resonant vibrations are induced by galloping or vortex shedding, but the long-term cumulative effects of natural wind and truck-induced gusts can also result in the development of fatigue damage. Therefore, an infinite life approach is specified for the fatigue design of cantilevered support structures. Fatigue critical details shall be designed with nominal stress ranges near the detail which are below the appropriate constant-amplitude fatigue limit.

To assist designers, a categorization of typical cantilevered support structure details to the existing AASHTO and AWS fatigue design categories is provided in Table 1.9.6.2 and Figure 1.9.6.1. Based on a review of state department of transportation standard drawings and manufacturer literature, the above-referenced list of typical cantilevered support structure connection details was produced. This list should not be considered as a complete set of all possible connection details, but rather it is intended to remove the uncertainty associated with applying the provisions of the AASHTO Bridge specification to the fatigue design of cantilevered support structures.

(C) Deflection

Because of the low levels of stiffness and damping inherent in cantilevered signal and single mast arm sign support structures, even structures which are adequately designed to resist fatigue damage may experience excessive vertical deflections at the free end of the horizontal mast arm. The primary objectives of this provision are to minimize vibration damage to signal/sign attachments and to reduce the number of motorist complaints. There is no requirement for the maximum displacement in the horizontal direction.

- II. *Section 1.9.1* - Make an addition which will instruct designers to calculate mast-arm tip deflections on cantilevered signal support structures. (See Item #3 of proposed modifications to the specification)
- III. *Sections 1.4.2 & 1.5.3* - Make additions which will instruct designers to refer to the fatigue categorization figures for improved weld details. (See Item #4 of proposed modifications to the specification)

Background:

The revisions to Sections 1.9.6(A)(1&2), 1.9.6(B) and 1.9.6(C) are based on the results of research on NCHRP Project 10-38. The slenderness provisions for truss members in Section 1.9.6(A)(3) is from the 1985 Standard Specifications for Structural Supports for Highway Signs, Luminaires and Traffic Signals.

Anticipated Effect on Cantilevered Support Structures:

Structures designed for Importance Factor Category I and II will require strengthening and/or the use of details with higher fatigue strengths to meet the fatigue and deflection provisions of the proposed specification. Those structures classified as Category III will, on average, require little strengthening to meet the proposed requirements.

References:

- 1. Kaczinski, M.R., Dexter, R.J., and Van Dien, J.P., "Fatigue Resistant Design of Cantilevered Signal, Sign and Light Supports," National Cooperative Highway Research Program, Final Report - NCHRP Project 10-38, Transportation Research Board, Washington, D.C., 1996.
- 2. McDonald, J.R., et al., "Wind Load Effects on Signals, Luminaires and Traffic Signal Structures," Report 1303-1F, Wind Engineering Research Center, Texas Tech University, Lubbock, TX, 1995.
- 3. DeSantis, P.V. and Haig, P., "Unanticipated Loading Causes Highway Sign Failure," Proceedings of ANSYS Convention, 1996.

**1994 Standard Specifications for Structural Supports
for Highway Signs, Luminaires and Traffic Signals**

Item 2

Add to the end of Section 1.3.4 the following:

(F) Anchor bolts shall be designed for wind-induced cyclic loads according to the provisions in Section 1.9.6.

(G) Anchor bolts shall be fabricated to conform to the provisions in the Standard Specification for Steel Anchor Bolts (AASHTO M314-90)

(H) All anchor bolts shall be pretensioned between nuts on either side of the base plate to 70 percent of the minimum tensile strength of the bolt. In addition, anchor bolts shall be installed with misalignments of less than 1:40 from vertical. Firm contact shall exist between the anchor bolt nuts and base plate on any anchor bolt installed in a misaligned position.

Other Affected Areas:

Section 1.3.4 (B) - The second sentence from this section should be deleted to remain consistent with the proposed addition in Section 1.3.4 (F)

The commentary to Section 1.3.4 shall be modified as follows:

1. Delete the last paragraph of the existing commentary. The paragraph starts as follows:

Research done with respect to fatigue failures in anchor bolt...

2. Add the following commentary.

(H) The fatigue strength of anchor bolt connections is directly influenced by several installation conditions. Most importantly, all anchor bolts should be installed in the fully tightened condition (i.e. 70 percent of minimum tensile strength) to eliminate the possibility of bolts becoming loose under service load conditions. Bolts which become loose, or bolts which were only snug tightened, are more susceptible to fatigue damage. The most common method of tightening anchor bolts is the turn-of-nut method. For small diameter bolts, this method specifies that the nut should be rotated 1/3 turn beyond the snug tight condition to ensure adequate pretension. Turning large diameter anchor bolts with coarse pitch threads 1/3 turn beyond snug will likely yield the bolt material. In general, most large diameter anchor bolts will require the use of a hydraulic wrench or other proven method of tightening and external lubrication of the threaded and bearing surfaces in order to achieve a fully-tightened condition. For double-nutted anchor bolt installations, snug tight shall be defined as the full strength of one man and until the base plate is in firm contact with the top and bottom nuts.

Misalignment is another common installation condition which can influence the fatigue strength of anchor bolts. However, recent research [1] has determined that bending stresses resulting from misalignments up to 1:40 do not need to be considered in stress calculations when designing anchor bolts for infinite life provided that firm contact exists between the anchor bolt nuts and base plate. Where appropriate, a beveled washer may be utilized.

Experiments to determine the relationship between column forces and anchor bolt stresses showed that inadequate column base-plate thicknesses can increase bolt stresses. As a rule-of-thumb, a base plate thickness equal to or greater than the bolt diameter will provide adequate stiffness. In addition, bending stresses in individual bolts can be ignored if the standoff distance between the top of the foundation and bottom of the leveling nut is less than one bolt diameter. For larger standoff distances, a fixed-fixed beam bending model should be used.

Background:

These additions incorporate the new AASHTO anchor bolt standard specification, as well as the results of research on NCHRP Project 10-38.

Anticipated Effect on Cantilevered Support Structures:

The proposed specification will tighten the requirements for the fabrication and installation of anchor bolts used in cantilevered support structures. Compliance to these requirements may create the need for a more detailed inspection program during construction.

References:

1. Kaczinski, M.R., Dexter, R.J., and Van Dien, J.P., "Fatigue Resistant Design of Cantilevered Signal, Sign and Light Supports," National Cooperative Highway Research Program, Final Report - NCHRP Project 10-38, Transportation Research Board, Washington, D.C., 1996.

**1994 Standard Specifications for Structural Supports
for Highway Signs, Luminaires and Traffic Signals**

Item 3

Add to the end of Section 1.9.1 the following:

(C) Cantilever Supports for Traffic Signals Subject to Fatigue Limit-State Wind Loads

The horizontal mast arms of cantilevered signal support structures shall be designed to minimize deflections due to wind-induced vibrations. Details regarding this serviceability requirement are found in Section 1.9.6(C).

Other Affected Areas:

Allowable deflection criteria is included in Section 1.9.6 of the specification.

Background:

Based on the results of research for NCHRP Project 10-38. Several states are currently specifying some form of wind load deflection criteria for cantilevered support structures. The existing AASHTO specification, however, only addresses dead load deflection requirements.

Anticipated Effect on Cantilevered Support Structures:

Excessive deflections in most cantilevered support structures will be eliminated by designing to resist the fatigue limit-state wind load. Those structures which still exceed this displacement limit will require additional stiffening.

References:

None

**1994 Standard Specifications for Structural Supports
for Highway Signs, Luminaires and Traffic Signals**

Item 4

Add to the end of Section 1.4.2(A) and Section 1.5.3 the following sentence:

Additional recommendations for proper detailing of fatigue critical welded connections are included in Table 1.9.6.2 and Figure 1.9.6.1.

Other Affected Areas:

None

Background:

The development of a detailed categorization of fatigue sensitive connection details can be used by designers and fabricators to produce more fatigue resistant cantilevered support structures.

Anticipated Effect on Cantilevered Support Structures:

Proper detailing will improve the fatigue resistance of these structures.

References:

None

**1994 Standard Specifications for Structural Supports
for Highway Signs, Luminaires and Traffic Signals**

Item 5

Incorporate into the "Nomenclature" section the following definitions:

- I_F = Importance factors applied to limit-state wind loads to determine fatigue resistance and/or mast arm displacements of cantilevered support structures
- P_G = Galloping-induced vertical shear pressure range used for vibration and fatigue design of cantilevered support structures
- P_{NW} = Natural wind gust pressure range used for vibration and fatigue design of cantilevered support structures
- P_{TG} = Truck-induced gust pressure range used for vibration and fatigue design of cantilevered support structures
- P_{VS} = Vortex shedding-induced pressure range used for vibration and fatigue design of cantilevered support structures

Other Affected Areas:

None

Background:

None

Anticipated Effect on Cantilevered Support Structures:

None

References:

None

